miR-542: a novel regulator for muscle mass and function

Roser Farré Garrós

Imperial College London

National Heart and Lung Institute

Submitted for the degree of Doctor of Philosophy (PhD)

November 2017

Declaration of Originality

I confirm that this thesis and the data presented within it are entirely my own work. Data or information which has been obtained from other members of the group, collaborators or the literature has been appropriately referenced.

Roser Farré Garrós

Copyright Declaration

The copyright of this thesis rests with the author and is made available under a Creative Commons Attribution Non-Commercial No Derivatives licence. Researchers are free to copy, distribute or transmit the thesis on the condition that they attribute it, that they do not use it for commercial purposes and that they do not alter, transform or build upon it. For any reuse or redistribution, researchers must make clear to others the licence terms of this work.

Acknowledgements

Firstly, I would like to sincerely thank my supervisor Dr Paul Kemp who gave me the opportunity to be part of his group and offered me unconditional support throughout all my PhD. I feel very lucky for having had you as my supervisor.

I also would like to thank the rest of the members of the Kemp group and all the other members of Imperial College London that had an input on my PhD project, I really appreciated all the suggestions and your help as it has contributed towards my both scientific and personal growth and I could not have done it without you all.

I also would like to mention some of the people that made of these three years of my life an unforgettable experience and with whom I have shared very long days in the lab, unsuccessful experiments and stress but also complicity and laughs. Particularly, Anna Cocking, David Cocoran, Martin Connolly, Victoria Juskaite and Despoina Gavriilidou thank you for all the good moments we have shared including BBQs, trips, nights out and festivals.

Per últim i no per això menys important, voldria agrair de tot cor als meus pares, Carlos Farré Melgosa i Maria José Garrós Torreguitart, per tot l'esforç que han fet perquè jo sigui on sóc avui i més important qui sóc. Sense ells, sense el seu suport i la seva plena confiança en mi mai ho hauria aconseguit. Així que moltes gracies per tot, mai us ho podré agrair. Moltes gràcies també als padrins que sé que tot i la distància sempre heu estat al meu costat. També agrair a tots els familiars i amics els moments de relaxació i desconnexió al vostre costat. Finalment, voldria agrair-te a tu Rubén la paciència que has tingut durant aquest últim període, gràcies per ajudar-me sempre que ho he necessitat, per saber contenir el meu estrès i per treure'm mil rialles i somriures.

Abstract

Loss of skeletal muscle mass and function is a common co-morbidity of a number of chronic diseases including chronic obstructive pulmonary disease (COPD) and a range of critical illnesses as well as in ageing, affecting the quality of life of these individuals. However, the mechanisms by which this occurs have not been completely elucidated.

Previous studies in the group identified changed in the levels of several microRNAs in the quadriceps of COPD patients. We focused on the microRNAs that showed the largest and most significant increased expression between patients and controls. One of the elevated microRNAs was miR-542-3p, which was chosen after performing a bioinformatics analysis and saw interesting predicted targets in the muscle wasting context. MiR-542-3p was also found to be elevated in the quadriceps muscle of sarcopenic patients. In this thesis, we aimed to determine if miR-542-5p was also elevated in those two cohorts and if a similar pattern for miR-542-3p/-5p was seen in critical illness such as patients with intensive care unit acquired weakness (ICUAW). We also aimed to identify the molecular pathways by which these miRNAs contributed to muscle impairment or dysfunction.

miR-542-3p/5p levels were found elevated in COPD and sarcopenic patients but more markedly elevated in patients with ICUAW. *In vitro*, miR-542-3p decreased the expression of mitochondrial (MRPS10) and cytoplasmic (RPS23) ribosomal proteins and reduced 12S and 18S ribosomal RNA (rRNA) suggesting mitochondrial and cytoplasmic ribosomal stress. miR-542-3p/-5p promoted the nuclear accumulation of phospho-SMAD2/3 and suppressed expression of SMURF1, SMAD7 and PPP2CA which are inhibitors of the system, indicative of increased TGF-β signalling. *In vivo*, miR-542 over-expression caused muscle wasting in the targeted muscle, decreased mitochondrial function, 12S rRNA and 18S rRNA levels and SMAD7 expression, consistent with the effects of the miRNA *in vitro*. In patients with ICUAW similar results were observed, the expression of 12S and 18S rRNA and SMURF1, SMAD7 and PPP2CA were reduced, suggesting mitochondrial and cytoplasmic ribosomal stress and increased TGF-β signalling.

Table of contents

Declaration of Originality 3
Copyright Declaration 3
Acknowledgements 4
Abstract 5
Table of contents 6
List of figures 12
List of tables 14
Abbreviations 15
Publications and abstracts arising from this thesis 19
Publications 19
Abstracts 19

CHAPTER 1: Introduction 20
1.1 Skeletal muscle overview 20
1.2 Skeletal muscle homeostasis: balance between muscle loss and synthesis 24
1.2.1 Mechanisms leading to muscle loss 25
1.2.2 Mechanisms involved in the gain of muscle 31
1.3 Skeletal muscle atrophy in disease 40
1.3.1 Chronic obstructive pulmonary disease 40
1.3.2 Intensive care unit acquired weakness 42
1.3.3 Sarcopenia 43
1.4 Mitochondria in atrophy 44
1.5 TGF-β ligands in muscle 48
1.5.1 Canonical pathway 49
1.5.2 Non-canonical pathways 53
1.6 MicroRNAs 55
1.7 Thesis aims and hypothesis 60

CHAPTER 2: Materials and methods 61

2.1 MATERIALS 61

2.1.1 Preparation of DNA plasmids 61

2.1.2 Protein synthesis experiment 61

2.1.3 Fixing and Staining 61

2.1.4 Western Blotting 62

2.1.5 Agarose gel 63

2.1.6 cDNA dilutions 63

2.2 METHODS 64

2.2.1 *In vitro* experiments 64

2.2.2 Protein synthesis experiment 67

2.2.3 Luciferase reporter assay 68

2.2.4 Mitochondria assays 69

2.2.5 Membrane potential assays 70

2.2.6 Proliferation assay 73

2.2.7 RNA extraction 73

2.2.8 cDNA synthesis 75

2.2.9 Primer validation 76

2.2.10 Real Time quantitative polymerase chain reaction (qPCR) 77

2.2.11 Protein extraction 80

2.2.12 Western blotting 81

2.2.13 Immunoprecipitation 83

2.2.14 Immunostaining for p-Smad-2/3 localisation 83

2.2.15 Hypoxia treatment 84

2.2.16 *In vivo* experiments 84

2.2.17 Data analysis 92

CHAPTER 3: Clinical observations of miR-542-3p & miR-542-5p in muscle wasting diseases 93

3.1 Rationale 93

3.2 Hypothesis 95

3.3 Results 96

3.3.1 miR-542-5p levels are increased in COPD patients and associate with reduced lung function 96

3.3.2 miR-542-5p associate with reduced physical performance in COPD patients 99

3.3.3 miR-542-5p levels inversely associated with physical performance in a cohort of older people 101

3.3.4 miR-542-5p levels inversely associated with lung function in a cohort of older people 104

3.3.5 miR-542-3p and miR-542-5p levels are increased in patients with ICUAW and associate with days of ICU stay 106

3.3.6 miR-542-3p expression is increased under hypoxia *in vitro* 108

3.3.7 Bioinformatic analysis predicts important targets for miR-542-3p and miR-542-5p in muscle wasting context 109

3.4 Discussion 113

3.4.1 Main findings 113

3.4.2 How might miR-542 contribute to muscle dysfunction in disease? 114

3.5 Conclusions 116

CHAPTER 4: Mechanism of the role of miR-542-3p and miR-542-5p in cytoplasmic and mitochondrial ribosomal stress 117

4.1 Rationale 117

4.2 Hypothesis 120

4.3 Results 121

4.3.1 miR-542-3p targets mitochondrial ribosomal proteins *in vitro* 121

4.3.2 Mitochondrial ribosomal RNA levels are decreased by miR-542-3p and miR-542-5p *in vitro* 122

4.3.3 miR-542-3p decreases CYTB protein levels *in vitro* 124

4.3.4 Mitochondrial membrane potential is reduced by miR-542-3p and miR-542-5p *in vitro* 125

4.3.5 Mitochondrial ribosomal RNA subunits are down-regulated in patients suffering from muscle wasting (COPD and ICUAW) 128

4.3.6 miR-542-3p/-5p levels associate with levels of mitochondrial ribosomal subunits in patients suffering from muscle wasting (COPD and ICUAW) 130

4.3.7 miR-542-3p targets cytoplasmic ribosomal proteins *in vitro* 133

4.3.8 Cytoplasmic ribosomal RNA levels were decreased by miR-542-3p and miR-542-5p *in vitro* 134

4.3.9 miR-542-3p and miR-542-5p suppress protein synthesis *in vitro* 136

4.3.10 Cytoplasmic ribosomal RNAs are down-regulated in patients suffering from muscle wasting (COPD and ICUAW) 137

4.3.11 LHCN-M2 myoblasts under hypoxia decreased the levels of mitochondrial and cytoplasmic ribosomal subunits *in vitro* 140

4.3.12 miR-542-3p increases GDF-15 expression *in vitro* in a positive feedback manner 142

4.4 Discussion 144

4.4.1 Main findings 144

4.4.2 miR-542 promotes mitochondrial ribosomal stress 144

4.4.3 The role of mitochondria in exercise performance 146

4.4.4 miR-542 suppresses protein synthesis 147

4.4.5 miR-542-3p elevates GDF-15 expression in muscle 147

4.4.6 Critique of the method 148

4.5 Conclusions 149

CHAPTER 5: Regulation of SMAD2/3 signalling by miR-542-3p and miR-542-5p 150

5.1 Rationale 150

5.2 Hypothesis 152

5.3 Results 153

5.3.1 miR-542-3p and miR-542-5p increase SMAD dependent luciferase activity in the absence of added ligand *in vitro* 153

5.3.2 miR-542-5p increase p-SMAD2/3 nuclear localisation independent from TGF-β ligand *in vitro* 156

5.3.3 miR-542-3p/-5p effects on TGF-β signalling are time dependent 160

5.3.4 miR-542-3p and miR-542-5p target inhibitors of TGF-β signalling *in vitro* . 162

5.3.5 miR-542-3p and miR-542-5p did not increase p-SMAD2/3 in the presence of TGF-β ligand *in vitro* 169

5.3.6 Increased TGF-β signalling in patients suffering from muscle wasting (COPD, ICUAW or older population) 174

5.3.7 Down-regulation of inhibitors of TGF-β system in ICUAW patients 176

5.4 Discussion 178

5.4.1 Main findings 178
5.4.2 Mechanism of SMAD2/3 activation 178
5.4.3 Time course of SMAD signalling 180
5.4.4 Increased p-SMAD2/3 in the muscle of wasting patients 181
5.4.5 TGF-β signalling and other members of the miR-542 cluster 182
5.4.6 Other roles of miR-542-3p 182
5.4.7 Critique of the method 183
5.5 Conclusions 184

CHAPTER 6: Effects of miR-542 *in vivo* via the development of a mouse model 185
6.1 Rationale 185
6.2 Hypothesis 188
6.3 Results 189
6.3.1 Predominant miR-542-5p expression from pCAGGS-EGFP-542 vector *in vitro* 189
6.3.2 miR-542-3p/-5p expression from pCAGGS-EGFP-542 vector *in vivo* 192
6.3.3 miR-542 induces wasting *in vivo* and electroporation efficiency varies along the TA muscle 193
6.3.4 miR-542 induces fibre diameter and area decrease *in vivo* 196
6.3.5 miR-542 causes mitochondrial impairment *in vivo* 198
6.3.6miR-542 causes cytoplasmic ribosomal stress *in vivo* 200
6.3.7 miR-542 increases TGF-β signalling *in vivo* 201
6.4 Discussion 204
6.4.1 Main findings 204
6.4.2 Expression of miR-542-3p/-5p from pCAGGS-EGFP-542 plasmid *in vitro* and *in vivo* 204
6.4.3 Muscle wasting is promoted by miR-542 *in vivo* 206
6.4.4 Increased mitochondrial and cytoplasmic ribosomal impairment by miR-542 *in vivo* 207
6.4.5 Increased TGF-β signalling by miR-542 *in vivo* 208
6.4.6 Critique of the method 208
6.5 Conclusions 210

CHAPTER 7: Discussion and further work 211
7.1 Summary of obtained results 211
7.2 Muscle mass and function regulation: genetics and epigenetics matter 212
7.3 Ribosomal stress as a contributor to muscle wasting 215
7.4 TGF-β pathway contributing to atrophy 216
7.5 General limitations 217
7.6 Clinical implications and future work 218
7.7 Conclusions 219

References 220
Appendix 1 254
Appendix 2 255

List of figures

Figure 1- Protein degradation and organelle removal in skeletal muscle via autophagy. _____ *29*
Figure 2- Schematic diagram of the initiation of transcription in eukaryotes. _____ *32*
Figure 3- Schematic diagram of mRNA translation. _____ *34*
Figure 4- Signalling pathways involved in protein synthesis regulation. _____ *36*
Figure 5- Electron transfer system in the mitochondria. _____ *45*
Figure 6- Scheme of the TGF-β pathway: Canonical (blue) and non-canonical (white background). ____ *51*
Figure 7- MicroRNA biogenesis. _____ *56*
Figure 8- Schematic representation of luciferase assay. _____ *68*
Figure 9- Chemical structure of MitoTracker® Red CMXRos. _____ *71*
Figure 10- Chemical structure of JC-1. _____ *72*
Figure 11- miR-542 orientation check in pCAGGS-EGFP vector. _____ *88*
Figure 12- Schematic representation of TA sectioning. _____ *91*
Figure 13- miR-542-3p/5p are increased in patients with COPD. _____ *97*
Figure 14- miR-542-3p/5p associated with lung function in patients with COPD. _____ *98*
Figure 15- In COPD patients miR-542-3p/5p levels are increased and associated with muscle physiology. _____ *100*
Figure 16- miR-542-3p/5p are associated with physical performance in healthy older individuals. ___ *102*
Figure 17- miR-542-3p/5p are elevated in sarcopenia. _____ *103*
Figure 18- miR-542-3p/5p are associated with lung function in healthy older individuals. _____ *105*
Figure 19- In patients with ICUAW miR-542-3p/5p levels are increased and associate with length on ICU. _____ *107*
Figure 20- miR-542-3p expression is elevated under hypoxia in vitro. _____ *108*
Figure 21- Cytoplasmic and mitochondrial ribosomal subunits. _____ *120*
Figure 22- Mitochondrial ribosomal protein is down-regulated by miR-542-3p. _____ *121*
Figure 23- miR-542-3p /-5p decrease levels of 12S and 16S rRNA in LHCN-M2 myoblasts. _____ *123*
Figure 24- Mitochondrial protein synthesis is down-regulated by miR-542-3p. _____ *124*
Figure 25- miR-542-3p/-5p inhibit mitochondrial function in vitro by decreasing membrane potential. *127*
Figure 26- Mitochondrial ribosomal stress in patients with COPD and ICUAW. _____ *129*
Figure 27- Associations between miR-542-3p/-5p and reduced rRNA in patients with COPD and ICUAW. _____ *132*
Figure 28- Cytoplasmic ribosomal protein down-regulation by miR-542-3p. _____ *133*
Figure 29- miR-542-3p /-5p decrease 18S and 28S levels of rRNA in LHCN-M2 myoblasts. _____ *135*
Figure 30- Protein synthesis is decreased by miR-542-3p and miR-542-5p in vitro _____ *136*
Figure 31- rRNA levels in patients with COPD and ICUAW and associations with interleukins. _____ *139*
Figure 32- Hypoxia drives down-regulation of 12S and 18S rRNA levels in vitro. _____ *141*
Figure 33- GDF-15 RNA up-regulation by miR-542-3p/-5p in vitro and positive feedback. _____ *143*

Figure 34- Proposed mechanism of action of miR-542-3p/-5p in cytoplasmic and mitochondrial ribosomal stress _____ *149*
Figure 35- Dose response of TGF-β at 6h activation period in C2C12. _____ *153*
Figure 36- miR-542-3p increases basal level of TGF-β signalling in C2C12. _____ *154*
Figure 37- miR-542-3p and miR-542-5p increased basal SMAD2/3 activity in LHCN-M2. _____ *155*
Figure 38- miR-542-5p increases p-SMAD2/3 accumulation in the nuclei. _____ *157*
Figure 39- miR-542-3p decreases TGF-β1 and myostatin RNA expression. _____ *158*
Figure 40- TGF-β receptor complex is required for SMAD phosphorylation in the presence of miR-542-5p. _____ *159*
Figure 41- miR-542-3p/-5p effects of TGF-β signalling are time dependent. _____ *161*
Figure 42- SMAD7 and SMURF1 are targeted by miR-542-3p/-5p. _____ *164*
Figure 43- miR-542-3p and miR-542-5p target PPP2CA and STRN in vitro. _____ *166*
Figure 44- miR-542-3p/-5p do not target CTDSP1 or CTDSP2 in vitro. _____ *168*
Figure 45- MG132 effects on TGF-β pathway are inconclusive. _____ *170*
Figure 46- Degradation of p-SMAD2/3 is promoted by TAK1 signalling. _____ *173*
Figure 47- CYR61 levels in COPD, ICUAW and older people cohort. _____ *175*
Figure 48- SMAD7 protein expression and SMAD7, SMURF1 and PPP2CA RNA levels are decreased in patients with ICUAW. _____ *177*
Figure 49- Proposed mechanism of action of miR-542-3p/-5p in the TGF-β pathway. _____ *184*
Figure 50- Schematic representation of DNA injection followed by electroporation used in in vivo experiments. _____ *188*
Figure 51- pCAGGS-EGFP-542 vector leads to an increase in miR-542-5p levels in vitro. _____ *191*
Figure 52- miR-542-3p/-5p expression of pCAGGS-EGFP-542 in vivo. _____ *192*
Figure 53- pCAGGS-EGFP-542 electroporation drives muscle wasting in vivo and its transfection efficiency varies within the muscle length and depth. _____ *195*
Figure 54- Fibre diameter and area are decreased in miR-542 positively electroporated fibres in vivo. *197*
Figure 55- miR-542 causes mitochondrial activity and ribosomal biogenesis impairment in vivo. _____ *199*
Figure 56- miR-542 causes cytoplasmic ribosomal stress in vivo. _____ *200*
Figure 57- TGF-β signalling was increased by miR-542 in vivo. _____ *203*
Figure 58- Schematic representation of miR-542 effects in vivo. _____ *210*
Figure 59- miR-542-5p does not affect proliferation in vitro. _____ *255*

List of tables

Table 1- Differences between the three types of muscle. 20
Table 2- Characteristics of the different muscle fibres types. 22
Table 3- COPD classification based on post-bronchodilator FEV_1. 40
Table 4- COPD patients' new assessment: ABCD. 41
Table 5- miR-542 accession number and mature sequence for human and mouse. 59
Table 6- Concentration of reagents used in 10 and 15% resolving gels. 62
Table 7- microRNAs used for cell transfection. 65
Table 8- Plasmids used for luciferase assays in vitro and in vivo. 66
Table 9- Forward and reverse sequences of primers used in qPCR using FAST sybr. 78
Table 10- MicroRNA probes and primers used for Taqman PCR. 79
Table 11-Antibodies and working concentrations used for Western Blotting and immunostaining. 82
Table 12- Potential pathways and RNA targets of miR-542-3p/-5p. 111

Abbreviations

6MW	Six-minute walk
aa	Amino acid
AIDS	Acquired immune deficiency syndrome
ATP	Adenosine triphosphate
B2M	Beta-2-microglobulin
Bcl	B-cell lymphoma
BMP	Bone morphogenic protein
BMPR	Bone morphogenetic protein receptor
BSA	Bovine serum albumin
CAT	COPD Assessment Test
CDK	Cyclin-dependent kinase
cDNA	Complementary deoxyribonucleic acid
CHF	Chronic heart failure
CMA	Chaperone-mediated autophagy
COPD	Chronic obstructive pulmonary disease
COX	Cytochrome c oxidase assembly protein
CTDSP	Carboxy-terminal domain small phosphatase
CYR61	Cysteine-rich angiogenic inducer 61
CYTB	Cytochrome b
DAPI	2-(4-amidinophenyl)-1H -indole-6-carboxamidine
DM	Myotonic dystrophy
DMD	Duchene´s muscular dystrophy
DMEM	Dulbecco's modified eagle medium
DNA	Deoxyribonucleic acid
dNTP	Deoxynucleotide
ECG	Electrocardiography
EDL	Extensor digitorum longus
eIF	Eukaryotic initiation factor
ELISA	Enzyme-linked immunosorbent assay
ERK	Extracellular signal-regulated kinase
ETS	Electron transport system
FADH2	Flavin adenine dinucleotide
FBS	Foetal bovine serum
FCP	Transcription factor IIF-interacting CTD phosphatase
FEV_1	Forced expiratory volume in 1 second
FFMI	Fat free mass index
FHL1	Four and a half LIM domain protein-1
FOX	Forkhead box
FVC	Forced vital capacity
GAPDH	Glyceraldehyde 3-phosphate dehydrogenase
GDF	Growth differentiation factor
GOLD	Global initiative for chronic obstructive lung disease

GSK3B	Glycogen synthase kinase 3 beta
GTP	Guanosine-5'-triphosphate
H/H	Hypnorm/Hypnovel
HDAC4	Histone deacetylase 4
HF	Heart failure
HPRT	Hypoxanthine guanine phosphoribosyltransferase
HSS	Hertfordshire sarcopenia study
ICU	Intensive care unit
ICUAP	Intensive care unit acquired paresis
ICUAW	Intensive care unit acquired weakness
IGF-1	Insulin-like growth factor-1
IL	Interleukin
IP	Intraperitoneal
ISCU	Iron-sulphur cluster scaffold
IVC	Individually ventilated cage
JNK	c-Jun N-terminal kinase
LAP	Latency associated peptide
LB	Luria broth
LCM	Laser- capture microdissection
LFFMI	Low fat free mass index
MAPK	Mitogen-activated protein kinase
met	Methionine
MH	MAD homology
MHC	Myosin heavy chain
MIC	Macrophage inhibitory cytokine
MKK	MAP kinase kinases
mMRC	Modified British medical research council
MNK	Mitogen-activated protein -interacting kinases
mOD /min	Milli-optical density units/min
MPS	Muscle protein synthesis
mRNA	Messenger ribonucleic acid
MRP	Mitochondrial ribosomal protein
mtDNA	Mitochondrial DNA
mTOR	Mammalian target of rapamycin
mtTFA	Mitochondrial transcription factor A
MuRF-1	Muscle ring finger-1
MVC	Maximal voluntary contraction
Myf	Myogenic factor
MyoD	Myogenic determination factor
NADH	Nicotinamide adenine dinucleotide
NEDD4L	Neural precursor cell expressed developmentally downregulated gene 4-like
NF-κB	Nuclear factor-κB
NFFMI	Normal fat free mass index
OCT	Optimal cutting temperature compound
OXPHOS	Oxidative phosphorylation

PAH	Pulmonary arterial hypertension
PaO2	Oxygen partial pressure (tension) in arterial blood
PBS	Phosphate buffered saline
PDK1	3-phosphoinositide-dependent kinase 1
PEN	Polyethylene naphthalate
PFA	Paraformaldehyde
PGC-1α	Peroxisome proliferator-activated receptor-gamma coactivator-1alpha
PI3K	Phosphatidylinositol 3-kinase
PIP	Phosphatidylinositol phosphate
PP2Cα	Protein phosphatase C alpha
PPM	Protein phosphatase, Mg2+/Mn2+ dependent
PPP	Phospho-protein phosphatase family
PPP2CA	Phospho-protein phosphatase 2 catalytic subunit alpha
pre-miRNA	Precursor microRNA
pri-miRNA	Primary microRNA
PVDF	Polyvinylidene fluoride
qPCR	Real time quantitative polymerase chain reaction
RISC	RNA-induced silencing complex
RNA	Ribonucleic acid
RNase III	Ribonuclease III endonuclease
ROS	Reactive oxygen species
RPS23	Ribosomal protein S23
RPS6	Ribosomal protein S6
rRNA	Ribosomal ribonucleic acid
RT	Room temperature
S	Svedberg unit
S/T	Serine/threonine
S6K1	Ribosomal protein S6 kinase beta-1
SCP	Small C-terminal domain S/T phosphatases
siRNA	Small (or short) interfering RNA
SMAD	Small mothers against decapentaplegic
SMURF	SMAD ubiquitination regulatory factor
SNIP1	SMAD nuclear-interacting protein 1
TA	*Tibialis anterior*
TAK1	TGF-β-activated kinase 1
TBE	Tris-borate-EDTA
TCA	Tricarboxylic acid
TE	Tris/EDTA
TGF-β	Transforming growth factor beta
TGFβR	Transforming growth factor beta receptor
TL_{CO}	Transfer factor for carbon monoxide
TMB	Tetramethylbenzidine
TNF-α	Tumour necrosis factor-alpha
TRAF6	Tumour necrosis factor receptor associated factor 6
tRNA	Transfer ribonucleic acid

TSC	Tuberous sclerosis
TUG	Timed up and go test
TUNEL	Terminal deoxynucleotidyl transferase-mediated deoxyuridine triphosphate nick end-labelling
TwQ	Twitch strength quadriceps
UTR	Untranslated region
VO_{2max}	Maximal rate of oxygen consumption
XPO5	Exportin-5

Publications and abstracts arising from this thesis

Publications

- miR-542 promotes mitochondrial dysfunction and SMAD activity and is raised in ICU acquired weakness.

  American Journal of Respiratory and Critical Care Medicine. 2017 Aug 15. DOI: 10.1164/rccm.201701-0101OC.

  Roser Farre Garros, Richard Paul, Martin Connolly, Amy Lewis, Benjamin E Garfield, S Amanda Natanek, Susannah Bloch, Vincent Mouly, Mark J Griffiths, Michael I Polkey, and Paul R Kemp.

Abstracts

- miR-542: a novel regulator of muscle mass and function.

  Journal of Muscle Research and Cell Motility. 2015 Dec. 36:593–594, Volume: 36. DOI 10.1007/s10974-015-9429-x.

  Roser Farre-Garros, S. Amanda Natanek, Susannah Bloch, Michael I. Polkey, Paul R. Kemp.

  44th European Muscle Conference in Warsaw, Poland. September 21 - 25, 2015. Selected for an oral presentation.

- A microRNA axis that regulates muscle mass and mitochondrial function in response to disease.

  Journal of Muscle Research and Cell Motility. 2017 Feb. 1-90, DOI 10.1007/s10974-016-9457-1

  Farre-Garros Roser, Paul Richard, Natanek Amanda, Griffiths Mark, Polkey Michael, Kemp Paul.

  45th European Muscle Conference in Montpellier, France. September 2 - 6, 2016.

CHAPTER 1: Introduction

1.1 Skeletal muscle overview

Skeletal muscle is the most abundant tissue in the body, accounting for up to 40% of total body mass and is one of the three types of muscle tissue found in mammals. The other muscle types, cardiac and smooth muscle, differ from skeletal muscle in structure and function *(Table 1)* (1).

Table 1- Differences between the three types of muscle.

TYPE OF MUSCLE			
	CARDIAC	**SMOOTH**	**SKELETAL**
LOCATION	Heart	Airways, vessels Hollow organs	Variable, but mostly attached to bones. There are some exceptions such as facial muscles and tongue.
CELL CHARACTERISTICS	Single nucleus Lightly striated	Single nucleus Non-striated	Multinucleated Heavily striated
FUNCTION	Involuntary Pumps blood around the body	Involuntary Slow contraction and relaxation Peristalsis	Voluntary Rapid contraction and relaxation Movement

The main role of skeletal muscle is to generate force and so enable the movement or provide support of parts or all of the body. Such movement is important in locomotion, postural support and ventilation (2). In addition to providing movement skeletal muscle has a major role in homeostasis for example contributing to thermoregulation (2) and the regulation of circulating glucose levels (3).

Mammalian skeletal muscle is first formed during embryogenesis by myogenesis. This process occurs within the mesoderm after the formation of the three germ layers (ectoderm, mesoderm and endoderm). During the neurula stage the neural plate transforms into the neural tube (the precursor to the central nervous system) (4). At the same time, the cells adjacent to the neural tube (the paraxial mesoderm) give rise

to the somites and these subdivide into sclerotomes, myotomes and dermotomes. The sclerotomes give rise to the axial skeleton, the myotomes give rise to skeletal muscle (5) and dermatomes to dermal tissue (skin and connective tissue) (6). Some myotome cells become committed muscle cell precursors (myoblasts) in response to paracrine factors and start to synthesise transcription factors such as MyoD or Myf5 (7) and divide in the presence of growth factors, primarily fibroblast growth factors (1). As the growth factors levels decrease, myoblasts stop dividing, align and fuse to form multinucleated myotubes (8). Myotubes then fuse to form muscle fibres (9,10). The described process is known as skeletal muscle myogenesis. In addition to the generation of skeletal muscle from the somites, some muscle is formed from other embryonic structures such as the cranial somitomeres. The cells in these cranial somitomeres go on to form some of the head skeletal muscle (11).

Each myofibre is surrounded by a cell membrane termed sarcolemma and contains many myofibrils, composed of contractile proteins, predominantly myosin and actin, which are organised in discrete functional units called sarcomeres. Sarcomeres are responsible for generating force and are repeated along the length of myofibrils giving skeletal muscle its particular striated appearance (12). The fibres are arranged in the muscle into small bundles known as fascicles. Surrounding the fascicles and separating them is the perimysium, which is a connective tissue that extends becoming the epimysium until the fascia. The fascia is another connective tissue, which separates the numerous muscle fibres belonging to a skeletal muscle from adjacent muscles or other tissue (13).

In mammals, there are 4 types of skeletal muscle fibre each type being identified by the isoform of myosin heavy chain (MHC) that it expresses. As no agreement has been made in the scientific community whether extraocular muscle should be considered as skeletal muscle, we will not consider it as the 5^{th} type of skeletal muscle in this thesis. The different MHC isoforms expressed in the fibres; Type I, IIA, IIX and IIB, have specific contraction kinetics and metabolic requirements such that the function of a muscle is governed by the type(s) of fibres that it contains *(Table 2).*

Table 2- Characteristics of the different muscle fibres types.

TYPE OF MUSCLE FIBRES				
	TYPE I	**TYPE IIA**	**TYPE IIX**	**TYPE IIB**
Contraction time	Slow	Moderately fast	Fast	Very fast
Size of motor neuron	Small	Medium	Large	Very large
Activity used for	Aerobic	Long-term anaerobic	Short-term anaerobic	Short-term anaerobic
Force production	Low	Medium	High	Very high
Capillary density	High	Intermediate	Low	Low
Mitochondrial density	High	High	Medium	Low
Oxidative capacity	High	High	Intermediate	Low
Glycolytic capacity	Low	High	High	High
Resistance to fatigue	High	Fairly high	Intermediate	Low
Major storage fuel	Triglycerides	Creatine phosphate, glycogen	Creatine phosphate, glycogen	Creatine phosphate, glycogen

Briefly, Type I fibres are red in colour, due to increased myoglobin, and have high numbers of mitochondria which confers resistance to fatigue. Therefore, Type I fibres can produce repeated low-impact contractions and obtain ATP though aerobic metabolic cycle (14). Conversely, Type II fibres are whiter in colour due to lower levels of myoglobin and fewer mitochondria, which results in relatively rapid fatigue. Type II fibres are therefore responsible for short and high impact movements (14). However, the three Type II fibres vary in MHC kinetics and mitochondrial content consequently have differences in fatigue resistance. For example, fibres IIX and IIB have fewer mitochondria so are easily fatigable while Type IIA fibres have more mitochondria and exhibit intermediate fatigue resistance (14).

However, there are some species differences between fibres characteristics. For example, relative to mitochondrial content, in humans the fibre type with highest content of mitochondria is Type I, followed by Type IIA > Type IIX, whereas in mouse the fibre with the highest content in mitochondria is Type IIA > Type IIX > Type I and Type IIB (15). These species differences need to be taken into account in the design and interpretation of experimental studies.

An individual muscle is rarely composed of a single fibre type with the proportion of each fibre varying in relation to the function of the muscle. For example, the *flexor digitorum profundus* muscle which is in charge of flexing the fingers has a high proportion of Type II fibres as its role requires speed rather than fatigue resistance (16). On the other hand, the soleus muscle requires high fatigue resistance, therefore it is composed of around 80% Type I and 20% Type II (17). However, some muscles require both fatigue resistance and strength such as the diaphragm, which in adult humans is composed of equal proportions of slow fibres and fast fibres (18).

Muscle phenotype is plastic and specific muscles can change fibre proportion dependent on the demand placed on the muscle as a consequence of different physiological and pathological conditions including training, hypoxia and age (18). For example, some studies have shown that high intensity training over short periods of time such as using high velocity isokinetic contractions and ballistic movements (sprints, bench press throws) induces a fibre shift, increasing Type II fibres and decreasing Type I fibres (19). On the other hand, training focusing on longer duration activity and higher volume endurance contributes to the shift from Type II to Type I fibres (20). Several mechanisms have been proposed to be involved in this fibre shift such as neurotrophic factors, electrical activity and hormones playing a role in the change of the contractile phenotypes (20). However, further research is needed. *Buller et al.* stated that nerves from fast and slow twitch muscles send out different signals that can change muscle fibres from fast to slow and vice versa (21). They proved this hypothesis by transplanting nerves from one fibre type to another and they proposed that the electrical signals and/or neurotrophic factors that nerves send could be altered (e.g. with exercise) determining the fibre type.

Another of the causes that may contribute to the fibre-shift is the fact that Type II fibres are more prone to atrophy than Type I fibres provoking an overall increase of Type I fibres. Therefore, muscle immobilization seems to lead to a decrease in fibres, particularly Type II fibres. For example, *MacDougall et al.* showed that after 5-6 weeks of muscle immobilization by elbow cast, there was a decrease in fibres, which affected the Type II fibres to a greater extent than the Type I fibres leading to an increase in the proportion of Type I fibres in the muscle (19).

1.2 Skeletal muscle homeostasis: balance between muscle loss and synthesis

In the absence of major environmental changes (starvation, disuse, etc.), muscle mass is maintained in healthy adults by balancing the mechanisms that promote muscle loss (apoptosis, protein degradation by ubiquitination/caspases or by autophagy) with those that promote muscle synthesis (satellite cell recruitment and protein synthesis) (22). The activity of these mechanisms is controlled by a number of different growth factors and signalling pathways that interact. Principal amongst these growth regulators are insulin-like growth factor-1 (IGF-1) (23) and myostatin (MSTN) (24) which promote muscle synthesis and muscle degradation respectively. Both of these pathways affect multiple aspects of muscle protein turnover by regulating both myofibrillar protein synthesis and/or degradation as well as satellite cell proliferation and activation.

The balance of synthetic and degradative processes that normally maintains muscle mass can change allowing the muscle to adapt to altered physiological or environmental stimuli, resulting in a change of phenotype by, for example, altering size or mass. Some studies have shown that in human skeletal muscle the increase in essential amino acids and insulin after food ingestion activates mTOR signalling and promotes protein synthesis (23). However, under inflammation, the MSTN-SMAD2/3 pathway is activated acting as a negative regulator of protein synthesis. Under inflammation, cytokines promote muscle degradation by activating FOXO transcription factors such as FoxO3 which activate the expression of atrophy related genes.

The individual mechanisms involved in regulating muscle mass are discussed in the following sections.

1.2.1 Mechanisms leading to muscle loss

1.2.1.1 Proteolysis

Increased protein breakdown is thought to be a significant contributor to the loss of muscle protein and therefore to muscle loss. This occurs by two major mechanisms the ubiquitin/proteasome pathway and the activity of caspases. Of these most studies have focussed on the proteasomal pathway that is initiated by protein ubiquitination.

1.2.1.2 Ubiquitination

The role of the ubiquitin/proteasome pathway in muscle was firstly identified by an elevation of atrogin-1 and muscle ring finger-1 (MuRF-1), both ubiquitin ligases, in muscle in response to a range of atrophic stimuli (25,26).

Further studies on these proteins have suggested that they are also increased in the muscle of patients with a range of diseases including COPD, chronic heart failure (CHF) and ICUAW (27-31). However, although increased MuRF-1 and atrogin-1 are consistently reported in ICUAW (32,33), the increase of these factors in chronic diseases such as COPD and CHF is not consistent as some reports indicate no or opposite changes in patients compared to control. For example, quadriceps atrogin-1 protein was decreased and no change in MuRF-1 protein levels was reported between COPD patients and controls (34). In HF mice model, an increase in atrogin-1 mRNA but not in MuRF-1 mRNA was seen in the *vastus lateralis* of mice (35). However, we have to consider that it is also likely that the increase in proteolysis that is required to get the sort of slow atrophy seen in many forms of wasting is too low to be measurable.

The proteasomal pathway is also known to be activated by several atrophic stimuli such as inactivity and inflammation (36) that are also present in COPD and ICUAW patients. Moreover, *in vivo* atrogin-1 and MuRF-1 knockout confers resistance to atrophy in response to denervation (37) suggesting they play a key role in the proteasomal pathway.

As described above, MuRF1 and atrogin-1 are components of the ubiquitin/proteasome pathway. The ubiquitin/proteasome machinery is complex and

the first step of this system consists of an ATP dependent ligation of ubiquitin to an E1 enzyme (38). The ubiquitin is then transferred to an E2 enzyme (ubiquitin-conjugating enzyme) (39). E3 enzymes (ubiquitin ligases) are needed to bind to E2 and the target protein to catalyse the transfer of ubiquitin from E2 to the target protein. Both MuRF1 and atrogin-1 are E3 ligases and as such confer substrate specificity. Once monoubiquitination has occurred, the target protein is poly-ubiquitinated, causing it to be targeted to the proteasome and degraded (40). Proteins involved in this process also contribute to muscle wasting. For example, ZNF216, is a protein that recognises ubiquitinated proteins and delivers them to the proteasome during muscle atrophy. Mice deficient in ZNF216 are more resistant to muscle atrophy during denervation than normal mice and showed an accumulation of poly-ubiquitinated proteins in the muscle (41). The ubiquitination process is reversible as polyubiquitin chains can be removed by ubiquitin-specific processing proteases (USPs) (42).

The targets of Atrogin-1 and MuRF-1 include many key cytoskeletal proteins including myosin light-chain-2, troponin I, troponin T1, troponin T3, titin, telethonin, myotilin and nebulin (43,44). *Witt SH et al.* also identified the interaction of MuRF-1 with 11 enzymes essential for ATP synthesis such as mitochondrial ATP synthase and cytoplasmic creatine kinase suggesting it could regulate energy metabolism (43). Moreover, Atrogin-1 controls the half-life of MyoD (a key transcription factor in muscle differentiation) in skeletal muscle (45) and overexpression of a mutant MyoDK133R lacking atrogin-1 mediated ubiquitination prevented atrophy of mouse primary myotubes and skeletal muscle fibres *in vivo* (46). Atrogin-1 also targets eIF3f (-eukaryotic initiation factor 3F- a protein involved in protein synthesis) in skeletal muscle (46) suggesting that increased atrogin-1 may impair protein synthesis (47,48). The transcriptional control of these two E3 enzymes is regulated differently; atrogin-1 levels are up-regulated by FoxO (49) whereas MuRF-1 transcription is controlled by the activation of NF- κB (nuclear factor κB) (50).

Other E3 ligases are also activated during atrophy to promote breakdown of other proteins, contributing to catabolism. For example, TRAF6 is important in activating the ubiquitin-proteasome system by promoting ubiquitination of its target proteins (51). TRAF6-mediated ubiquitination is essential for activation of several signalling pathways

including the JNK, AMPK, FoxO3 and NF-κB pathways (52). Consistent with a role for TRAF6 in skeletal muscle atrophy, starved TRAF6 knockout mice had reduced levels of poly-ubiquitinated proteins and had almost no Lys63-polyubiquitylated proteins in their muscle. Moreover, TRAF6 knockout mice seem to be resistant to muscle atrophy caused by cancer, starvation or denervation (51-53). Moreover, TRAF6−/− mouse embryonic fibroblasts showed the decrease of some atrophy activators such as MAFBx, MuRF1, p62, LC3B, Beclin1, Atg12, and Fn14.

As the ubiquitination pathway is complex, de-regulation of the system in any of the four main steps could lead to muscle wasting (54). The four main events which have been shown to be de-regulated in atrophy are: 1) augmentation of ubiquitin conjugation to protein in the muscle, which, for example, has been shown to be induced by starvation through TRAF6. 2) Increased ATP-dependent activity of the proteasome. In rats with chronic renal failure an increased expression of genes encoding proteins of the ATP-dependent ubiquitin-proteasome pathway was associated with increased muscle proteolysis (55) and a similar observation was made in rats suffering from diabetes mellitus (56), suggesting that the stress of these diseases can dysregulate this step. 3) Increased transfer of ubiquitin from E2 to the target protein; for example, some mutations in UBE2A enzyme have increased its activity by three-fold, compared to the wild type enzyme (57), increasing proteolysis and contributing to muscle wasting. 4) Overexpression of ubiquitin, E2, E3 or proteasome subunits. It has been shown that several different stresses can increase components of the proteasome pathway. For example, 14 days leg immobilization increases 20S Proteasome and atrogin-1 expression (58) and 0-10 days immobilization increases MuRF1 mRNA (59). Similarly, ubiquitin protein was increased in the muscle of patients 1-25 days after admission to ICU (60). In non-pathological states some de-regulation can also occur due to fasting, vitamin D deficiency, ageing and hyperthermia leading to an increase of an E2 enzyme expression (UBE2B) (61).

The ubiquitin/proteasome pathway has other functions apart from degrading proteins to reduce total protein content as it contributes to the regulation of specific pathways such as the TGF-β signalling pathway as will be described later.

1.2.1.3 Autophagy

Autophagy is a regulated process that degrades damaged or unwanted cell components and therefore plays an important role in the size reduction of skeletal muscle. Autophagy occurs at a low rate constitutively where it contributes to cellular housekeeping but it can be activated by stimuli such as cellular stress, starvation and in response to cytokines (62). This process is mainly a non-selective degradation pathway; however, removal of specific organelles can also occur as exemplified by the removal of mitochondria via mitophagy. There are three different systems of autophagy *(Figure 1)* according to how the autophagic cargo is delivered to the lysosomes: macroautophagy, chaperone-mediated autophagy (CMA) and microautophagy.

Macroautophagy is the main pathway to eliminate damaged cell organelles or proteins that are no longer required (63) and is induced by the activation of a complex including Vps34 (64,65), Beclin 1 (also known as Atg6) (64,66), Vps15 (67), Ambra1 (68) and Atg14 (66,69). The initial step in macroautophagy is the formation of a double membrane and the regulatory complex (containing Vps34, Beclin 1, Vps15, Ambra1 and Atg14) recruits LC3 on the membrane of the nascent autophagosome (2). For mitophagy, a specific form of macroautophagy, PINK1 recruits parkin to mitochondria, promoting ubiquitination of outer mitochondrial membrane proteins. p62 recognizes these ubiquitinated proteins and recruits autophagic vesicles (70,71). Bnip3 and Bnip3L are known to directly bind to LC3, recruiting a growing autophagosome to the mitochondria (72,73).

In atrophy, mitochondria are removed through autophagy during fasting and denervation (14,74). Alterations in mitochondrial number, morphology or function can lead to mitophagy to eliminate defective organelles, which in turn can increase muscle atrophy. A reduced number of mitochondria has been reported in the quadriceps fibres of COPD patients (75). Moreover, in other muscle wasting conditions a decrease in mitochondrial biogenesis and function has also been reported for example in both heart and skeletal muscle in heart failure patients (76) and in the muscle of ageing humans (77).

As described above there are other autophagy systems including microautophagy and CMA but unlike macroautophagy their function in skeletal muscle it is still unknown.

Microautophagy consists of direct engulfment of cytoplasmic material into the lysosome by invagination of the lysosomal membrane. Some studies indicate that microautophagy can contribute to glycogen uptake into lysosomes in skeletal muscle when macroautophagy is blocked (78,79). CMA is a very specific and complex pathway. Proteins damaged by reactive oxygen species (ROS) or other agents expose a KFERQ motif, a specific amino acid sequence that is recognised and bound by the Hsc70 chaperone to form a CMA- substrate/chaperone complex. This chaperone interacts with Lamp2a receptor on the lysosome to deliver the damaged protein (2). However, in fasted rats an activation of CMA and an increase in protein breakdown was seen in the liver and the heart but not in skeletal muscle so its role in muscle homeostasis and atrophy is still unknown (79).

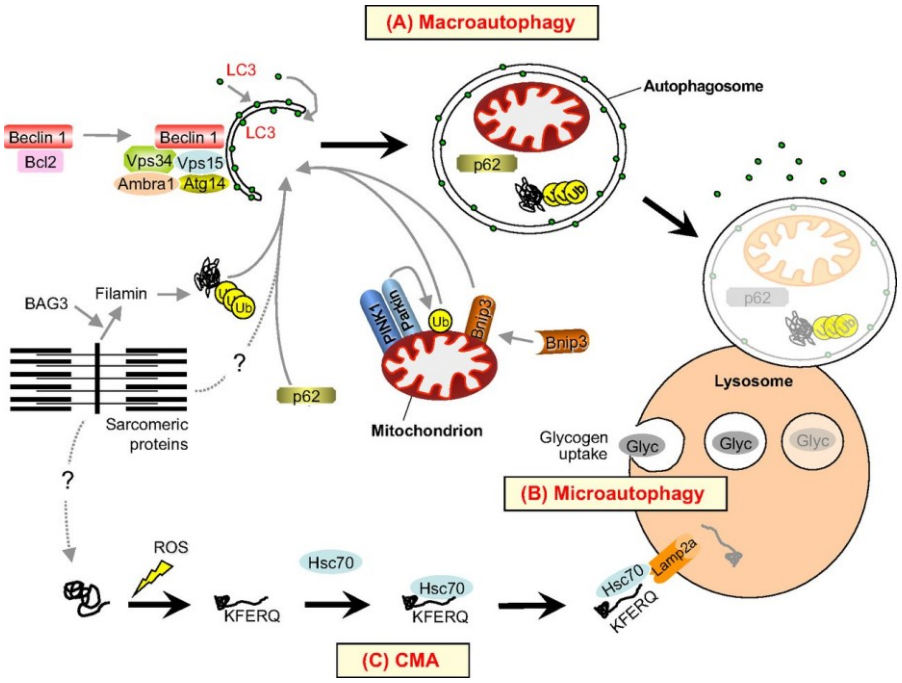


Figure 1- Protein degradation and organelle removal in skeletal muscle via autophagy.

(A) During macroautophagy, a regulatory complex (Beclin1, Vsp34, Vsp15, Ambra1 and Atg14) is responsible for LC3 recruitment into the nascent autophagosome. Proteins that need to be degraded are labelled with polyubiquitin chain and delivered to the autophagosome by p62 protein. A form of macroautophagy is mitophagy which consists on the removal of mitochondria via the PINK-parkin complex and Bnip3 factors. (B) Microautophagy consists on direct engulfment of small parts of the cytoplasm into lysosomes. In skeletal muscle, glycogen is taken up and broken down by this method. (C) CMA plays a role in removing proteins that are damaged (e.g. by ROS). Damaged proteins expose a KFERQ amino acid motif, which is recognised by the chaperon Hsc70 and delivered to the lysosome via Lamp2a receptors interaction. Source: doi: 10.1242/dmm.010389 and permission was obtained (2).

1.2.1.4 Apoptosis

From the three muscle loss mechanisms, apoptosis in skeletal muscle is the least well defined. However, the fact that apoptosis is increased in the skeletal muscle of patients with a number of diseases such as chronic heart failure (80), skeletal muscle denervation (81), muscular dystrophy and skeletal muscle atrophy due to limb immobilization (82) measured by DNA fragmentation in gel electrophoresis or by terminal deoxynucleotidyl transferase-mediated deoxyuridine triphosphate nick end-labeling (TUNEL) suggests it plays an important role in muscle loss.

Mechanistically, apoptosis also known as programmed cell death occurs as a response to death-inducing signals such as ROS, nitrogen species, impairment in calcium regulation and modification of the abundance of B-cell lymphoma (Bcl)-2 family such as Bax, Bad, Bcl-2 and Bcl-xl (83). Following these signals, the activated mitochondrial apoptotic pathway promotes cell death (84). Protein-cleaving enzymes such as caspases, which are cysteine-dependent aspartate-directed proteases, play a main role in the initiation (caspase-8, -9, -12) and execution of apoptosis (caspase-3, -6, -7) by cleaving multiple cellular targets (85). For example, caspase-3 is known to degrade filamentous actin (86). Other factors contributing to apoptosis independent of caspases are apoptosis-inducing factor and endonuclease G from mitochondria which are responsible for DNA fragmentation (84).

1.2.2 Mechanisms involved in the gain of muscle

1.2.2.1 Protein synthesis

One of the major contributors to muscle growth is new protein synthesis, a process that occurs on the ribosomes and is modulated in response to a variety of stimuli such as activity, disease and nutrition. In cells, there are two types of ribosomes, cytoplasmic ribosomes, which are found free in the cytoplasm or on the external membrane of the endoplasmic reticulum and mitochondrial ribosomes, which are found in the matrix of mitochondria (87). Both types of ribosomes vary slightly in their structure, although both are formed by two major components: the small ribosomal subunit, which reads the RNA and is less stable, and the large subunit, which creates polypeptides chains by attaching amino acids together. Each of the subunits is composed of one or more rRNA molecules and multiple ribosomal proteins (88) as described later in the introduction. However, the ratio rRNA/ribosomal protein differs between the two types of ribosomes as there is less rRNA in mitochondrial ribosomes (89).

The initiation of cytoplasmic protein synthesis occurs with the formation of the 43S pre-initiation complex. This complex contains the small ribosomal subunit together with some additional initiation factors including eIF3 and eIF4. The mRNA is loaded into this complex as part of a second complex containing multiple eIFs and along with the initiator tRNA (met-tRNA) in combination with eIF2-GTP to form the 48S pre-initiation complex *(Figure 2)*. Formation of both the eIF2-GTP-met-tRNA and the mRNA-eIF complexes is controlled by signalling pathways such that the formation of the pre-initiation complex marks a main regulatory step in protein synthesis. Initiation of translation in mitochondria is more similar to that which occurs in bacteria. This process also requires the formation of a pre-initiation complex containing the small ribosome subunit, the met-tRNA^{met} bound to mitochondrial initiation factor 2-GTP and the RNA (90). In both cases once the pre-initiation complex has formed the large subunit joins the complex to form the initiation complex.

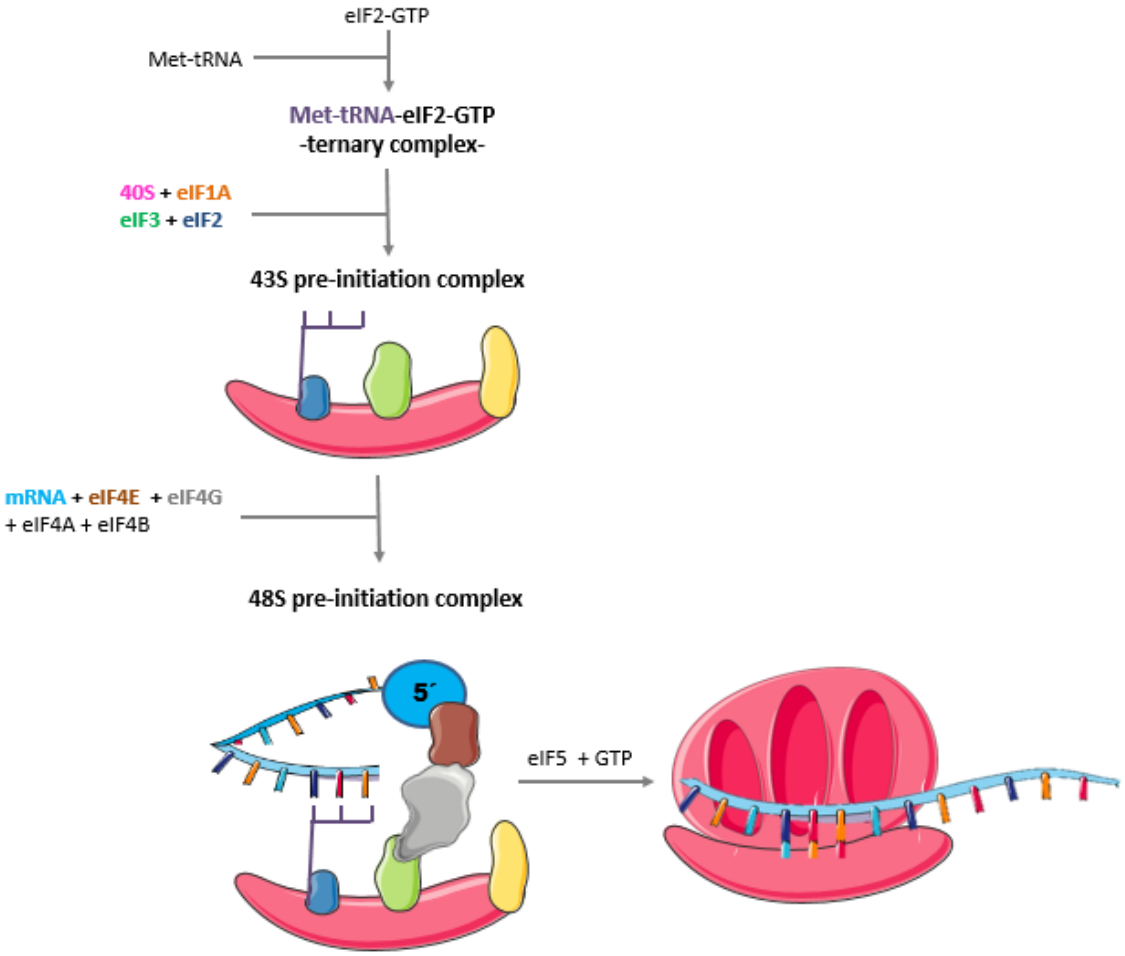


Figure 2- Schematic diagram of the initiation of transcription in eukaryotes.

Initiation of transcription starts with the formation of the 43S pre-initiation complex via the assembly of the ternary complex with the 40S ribosomal subunit (to which eIF1A and eIF3 are already attached). The binding of the mRNA to form the 48S pre-initiation complex requires other initiation factors eIF4E, 4G, 4A and 4B. Finally, the binding of the 60S ribosomal subunit, which requires eIF5 and GTP, occurs allowing protein synthesis to begin. Adapted from (91).

One significant difference in this step between the ribosome types is how the ribosome enters the mRNA. As mitochondrial transcripts are often polycistronic, ribosomes can bind the mRNA directly at the translation start site (92). However, eukaryotic mRNAs are monocistronic forcing the ribosomes to bind the mRNA though the 5' end (a methylated guanine residue) and move downstream to the translation site (in a process called scanning) (93). The recognition of the initiation site is done in the mitochondrial ribosomes by complementary base-paring on the 3' terminus of the 16S rRNA (92) while in cytoplasmic ribosomes for the ribosome to recognize the 5' CAP of an mRNA several protein factors are required. For example, eIF-3, a factor

associated to the 40S subunit interacts with eIF-4F which binds to the 5’ CAP of the mRNA (93).

An enzyme called aminoacyl tRNA synthetase is the responsible for attaching amino acid (aa) to the 3’ end of the tRNA using ATP, activating the tRNA (90). During the elongation step, with the exception of the first tRNA, which enters into the P site, the following tRNAs enter the ribosome and hybridise to the mRNA in the A site (entry site) carrying the appropriate aa and binding of the GTPase EF-G promotes the cleavage of the petidyl-tRNA bond in the P site and the formation of a new peptide bond between the growing polypeptide and the amino group in the amino acid-tRNA in the A site. The elongated peptidyl-tRNA is then moved from the A site to the P site and the newly deacylated tRNA moves from P site to the E site (exit site) by GTP hydrolysis *(Figure 3)* (90). Finally, the termination step is reached when a stop codon is reached by the ribosome and the polypeptide is released. The main difference in this termination step between the mitochondrial and cytoplasmic ribosomes is due to the genetic code, while UAA, UAG and UGA are read as stop codons by the cytoplasmic ribosomes (94), mitochondrial ribosomes read as stop codons AGA and AGG but not UGA, which encodes for tryptophan in mitochondria (95). There is also another aa coding difference, while AUA encodes for isoleucine it encodes for methionine in mitochondria (96).

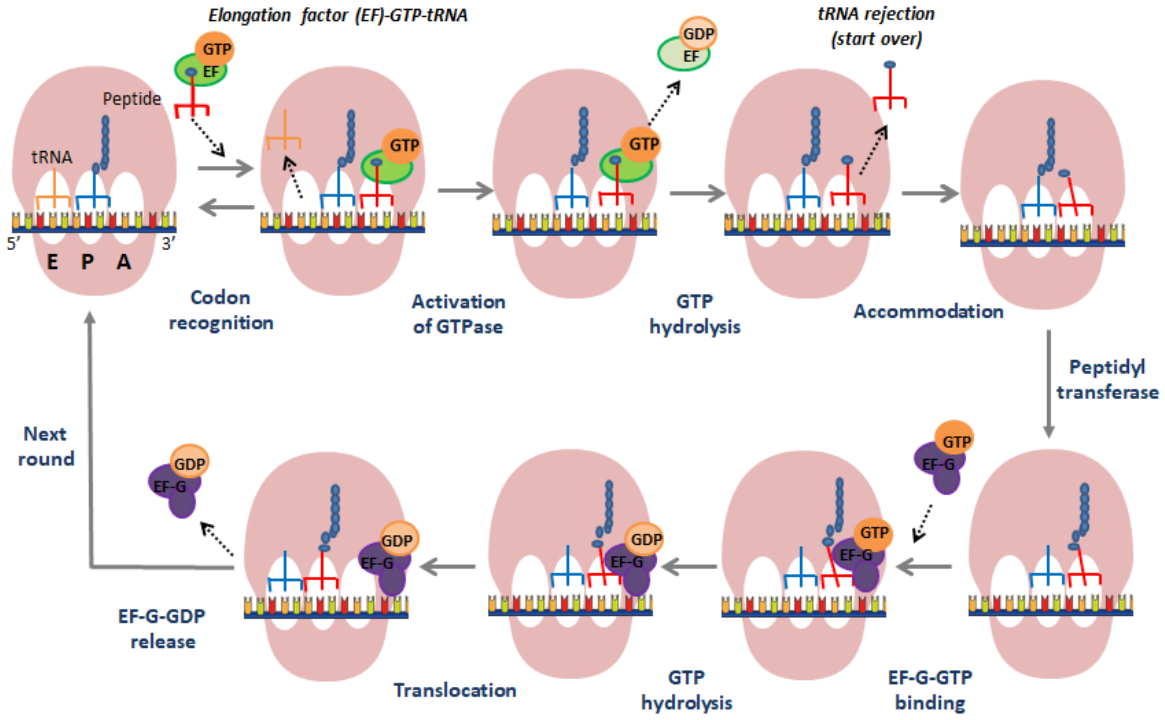


Figure 3- Schematic diagram of mRNA translation.

The binding of met-tRNA^{met} into the P site initiates mRNA translation. The complex formed by an incoming tRNA and EF-GTP enters the A site and the codon-anticodon pairing activated the GTPase, provoking the release of the aminoacyl end of the tRNA from EF. The tRNA binding also causes conformational changed in the rRNA that helps the transfer of the peptide chain onto the A-site tRNA. The translocation of the deacylated tRNA from the P site to the E site and of the peptidyl-tRNA from the A site to the P site occurs due to GTPases and EF. The deacylated tRNA in the E site is released when the next aminoacyl-tRNA binds to the A site. The elongation step finished when the ribosome meets a stop codon, releasing the polypeptide. Adapted from (90).

It is important to note that ribosomes in the mitochondria are responsible for the synthesis of only 13 key proteins needed in oxidative phosphorylation. These proteins form part of complexes I (NADH dehydrogenase), complex III (cytochrome b-c_1) and complex IV (cytochrome c oxidase) and the ATP synthase but not complex II, which is entirely encoded in the nucleus and synthesised in the cytoplasm (97).

1.2.2.1.1 Regulation of protein synthesis

The best studied signalling pathways that stimulate protein synthesis in adult muscle are those activated by IGF-1 and insulin. These pathways are the phosphatidylinositol 3-kinase/Akt (PI3K/AKT) pathway and the Ras-Raf-MEK-ERK pathway (98) *(Figure 4).*

Activation of PI3K promotes the phosphorylation of PIP2 to PIP3 leading to the activation of 3-phosphoinositide-dependent kinase 1 (PDK1) (37). Activated PDK1 phosphorylates AKT a protein kinase with multiple targets in the protein synthetic and protein breakdown pathways. AKT activates protein synthesis by phosphorylating and inactivating glycogen synthase kinase 3 beta (GSK3B) and tumour suppressor protein tuberous sclerosis 1 (TSC1) and 2. This latter phosphorylation releases the inhibition of mammalian target of rapamycin complex 1 (mTORC1) thereby promoting the phosphorylation and activation of ribosomal protein S6 kinase beta-1 (S6K1) (99) and the inhibition of 4E-BP1. Activated S6K1 phosphorylates its substrate, the ribosome protein S6 (RPS6) which is part of the 40S ribosomal subunit, and phosporylation of 4E-BP1 results in dissociation of 4E-BP1 from the initiation factor eIF4E and thus in de-repression of the latter protein (100) thereby promoting protein synthesis.

Activated AKT also blocks FoxO transcription factors by phosphorylation which causes their sequestration in the cytoplasm (101) so that they cannot enter the nuclei and activate growth suppression and apoptosis related genes (102). Consistent with the promotion of protein synthesis and inhibition of protein breakdown, the inhibition of PI3K and the expression of a dominant-negative AKT reduce the size of myotubes in culture (103). *In vivo*, muscles from mice that lack both AKT1 and AKT2 are smaller than those from control animals (104). Moreover, AKT activation in rat muscle prevents atrophy in response to denervation (105). Consistent with these data, sarcopenia was also partly prevented in transgenic mice over-expressing IGF-1 (106).

The other pathway that gets activated by anabolic stimuli is the Ras-Raf-MEK-ERK pathway. This pathway gets activated when an extracellular mitogen such as IGF-1 binds to the membrane receptor allowing Ras to exchange the GDP to GTP (107). Ras-GTP then activates Raf to start of a protein phosphorylation cascade in which Raf phosphorylates and activates MAP2K, which phosphorylates and activates MAPK (108),

which (like mTORC1) phosphorylates 40S ribosomal protein S6 kinase which phosphorylates RPS6 (109). MAPK also phosphorylates and activates MAPK-interacting kinases (MNK) (110), leading to the phosphorylation and activation of CREB. Apart from RPS6 and CREB, MAPK can also activate Myc. Myc activates the transcription of genes that are important for the cell cycle as well as increasing the expression of ribosomal RNAs (110). However, its role in muscle mass has been less described than PI3K/AKT pathway.

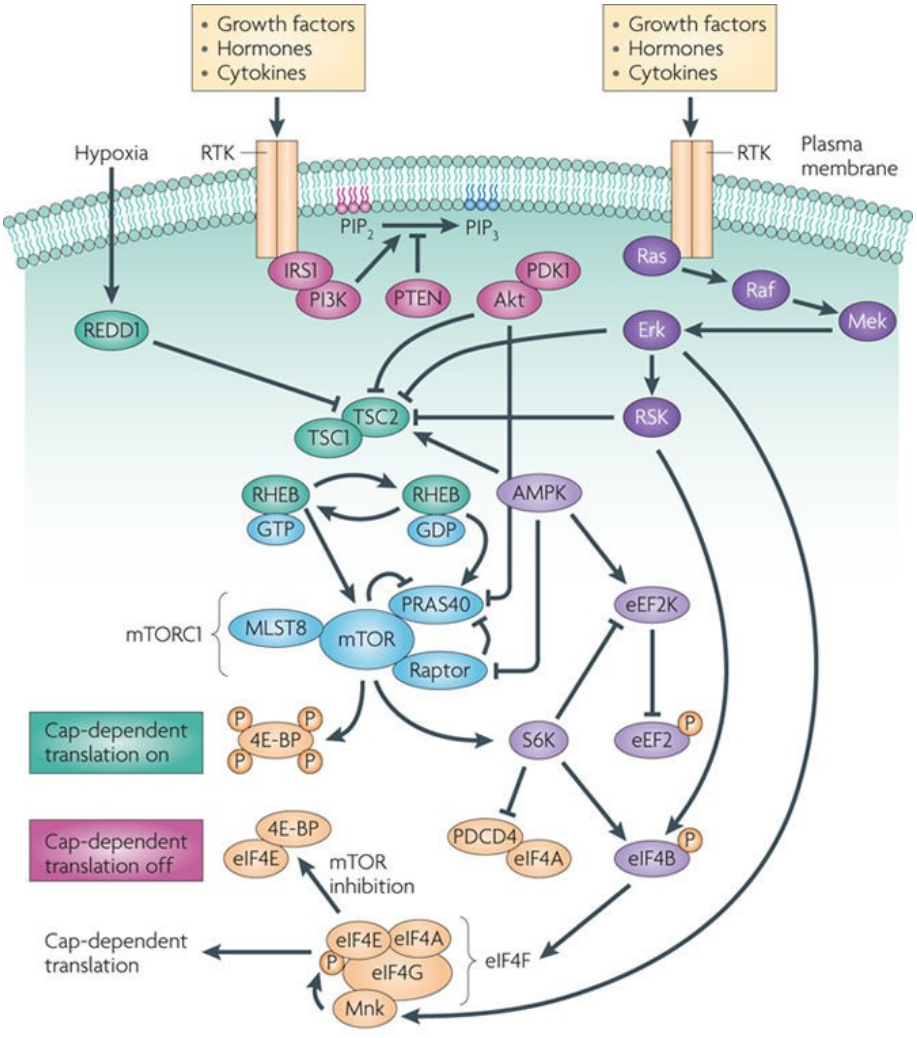


Figure 4- Signalling pathways involved in protein synthesis regulation.

Growth factors, hormones or cytokines can act through receptor tyrosine kinases to activate Ras GTPases and PI3K. Ras activates the Raf-Mek-Erk kinase pathway. Erk stimulates protein translation via p90RSK which phosphorylates eIF4B increasing its mRNA binding activity. Erk inhibits the activity of TSC1 and TSC2 leading to stimulation of mTOR complex 1. PI3K activation leads to Akt pathway stimulation where Akt activates mTORC1 by inhibiting its inhibitor PRAS40. Activated mTORC1 phosphorylates S6Ks, which phosphorylates elongation factor kinase eEF2K which activates eEF2, promoting translation elongation. Activated mTORC1 also inhibits eIF4E inhibitory binding proteins via phosphorylation, promoting cap-dependent translation. Source: doi:10.1038/nrc2824 and permission was obtained (111).

1.2.2.1.2 Ribosomes synthesis and turnover

After activation of the anabolic pathways, protein synthesis takes place in the ribosomes, therefore the synthesis and turnover of these organelles can have an impact on protein translation.

The production of both ribosomal subunits (small and large) is carried out in the nucleolus under strict regulation to achieve proper cellular proliferation and growth (112). The majority of this process is conserved between eukaryotic organisms, from yeast to human (113). Ribosomal biogenesis starts by the transcription of ribosomal DNA by RNA polymerase I to obtain the 47S precursor ribosomal RNA transcript which is processed by small nucleolar ribonucleoproteins to generate 28S, 18S and 5.8S rRNAs. These rRNAs are assembled with the appropriate ribosomal proteins to form the small subunit (containing the 18S rRNA) and the large subunit (containing the 28S and 5.8S rRNAs) which are separately exported to the cytoplasm to undergo final processing and to become the mature 40S and 60S ribosomal subunits, respectively (114). Efficient ribosomal biogenesis is essential to translation but because it requires high levels of energy (ATP) under stress conditions such as nutrient deprivation or hypoxia, ribosomal biogenesis is decreased as a strategy to preserve cellular energy, leading to ribosomal or nucleolar stress (114). Conversely in response to exercise there is a marked increase in ribosomal biogenesis. For example, increased markers of ribosomal biogenesis such as total RNA (115), S6K1 levels and RPS6 phosphorylation (116) was observed after resistance exercise in the *vastus lateralis* muscle of middle-aged and young individuals respectively.

Under stress stimuli such as lack of nutrients (117), muscle disuse (118) or disease such as diabetes mellitus, renal failure and cancer (117), ribosomal biogenesis is impaired causing a reduction in ribosome number to ensure cell viability, a process known as ribosomal stress. One of the effects of ribosomal stress has been shown to be p53 activation (119). Under normal physiological conditions, p53 levels are kept low due to ubiquitination by HDM2 which is an E3 ubiquitin ligase (in mice the gene is Mdm2). However, in response to ribosomal stress there is an accumulation of free ribosomal protein RPL11, which can bind to HDM2 and cause it to dissociate from p53. This

sequestration of HDM2 therefore suppresses the ubiquitination and destruction of p53 leading to an increase in p53 activity (119). Consistent with this observation a reduction of RPs can cause p53 activation as demonstrated by knocking down RPS6 leading to a reduction in the formation of the 40S small ribosomal subunit, increased free RPL11 and thereby activation of p53 (120).

In mice lacking RPL29, a decrease in cell proliferation and protein synthesis was reported (121) suggesting that ribosomal stress or impairment in ribosomal biogenesis could also impair protein synthesis.

1.2.2.2 Satellite cell recruitment

Satellite cells are myogenic cells that play an important role in adult skeletal muscle growth and repair through a process termed satellite cell recruitment (122). During this process, the quiescent satellite cells that are between the myofibre plasmalemma and the basal lamina surrounding the fibres are activated, commit to myogenic cell lineage, proliferate and differentiate into myoblasts to fuse to established myofibres, increasing the number of nuclei in the fibre to repair an injury (9,10). To preserve the satellite "pool", satellite cells divide asymmetrically so that some of the daughter cells can differentiate and fuse with the myofibres and others can return to the quiescent state so that they are available for future rounds of regeneration (10). It is known that the number of satellite cells per myofibre or cross-sectional area varies between muscles. For example, the *extensor digitorum longus* (EDL) muscle which has mainly Type II fibres contains fewer satellite cells than the *soleus* muscle which contains mainly Type I fibres (10). The importance of satellite cells in atrophy has been suggested by a study which found an increase in the number of senescent satellite cells in *vastus lateralis* biopsies from COPD patients with Global initiative for chronic obstructive lung disease (GOLD) III-IV (for further explanation see 1.3.1 section) compared to healthy controls (123). The number of satellite cells has also been reported to decline with age (124) suggesting the role of these cells on muscle mass maintenance. Other studies have also suggested that satellite function declines with age (125). Trying to elucidate the satellite cell requirement with age, *Murach et al*. designed a study with young and old mice using a $Pax7^{CreER}$-$R26R^{DTA}$ model where

muscle hypertrophy was induced with mechanical overload (126). Data showed that satellite cells are not required for hypertrophy measured by fibre cross sectional area in fully grown adult mice whereas they do play an important role in young mice. They determined that myonuclei in adult mice had the transcriptional capacity to contribute to hypertrophy in the absence of satellite cell/fibre fusion (127). These data may suggest that in patients suffering from sarcopenia, protein synthesis may be decreased (either by impaired translation and/or anabolic resistance) rather than an inability to adapt to the absence or decrease of satellite cells, impairing muscle regeneration.

1.3 Skeletal muscle atrophy in disease

Skeletal muscle atrophy is a co-morbidity of a wide range of diseases such as COPD (128), cancer, heart failure, diabetes, critical care (33), pulmonary arterial hypertension (PAH) and acquired immune deficiency syndrome (AIDS). Moreover, skeletal muscle wasting also occurs during ageing. The loss of muscle mass and function reduces quality of life of those patients by decreasing their ability to perform their normal daily tasks and it is associated with increased mortality (129,130). These associations with quality and quantity of life are well demonstrated in studies of COPD, where muscle strength and endurance as contributors to physical performance, and muscle mass are associated with increased mortality and poorer quality of life scores (130). Muscle wasting also occurs rapidly in acute diseases such as critical illness where it extends weaning from mechanical ventilation (131) and is associated with mortality and long-term disability (33).

1.3.1 Chronic obstructive pulmonary disease

COPD, one of the chronic diseases where muscle wasting is a common comorbidity, is the most common chronic lung disease in adults and globally it is estimated that it caused 3 million deaths in 2015 (132). COPD is characterised by persistent airflow limitation and airway and parenchymal inflammation and, in the western world, is primarily caused by cigarette smoke. Patients are classified in GOLD stages or grades according to their airflow limitation, in COPD patients with forced expiratory volume in 1 second (FEV_1)/ Forced vital capacity (FVC) ratio < 0.70 (133) (Table 3).

Table 3- COPD classification based on post-bronchodilator FEV_1.

COPD classification based on airflow limitation		
GOLD 1	Mild	$FEV_1 \geq 80\%$ predicted
GOLD 2	Moderate	$50\% \leq FEV_1 < 80\%$ predicted
GOLD 3	Severe	$30\% \leq FEV_1 < 50\%$ predicted
GOLD 4	Very Severe	$FEV_1 < 30\%$ predicted

However, the systemic complications of COPD make airflow limitation a simplistic and incomplete way of classifying disease severity. Therefore, a new assessment tool has been proposed which classifies patients in A-D groups (134). This new assessment tool takes into account the exacerbation history as well as general symptoms such as coughing, and chest pain assessed by the COPD Assessment Test (CAT) and breathlessness by the Modified British Medical Research Council (mMRC) Questionnaire (Table 4).

Table 4- COPD patients' new assessment: ABCD.

COPD classification based exacerbation			
Group	**Exacerbation**	**mMRC**	**CAT**
A	0 or 1 not leading to hospital admission	0-1	< 10
B	0 or 1 not leading to hospital admission	≥ 2	≥ 10
C	≥ 2 or ≥ 1 leading to hospital admission	0-1	< 10
D	≥ 2 or ≥ 1 leading to hospital admission	≥ 2	≥ 10

The myopathy accompanying COPD affects approximately 30% of patients and is characterised by skeletal muscle wasting and weakness due to a reduction in fibre size and muscle mass (135). A shift from a predominance of Type I (oxidative) fibres to a predominance of Type IIA (more glycolytic) fibres is also very common in COPD affecting more than 50% of moderate to very severe patients (136). The combined effect of muscle atrophy and fibre shift is a marked decrease in exercise performance and quality of life as well as increasing mortality. Surprisingly, for patients with moderate or severe COPD, reduced muscle mass and strength are better predictors of mortality than the standard clinical measurement of FEV_1 and more recently it has been demonstrated that loss of Type I fibre proportions is also an independent risk factor for death in COPD patients (137). Hence, mechanisms involved in regulating muscle phenotype in disease such as increased inflammation, oxidative stress or inactivity that have already been described in COPD patients (138) and to contribute to muscle wasting are of significant interest.

1.3.2 Intensive care unit acquired weakness

ICUAW or intensive care unit acquired paresis (ICUAP) is a complication in critical illness that is increasing in occurrence and that reduces patient survival (139). The reported incidence of this condition varies depending on the cohort of patients examined and ranges from 25% to 100% (33). For example, from a study performed in France, it is estimated that more than 25% of patients admitted to ICU who are intubated for more than 7 days develop ICUAW (131). ICUAW is characterised by skeletal muscle weakness and wasting (both limb and respiratory muscles) resulting in a range of physical disabilities from mild loss of muscle function to complete muscle paralysis and inability to wean from mechanical ventilation (140). The myopathy accompanying ICUAW affects both muscle mass and muscle exercise capacity by disrupting the muscle architecture organization. There is a significant decrease of thick myosin filaments with disruption of both the actin:myosin ratio (141,142) and myofilament organization in patients compared to healthy controls (143,144). Atrophy of both Type I and II fibres is present on ICUAW muscle (145) but fast Type II fibres were reported to waste quicker in muscle biopsies taken from seven critically ill patients (146). This data suggests that, as mentioned earlier, Type II fibres are more susceptible to atrophy. One potential contributor to the greater sensitivity of Type II fibres to atrophy is their higher myosin:actin ratio compared to Type I fibres as MuRF-1 (ubiquitin ligase), is known to target preferentially myosin filaments contributing to their degradation (32).

1.3.3 Sarcopenia

Sarcopenia is the age-associated loss of skeletal muscle mass and function and is associated with disability, morbidity and mortality. The prevalence of sarcopenia varies worldwide but is estimated to be from 3% to 30%. Sarcopenia leads to a loss of muscle mass of 30-50% in individuals between the ages of 40 and 80 years old and the average annual decline in functional capacity has been reported to be around 1-2% per year after the age of 50, increasing to 3% per year after the age of 60 (147). Sarcopenia can be described as a decrease in anabolism and/or an increase in catabolism together with a loss of regeneration capacity of the muscles (148). Consistent with decreased anabolism, growth hormone, IGF-1 and androgens are reduced in ageing. As shown by *Chakravarthy MV et al.* IGF-1 is key in regulating satellite cell proliferation in old skeletal muscle. In this study immobilizing the *gastrocnemius* muscle of aged rats (25 to 30-month-old) caused a decrease in the proliferative potential of the satellite cells. However, administration of IGF-1 to the atrophied *gastrocnemius* muscle for two weeks rescued 46% of the lost muscle mass and increased the proliferation potential of the satellite cells (149).

The increase in catabolism that occurs during ageing may be a consequence of an increase in inflammatory activity reflected by an increase in TNF-α and interleukins (IL-6 and IL-1) as cytokines become dysregulated (150). A cross-sectional study of older people has shown an association between high levels of IL-6 and TNF-α with low muscle mass and strength (151) and with low physical performance (152,153). These data together with experimental studies showing that administration of IL-6 and TNF-α in rats causes muscle breakdown (154,155) suggest that inflammation may contribute to muscle loss and muscle weakness in ageing.

Supporting the loss of regenerative capacity, the loss of both satellite cell number and their ability to fuse with muscle fibres in sarcopenia have been reported (156). Other factors likely to contribute to sarcopenia that occur with age are a reduction in activity and dietary protein intake together with hormonal changes that lead to a loss of muscle fibres, and its replacement with fat (157).

1.4 Mitochondria in atrophy

Mitochondria are organelles with an inner and an outer membrane, with the matrix inside the inner membrane. Mitochondria possess their own genome and their main function is producing ATP as a consequence of oxidation of carbon substrates with molecular oxygen as the final electron acceptor (158). The oxidation of these carbon substrates occurs via the tricarboxylic acid (TCA) cycle with the electrons passed through the electron transport system (ETS). The energy from the TCA is transferred to the coenzymes NAD+ and FADH which have a high reduction potential (tendency to acquire electrons) so they get reduced to NADH and $FADH_2$ (159) *(Figure 5)*. The energy is transferred in the form of electrons to the ETS, which contains four different complexes (I-IV) embedded in the inner membrane of the mitochondria. The electrons are transferred to molecules between the complexes and each movement is a reduction-oxidation reaction in which electrons move to a lower energy state until they reach complex IV where O_2 is the final acceptor (159). The energy released in transferring electrons along the ETS to molecular oxygen is used to transport hydrogen ions out of the matrix creating a proton gradient and a membrane potential that allows ATP synthesis as the protons re-enter the matrix via complex V (ATP synthase). This overall process is called oxidative phosphorylation (OXPHOS) (159).

During OXPHOS, the bulk production (around 90%) of ROS is generated. The production of ROS can be part of normal metabolism as they are produced by macrophages in the presence of bacterial invasion and other cell types in response to xenobiotics or cytokines. ROS are critical to cell survival as they directly interact with critical signalling molecules in a variety of cellular processes such as proliferation and survival (MAP kinases, PI3 kinase, PTEN, and protein tyrosine phosphatases), ROS homeostasis and antioxidant gene regulation (thioredoxin, peroxiredoxin, Ref-1, and Nrf-2), mitochondrial oxidative stress, apoptosis, and aging (p66Shc), iron homeostasis through iron–sulfur cluster proteins (IRE–IRP), and ATM-regulated DNA damage response (160). An excess of ROS or oxidants could lead to oxidative stress in a cell, but mitochondrial oxidant scavenging, for example by detoxifying enzymes and non-enzymatic antioxidants, prevents cellular oxidative damage almost completely (161).

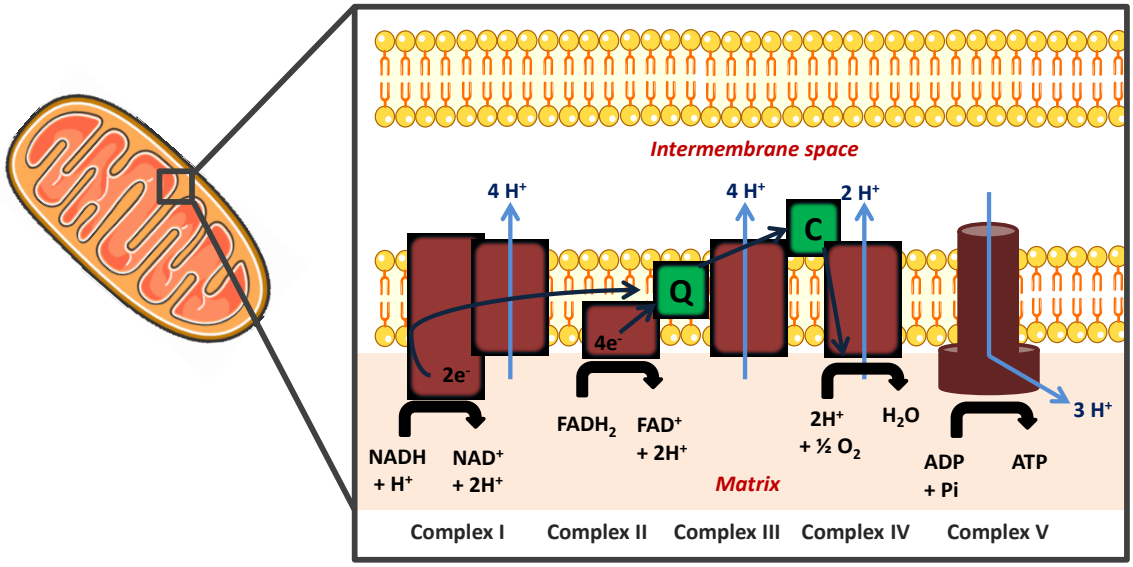


Figure 5- Electron transfer system in the mitochondria.

Electron transfer along the complexes I-IV embedded in the inner membrane of the mitochondria generates a proton gradient causing hydrogen ions to flow back into the mitochondrial matrix via the complex V, producing energy in the form of ATP. Adapted from (77).

Due to their function, mitochondria need to be dynamic and be able to adjust to cellular requirements through biogenesis and turnover, including fission, fusion or autophagy. For example, exercise training promotes mitochondrial biogenesis to meet the increased muscle energetic demand (77) whereas a reduction in mitochondrial number often accompanies loss of activity (162). However, some studies define mitochondria as a reticulum along the length of the muscle fibre instead of single organelles, but as there is no consensus in this thesis we considered mitochondria as single entities (163).

Impaired mitochondria are thought to play an important role in muscle atrophy, particularly in muscle functional decline, since mitochondria are the main producers of cellular energy in the form of ATP. For example, in studies of the effect of ageing, ATP measured by NMR was around 50% lower in the gastrocnemius-soleus of elderly (70±2 years old) study participants compared to young participants (27±2 years old) (164). Similarly, a 50% ATP reduction in the quadriceps muscle of elderly was seen compared to young individuals (165). Changes in mitochondria during ageing or chronic diseases have also been reported including accumulation of mutations in mitochondrial DNA,

decreased mitochondrial activity, and impairment in mitochondrial respiration (77). These changes can lead to a reduction in mitochondrial density (166,167) and to mitochondrial dysfunction the latter of which increases the production of ROS and cellular oxidative stress. Consistent with such dysfunction, in ageing and in conditions including acute muscle atrophy or sarcopenia an excessive ROS generation, a defective oxidant scavenging or both have been reported (168-170).

ROS, including O_2^- and H_2O_2, occur as a result of premature exit of electrons from the complex I, II and III of ETS, with complexes I and III known to be the major sites of mitochondrial superoxide generation (77). ROS cause oxidation of cellular components such as lipids and mitochondrial DNA (mtDNA) leading to mutations as the DNA repair mechanisms are weaker than those of nuclear DNA promoting further mitochondrial and cellular dysfunction (171). Age seems to also impact mtDNA and its integrity. For example, some studies reported a decrease of mtDNA in skeletal muscle with age (172) and several studies have shown that mtDNA damage such as deletions and oxidative damage, single point mutations, rearrangements and tandem duplications can occur both with ageing and in myopathies (173,174).

Mutations in mtDNA are important as the mtDNA encodes for 13 proteins all of which are involved in OXPHOS, encoding part of complexes I, III, IV and V as well as 22 tRNAs and 2 rRNAs (12S and 16S). Between 1,000 and 10,000 copies of mtDNA are found in mammalian cells. The 13 proteins essential for OXPHOS complexes are translated by mitochondrial ribosomes but the mitochondrial ribosomal proteins (MRPs) and complex II from the ETS are all encoded in the nucleus (175) perhaps explaining why complex II activity is less susceptible to ageing (176,177) than the other complexes.

Consistent with the importance of mtDNA mutations, a decrease in the transcription of mitochondrially encoded components of the ETS complexes in older individuals has been reported. For example, a decrease of complex I and complex IV activity was found in elderly human skeletal muscle (178). Consequently, a decrease in ATP synthesis in myopathies and in ageing have been reported with one study identifying a 50% reduction in oxidative capacity per unit muscle volume and a 30% reduction per

unit mitochondrial volume (165). Interestingly, there is an association between physical inactivity and mitochondrial function decline (179).

Mutation and loss of transcription of ETS proteins translated in the mitochondria are not the only mechanisms that lead to mitochondrial dysfunction. Other mechanisms including mutations of the mitochondrial ribosomal proteins can also lead to the same outcome. For example, a mutation in the gene encoding MRPS16 was found in a patient with agenesis of the *corpus callosum* (a congenital neuronal disorder) and lactic acidosis. The patient had decreased complex I and IV activity in muscle and reduced 12S rRNA (180). Similarly, a mutation in MRPS22 was identified in patients with antenatal skin oedema, cardiomyopathy and hypotonia which also resulted in a decrease in complex I and IV activity and a reduction in 12S rRNA. Transfection of patients' cells with wild-type MRPS22 cDNA lead to an increase in mitochondria respiration and an increase in 12S rRNA levels (181).

1.5 TGF-β ligands in muscle

The TGF-β superfamily contains a wide range of factors, including isoforms of TGF-β (1-3), bone morphogenic proteins (BMPs 1-20), growth differentiation factors (GDFs), leftys (1 and 2), activins (A and B), inhibins (A and B), nodal, and Mullerian inhibiting substance (182). In skeletal muscle, some of the most relevant molecules playing a role in TGF-β pathway are MSTN also known as GDF-8, GDF-15 and TGF-β1 and their roles are described below.

MSTN is a negative regulator of muscle growth, inhibiting activation, differentiation and self-renewal of satellite cells (183-185) and muscle regulatory factor expression as well as promoting protein degradation in myofibres (186). Mutations in the MSTN gene, causing down-regulation of the gene or non-functional protein, are associated with an increase in muscle mass due to hyperplasia (increased cell number) and hypertrophy (increased cell size) (187-189). For example, naturally occurring mutations in the MSTN gene in Belgian Blue and Piedmontese cattle lead to a hyper-muscular phenotype (190). Moreover, deletion of the MSTN gene in mice causes a phenotype similar to the muscular hypertrophy in cattle (191,192). This phenomenon has been described as well in sheep (187) and humans (193), as the MSTN gene is well conserved across species. An increase in MSTN levels has been associated with muscle wasting as it causes a reduction in myogenic gene expression (MyoD and Pax3) and an increase in the expression of genes involved in ubiquitin-mediated proteolysis such as atrogin-1, MuRF-1, and E214k. MSTN also inhibits protein synthesis by inhibiting AKT phosphorylation in the IGF-1/PI3K/AKT pathway (194) which further contributes toward muscle wasting.

GDF-15 also known as macrophage inhibitory cytokine-1 (MIC-1) is a cytokine which gets induced in response to stress such as inflammation, oxidative stress and hypoxia and seems to promote muscle wasting. For example, the injection of cancer cells transfected with GDF-15 into the flanks of immunodeficient mice to establish xenografted tumours resulted in weight loss after 6 weeks that could be inhibited by a GDF-15 neutralising antibody (195). Moreover, GDF-15 caused myotube atrophy *in vitro* (196). In patients on the ICU with established ICUAW, circulating GDF-15 levels

(196) and muscle GDF-15 levels were markedly elevated (30). Similarly, in two COPD cohorts muscle mass associated with circulating GDF-15 (197). The effects of GDF-15 have been suggested to occur via appetite suppression as well as via direct effects on the muscle.

TGF-β1 is expressed during myogenesis and regulates the fibre type of the surrounding myotubes. In the absence of TGF-β1, myotubes develop into slow fibres while, when TGF-β1 is expressed by adjacent connective tissue, myoblasts develop into fast fibres (198). In fetal myoblasts, TGF-β1 inhibits differentiation (199) and, in adult muscle, TGF-β1 inhibits regeneration by reducing satellite cell proliferation, myofibre fusion, and expression of some muscle-specific genes. In addition, TGF-β1 triggers the conversion from myogenic cells into fibrotic cells after damage (200) so could be involved in a transient inflammatory response to muscle damage (201).

TGF-β family ligands are synthesised as inactive precursors that are cleaved intracellularly into the active peptide and a non-covalently bound latency associated peptide (LAP) or pro-peptide. The mature protein is secreted either as an inactive form, still associated with the LAP (in the case of TGF-β1, a latent transforming growth factor-binding protein-4 binds TGF-β1-LAP complex causing its secretion (202)) or in the active form (e.g. activin). Proteins secreted in the inactive form are activated by removal of the LAP. In TGF-β1, this occurs by proteolysis (via thrombin, plasmin, plasma transglutaminases or endoglycosylases) or by physical interaction of LAP with other proteins (203).

1.5.1 Canonical pathway

TGF-β receptors (TGFβR) complexes are heterotetramers of two types of subunit, type I and type II receptors, for which 7 and 5 different types respectively have been described. TGF-β1 can bind to a type I receptor (normally activin receptor-like kinase 5 (ALK 5)) and type II (normally TGFβR-II). Once the ligand/receptor complex is formed, a dimer of type I receptors and a dimer of type II receptors aggregate to form the heterotetramer complex. The type II receptor, which has a constitutively active serine

threonine kinase domain, phosphorylates and activates the type I receptor, which also contains a serine threonine kinase domain (204,205). Adaptor proteins recruit SMAD (small mother against decapentaplegic) transcription factors termed receptor regulated SMADs or R-SMADs such as SMAD2 and SMAD3. Members of the TGF-β superfamily are classified in two groups depending on the use of R-SMADs. The TGF-β group including TGF-β, activin, nodal, and MSTN (GDF-8), uses R-SMADs 2 and 3 for signalling while the BMP group, comprising BMPs and several other GDFs, uses R-SMADs 1, 5 and 8.

R-SMADs have three defined structural domains: a Mad homology 1 (MH1) domain at the N-terminus which provides the DNA binding specificity, the Mad Homology 2 (MH2) domain at C-terminus that is responsible for interaction with the receptor, SMAD complex formation and interactions with DNA binding partners, and the linker region which contains Serine/threonine resides that are phosphorylated by various kinases and a motif which interacts with E3 ubiquitin ligases that inhibit SMAD activity. Activation of R-SMADs requires phosphorylation by the type I receptor of two serine residues in the C-terminal domain (206), initiating the canonical signalling pathway *(Figure 6).*

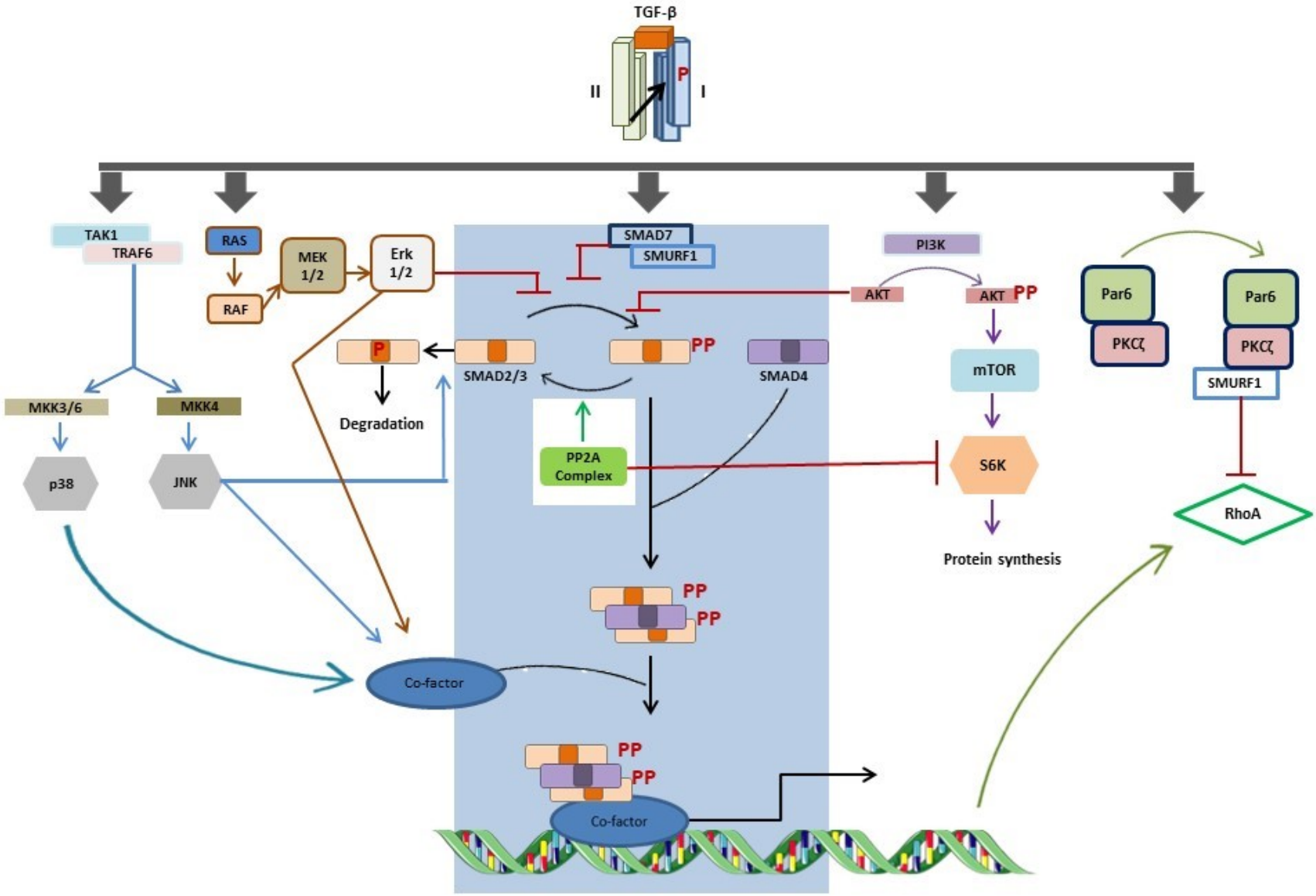


Figure 6- Scheme of the TGF-β pathway: Canonical (blue) and non-canonical (white background).

BMP ligands bind to BMP receptors (BMPR), heterotetramers formed by two subunits of type I (BMPR1A or ALK-3, BMPR1B or ALK-6, and ACVR1A or ALK-2) and two type II (BMPR2, ACVR2A, and ACVR2B) receptors (207). BMPR signals thought phosphorylation of SMAD1, 5 and 8. Phosphorylated R-SMADs bind to the common mediator SMAD (co-SMAD), SMAD4, and translocate to the nucleus to act as transcription factors where they activate downstream gene transcription (208).

Several molecules are responsible for modulating the TGF-β pathway including inhibitory SMAD proteins, phosphatases and ubiquitin ligases. The main inhibitory SMADs are SMAD7, SMAD6 and Smad nuclear-interacting protein 1 (SNIP1). SMAD7 regulates both (TGF-β and BMP signalling), competing with R-SMADs for interaction with type I receptor, whilst SMAD6 only regulates BMP signalling by competing with SMAD4 binding to SMAD1. SNIP1 binds the transcriptional coactivator CBP/300, blocking its interaction with SMAD4 and p65/RelA, thereby, inhibiting TGF-β and NF-κB signalling (209).

Several phosphatases can also modulate R-SMADs. Since phosphorylation sites in R-SMADs are on serine/threonine (S/T) residues I will focus on the 3 categories of S/T phosphatases: the phospho-protein phosphatase family (PPP), the protein phosphatase Mg2+/Mn2+-dependent (PPM) family and the transcription factor IIF-interacting CTD phosphatase (FCP) family (206). The PPP family proteins are normally trimeric containing a structural, a regulatory and a catalytic subunit. One member of this family known to regulate TGF-β signalling is the PP2A complex where PPP2CA is the catalytic subunit. This protein was reported to dephosphorylate the C-terminal domain of SMAD3 but not SMAD2 in response to hypoxia leading to a decrease in the transcription of the SMAD3-activated genes (210). The PPM family are monomeric and the prototypic member PPM1A, also known as PP2Cα, was reported to dephosphorylate SMAD2 and SMAD3 in the C-terminal domain (211). Finally, the FCP family are also monomeric proteins and the family contains the Small C-terminal domain S/T phosphatases (SCPs) (212). SCP1 and SCP2, also known as CTDSP1 and CTDSP2, dephosphorylate SMAD2 and SMAD3 in the linker domain thereby enhancing TGF-β signalling (213).

An alternative to reducing active protein levels by dephosphorylation is to destroy the protein completely. As targeted protein destruction is achieved by ubiquitination, several components of the ubiquitin/proteasome pathway also contribute to the regulation of TGF-β signalling. For example, SMURF1, an E3 ubiquitin ligase, associates with TGFβR type I via SMAD7 resulting in ubiquitination and turnover of TGFβR and SMAD7. SMURF1 can also induce ligand-dependent and independent ubiquitination and degradation of SMAD1 and SMAD5 through binding to the linker region (214). R-SMAD linker region ligand-induced phosphorylation by MAPK or nuclear kinases such as CDK8 and CDK9 leads to impairment of nuclear localisation. Moreover, linker phosphorylation of SMAD3 triggers polyubiquitylation by the ubiquitin ligase NEDD4L and further proteasome-mediated degradation (215).

1.5.2 Non-canonical pathways

In addition to SMADs signalling, TGF-β binding to its receptor activates a number of other intracellular pathways to modulate downstream cellular responses (216). Such non-canonical pathways include mitogen-activated protein kinase (MAPK), PI3K/AKT and Rho-like GTPase signalling pathways which are described below and are represented on *Figure 2.*

The MAPK family includes isoforms of extracellular signal-regulated kinases (ERKs) (1 and 2), p38 (α, β, γ and δ), and c-Jun N-terminal kinase (JNK) (1-3).

The ERK pathway is activated by TGF-β induced phosphorylation of tyrosine residues on both type I and type II TGF-β receptors and/or ShcA. The activation of ShcA leads to formation of a ShcA/Grb2/Sos complex which can activate Ras, leading to activation of c-Raf, MEK and ERK. ERK can phosphorylate receptor-activated SMADs such as SMAD1, 2 and 3 in the linker region inhibiting the nuclear accumulation of the SMADs (216).

The JNK/p38 pathway also gets activated in response to TGF-β family signalling through the interaction between TGF-β receptors and TRAF6 inducing the poly-ubiquitination of TRAF6 followed by recruitment of TGF-β-activated kinase 1 (TAK1) (216). TAK1 is one of the MAP3Ks that activates MAP kinase kinases (MKK) such as

MKK3/6 and MKK4 leading to p38 and JNK activation, respectively (216). Activated JNK/p38 together with SMADs modulate apoptosis. JNK/p38 can also phosphorylate receptor-activated SMADs in the linker region inhibiting SMAD nuclear accumulation (217). Activation of the JNK pathway leads to the activation of the transcription factor c-Jun which can interact with TGIF (a nuclear transcriptional corepressor- TG-interacting factor) to repress SMAD2 activity. This interaction between c-jun and the R-SMAD blocks the recruitment of p300/CBP required for SMAD2 transcriptional activity as demonstrated *in vitro* in COS-7 cells (monkey fibroblast from kidney tissue) (218).

Another non-canonical pathway activated by TGF-β family signalling is the PI3K/AKT pathway. Upon TGF-β stimulation, association between TGF-β type I receptor and p85, the regulatory subunit of PI3K, occurs promoting AKT activation. The PI3K/AKT pathway regulates translational responses by a downstream effector of ATK, mTOR, thereby regulating protein synthesis trough phosphorylation of S6K (216) potentially contributing to skeletal muscle hypertrophy.

Lastly, the Rho-like GTPase signalling pathway is activated by TFG-β which causes down-regulation of RhoA protein, an important mediator of skeletal muscle differentiation that increases MyoD expression (219). The RhoA down-regulation occurs via Par6 which gets phosphorylated by TGF-β receptor type II and activated leading to SMURF1 (E3 ligase) and PKCζ (an effector of the Cdc42/Rac1-Par6 polarity complex) recruitment which ubiquitinylates and promotes RhoA turnover in skeletal muscle cells (220). However, TGF-β has been reported to increase RhoA expression in smooth muscle cell lines (221).

1.6 MicroRNAs

MicroRNAs are small (21-25 nucleotides) non-coding ribonucleic acids (RNAs) present in the genomes of plants, animals and some viruses (222). They were originally identified through a genetic screen to identify the development regulating gene lin-4 in *C. elegans* (a nematode) in 1993 (223). Experimentally, they found that lin-4 did not encode a protein but expression of lin-4 negatively regulated LIN-14 protein levels. Two lin-4 transcripts of approximately 22 and 61 nucleotides were identified and these contained sequences complementary to the 3'UTR region of lin-14 RNA suggesting that lin-4 regulated lin-14 translation via an antisense RNA-RNA interaction, establishing a new regulation level for protein expression. Following on from this initial discovery and the demonstration that microRNAs were also present in other organisms (224), an increasing research effort has identified the mechanisms by which these regulators are synthesised and elucidated their function.

MicroRNAs are transcribed by RNA polymerase II or III from independent genes from a microRNA-specific promoter, from introns of protein-coding genes or from the exons of non-coding RNAs (e.g. H19) *(Figure 7)*. The initial transcript, described as a primary microRNA (pri-microRNA), can be several kilobases long (225) and may contain several microRNA precursors. Pri-microRNAs are processed by a complex containing Drosha, a ribonuclease III endonuclease (RNase III), and Pasha (DGCR8), an essential co-factor for microRNA processing. Drosha cleaves the pri-microRNA to produce a pre-microRNA of 70 nucleotides. These pre-microRNAs are double-stranded RNAs containing a hairpin loop (226), which are exported from the nucleus to the cytoplasm by exportin-5 (XPO5) (227). In the cytoplasm, a second RNase III, Dicer, cleaves the hairpin loop to obtain an approximately 20 nucleotide microRNA duplex. One strand of the duplex is degraded and the other, representing the mature microRNA, is incorporated into the RNA-induced silencing complex (RISC) (228). Depending which of the arms of the precursor is integrated in RISC, microRNAs are named -5p (from the 5' arm) or -3p (from the 3' arm) (229). By complementary base pairing, this complex identifies and binds mRNA targets (225) and in most cases this interaction decreases the half-life or rate of translation of the mRNA. Consequently, microRNAs regulate cell phenotype 'fine-tuning' the proteome and it is estimated that 60% of genes are regulated by

microRNAs (230). MicroRNA target recognition appears to differ between plants and animals. In plants, there is a complementary binding of the whole microRNA with the 3'UTR of target mRNAs, making target prediction quite straightforward (231). In animals, the binding occurs between a "seed sequence" (the region spanning the 2nd and the 8th nucleotides at the 5' end of the microRNA), and the pairing is often imperfect. Therefore, each microRNA is thought to regulate tens to hundreds of genes simultaneously due to redundancy in complementary sequences between targets and microRNAs (222) and each target can also be regulated by multiple microRNAs. However, many of the target predictions remain to be experimentally validated (232).

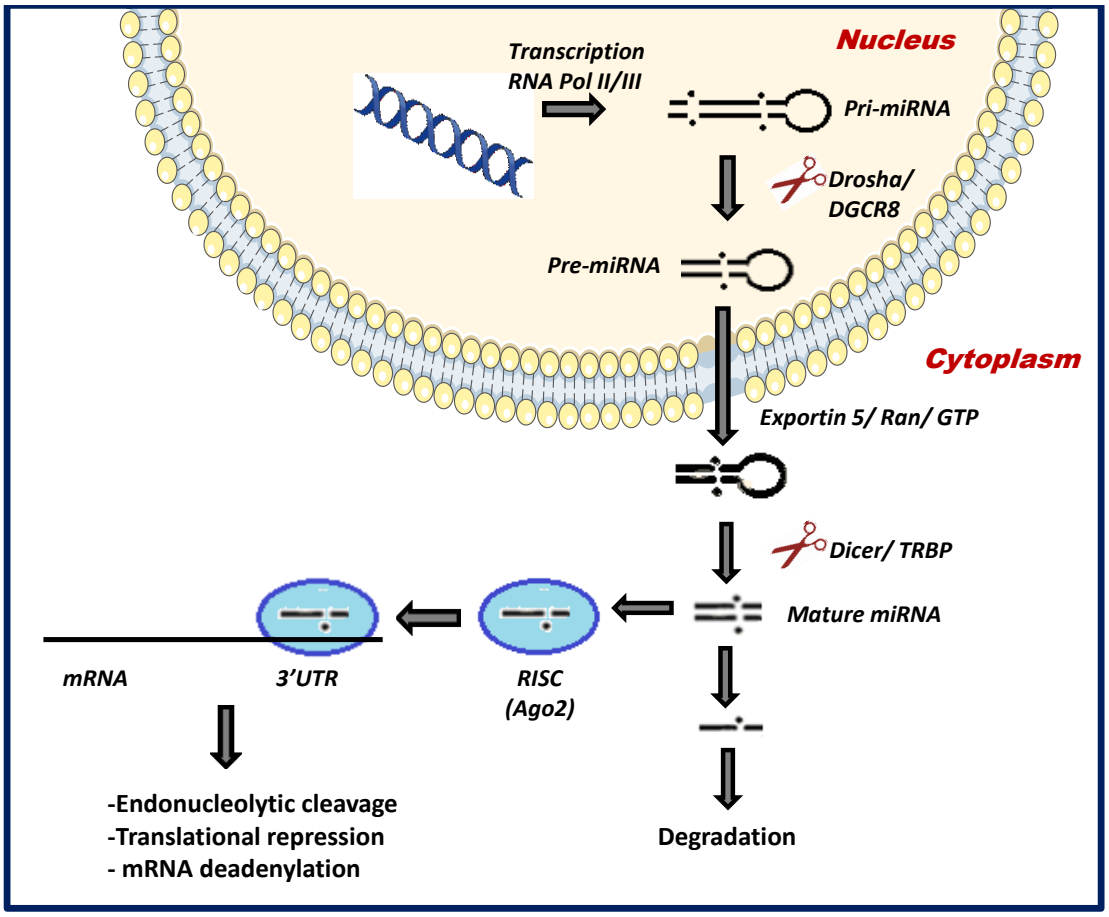


Figure 7- MicroRNA biogenesis.

The microRNA biogenesis starts with the production of the pri-miRNA by RNA polymerase II or III and further cleavage by the Drosha-DGCR8 in the nucleus to obtain the pre-miRNA. The latest is exported to the cytoplasm by the complex Exportin-5, Ran and GTP. In the nucleus, the pre-miRNA is cleaved by the complex Dicer and TRBP (double-stranded RNA binding protein) to obtain the mature miRNA. One strand of the mature miRNA is degraded and the other is loaded together with Ago2 to RISC to silence target mRNA through cleavage, translational repression or deadenylation. Adapted from (233)

A specific group of microRNAs are restricted to -or much more highly expressed in- muscle and are known as myomiRs. This group includes miR-1, miR-133a, miR-133b, miR-206, miR-208a, miR-208b and miR-499. Some myomiRs are transcribed as bi-cistronic transcripts (e.g. miR-1/miR-133a and miR-206/miR-133b) (234). Modification of expression levels of these microRNAs was associated with decreased muscle function in both cardiac and skeletal muscle (235). The importance of microRNAs in skeletal muscle was identified in 2005, when it was shown that deletion of miR-1 in drosophila caused incomplete skeletal muscle growth during early development leading to premature death (236). Later studies in mammals confirmed important roles for the myomiRs in muscle as miR-206 knockout mice exhibited a delay in muscle recovery after denervation (237). Other microRNAs are also present in muscle but are not tissue-restricted and are widely or ubiquitously expressed. However, these miRNAs also play important roles in controlling skeletal muscle homeostasis.

Emerging evidence suggests that a change in metabolic demands in skeletal muscle such as exercise alters microRNA expression which may contribute to the muscle adaptation to the new metabolic demand. For example, miR-208b and miR-499 are essential to establish and/or maintain the Type I fibre phenotype as knockout mice for each of them resulted in muscle with significantly more Type II fibres, leading to reduced exercise capacity when the mice were subjected to forced running (238). Acute bouts of endurance exercise in mice significantly increase the levels of miR-181, miR-1 and miR-107 by 37%, 40% and 56%, respectively, and reduce miR-23 expression by 84% in skeletal muscle. The reduction in miR-23 increases *Pgc-1α* so is likely to contribute to increased mitochondrial biogenesis following exercise (239). Similarly, in untrained human participants, 60 min of endurance exercise increased the levels of miR-1 and miR-133 in the *vastus lateralis*. However, the elevation of these miRs was not seen after post-training suggesting that microRNA levels are very sensitive to muscle activity (240).

MicroRNA expression in skeletal muscle has been reported to be altered in several diseases including Duchenne´s muscular dystrophy (DMD), myotonic dystrophy (DM) and amyotrophic lateral sclerosis (ALS) (241-243). For example, miR-206 was up-regulated in the diaphragm of mdx mice (animal model for DMD), which was the most

dystrophic muscle in these animals (244). Moreover, miR-206 was also found to be upregulated in the muscle of DMD patients (245). Similarly, miR-31 was increased in the skeletal muscle and isolated myoblasts from DMD patients and it was reported that this miR repressed dystrophin expression, a protein required for sarcolemmal integrity (246). In addition to miR-206, other microRNAs including miR-210 and miR-335 were up-regulated in muscle biopsies of patients with DM type 1 (247-249). In patients with amyotrophic lateral sclerosis, several microRNAs including miR-206, miR-23a, miR-29b and miR-455 are up-regulated in the skeletal muscle. As miR-23a represses Pgc-1α the increase in this microRNA may contribute to the mitochondrial dysfunction in the skeletal muscle of these patients (242).

MicroRNA changes have also been reported in diseases studied in this thesis which result in muscle wasting: ICUAW and COPD (250). In the *rectus femoris* muscle of patients with ICUAW a decrease in the levels of miR-1, miR-133a and miR-499 by 39%, 38% and 27%, respectively, was found. Interestingly, miR-181a is also suppressed in these patients, and like miR-1 and miR-499 which target the ligand myostatin (251) and the receptor activin IIB (252), this microRNA also reduces TGF-β signalling by targeting SMAD7. Therefore, a decrease of these microRNAs could lead to a removal of a level of inhibition of the TGF-β signalling pathway causing a sensitization of the muscle of COPD and ICUAW patients to TGF-β signalling and consistent with this suggestion the ICUAW patient biopsies had increased CYR61 mRNA levels and increased localization of p-SMAD2/3 into the nuclei (30). Another microRNA that targets inhibitors of the TGF-β signalling is miR-424 (253) which targets SMAD7 and SMURF2.

In skeletal muscle of COPD patients, a reduction in miR-1 was observed whereas no change in miR-133 and miR-206 levels was found (254). One other finding from this study was an inverse correlation of miR-499 with muscle mass in the patients. However, a reduction in the expression of these microRNAs in COPD has not been universally reported as other studies have shown increased myomiR expression in COPD patients. The reasons for this discrepancy are not clear but may be due to the choice of controls or other factors relating to physical activity or disease severity (255,256).

As further described in Chapter 3, our preliminary data identified several microRNAs that were differently expressed in the quadriceps of COPD patients compared to controls. The up-regulated microRNAs included both -3p and -5p forms of miR-542. Moreover, the expression of miR-542-3p was associated with lung function and physical performance in a COPD cohort (162). A similar association of miR-542-3p with physical performance in older people was also identified. Bioinformatics analysis (presented in Chapter 3) predicted that miR-542 would target a number of proteins or pathways associated with the maintenance of muscle mass and muscle wasting including mitochondrial and cytoplasmic ribosomal proteins and the TGF-β and IGF-1 pathways suggesting functional consequences of the altered microRNA expression. Together with the expression data this bioinformatic analysis prompted us to investigate further the expression and function of miR-542 in the context of atrophy.

In order to interpret results between the most commonly used *in vitro* cells, C2C12 myoblasts, and human data it is useful to know the mature sequence of these microRNAs *(Table 5).* Human and mouse miR-542-3p have the same mature sequence whereas human and mouse miR-542-5p do not share the same sequence.

Table 5- miR-542 accession number and mature sequence for human and mouse.

miR-542 information		
MicroRNA	**Accession**	**Mature Sequence**
hsa-miR-542-3p	MIMAT0003389	UGUGACAGAUUGAUAACUGAAA
mmu-miR-542-3p	MIMAT0003172	UGUGACAGAUUGAUAACUGAAA
hsa-miR-542-5p	MIMAT0003340	UCGGGGAUCAUCAUGUCACGAGA
mmu-miR-542-5p	MIMAT0003171	CUCGGGGAUCAUCAUGUCACGA

1.7 Thesis aims and hypothesis

miR-542-3p and miR-542-5p were identified as being up-regulated in COPD patients compared to a control healthy group in a previous array and their role in muscle atrophy has not yet been explored. Moreover, the pathways that miR-542-3p/-5p are predicted to target (TGF-β and IGF-1 signalling and both cytoplasmic and mitochondrial ribosomal proteins) have been shown to be of importance in maintaining muscle homeostasis. Therefore, the work presented in thesis was designed to examine the role of both miR-542-3p and miR-542-5p in TGF-β signalling and ribosomal protein synthesis in the context of skeletal muscle wasting in relation to acute and chronic myopathies such as ICUAW and COPD as well as ageing. Thus, the main hypotheses of this thesis can be stated as follows:

- miR-542-5p expression will associate with muscle function.
- miR-542 expression will be increased in patients with established ICUAW.
- miR-542-3p and miR-542-5p will decrease mitochondrial protein synthesis.
- miR-542-3p and miR-542-5p will decrease ribosomal biogenesis.
- miR-542-3p and miR-542-5p will increase TGF-β signalling.
- Increased miR-542-3p and miR-542-5p will cause muscle wasting.

CHAPTER 2: Materials and methods

2.1 MATERIALS

All reagents were purchase from Thermo Scientific unless otherwise stated. Water used to prepare solutions was MilliQ purified unless differently specified.

2.1.1 Preparation of DNA plasmids

2.1.1.1 1% Luria Broth (LB) agar plates

2.5g of agar powder were diluted in 250mL of LB media and pH was adjusted to 7.2. After the mixture was autoclaved and the temperature was below 60°C, 250µL of 10mg/mL of antibiotic (ampicillin) were added for the selection of the desired bacteria. Around 20mL of LB agar mix was poured into each 100mm petri dish and allowed to set.

2.1.1.2 Ampicillin solution

0.05g of ampicillin were dissolved in 5mL of H_2O to obtain a 10mg/mL stock solution.

2.1.2 Protein synthesis experiment

2.1.2.1 50mM Sodium Bicarbonate pH 9.6

4.2g of $NaHCO_3$ were dissolved in H_2O and the pH was adjusted to 9.6 with 5M NaOH. Water was then added to make up a 1000mL solution.

2.1.3 Fixing and Staining

2.1.3.1 1x Phosphate buffered saline (PBS)

8g of NaCl, 0.2g of KCl, 1.44g of Na_2HPO_4, 0.24g of KH_2PO_4 *(Sigma, USA)* were dissolved in 800mL of H_2O and pH was adjusted to 7.4. H_2O was added to make up 1000mL of solution followed by sterilization via autoclaving.

2.1.3.2 1x Phosphate buffered saline supplemented with 0.05% Tween 20 (PBST)

1mL Tween 20 *(Sigma, USA)* was added to 1999mL of 1X PBS.

2.1.3.3 4% paraformaldehyde (PFA) in PBS

4g of PFA *(Sigma, USA)* in 80mL of H_2O were heated to 60°C followed by the addition of NaOH until PFA was dissolved. 10mL of 10X PBS were added and pH adjusted to 7.4 using 5M HCL. H_2O was added to make up a 100mL solution.

2.1.3.4 5% Bovine serum albumin (BSA) in PBS (BSA-PBS)

5g of bovine serum albumin *(Sigma, USA)* were dissolved in 100mL of 1X PBS.

2.1.4 Western Blotting

2.1.4.1 2x Igepal NP40 buffer

Lysis buffer was made by mixing 8.76g of NaCl, 10mL NP-40, 50mL of 0.5M EDTA and 1.21g Tris *(Sigma, USA)* in water followed by adjusting the pH to 7.3 and the solution was brought to a final volume of 500mL with H_2O. To avoid proteolysis and dephosphorylation, protease inhibitor cocktail and phosphatase inhibitor *(Sigma, USA)* were added to the mix 1% (v/v), before use.

2.1.4.2 2x SDS protein sample buffer

4mL 10% Sodium dodecyl sulphate (SDS), 1mL Tris-HCl (1M, pH 6.8), 2mL glycerol and 0.5mL 1% bromophenol blue were dissolved in 10mL of H_2O. Before use, 10% mercaptoethanol (v/v) was added to the mixture.

2.1.4.3 Resolving gel

Two different resolving gels were used so the concentrations of each reagent were adjusted appropriately as detailed in *Table 6.*

Table 6- Concentration of reagents used in 10 and 15% resolving gels.

Reagents	10% Resolving gel	15% Resolving gel
H_2O	4.02mL	2.3mL
30% (w/v) Acrylamide:0.8% (w/v) Bis-Acrylamide	3.33mL	5mL
1.5M Tris-HCl pH 8.8	2.5mL	2.5mL
10% SDS	100µL	100µL
10% APS	50µL	50µL

2.1.4.4 Stacking gel

The stacking gel was made up from 2.11mL H_2O, 0.83mL of 30% (w/v) Acrylamide:0.8% (w/v) Bis-Acrylamide, 1.26mL of 0.5M Tris-HCl pH 6.8, 50µL 10% SDS, 25µL 10% APS and 5µL of TEMED to give a final gel containing 5% Acrylamide.

2.1.4.5 10x Running buffer

30.3g of Trizma® Base, 140.4g of glycine and 10g of SDS were dissolved in H_2O, pH was adjusted to 8.3 with 5M HCl and final volume made up to 1L.

2.1.4.6 10x Transfer buffer

24.7g of Trizma® Base and 112.6g of glycine were dissolved into 1L of H_2O. H_2O was used to dilute the buffer to 1x.

2.1.5 Agarose gel

2.1.5.1 0.5x Tris-borate-EDTA (TBE) buffer

108g of Tris base, 55g of boric acid and 40mL of 0.5M EDTA (pH 8) were mixed in H_2O and made up to 1L. To prepare a 0.5x working solution from the 10x stock, we mixed the 10x stock with H_2O in 1/20 (v/v) ratio.

2.1.6 cDNA dilutions

2.1.6.1 0.1x Tris/EDTA (TE)

10x TE was prepared by mixing 10mM Tris-HCl, pH 8.0 with 1mM ethylenediaminetetraacetic acid (EDTA) *(Sigma, USA)*. To obtain 0.1X, the solution was diluted 1/100 with H_2O.

2.2 METHODS

2.2.1 *In vitro* experiments

2.2.1.1 Cell culture

Immortalised mouse skeletal myoblast C2C12 (257) cells were maintained in Dulbecco's Modified Eagle Medium (DMEM) which was supplemented with 10% (v/v) foetal bovine serum (FBS) *(GE Healthcare, UK)*, penicillin (100U/mL) and streptomycin (100mg/mL) at 37°C in humidified 5% CO_2, 95% atmospheric air (standard incubation). Immortalised human skeletal myoblast cells isolated from the *pectoralis* major muscle of a 41-year-old male Caucasian heart-transplant donor, LHCN-M2 (258), were grown in skeletal muscle growth media *(PromoCell, Germany)* supplemented with 20% (v/v) FBS at standard incubation conditions. Cells were maintained at sub-confluent levels by trypsinisation every 2-3 days (split ratio 1:5 for C2C12 and 1:4 for LHCN-M2) (257,258).

2.2.1.2 Preparation of DNA plasmids

Plasmids used were obtained from bacterial transformation and DNA extraction and purification. For this purpose, 40µL of competent *E. Coli (Biolab, UK*) were mixed with 5µL of the plasmid of interest and incubated on ice for 15 minutes. The sample was heat shocked at 42°C for 90s to promote uptake of the DNA by bacteria. The mix was then placed on ice for 2 minutes followed by the addition of 500µL of LB broth. 200µL of bacteria were plated on to LB-agar plates containing ampicillin (100µg/mL) *(Sigma, USA)* and incubated at 37°C overnight. Single colonies were picked using a sterile pipette tip and inoculated into 3mL of LB broth containing 30µL of 10mg/mL ampicillin. Samples were incubated at 37°C overnight under agitation. QIAprep SPIN Miniprep Kit *(Qiagen, UK)* was used to lyse cells and purify plasmid DNA according to the manufacturer's instructions. DNA quantification was performed using a Nanodrop spectrophotometer (*ND1000, Wilmington, USA).*

2.2.1.3 microRNA transfection

C2C12 and LHCN-M2 cells were seeded at a density of $5x10^4$ cells/mL (seeding 6250 cells in a 96-well plate well and scaling it for the appropriate growth area). 24 hours later, cells were observed using an optical microscope to ensure confluence was

between 60-80% for transfection. For a single 96-well plate well, 0.5µL of 20µM mirVana microRNA mimics in 12.5µL of Opti-MEM and 0.5µL Lipofectamine 2000 in 12.5µL of Opti-MEM were mixed and incubated for 15min. 100µL of serum-free DMEM per well were added to the mixture. Growth media was removed, cells were washed twice with serum-free DMEM and 125µL of the reaction mixture were added to each well. Cells were then placed into the incubator at 37°C and 5% CO_2 for 4h. Transfection media was removed and replaced with DMEM + 10% FBS for C2C12 cells or skeletal muscle growth media + 20% FBS for LHCN-M2 cells, and returned to the incubator for the required length of time. Volumes were scaled up when necessary. A list of the mirVana microRNA mimics used for transfection is provided in *Table 7*.

Table 7- microRNAs used for cell transfection.

Mature ID	Species	Mature microRNA sequence
mirVana® microRNA		
Scrambled	*Mus musculus* *Homo sapiens*	Random sequence microRNA mimic molecule that does not produce identifiable effects on any gene.
mmu-miR-542-3p hsa-miR-542-3p	*Mus musculus* *Homo sapiens*	UGUGACAGAUUGAUAACUGAAA
hsa-miR-542-5p	*Homo sapiens*	UCGGGGAUCAUCAUGUCACGAGA
Anti-miR™ microRNA Inhibitor		
AntagomiR-mmu-miR-542-3p AntagomiR-hsa-miR-542-3p	*Mus musculus* *Homo sapiens*	UGUGACAGAUUGAUAACUGAAA
AntagomiR-hsa-miR-542-5p	*Homo sapiens*	UCGGGGAUCAUCAUGUCACGAGA

2.2.1.4 Transfection of DNA plasmids

Cells were seeded at a density of $5x10^4$ cells/mL in 6 (2mL/well) or 96 (0.125mL/well) well culture plates as appropriate for the experiment. Two different experiments were performed: 1) DNA plasmid after microRNA transfection (the majority) or 2) DNA plasmid without microRNA transfection (pCAGGS-EGFP-miR-542 and pCAGGS-EGFP). In

the former experiments, 24h after miR transfection, cells were transfected with DNA plasmids whereas in the latter 24h after seeding, cells were observed under the optical microscope to ensure confluence was between 60-80% to proceed to transfection. The process that follows was the same for the two types of experiments. For a single 96-well plate well, 0.4µg of plasmid DNA was added to 20µL of Opti-MEM and incubated at room temperature for 15min together with a second mix containing 2µL of Lipofectamine and 20µL of Opti-MEM. 165µL of serum-free DMEM were then added to the reaction mixture per well and mixed. Growth media was removed and cells were washed twice with serum-free DMEM before adding 200µL per well of the final transfection mix. Cells were then incubated at 37°C and 5% CO_2 for 4.5h before the transfection media was removed and replaced with the appropriate growth medium according to the manufacturer's instructions. Volumes were scaled up when necessary. A list of the plasmids used for transfection is provided in *Table 8.*

Table 8- Plasmids used for luciferase assays *in vitro* and *in vivo.*

Plasmid	Functional gene	Vector	Origin
pCDNA.3	Empty vector	-	Promega
p(CAGA)$_{12}$-luc	Luciferase	pGL3	Susumu Itoh (sitoh@md.tsukuba.ac.jp)
PRL-TK	Luciferase	pRL	Promega
TGBR truncated	TGBR truncated	pGL3	B. Garfield
pCAGGS-EGFP	EGFP	pCAGGS	D. Lori
pCAGGS-EGFP-miR-542	EGFP-miR-542	pCAGGS	R. Farré Garrós

2.2.2 Protein synthesis experiment

2.2.2.1 Puromycin experiment

Human myoblasts were seeded at $5x10^4$ cells/mL in a 24 well plate. After 24h, myoblasts were serum and leucine starved for 2h, culturing myoblasts in Dulbecco's Modified Eagle's Limiting Media (DMEM-LM) at 37°C in humidified 5% CO_2, 95% atmospheric air. Media was changed to serum free skeletal muscle growth media containing leucine for 45min before puromycin was added to a final concentration of 100ng/mL *(Sigma, USA)* and incubation was continued for 30min at 37°C. LHCN-M2 myoblasts were harvested and protein was quantified as detailed in Protein extraction section 2.2.11.1.

2.2.2.2 Puromycin enzyme-linked immunosorbent assay (ELISA)

Protein extracts were diluted to 300ng/µL. 100µL of 50mM sodium bicarbonate pH 9.6 *(Sigma, USA)* were added per well into a 96-well plate followed by the addition of 1µL/well protein extract (300ng). A standard curve containing 1200, 600, 300, 150, 75 and 37.5ng of protein as well as a blank were prepared in the plate to allow quantification. The plate was incubated at 37°C in humidified 5% CO_2, 95% atmospheric air for 2h, and then washed once with PBS. To block non-specific interactions, 200µL of 5% BSA in PBS were added to each well and incubated for 30min at room temperature. After blocking, 100µL of mouse anti-puromycin *(Millipore, USA)* were added at 1:10000 in PBS 1x containing 5% BSA and the reaction was incubated for 1h. After two 1x PBS washes, protein was incubated with 100µL of anti-mouse secondary antibody *(GE healthcare, UK)* at 1:1000 in blocking solution for 1h at RT. After four 1x PBS washes, 100µL of the reaction substrate, tetramethylbenzidine (TMB) *(Sigma, USA)*, were added and when a blue colour had developed 100µL of stop solution *(Sigma, USA)* were added and absorbance was measured at 450nm in a plate reader *(BioTek, USA).*

2.2.3 Luciferase reporter assay

The luciferase assay was used to determine TGF-β activity as the plasmids used for this experiment have a $CAGA_{12}$ promoter which contains 12 tandem copies of the sequence "CAGA" which constitutes a SMAD binding element. SMAD2/3-SMAD4 binding to this promoter region increases *firefly* luciferase gene expression *(Figure 8).* To account for variable transfection efficiency the dual-luciferase® reporter assay system *(Promega, UK)* was used consisting of measuring the activities of two luciferases from a single sample. Therefore, cells were co-transfected with a pRL-TK vector which is a *Renilla* luciferase control reporter vector that it is constitutively expressed.

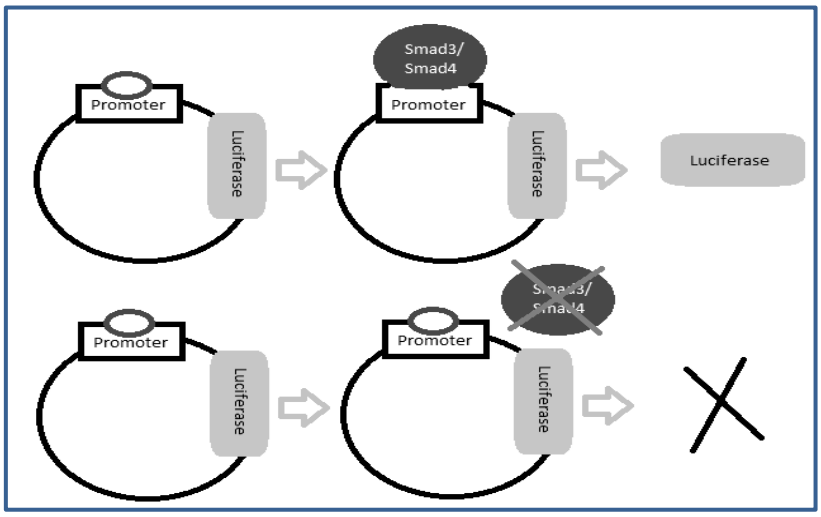


Figure 8- Schematic representation of luciferase assay.

Cells are transfected with the dual reporter system, as there is simultaneous expression and measurement of two individual reporter enzymes. The experimental reporter used had a binding region (CAGA sequence) for SMADs. Binding of SMADs resulted in *firefly* luciferase gene expression. Therefore, firefly luciferase expression correlated with SMAD binding. Less or no SMAD on the system, results in less or no expression of the *firefly* luciferase gene. On the other hand, the control reporter expression is regulated by a constitutively active promoter.

Cells were seeded at a density of $5x10^4$ cells/mL in a 96 well plate (0.125mL/well). 24h later cells were transfected with miRVana microRNA mimics as described above and allowed to recover for 24h. The cells were transfected with luciferase reporter vectors: 1.5µg/mL of $p(CAGA)_{12}$-luc (0.094µg in a 96-well plate well) and 0.5µg/mL of pRL-TK construct (0.094µg in a 96-well plate well) using Lipofectamine as described in section 2.2.1.4. Cells were allowed to recover overnight in complete growth medium before

being washed twice with serum free (SF) DMEM, treated if necessary with inhibitors and then stimulated with ligand at the appropriate concentration in SF medium as described in the appropriate figure

legends. After washing with PBS (1x), cells were lysed with 50µL of 1x Passive Lysis Buffer *(Promega, UK)* with shaking on a horizontal shaker for 15min. To quantify luciferase activity, 10µL of lysed cells were placed into a well of a white 96-well polystyrene plate *(Costar, UK)* followed by the addition of 50µL of a 1:1 luciferase assay substrate and luciferase assay buffer mix. Firefly luciferase activity was measured using a Lumimark plate-reader *(Bio-Rad, UK)*. 50µL of 1:50 Stop Substrate and Stop and Glo buffer *(Promega, UK)* were added to each well to quench Firefly *(Photinus pyralis)* luciferase activity followed by the measurement of the control Renilla *(Renilla reniformis)* luciferase activity using the same parameters. Firefly luciferase activity was normalised to Renilla luciferase activity.

2.2.4 Mitochondria assays

2.2.4.1 Cell fractionation

Cell fractionation was performed from half of the TA muscle of the mice using a mitochondria isolation kit for tissue *(ThermoFisher Scientific, UK)*. After extraction, samples were weighed and from each muscle we used approximately 20mg. Samples were kept on ice at all times. TA muscles were washed twice with 2mL of 1x PBS and the tissue was cut in a Petri dish and put with tweezers in the neck of a pre-chilled collector tube of a dounce homogeniser. Next, 400µL of BSA and Reagent A solution were added to the tube. The latter solution was made fresh containing 4mg/mL BSA in Reagent A and 1 tablet of protease inhibitor cocktail *(Roche, UK)* in 10mL. Rupture of cells was achieved by 10 strokes with Dounce homogeniser A and 40 strokes with Dounce homogeniser B *(Sigma, USA).* Disrupted cells were transfered from the collector tube to a microcentrifuge tube and 400µL of Reagent C were added followed by tube inversion. Samples were centrifuged at 700x g for 10min at 4°C and the obtained pellet corresponding to the nuclear fraction that was stored at -80°C. The supernatant was transfer to a new microcentrifuge tube and centrifuged at 12.000x g

for 15min at 4°C. The supernatant corresponded to the cytoplasmic fraction that was stored at -80°C and the pellet corresponded to the mitochondrial fraction. The mitochondrial pellet was dissolved in 100µL of PBS and protein was measured as described in section 2.2.10.3 and functional analyses were performed immediately.

2.2.4.2 Complex I activity

Complex I activity was analysed using the complex I enzyme activity microplate assay kit *(Abcam, UK).* In each well of the plate, 20µg of extracted mitochondria were added, previously dissolved in incubation solution and made up to 200µL, and the plate was incubated for 3h at RT. The solution was removed by turning the plate over and 300µL of 1x Buffer solution were added to each well. The wells were emptied and rinsed again with 1x Buffer solution. After removing the Buffer, 200µL of Assay Solution were added to each well. In each ELISA strip, the Assay Solution contained 1.67mL of 1x Buffer, 84µL of 20x NADH and 17µL of 100x Dye. The plate was placed in a Lumimark plate-reader *(Bio-Rad, UK)* and measurements were taken at RT and at 450nm at intervals of 1min for 30min and shaking between readings. In order to plot the data, we calculated the mOD per min.

2.2.5 Membrane potential assays

2.2.5.1 MitoTracker® Red CMXRos staining

MitoTracker® Red CMXRos is a red-fluorescent dye which passively diffuses across the plasma membrane and accumulates in a membrane potential dependent manner in active mitochondria. When entering in actively respiring cells, the dye is oxidised and sequestered in the mitochondria where its mildly thiol-reactive chloromethyl moiety *(Figure 9)* reacts with thiols on proteins and peptides to form an aldehyde-fixable conjugate. MitoTracker® Red CMXRos is retained in cells after aldehyde-based fixation and after permeabilisation. As staining of the nucleus with 2-(4-amidinophenyl)-1H -indole-6-carboxamidine (DAPI) was needed to quantify mitochondrial staining per cell, MitoTracker® Red CMXRos was our dye of choice. Other conventional fluorescent dyes

such as rhodamine 123 or tetramethylrosamine were discarded as they are not resistant to cell fixation.

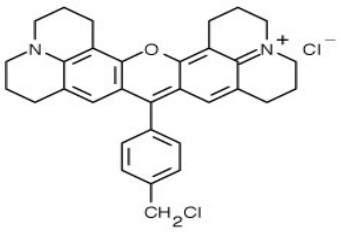


Figure 9- Chemical structure of MitoTracker® Red CMXRos.

Cells were seeded at a density of $4x10^4$ cells/mL in a 96 well plate (0.125mL/well). The cells were transfected with miRVana microRNA mimics 24h later as described in section 2.2.1.3 and then allowed to recover for 24h. Growth media was removed and cells were washed with PBS (1x). 125µL of 250nM MitoTracker® Red CMXRos dissolved in growth media were added to each well and incubated for 15min at 37°C. After washing twice the cells with PBS (x1), cells were fixed with 50µL 4% paraformaldehyde (PFA) *(Sigma, USA)* for 10min at RT. After washing cells twice with PBS-T (0.05% Tween), cells were incubated with 50µL of 1xPBS with 0.3% Triton X-100 detergent *(Sigma, USA)* for 15min to permeabilise the cell membranes. Cells were washed twice with PBS-T and the nuclei stained with 50µL 1:10000 DAPI in PBS-T (1x) for 1 min. Cells were washed with PBS-T then observed by fluorescence microscopy *(Zeiss Anxiovert 200M inverted, Carl Zeiss microimaging, Germany).* The excitation maximum of MitoTracker® Red CMXRos is 579nm and emission maximum is 599nm, therefore a rhodamine filter set was used. MitoTracker® Red CMXRos stock solution was dissolved in dimethyl sulfoxide (DMSO) *(Sigma, USA)* to a final concentration of 1mM. Product was kept at –20°C and protected from light until used.

2.2.5.2 JC-1 staining

JC-1 is a cationic carbocyanine dye *(Figure 10)* which accumulates in mitochondria in a membrane potential dependent manner. The positive charge of the dye allows passive diffusion and accumulation in the negatively charged interior of mitochondria. In a monomeric form, the dye fluoresces in the green region of the

spectrum. When the dye aggregates inside mitochondria it forms J-aggregates which have a different fluorescence spectrum (red region). These characteristics allow the measurement of a ratio which confers sensitivity to the method as well as accounting for any variation in dye concentration and cell number between samples.

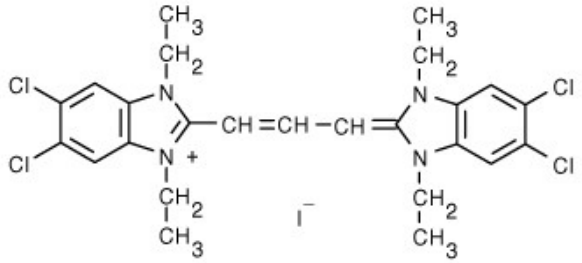


Figure 10- Chemical structure of JC-1.

Cells were seeded at a density of $2.4x10^4$ cells/mL in a 96-well plate (0.125mL/well). 24h later cells were transfected as previously described with miRVana microRNA mimics and were allowed to recover overnight. Growth media was removed and cells were washed with PBS (1x). 125µL of 10µM JC-1 solution *(Thermofisher, UK*) dissolved in growth media were added to each well and incubated for 15min at 37°C. After washing the cells twice with PBS (x1), PBS was added to cells and dye intensities (monomer as green and potential-dependent aggregates in red) were quantified. Fluorescence intensity was measured at paired excitation and emission wavelengths of 485/530nm for green fluorescence and 530/590nm for red fluorescence using a plate reader *(CytoFluor®, Applied Biosystems, US)*. The stock solution was prepared by dissolving the lyophilized JC-1 product in DMSO to a final concentration of 15mM and was kept protected from light at –20°C until used. The ratio between red and green emission (590/530) reflects the mitochondrial membrane potential.

2.2.6 Proliferation assay

Cells were seeded at a density of 500 cells per well in a 96-well plate. A total of three plates were prepared, Plate A, B and C. After 24h cells were transfected with the microRNAs of interest and 24h (for plate A), 48h (for plate B) and 72h (for plate C) after transfection cells were fixed and stored at 4°C before assay. The day prior to fixation different cell densities were seeded in each plate to obtain a standard curve, consisting of 0, 500, 1000, 2000, 4000, 6000, 10000 and 20000 cells per well. The assay consisted of removing PBS from fixed cells and adding 100µL of the Dye Binding Solution to each well (2.2 mL 5x Hank's balanced salt solution (HBSS) buffer to 8.8mL distilled H_2O were mixed with 22µL CyQUANT® NF Dye Reagent) *(CyQUANT® NF Cell Proliferation Assay Kit, Invitrogen, UK).* The mix was incubated at 37°C for 60min before reading the fluorescence in a CytoFluor® plate reader *(Applied Biosystems, US)* according to the manufacturer´s instructions. Measurements were taken using 485nm as the excitation wavelength and 530nm as emission wavelength. Four reads per well were taken and an empty well and a well just with Dye Binding solution were used as controls.

2.2.7 RNA extraction

2.2.7.1 RNA extraction from cells in a 96-well plate using a kit

In experiments carried out in 96-well plates, 125µL of cells at $5x10^4$ cells/mL were seeded per well. For harvesting, a CellAmp Direct Prep Kit for RT-PCR *(Takara Bio Europe/Clontech, France)* was used. Growth medium was removed and 125µL of CellAmp Washing Buffer was added to each well. After removing the Washing buffer, 50µL of the Processing Solution (49:1, Cell Amp Processing Buffer and DNAse I for Direct RNA prep, respectively) were added per well and incubated for 10min at RT. The cell lysate was then incubated for 5min at 75°C to stop the reaction then placed on ice. RNA was quantified using a NanoDrop spectrophotometer *(ND1000, Wilmington, USA)* and RNA purity was determined using the 260/280nm absorption ratio which gives information about presence of protein in the sample and 260/230nm ratio which gives

information about extraction reagents contamination. In both ratios, an outcome of 2 is used as an indicator of pure RNA. RNA was stored at -80°C.

2.2.7.2 RNA extraction from cells in a 6-well plate using phenol-chloroform method

In experiments carried out in 6-well plates, cells were seeded at $5x10^4$ cells/mL using 2mL per well. The extraction was carried out using the phenol-chloroform method. Cells were washed twice with cold PBS(x1). Cells were lysed in 500µl Trizol Reagent on ice with vigorous scrapping, the lysate was transferred to a 1.5mL microcentrifuge tube and thoroughly vortexed to enhance cell membrane breakdown. 100µL of chloroform were added to the sample, mixed by vortexing and let settle at RT for 3min.

The samples were centrifuged at 12,000x g for 20min at 4°C to ensure separation of the RNA containing phase (upper aqueous phase) and this supernatant was transferred to another microcentrifuge tube without disturbing the protein layer underneath. To precipitate RNA, 250µL isopropanol were added and the samples were mixed and incubated overnight at -80°C. Samples were centrifuged as above to precipitate the RNA pellet. The supernatant was removed and the pellet washed twice with 500µL of 75% ethanol. The ethanol was removed and pellet was allowed to air dry until the ethanol had evaporated. The RNA was dissolved with 30µL RNAse-free H_2O and RNA quantified as above and stored at -80°C.

2.2.7.3 RNA extraction from tissue using phenol-chloroform method

Between 0.1 and 0.2g of frozen muscle were transferred to CKD-14 ceramic beaded tubes *(Qiagen, Germany)* and 500µL of Trizol were added to each sample. Homogenisation of the sample was performed under rapid agitation of the sample 2x20 sec cycles at 5000x g using a Precellys 24 Tissue homogeniser *(Stretton Scientific, UK)* which allowed the beads to crush and breakdown the tissue. Agitation cycles were repeated if needed. Samples were centrifuged at 5000x g at 4°C for 3min to allow the removal of the insoluble fraction and the supernatant was transferred to another microcentrifuge tube. 100µL of chloroform were added to each sample and RNA extraction from that step continued as described in section 2.2.7.2.

2.2.7.4 RNA extraction from adhesive cup

Extraction from adhesive cups *(Carl Zeiss, Germany)* was achieved using the RNeasy® Micro Kit *(Qiagen, Germany)*. 300µL of lysis buffer were added to the cup and vortexed for 1h. The content was transfer to a 1.5mL microcentrifuge tube and extraction was carried out as described in the manufacturer's instructions.

2.2.8 cDNA synthesis

2.2.8.1 cDNA synthesis using Omniscript reverse transcription for RNA analysis

150ng of total RNA were diluted in RNAse-free H_2O to obtain an 11-µL-solution and denatured at 65°C for 5min then cooled on ice for 2min. 9µL of cDNA mastermix *(Qiagen, UK)* containing 2µL 10x reverse transcription buffer, 1µL 5nM dNTPs, 3.5µL RNAse-free H_2O, 0.5µL reverse transcriptase (Ominiscript), 1µL 0.1M DTT, 0.5µL random hexamer primers, 0.5µL RNAse inhibitor (Ribolock) were added and the samples were incubated at 42°C for 2h. The cDNA was diluted with 180µL of RNAse-free H_2O and stored at -80°C.

2.2.8.2 cDNA synthesis using megaplex reverse transcription with preamplification for microRNA analysis

150ng of total RNA were diluted in RNAse-free H_2O to obtain a 3-µL-solution in PCR tubes. Four and a half microliters of reverse transcription mastermix *(Qiagen, UK)* containing 0.8µL 10x Megaplex reverse transcription primers (Pool A), 0.2µL 100nM dNTPs with dTTP, 1.5µL 50U/µL multiscribe reverse transcriptase, 0.8µL 10x reverse transcription Buffer, 0.9µL 25mM $MgCl_2$, 0.1µL 50 U/µL RNAse inhibitor, 0.2µL RNAse-free H_2O were added to each tube and were incubated on ice for 5min. Samples went through 40 cycles of 16°C for 2min, 42°C for 1min and 50°C for 1s before being heated at 85°C for 5min then held at 4°C. To increase the quantity of desired cDNA a preamplification step was performed. 2.5 µL of cDNA were added to 22.5µL of preamplification mastermix consisting in 12.5µL 2x TaqMan PreAmp Master Mix, 2.5µL 10x Megaplex PreAmp primers (Pool A), 7.5µL RNAse-free H_2O and mixed. Samples

were heated at 95°C for 10min, followed by 55°C for 2min and 72°C for 2min. Samples underwent 12 cycles of 95°C for 15s and 60°C for 4min, followed by an inactivation of the enzyme at 99.9°C for 10min. Samples were diluted with 75µL of 0.1x TE pH 8.0 then stored at -80°C.

2.2.8.3 cDNA synthesis using megaplex reverse transcription without preamplification for microRNA analysis

Between 300 and 500ng of total RNA were diluted in RNAse-free H_2O to obtain a 3-µL-solution in PCR tubes. A reverse transcription primer pool was made by adding 2.5µL of the reverse transcription primers of interest and 1x TE solution to make a total volume of 1000µL. In each tube 12µL of reverse transcription mastermix *(Qiagen, UK)* containing 6µL reverse transcription primer pool, 0.3µL 100mM dNTPs with dTTP, 3µL 50U/µL multiscribe reverse transcriptase, 1.5µL 10x reverse transcription Buffer, 0.19µL 20U/µL RNAse inhibitor, 1.01µL RNAse-free H_2O were added. Samples were incubated at 16°C for 30min, then at 42°C for 30min and finally at 85°C for 5min before being held at 4°C. Samples were stored at -80°C.

2.2.9 Primer validation

Primer sequences were selected from the literature or designed to specifically amplify the gene of interest and validated through sequencing. To determine whether a set of primers was specific, 3µL of a pooled cDNA sample were mixed with 17µL of mastermix containing 10µL FAST sybr *(Qiagen, UK)*, 5µL sterile H_2O and 2µL of 2µM forward and reverse primer mix *(Sigma, USA)*. DNA was amplified using a 50-cycle PCR of 95°C for 10min initially, then 95°C for 10s and a 30s annealing/extension at different temperatures around primer melting temperatures. PCR products were analysed by electrophoresis on a 2% (w/v) agarose gel containing SYBR safe to confirm product sizes and exclude primer-dimer formation.

2.2.9.1 Agarose gel

Depending on the number of samples and the product size, different percentage or size of agarose gels were required *(Bioline, UK).* The required amount of agarose was added to the appropriate volume of 0.5xTBE followed by the addition of SYBR Safe (diluted to 1:10000 final) before microwaving the mix until the agarose had dissolved (for a 1.5% gel 1.13g of agarose and for a 2% gel 1.5g of agarose were dissolved in 75mL of 0.5xTBE). The solution was allowed to cool and poured into a tray. The gel was left to solidify before being submerged in 0.5xTBE in the gel tank. Samples were mixed with 5x loading buffe*r (Bioline, UK)* and the gel was run for 1h at 80V. Standard DNA ladders *(Bioline, UK)* were run alongside the samples to help identify the size of the product.

2.2.10 Real Time quantitative polymerase chain reaction (qPCR)

2.2.10.1 qPCR using FAST sybr for RNA analysis

SYBR green is a dye which binds to the minor groove of double stranded DNA, therefore specificity lies with sequence specific primers. Consequently, SYBR green can bind to non-specific amplicons as well as the desired product. Detection is measured by an increase in fluorescence due to dye binding.

qPCR was carried out in a 7500 FAST qPCR machine *(Applied Biosystems, UK)* using qPCR SYBR green reagents *(Qiagen, UK)*. Desired regions of DNA were amplified using primers listed in *Table 9.* In a 96-well plate, 3µL of cDNA were mixed with 17µL of mastermix containing 10µL FAST sybr, 5µL sterile H_2O and 2µL of 2µM forward and reverse primer mix. Plates were sealed with MicroAmp optical adhesive film and centrifuged at 200x g for 1min to help mixing and to remove air bubbles. Samples were heated to 95°C for 5 minutes and underwent 40 cycles of 95°C for 10 seconds followed by 65°C for 30 seconds (259). In order to further exclude non-specific binding a melt curve was performed.

To process the data, for each gene the baseline and the threshold were set up manually and when appropriate kept constant between different PCR plates. The C_T (threshold cycle) mean value of two qPCR replicates for each sample was normalised against the appropriate housekeeping genes and negative water control was added for every analysed gene. C_T is a relative measure of a target mRNA concentration in the sample and it is the intersection between the set threshold line and the amplification curve. Normalisation was carried out using the ΔΔCT method (260). When several housekeeping genes were used for data normalisation the geometric mean of those was calculated. Exclusion criteria were melt curve showing non-specific amplification or inconsistency between duplicates.

Table 9- Forward and reverse sequences of primers used in qPCR using FAST sybr.

	Gene	Primer forward sequence	Primer reverse sequence
HUMAN	*B2M*	TGCTGTCTCCATGTTTGATGTATCT	TCTCTGCTCCCCACCTCTAAGT
	CTDSP1	GACCCCAGTCCAATACCTGC	TCACTGGCTTGAAGGAGCTG
	CTDSP2	GCCAGTCAAGTTCCTCCACT	GTCCCTGGGATCTGGTAGAA
	CYR61	ACTTCATGGTCCCAGTGCTC	TGCTGCATTTCTTGCCCTTTT
	CYTB	TAGCAATAATCCCCATCCTCCATATAT	ACTTGTCCAATGATGGTAAAAGG
	GDF-15	TGCCCGCCAGCTACAATC	TCTTTGGCTAACAAGTCATCATAGGT
	GAPDH	GGTGGTCTCCTCTGACTTCAACA	GTTGCTGTAGCCAAATTCGTTGT
	HPRT	GCTATAAATTCTTTGCTGACCTGCTG	AATTACTTTTATGTCCCCTGTTGACTGG
	MSTN	ACATGAACCCAGGCACTGGT	GGTTGTTTGAGCCAATTTTGC
	PPP2CA	TGGTGGTCTCTCGCCATCTA	CATTGGACCCTCATGGGGAA
	SMAD7	TCGGACAGCTCAATTCGGAC	GGTAACTGCTGCGGTTGTAA
	SMURF1	TCGTGAGTTTATTGCATATGTAACA	CTTCCCACTGTTTTTATCACTGA
	STRN	ATCTAGAAGTGCAGGCGATGG	CTATTGGGCCTCTTCACCCCC
	TGF-β1	CCTGGCGATACCTCAGCAA	CCGGTGACATCAAAGATAACCA
	12S	AAACTGCTCGCCAGAACACT	CATGGGCTACACCTTGACCT
	16S	GCTAAACCTAGCCCCAAACC	TTGGCTCTCCTTGCAAAGTT
	18S	GTAACCCGTTGAACCCCATT	CCATCCAATCGGTAGTAGCG
	28S	ACGGCGGGAGTAACTATGACT	CTTGGCTGTGGTTTCGCT
MOUSE	*B2m*	CCGTCTACTGGGATCGAGAC	GCTATTTCTTTCTGCGTGCAT
	Cyr61	GGATGAATGGTGCCTTGC	GTCCACATCAGCCCCTTG
	Cytb	TGTTCGCAGTCATAGCCACA	TGGGATGGCTGATAGGAGGT
	Gdf-15	GGCTGCATGCCAACCAGAG	TCTCACCTCTGGACTGAGTATTCC
	Gapdh	ACTCCACTCCACGGCAAATTCA	CGCTCCTGGAAGATGGTGAT
	Hprt	GCAGTACAGCCCCAAAATGG	AACAAAGTCTGGCCTGTATCCAA
	Ppm1a	TCACCCAGGCTCATGGAAAC	TTGGCTACGAGGAGAGGACA
	Smad7	TCGGACAGCTCAATTCGGAC	GGTAACTGCTGCGGTTGTAA
	Smurf1	TGAGGAGAGGAGAGCCAGAC	CGCCTGTAGAGCCTTGCAGA
	Strn	CGATGGAACCGACTGGGAAA	CTATTGGGCCTCTTCACCCC

	12S	AAACTGCTCGCCAGAACACT	CATGGGCTACACCTTGACCT
	16S	GCTAAACCTAGCCCCAAACC	TTGGCTCTCCTTGCAAAGTT
	18S	GTAACCCGTTGAACCCCATT	CCATCCAATCGGTAGTAGCG
	28S	TGCCATGGTAATCCTGCTCA	CCTCAGCCAAGCACATACACC

2.2.10.2 qPCR using TaqMan universal PCR master mix for microRNA analysis

Taqman detection is based on a single stranded probe which is sequence specific and has been modified to contain a fluorescent tag on a terminal nucleotide and a quencher tag on the opposite end of the probe to absorb fluorescence. After binding to the region of interest the probe is cleaved by the 5'-exo-nuclease activity of the Taq polymerase and this separates the fluorophore from the quencher allowing the fluorescence to be detected. Therefore, TaqMan provides high specificity and sensitivity but the probes increase the cost of each reaction. Taqman based qPCR was used for microRNA detection to maintain specificity as microRNAs are very small in size.

qPCR was performed using a 7500 FAST qPCR machine using a 96-well plate. 1.5µL of cDNA were mixed with 18.5µL of mastermix containing 10µL 2x TaqMan Universal PCR Master mix -No uracil-N-glycosylase, 6.5µL nuclease-free H_2O and 2µL of 20x specific forward and reverse primer mix that also contained the probe *(Applied Biosystems, USA).* The 96-well plate was centrifuged at 200x g for 1min. Samples were heated to 50°C for 2min and to 95°C for 10min before undergoing 40 cycles of 95°C for 15s followed by 65°C for 1min.

Data processing was carried out as described in 2.2.10.1. A list of the analysed microRNAs and housekeeping genes can be seen in *Table 10*. Exclusion criterion was inconsistency between duplicates.

Table 10- MicroRNA probes and primers used for Taqman PCR.

MicroRNA
hsa-miR-542-3p
hsa-miR-542-5p
U6
mmu-miR-542-3p
mmu-miR-542-5p
U6

2.2.11 Protein extraction

2.2.11.1 Protein extraction from cells

C2C12 and LHCN-M2 cells were seeded at a density of $1x10^5$ cells/mL in a 6-well plate (2mL/well) and transfected 24 hours later with mirVana microRNA mimics. After incubation for 48 hours at 37°C, the medium was removed and cells were washed twice with cold 1x PBS. Cells were scraped in 1mL of ice-cold 1x PBS then incubated on ice for 5min. The suspension was transferred to a microcentrifuge tube and centrifuged for 2min at 300x g at 4°C. The supernatant was discarded and the pellet was resuspended in a mix of 100µL of 1x lysis buffer *(Cell Signaling, USA)* and 1:100 protease inhibitor cocktail *(Sigma, USA)* and left for 10min on ice. To remove cell debris, the lysate was centrifuged as described above and the supernatant containing the protein was transferred to a clean microcentrifuge tube. Samples were stored at -80°C.

2.2.11.2 Protein extraction from tissue

Between 0.1 and 0.2g of frozen TA or quadriceps muscle were transferred to CKD-14 ceramic beaded tubes and homogenised in 200µL 2x Igepal NP40 buffer *(Sigma, USA)* with Protease and Phosphatase inhibitor cocktail (100:1:1) *(Sigma, USA).* The inhibitor cocktail was added to NP40 buffer before the experiment to avoid loss of activity. Homogenisation was achieved by rapid agitation of the samples 2x20 sec cycles at 5000x g using a Precellys 24 Tissue homogeniser *(Stretton Scientific, UK)* which allowed the beads to crush and breakdown the tissue. Agitation cycles were repeated if needed. Samples were centrifuged at 10000x g at 4°C for 5 min to allow the removal of the insoluble fraction (cell debris) and supernatant (soluble protein fraction) was collected and stored at -80°C.

2.2.11.3 Protein quantification

Determination of protein concentration of the samples was performed using the DC™ Protein Assay *(Bio-Rad, USA).* In a 96-well plate well, 3µL of the sample were mixed with 20µL of Reagent S and Reagent A solution (1:50). 200µL of Reagent B were further added to the well and incubated under agitation for 15min. Absorption was read at

750nm in a micro-plate reader *(Bio-Tek, USA)* and sample concentration was calculated against the standard curve. Standards were prepared with BSA dissolved in cell lysis buffer used for protein extraction at 0, 0.125, 0.25, 0.5, 0.75, 1, 1.5 and 2 mg/mL.

2.2.12 Western blotting

2.2.12.1 SDS-Polyacrylamide gels electrophoresis

Separation of proteins by their molecular weight was performed by sodium dodecyl sulphate polyacrylamide gel electrophoresis (SDS-PAGE). Polyacrylamide gels with a 10% or 15% resolving gel and 5% stacking gel were prepared as described in section 2.1.4. 5µL of TEMED were added to the resolving and stacking gel immediately prior to their use as this reagent initiates polymerisation. The resolving gel mix was poured into a 1mm glass plate cast covered with a layer of water saturated butanol while allowing polymerisation. Once polymerisation was complete, the butanol was washed off with water and 2.5mL of the stacking gel solution was set above the resolving gel with the appropriate comb to create loading wells. Samples were diluted 5:1 with sample buffer (2x SDS) and heated at 95°C for 5min to denature proteins. Samples were loaded into a gel tank *(Bio-Rad, USA)* in 1x Running Buffer at 120V until the ladder had run though the resolving gel and was properly separated.

2.2.12.2 Protein transfer, blocking and antibody incubations

Proteins from the gel were transferred to a PVDF membrane *(Bio-Rad, USA)* (previously activated with methanol) using semi-dry transfer technique in a semi-dry transfer cell *(Bio-Rad, USA)* at 20V for an appropriate length of time dependent on the size of the protein of interest. 1x transfer buffer containing 20% methanol was used to soak the filter paper-gel-PVDF membrane-filter paper sandwich.

After the transfer, the membrane was washed with distilled water and stained with Ponceau S *(Sigma, USA)* to confirm protein transfer. The membrane was blocked by incubation in 1x TBST containing 5% milk for 1 hour at RT under agitation. The membrane was washed twice with 1x TBST and incubated with primary antibody in

blocking solution at RT for 1 hour under agitation. 2 washes with 1xTBST were performed followed by incubation with the secondary antibody in blocking solution at RT for 1 hour under agitation. The antibody working concentrations used can be found in *Table 11.* The membrane was washed twice with 1x TBST and protein detection was carried out with ECLPlus detection kit as described in the manufacturer's instructions. An Ettan DIGE imager *(GE healthcare, UK)* was used to obtain images. Image analysis was performed in Image J software *(National Institutes of Health, USA).*

Standard ladder *(Bio-Rad, USA)* was used to check that the protein band appears at the predicted molecular weight to control for primary antibody specificity. Secondary specificity was checked by incubation of the membrane with secondary antibody without primary blotting to guarantee that no signal was observed.

Ponceau red staining (after transfection) or Amido black staining (after blot developing) were used to control for protein loading and transfer efficiency. Membranes were briefly incubated with the staining solution then rinsed with 1x TBST for Ponceau or with de-staining solution for Amido Black and scanned. The bands from the protein of interest were normalised against the Ponceau or Amido Black staining scanned image by Image J.

Table 11-Antibodies and working concentrations used for Western Blotting and immunostaining.

	Antibody	Working concentration	Protein size (KDa)	Company
1a Ab	Goat anti-SMAD7	1/200	46	Santa Cruz
	Rabbit anti-SMURF1	1/200	86	Life technologies
	Goat anti-P-SMAD2/3	1/50	58	Santa Cruz
	Rabbit anti-CYTB5	1/500	38	Pierce
	Rabbit anti-MRSP10	1/500	21	Pierce
	Rabbit anti-RPS23	1/100	16	Novus
	Mouse anti-puromycin	1/10000	-	Millipore
2a Ab	Polyclonal goat anti-rabbit	1/3000	-	Dako
	Polyclonal rabbit anti-goat	1/3000	-	Dako
	Polyclonal sheep anti-mouse	1/10000	-	GE Healthcare
	Alexa Fluor 488 goat anti-rabbit IgG (H+L)	1/500	-	Invitrogen
	Alexa Fluor 568 goat anti-rabbit IgG (H+L)	1/500	-	Invitrogen

2.2.13 Immunoprecipitation

In transfected cells, SMAD7 protein expression was low and protein detection was not possible by Western blot. To increase the SMAD7 concentration in the sample we performed an immunoprecipitation. Pre-equilibration of protein A/G PLUS-Agarose beads *(Santa Cruz Biotechnology, Germany)* consisted of centrifuging 150µL of beads at 200x g for 5min at 4°C. The supernatant was discarded and the beads were washed three times with 750µL of 1x PBS by centrifuging at 200x g for 1min at 4°C. After the final centrifugation, the beads were resuspended in 300µL of PBS. Pre-clearing of the sample was performed at 4°C for 2h by adding 20µL of pre-equilibrated beads to 60µL of cell lysate or 5µg of muscle homogenate and to facilitate mixing in the rotating wheel 400µL of 1x PBS were also added. In parallel, 100uL of pre-equilibrated beads were blocked with 1mg/mL BSA during 2h at 4°C under rotation. Blocked beads were washed with 25µL 1x PBS three times and they were collected by centrifugation at 500x g at 4°C for 1min. The pre-cleared sample was centrifuged at 500x g at 4°C for 1min and the supernatant was transferred to a microcentrifuge tube containing the 20µL of blocked beads. 5µL of primary antibody (rabbit anti-SMAD7 antibody H-79, *Santa Cruz*) were added and samples were incubated overnight at 4°C on a rotating wheel. Immunoprecipitates were collected by centrifugation at 200x g for 5min at 4°C and supernatant was discarded. The pellets were washed four times with 1x PBS and finally diluted in 20µL of 1x PBS. The beads were diluted 1:1 with sample buffer (1x RSTB containing 2% mercaptoethanol) then analysed by Western blotting as described in section 2.2.12. To assure specific binding, a different anti-SMAD7 antibody (*goat, P20, Santa Cruz)* was used in the Western blot.

2.2.14 Immunostaining for p-Smad-2/3 localisation

After treatment, cells were washed twice with 1x PBS then fixed with 4% PFA followed by 2 washes with 1x PBST (0.05% Tween). Cells were incubated with 1xPBS containing 0.3% Triton X-100 detergent *(Sigma, USA)* for 15 minutes at RT and washed twice with 1x PBST. After 1 hour incubation with a blocking solution of 1x PBST containing 5% BSA, the primary antibody (p-SMAD2/3) *(Table 11)* in blocking solution was added to

cells for 1 hour at RT. The cells were washed 3 times with 1x PBST then incubated with secondary antibody in blocking solution for 1 hour at RT. Cells were then incubated in 1x PBST supplemented with DAPI (stock solution of 5mg/ml diluted 1:10000 in 1xPBS) to stain nuclei, then washed a final two times in 1x PBST. Images were taken under 20x objective and the immunofluorescent signal was analysed using a Zeiss Axiovert 200 microscope and Velocity software *(Perkin Elmer, USA).* Using Image J software, a macro was used to detect the blue nuclei, create a mask and measure the average of green or red (p-SMAD2/3) intensity in each nucleus, and thereby determining the mean fluorescence per nucleus. All parameters such as thresholds, exposure times and brightness were kept constant for all image acquisitions.

2.2.15 Hypoxia treatment

C2C12 and LHCN-M2 cells were seeded at a density of $5x10^4$ cells/mL in 6-well plates (2mL/well) and were left to recover overnight. Cells were incubated under hypoxia (2% O_2) or normoxia (16% O_2) at 37°C and 5% CO_2 for 48h (C2C12) or 48h, 72h and 96h (LHCN-M2). RNA was extracted and miR-542-3p and miR-542-5p levels were measured as described above (Sections 2.2.7.2 and 2.2.8.3).

2.2.16 *In vivo* experiments

2.2.16.1 Insert miR-542 immature sequence in pCAGGS-EGFP vector

2.2.16.1.1 Preparation of miR-542 immature sequence insert

Forward and reverse primers for a 500bp DNA fragment containing the entire pri-miR-542 sequence were designed including a restriction enzyme site for BglII at the beginning of each primer to allow for cloning of the miR-542 sequence into the 3'-UTR of the EGFP in pCAGGS-EGFP vector. The miR-542 sequence was obtained from Ensembl: Gene-sequence *(http://www.ensembl.org/index.html)* and BglII was chosen because no restriction sites for this enzyme were found in the vector nor in miR-542 sequence. miR-542 sequence amplification was performed by PCR from mouse

genomic DNA obtained from C2C12 cells. Genomic DNA was obtained by seeding C2C12 cells at a density of $5x10^4$ cells/mL in 6-well plates (2mL/well) and allowing them to recover and grow overnight. Cells were washed with 1xPBS and incubated with 800µL of lysis buffer (200mM Tris-HCl pH 7.5, 25mM EDTA pH 8.0, 250mM NaCl, 0.5% SDS) at 37°C for 1h. Cell lysates were transferred to microcentrifuge tubes and 8µL of Proteinase K solution (10mg/mL) *(Sigma, USA)* and 2µL RNAse solution (10mg/mL) *(Qiagen, Germany)* were added into each tube and samples were mixed and incubated at 50°C for 1h. 280µL of saturated NaCl were added to the samples and vortexed for 5 min. Samples were centrifuged at 6000x g for 10min and the supernatant was transferred to another microcentrifuge tube. 600µL of isopropanol were added and the samples were mixed and then incubated for 3min before centrifuging at 6000x g for 3min. The pellet was washed with 1mL of 70% ethanol and the samples were centrifuged at 6000x g for 10min. The pellets were allowed to air-dry before being resuspended in 80µL of 1xTE. Quantification of DNA was performed using a Nanodrop spectrophotometer *(ND1000, Wilmington, USA).* The genomic DNA was then amplified by PCR using Taq polymerase because it adds a 3' A-overhang to the end product needed for the ligation with PGEM-T vector.

0.25µL of mouse genomic DNA template (10-100ng) was mixed in a PCR tube with 19.75µL of mastermix containing 2µL 4µM miR-542 forward primer, 2µL 4µM miR-542 reverse primer, 0.8µL dNTPs, 0.1µL Taq polymerase (Qiagen, Germany), 2µL 10x Taq Buffer and 12.85µL ddH_2O. Samples were denatured at 94°C for 5min before undergoing 25 cycles of 94°C for 30s, 60°C for 30s and 72°C for 30s. Samples were heated at 72°C for 10min and were held at 4°C. Samples were kept at -80°C.

2.2.16.1.2 TA cloning into a pGEM-T vector

TA cloning relies on the lack of proof reading ability of some DNA polymerase, such as Taq polymerase, which results on the non-removal of the extra nucleotide it adds. In the majority of the cases, it adds an adenine (A) overhang in the 3' of each end of the PCR product. The 3'-A on each end of the product facilitates the direct cloning through hybridisation into a linearized cloning vector which contains a 3' thymine overhang on each end.

The PCR product obtained before was run on a 2% agarose gel after adding 5x loading dye *(Bioline, UK).* The gel was run at 80V for 90-120 min. miR-542 sequence bands were visualized under UV light *(ChemiDoc XRS+, Bio-Rad, USA)* and were extracted using a scalpel and put into a microcentrifuge tube. Immediately after, DNA extraction was performed with a Mini Elute Gel Extaction kit *(Qiagen, Germany)* consisting of adding into the microcentrifuge tube 3 volumes of QG buffer per volume of gel. Samples were heated at 50°C for 10min, vortexing every 2min. 1 volume of isopropanol was added and samples were inverted. The mixture was placed into an extraction column before centrifuging at 3500x g for 1min at RT. 500uL of QG buffer were added to the column and samples were centrifuged at 3500x g for 1min. 750uL of PE Buffer were added to columns and the samples allowed to stand for 5min before centrifuging at 3500x g for 1min. The DNA was eluted into a new microcentrifuge tube by adding 20uL of EB Buffer into the column, allowing the column to stand for 1min before centrifuging at 3500x g for 1min. A further 10uL of EB Buffer were added to the column and the same process as before was repeated. 30uL of miR-542 DNA were kept on ice for use.

Ligation of the miR-542 sequence and PGEM-T was performed by mixing into a 0.2-mL PCR tube 5µL of 2x Rapid Ligation Buffer, 1µL of pGEM-T vector (50ng), 1µL of gel extraction product (a molar ratio of 1:3 vector:insert was used), 1µL of T4 DNA Ligase and 2µL nuclease-free water. The reaction was incubated overnight at 4°C.

E. Coli were transformed with the ligated miR-542 and pGEM-T vector and the plasmid was obtained as described in section 2.2.1.2. However, before spreading the transformed bacteria on the LB-Agar Ampicillin plates, plates were prepared for blue-white screening (261) by spreading 40µL of 0.1 M Isopropyl β-D-1-thiogalactopyranoside *(IPTG, Sigma, USA)* and 16µL of 50 mg/mL 5-bromo-4-chloro-3-indolyl-β-D-galactopyranoside *(X-gal, Sigma, USA)* on top of each LB-Agar Ampicillin plate and allowing 30min for absorption. Only white colonies were picked for further screening. Blue-white screening is a technique that allows a rapid detection of recombinant bacteria containing a plasmid and a sequence of interest. The technique is based on *E. Coli* carrying the lacZ deletion mutation which contains the ω-peptide, while the plasmids used for transfection carry the lacZa sequence which encodes for

the α-peptide, which are the first 59 amino acids of β-galactosidase enzyme (261). Neither of the peptides is functional by itself. However, when they are expressed together they form a functional β-galactosidase enzyme. Therefore, if the insert is ligated in the vector, it causes the disruption of lacZa gene preventing the production of functional β-galactosidase. If the insert is not present, the enzyme is produced and X-gal hydrolysis occurs producing galactose and an indigo compound that turns colonies blue. Purified plasmids were digested with BglII restriction enzyme to release the insert from the vector. miR-542 pGEM-T digestion consisted on mixing 2µL of 10x Buffer (3.1), 1µL of restriction enzyme (BglII), 0.5µL of BSA, 4µL of plasmid and 12.5µL of nuclease-free water in a microcentrifuge tube and incubating the solution at 37°C for 90min.

To confirm the size of the insert, digests were run in a 2% agarose gel. Plasmids positive for miR-542 sequence of the correct size were Sanger DNA sequenced by Beckman Coulter Genomics *(UK)* using the forward T7 promoter sequencing primer (as PGEM-T contains a T7 promoter).

2.2.16.1.3 Cloning into the mammalian expression vector (pCAGGS-EGFP)

To facilitate ligation between the mammalian expression vector and the miR-542 purified and digested insert, pCAGGS-EGFP plasmid was cut by BglII restriction enzyme and the 5' phosphates were removed with calf intestinal alkaline phosphatase *(*CIAP*, New England BioLabs, UK)* to reduce self-ligation. Digestion of the pCAGGS-EGFP plasmid was carried out by mixing in a microcentrifuge tube 5µL of 10x Buffer (3.1), 5µL of restriction enzyme (BglII), 2.5µL of BSA, 16µL of plasmid, 5µL of CIAP and 16.5µL of nuclease-free water and incubating the mixture at 37°C for 90min followed by a phosphatase deactivation step at 65°C for 20min. Ligation was performed at 4°C overnight in 0.2-mL PCR tubes containing a molar ratio of 1:3 vector:insert with 50ng of cut plasmid, 1µL of T4 DNA ligase, 2µL of Ligase Buffer T4 DNA and nuclease-free water to make a 10-µL reaction. *E. Coli* were transformed with the ligated miR-542 and pCAGGS-EGFP vector and the plasmid was obtained as described in section 2.2.1.2. The orientation of miR-542 insert was checked by restriction enzyme digestion (using HindIII and EcoNI). The size of the products was determined by agarose gel

electrophoresis and compared to the expected sizes *(Figure 11).* Vectors with an insert in the correct orientation were sent for Sanger DNA sequencing by Beckman Coulter Genomics *(UK)* using the miR-542 forward primer and miR-542 reverse primer separately (primers used to amplify mouse genomic DNA). Sequencing confirmed the correct pCAGGS-EGFP-miR-542 vector had been obtained.

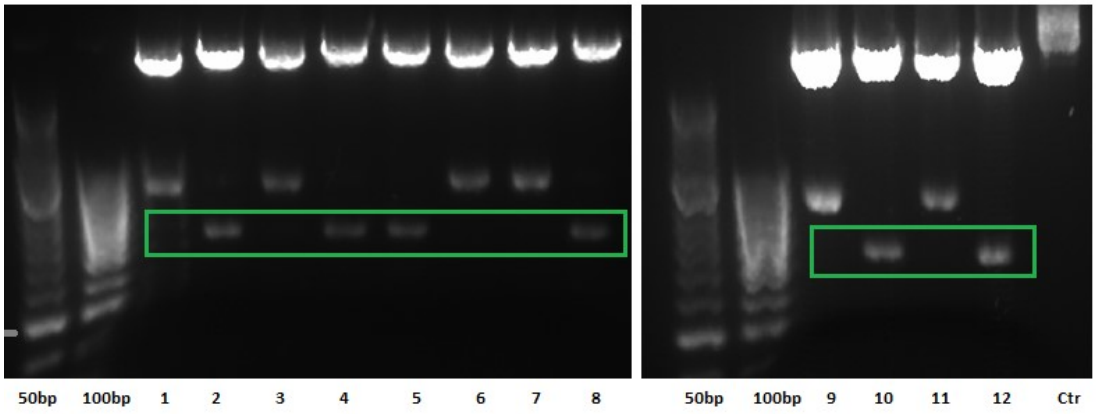


Figure 11- miR-542 orientation check in pCAGGS-EGFP vector.

Products of the pCAGGS-EGFP and miR-542 ligation were digested and run on an agarose gel to determine orientation. The expected size bands if the insert orientation was correct were 573 bp (squared in green) and 5169 bp whereas opposite insert orientation would produce 2 bands at 866 bp and 4876 bp. Therefore samples 2, 4, 5, 8, 10 and 12 were sent to be sequenced.

2.2.16.2 Mouse preparation and electroporation

All *in vivo* work was performed under the project license PPL 70/8297 and in accordance with the Animals Scientific Procedures Act 1986. Home Office licensed me with Personal License (PIL number: IDF691606) to carry out regulated procedures on living animals.

2.2.16.2.1 Mice description

Six-week old male mice of the C57BL/6 strain were used. Once received in the facility, up to 5 mice were kept in an individually ventilated cage (IVC) and allowed to acclimatise for 1 week. Health monitoring and handling was carried out daily.

2.2.16.2.2 Mouse preparation

The day that the procedure was carried out mice were weighed to determine the correct amount of anaesthesia given by intraperitoneal (IP) injection. 5µL/g of Hypnorm/Hypnovel (H/H) *(Janssen Animal Health, UK and Roche, UK, respectively)* mix were injected in each mouse. H/H mix was prepared by mixing 1:1 v/v Hypnorm and water and separately 1:1 v/v Hypnovel and water. Finally, both solutions were mixed 1:1 v/v to obtain the H/H mix. When mice lost pedal reflex, both back legs were shaved using a small trimmer *(WAHL, USA)* and 25µL of 0.4U/µL bovine hyaluronidase *(Sigma, USA)* were injected into both TAs. Hyaluronidase is an enzyme that breaks down hyaluronan, a component of the extracellular matrix, which facilitates DNA electroporation by improving penetration of the tissue by the injected DNA (262). Animals were returned to a cage which was placed half on a heat mat at 37°C and were allowed recovery for 2h.

2.2.16.2.3 Electroporation

Animals were anaesthetised via inhalation with isofluorane *(IsoFluo, USA)* using 5% anaesthetic for induction and 2-3% for maintenance of anaesthesia in oxygen. 25µL of 1µg/µL plasmid were injected in the TA of mice with an insulin syringe, pCAGGS-EGFP (control vector) in the left leg and pCAGGS-EGFP-542 in the right leg. Plasmids were diluted to the appropriate concentration with ddH_2O. Tweezerodes were placed side to side the TA and the distance between the tweezerode plates was measured so that the appropriate voltage could be applied. Electrocardiography (ECG) gel *(Parker Laboratories, USA)* was used on the top of the tweezerodes to facilitate current transmission in the skin. Electroporation was performed at 175V/cm, pulse length of 20ms and 10 pulses 1Hz *(ECM830 Electro Square Porator, BTX, USA)* (263). Immediately after electroporation, animals were removed from anaesthesia and placed in a cage which was placed half on a heat mat at 37°C to allow recovery. Animals showed no signs of altered behaviour and were fed with normal chow.

2.2.16.3 Refinements

Following electroporation, animals were constantly observed and checked for signs of dehydration or lameness until full recovery, if dehydration was observed sodium chloride 0.9 % was given subcutaneously or if lameness was observed temgesic

(analgesic) was provided, respectively. 30G needles were used for the H/H IP. When animals were submitted to the first anaesthesia, eye ointment *(Lacri-lube, Allergan, UK)* was applied to their eyes to help lubricating and moistening the eyes and avoid dryness.

2.2.16.4 Processing samples

3 days after electroporation, mice were humanely killed by cervical dislocation using as a confirmation method the permanent cessation of the circulation. Immediately after sacrifice the TA muscles were excised and weighed. TA muscles were mounted on a cork leaning the bottom against a needle. A minimal amount of cryo-embedding media, Optimal Cutting Temperature compound (OCT) *(Tissue-Tek, NL)*, was placed at the bottom of the TA to fix the muscles onto the cork and they were snap frozen using isopentane chilled in liquid nitrogen. This technique consists of placing liquid nitrogen in a Dewar flask and lowering a stainless steel container of isopentane *(Sigma, USA)* into the liquid nitrogen using tongs (adapted from (264)). When freezing, isopentane becomes white and opaque and can be taken out of the liquid nitrogen. TA muscles embedded onto the cork were placed into the nitrogen-cold isopentane and then wrapped up with foil and placed into liquid nitrogen and stored at -80°C.

2.2.16.5 Sectioning

The cork containing the TA was fixed onto a metal block with OCT allowing sectioning. Sectioning of the TA muscles was performed starting from the top of the muscle towards the base fixed on the cork. The microtome *(Bright Instruments, UK)* was placed on a cryostat at -20°C and the freezing shelf was set to -30°C. Sections were cut in 10µm thickness using a 5° angled knife from 5 evenly spaced levels (adapted from (263)). A representative section from each of the 5 levels was captured onto a frost-free glass slide, obtaining a total of 5 slides to be used for histological purposes. 10-15 sections from levels 3 and 4 were captured onto a polyethylene naphthalate (PEN) membrane slides for mRNA and microRNA analysis and this was repeated 4 times per muscle. The subsequent 40 sections from each level were divided into two different microcentrifuge tubes for mRNA and protein analysis and stored at -80˚C *(Figure 12).* The slides were allowed to air dry for 15min before storage at -80˚C until use. This chosen sectioning approach allowed the analysis of protein and

RNA/microRNA from the same region of each muscle (or levels) as the electroporation efficiency is unequal through the muscle. This technique allowed us to analyse the areas with highest electroporation efficiency.

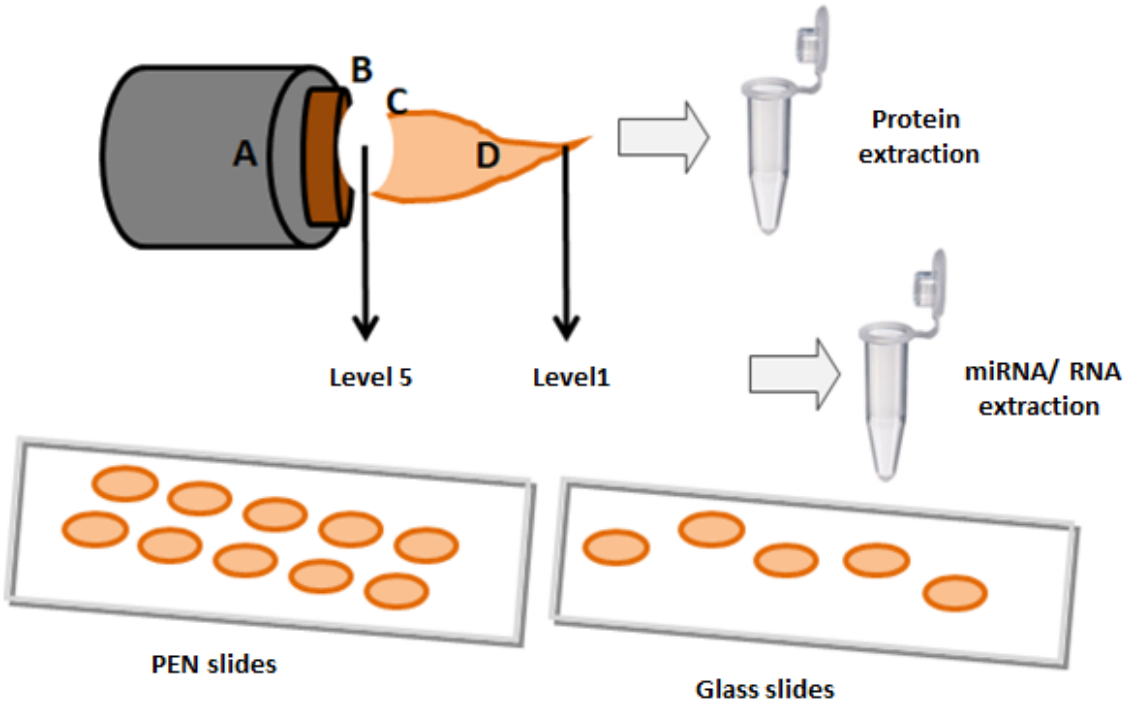


Figure 12- Schematic representation of TA sectioning.

TA muscle (D) was attached to a cork base (B) through OCT embedding (C). The cork base was then attached to a metal cylinder (A) applying also OCT in the base of the cork. The metal cylinder was then placed in the microtome and sections from different levels were taken and either placed on slides or on microcentrifuge tubes. From each sample, we had 4 different sampling methods: 2 collection microcentrifuge tubes for protein or microRNA/RNA extraction and two types of slides, glass slides or PEN slides for laser capture.

2.2.16.6 Laser-capture microdissection (LCM)

PEN sections were submerged for 30s in cold RNAse free water to remove any remaining OCT surrounding the muscle section. To minimise RNA degradation, sections were dehydrated with alcohol by submerging the samples in increasing concentrations of alcohol (70% ethanol for 30s, 90% ethanol for 30s and 100% ethanol for 30s). The PALM laser capture microdissection system *(Carl Zeiss, Germany)* with a 20x objective and a fluorescein isothiocyanate (FITC) filter was used to select fluorescent, positive electroporated fibres (265). This approach was selected because electroporation efficiency was less than 50%, thus it allowed us to only select the fibres that have been

transfected with our control and treated vectors and to compare gene expression more precisely. Fibres of interest were laser-captured using RoboLPC mode on the PALM Robo software *(Carl Zeiss, Germany)*. 600 regions of interest were marked and the laser option was switched on to produce the cuts after optimising the energy and focus (values were around 48 and 70, respectively). An opaque, adhesive cup microcentrifuge tube was placed on the top of the sample and the selected fibres were catapulted into the cup using a laser pulse. RNA was extracted as described in section 2.2.7.4.

2.2.17 Data analysis

Statistical analysis was performed in Graphpad® Prism Version 5.0 software *(GraphPad Software, USA).* Data are expressed as mean± SEM or median and 10-90 percentiles or inter-quartile range (IQR) depending on whether the data were normally or non-normally distributed, respectively. Normality was assessed by Kolmogorov-Smirnov test, d'Agostino and Pearson omnibus normality test and Shapiro-Wilk normality test. For analysis including multiple groups, an ANOVA analysis was performed. For statistical analysis of qPCR, data was log transformed to equalise variance and Student's T-Test for normally distributed data or Mann-Whitney U test for non-normally distributed data were used. Correlations analysis was performed using the Pearson correlation test to identify linear associations, or using the Spearman test for non-linear correlations. For *in vivo* data, comparison between groups was performed using ANOVA analysis and differences between two groups were further analysed using Paired-t-test (normally distributed data) or Wilcoxon matched-pairs signed rank test (not normally distributed data). $p<0.05$ was considered statistically significant.

CHAPTER 3: Clinical observations of miR-542-3p & miR-542-5p in muscle wasting diseases

3.1 Rationale

Skeletal muscle wasting is a common comorbidity in a range of acute and chronic diseases. A wide range of mechanisms have been studied to try to understand the mechanisms driving this wasting examining the contribution of both intracellular and extracellular factors. For example, our group has analysed the expression and activity of several pathways including the signalling pathways regulated by myostatin and GDF-15 (30,266). Recently, the group has started to investigate the role of microRNAs as they can target multiple components of different pathways so could regulate several different pathways leading to atrophy. Moreover, microRNA expression is altered in response to muscle use and disease for example in response to exercise (240,267-270), and in primary myopathies (241). Previous studies in patients with muscle dysfunction as a consequence of chronic disease have also shown changes in microRNA expression. For example, in COPD patients, miR-1 levels are suppressed in quadriceps of COPD patients compared to controls and miR-499 levels associate with fat free mass index (FFMI) (250). This decrease in miR-1 is associated with an increase in one of its targets, HDAC4, a change that may contribute to the reduction in MHCI and to a fibre shift from a predominance of slow fibres to a predominance of fast fibres. Having established that muscle of COPD patients had an altered microRNA expression profile, our group performed a microRNA screen to identify differences in microRNA expression in the quadriceps of COPD patients with a low fat free mass index (LFFMI) compared to those with a normal FFMI (NFFMI). This study showed that quadriceps expression of miR-675 was different between LFFMI and NFFMI patients, being higher in LFFMI patients (271) and negatively associated with muscle mass, but no association was found in healthy individuals. Re-analysis of the screen data comparing COPD patients as a whole group with controls, identified eighteen microRNAs that were differentially expressed in the COPD patients, six microRNAs were up-regulated in the patients compared to controls, 5 of which were derived from a single cluster on the X

chromosome (miR-542-3p and -5p, miR-424-3p and -5p, miR-450a and miR-450b), and 12 microRNAs were down-regulated in the COPD patients compared to controls, including miR-210 (162).

Analysis of microRNA expression in a larger cohort of patients suffering from muscle wasting showed that miR-542-3p expression was associated with lung function and physical performance in COPD patients as well as in a healthy older cohort *(experiments performed by Dr Jen Lee)*.

COPD is primarily a disease of the lungs in which a chronic obstruction of the lung airflow interferes with normal breathing and it is not fully reversible. However, it also has systemic complications that include a loss of exercise capacity (272). As a consequence, measurements of disease severity include both measurements of lung function and exercise performance. Lung function measurements include measurements of airflow obstruction, lung volumes and gas diffusion. These measurements analyse different components of the lung impairment. To quantify gas diffusion the transfer factor for carbon monoxide (TL_{CO}) is measured (273,274). This analysis determines the ability of carbon monoxide to diffuse from the alveoli into the blood and is primarily a measure of emphysema. A related parameter is the oxygen partial pressure (tension) in arterial blood (PaO_2) (275). Large airway obstruction is determined by measuring FEV_1 after taking a breath with a maximal inspiratory effort and is also considered to be an important measure of pulmonary function (276,277). The FEV_1/FVC ratio, also known as Tiffeneau-Pinelli index, is used in the diagnosis of obstructive and restrictive lung disease (278,279). It represents the proportion of a person's vital capacity that they are able to expire in the first second of forced expiration. FEV_1/FVC=0.7 is used as a cut off value, for the diagnosis of restrictive lung diseases with airflow obstruction at lower values and normal airflow at higher values (280). To analyse exercise capacity, several measurements can be used. The six-minute walk (6MW) test measures the distance an individual is able to walk over a total of six minutes on a hard, flat surface and has been used extensively to measure muscle exercise tolerance in chronic respiratory disease (281) and heart failure (282) as well as in other populations suffering from muscle loss such as the healthy elderly population (283,284). Similar tests include the 3m walking test in which the time that takes to

walk 3m at normal walking speed is measured. The timed up and go test (TUG) is a simple test used to assess a person's mobility and requires both static and dynamic balance. It uses the time that a person takes to rise from a chair, walk three meters, turn around, walk back to the chair, and sit down. The TUG test is used frequently in the elderly population, as it is easy to perform and can generally be completed by most older adults (285). FFMI which is calculated as fat-free body mass in kg divided by the square of the height in meters has been shown to accurately determine the nutritional status of subjects and *Luo Y. et al*. found correlations between low FFMI and several parameters such as frequent exacerbation, decreased pulmonary function, older age, 6MW test and worsened dyspnoea in COPD (286). Muscle strength can be quantified as a volitional manoeuvre using the maximal voluntary contraction (MVC) test which is the maximum force which a subject can produce in a specific isometric exercise or it can be measured using a non-volitional manoeuvre by electrical or magnetic stimulation of peripheral nerves to provoke muscle contractions (Twitch strength, Tw) with the resulting force is measured (287).

Since Dr Jen Lee showed that miR-542-3p expression was associated with lung function and physical performance in COPD patients as well as in a healthy older cohort, in this chapter we aimed to determine whether miR-542-5p was also associated with the same parameters in these cohorts and whether miR-542-3p/5p expression was elevated in patients with established ICUAW.

3.2 Hypothesis

The above rational suggested the following hypothesis:

1) miR-542-3p and miR-542-5p expression would be elevated in the quadriceps of patients suffering from muscle wasting.
2) Increased miR-542-5p levels would associate with poor lung capacity and physical performance.

3.3 Results

3.3.1 miR-542-5p levels are increased in COPD patients and associate with reduced lung function

Previous work in the group had shown that miR-542-3p was increased in a large cohort of COPD patients *(Figure 13, A)* and was associated with reduced lung function as shown by TL_{CO} *(Figure 14, A)*, PaO_2 *(Figure 14, C)* and FEV_1 *(Figure 14, E).*

To determine whether miR-542-5p was also elevated in the muscle of COPD patients we analysed its expression in patients and controls and found a 6-fold increase ($p<0.001$) in the quadriceps of the COPD patients (both sexes and all GOLD grades) *(Figure 13, B)*, whereas miR-542-3p only showed a 4-fold increase. Interestingly, a strong association was found between miR-542-3p levels and miR-542-5p levels in the COPD cohort *(Figure 13, C)*, suggesting that miR-542-5p would also associate with reduced lung function. As expected, miR-542-5p also inversely correlated with TL_{CO}% predicted ($r=-0.62$, $p<0.001$, *Figure 14, B*) and PaO_2 ($r=-0.38$, $p<0.001$, *Figure 14, D*). miR-542-5p also inversely correlated with FEV_1 measurements in the patients ($r=-0.59$, $p<0.001$, *Figure 14, F*). Both miR-542-5p and miR-542-3p were more tightly correlated with TL_{CO} measurements than with PaO_2 or FEV_1.

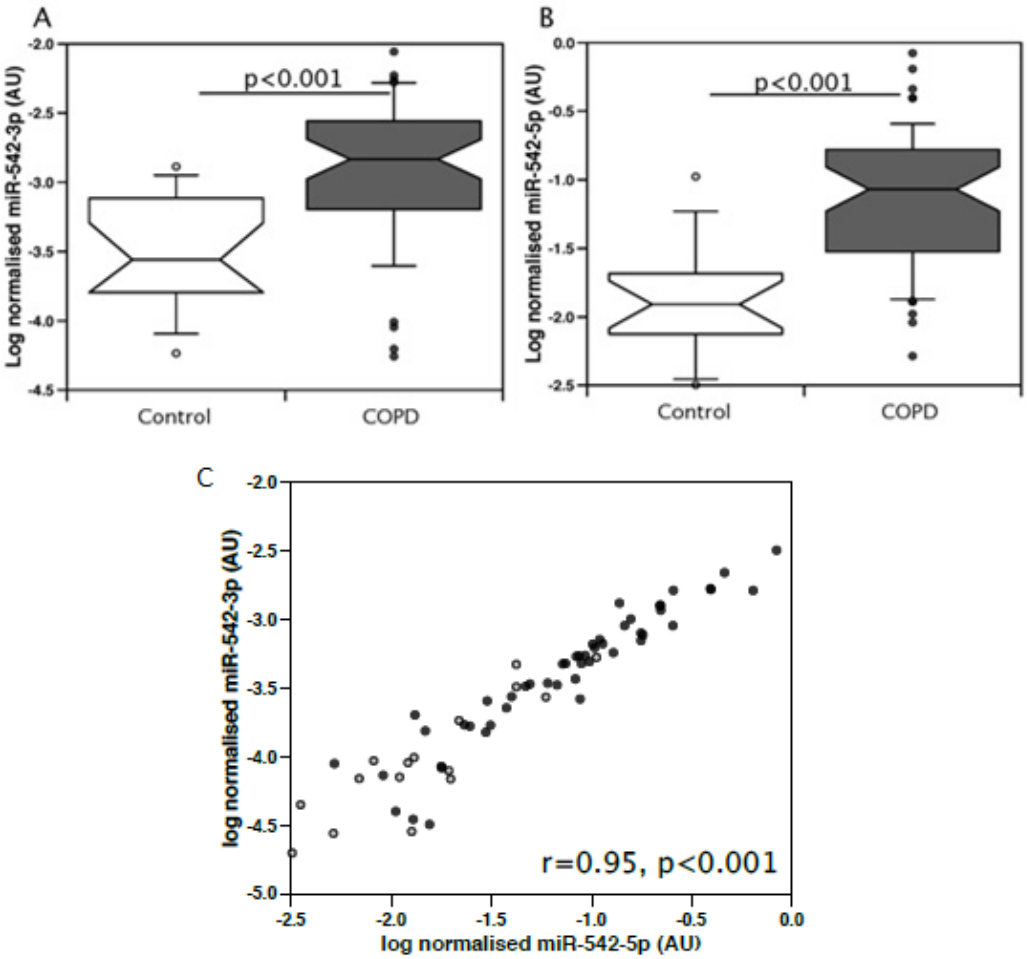


Figure 13- miR-542-3p/5p are increased in patients with COPD.

miR-542-3p/5p were quantified in quadricep biopsies from COPD patients (n=52) and healthy age-matched controls (n=16). miR-542-3p data were generated by Dr Jen Lee. Box and whiskers plot showing that the expression of miR-542-3p (A) and miR-542-5p (B) are increased in patients compared to controls (whiskers to 90% with outliers shown). There is an association between miR-542-5p expression and miR-542-3p expression in the COPD cohort (C). Patients are shown as filled circles, controls as open circles. Correlations were analysed by Pearson´s test as data had a linear association, showing p and r values. miR-542-3p and miR-542-5p levels were normalised to U6 and RNU48.

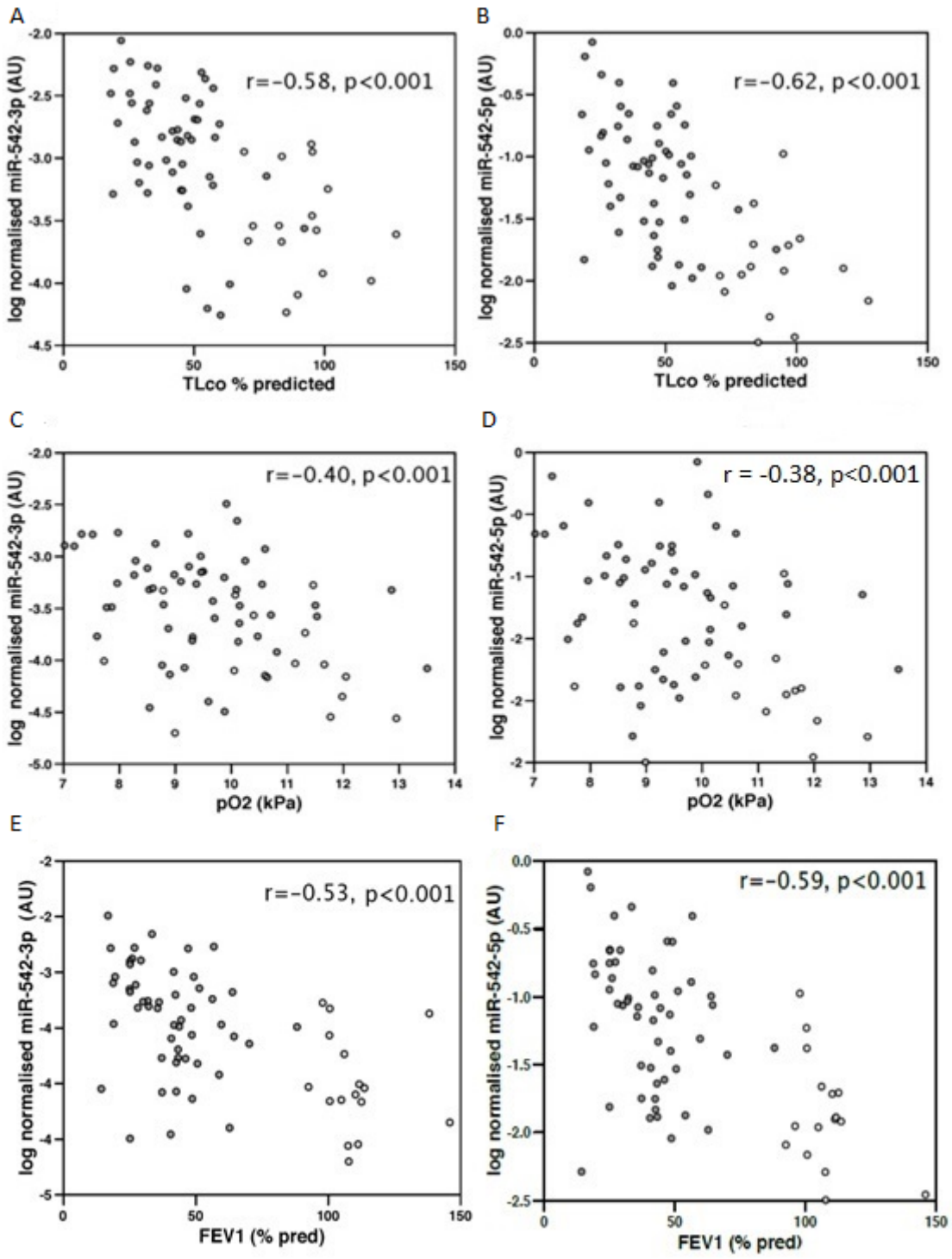


Figure 14- miR-542-3p/5p associated with lung function in patients with COPD.

miR-542-3p/5p were quantified in quadriceps biopsies from COPD patients (n=52) and healthy age-matched controls (n=16). miR-542-3p data were generated by Dr Jen Lee. miR-542-3p/5p expression was inversely correlated with lung function measured as TL_{CO} % predicted (A-B) and as pO2 (C-D). miR-542-3p/-5p levels also inversely associated with FEV_1 measurements (E-F). Patients are shown as filled circles, controls as open circles. Correlations were analysed by Pearson´s test as data had a linear association, showing p and r values. miR-542-3p and miR-542-5p levels were normalised to U6 and RNU48.

3.3.2 miR-542-5p associate with reduced physical performance in COPD patients

As previous work in the group had shown that miR-542-3p was associated with reduced physical performance in COPD patients as shown by 6MW distance % predicted *(Figure 15, A)*, MVC % predicted *(Figure 15, C)* and TwQ % predicted *(Figure 15, E)* we analysed if miR-542-5p also associated with these parameters.

miR-542-5p was inversely associated with the exercise capacity measurement (6MW distance % predicted) ($r=-0.59$, $p<0.001$, *Figure 15, B*) and with strength assayed both as a volitional manoeuvre (maximal voluntary contraction as a % of predicted, MVC%, *Figure 15, C-D*) and as a non-volitional manoeuvre (as twitch quadriceps force, TwQ%, *Figure 15, E-F*). Stronger associations were seen between miR-542-5p and in MVC ($r=-0.43$, $p<0.001$, *Figure 15, D*) than TwQ ($r=-0.29$, $p=0.024$, *Figure 15, F*). In this cohort, miR-542-3p/-5p expression was not higher in patients with a low FFMI compared to those with a normal FFMI, nor in weak patients compared to those with a normal strength (data not published). The physical performance measurement that correlated most strongly with miR-542-5p and miR-542-3p levels was 6MW test.

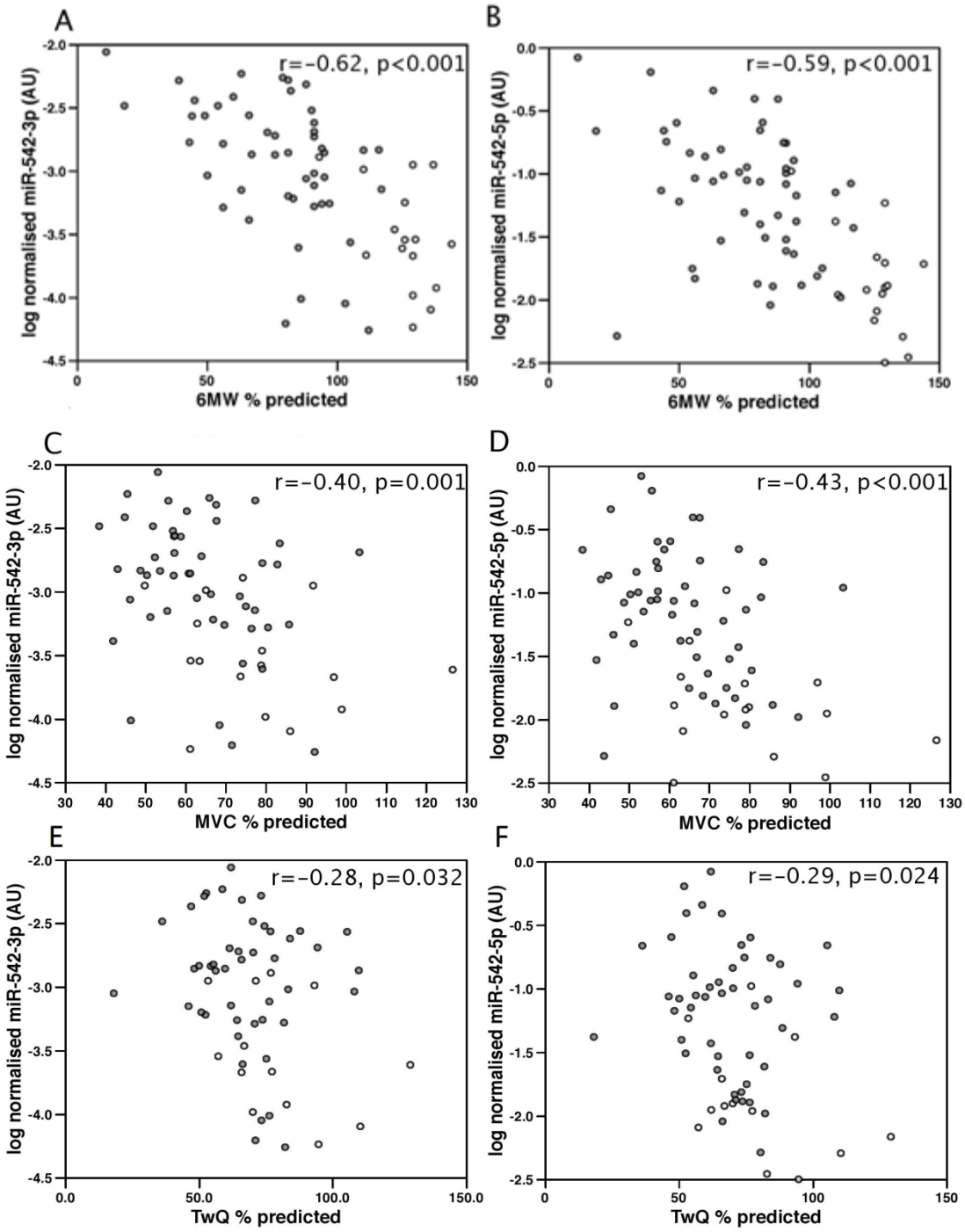


Figure 15- In COPD patients miR-542-3p/5p levels are increased and associated with muscle physiology.

miR-542-3p/5p was quantified in quadriceps biopsies from COPD patients (n=52) and healthy age-matched controls (n=16). miR-542-3p data were generated by Dr Jen Lee. miR-542-3p/5p were inversely correlated with 6MW test (A-B) and strength as MVC % predicted (C-D) and as TwQ (E-F). Patients are shown as filled circles, controls as open circles. Correlations were analysed by Pearson´s test as data had a linear association, showing p and r values. miR-542-3p and miR-542-5p levels were normalised against U6 and RNU48.

3.3.3 miR-542-5p levels inversely associated with physical performance in a cohort of older people

Previous work in the group had shown that quadriceps expression of miR-542-3p was associated with reduced physical performance in a cohort of older people (population susceptible to muscle loss). Samples were obtained from the Hertfordshire sarcopenia study (HSS) (288,289) and associations were found with 6m TUG test *(Figure 16, A)* and 3m gait speed test *(Figure 16, C)*. However, no association was found with FFMI *(Figure 16, E)*. Interestingly, miR-542-3p levels were elevated in the patients defined as having sarcopenia *(Figure 17, A)*.

To determine if miR-542-5p was also associated with these parameters in this cohort, we quantified its expression in the same samples. Consistent with the observations in the COPD patients there was a strong association between miR-542-3p levels and miR-542-5p levels in the HSS cohort *(Figure 17, C)*, which raised the hypothesis that miR-542-5p might also associate with reduced physical performance. As expected, increased expression of miR-542-5p also associated with poorer physical performance as indicated by longer times to complete the 6m TUG test (r=0.30, p=0.019, *Figure 16, B*). Moreover, miR-542-5p also directly associated with a slower 3m gait speed (r=0.41, p=0.001, *Figure 16, D*), suggesting an association with quadriceps function. Although miR-542-5p was not associated with FFMI in the HSS participants (r=-0.25, p=0.05, *Figure 16, F*), it was elevated in those defined as having sarcopenia (p=0.012, *Figure 17, B*). miR-542-5p was more tightly correlated with the 3m gait speed test whereas miR-542-3p was more tightly correlated with the TUG test. Finally, a larger increase in miR-542-5p was seen in patients defined as having sarcopenia (6.7-fold increase, compared to 2.7 fold increase seen for miR-542-3p levels).

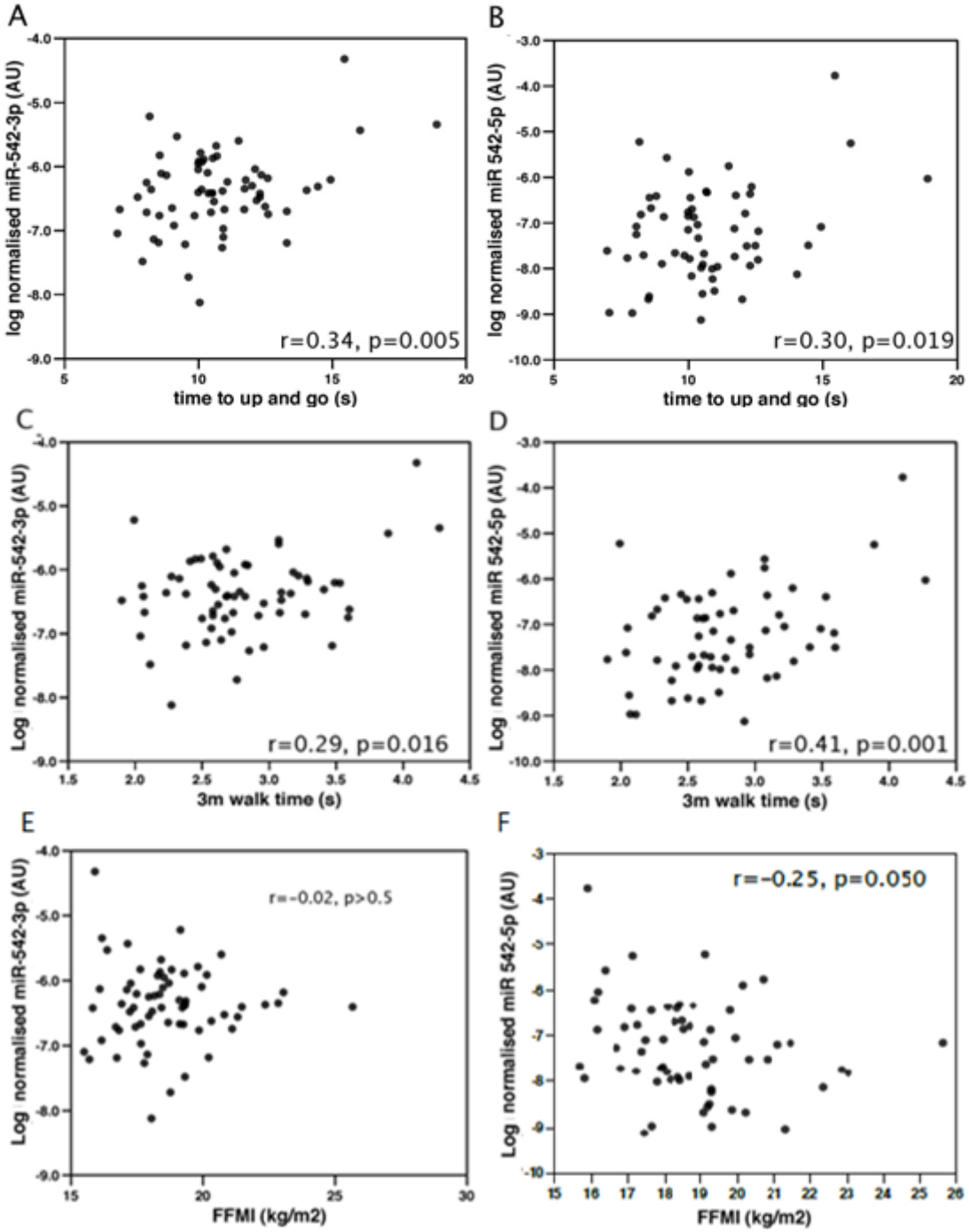


Figure 16- miR-542-3p/5p are associated with physical performance in healthy older individuals.

miR-542-3p and miR-542-5p were quantified in quadriceps biopsies from male participants in the HSS study. miR-542-3p data were generated by Dr Jen Lee. In these individuals miR-542-3p [A] and miR-542-5p [B] were directly associated with slower 6m and slower 3m gait speed test [C-D]. No association was seen between miR-542-3p or miR-542-5p levels and FFMI [E-F]. Correlations were analysed by Pearson´s test as data had a linear association, showing p and r values. miR-542-3p and miR-542-5p levels were normalised to U6 and RNU48.

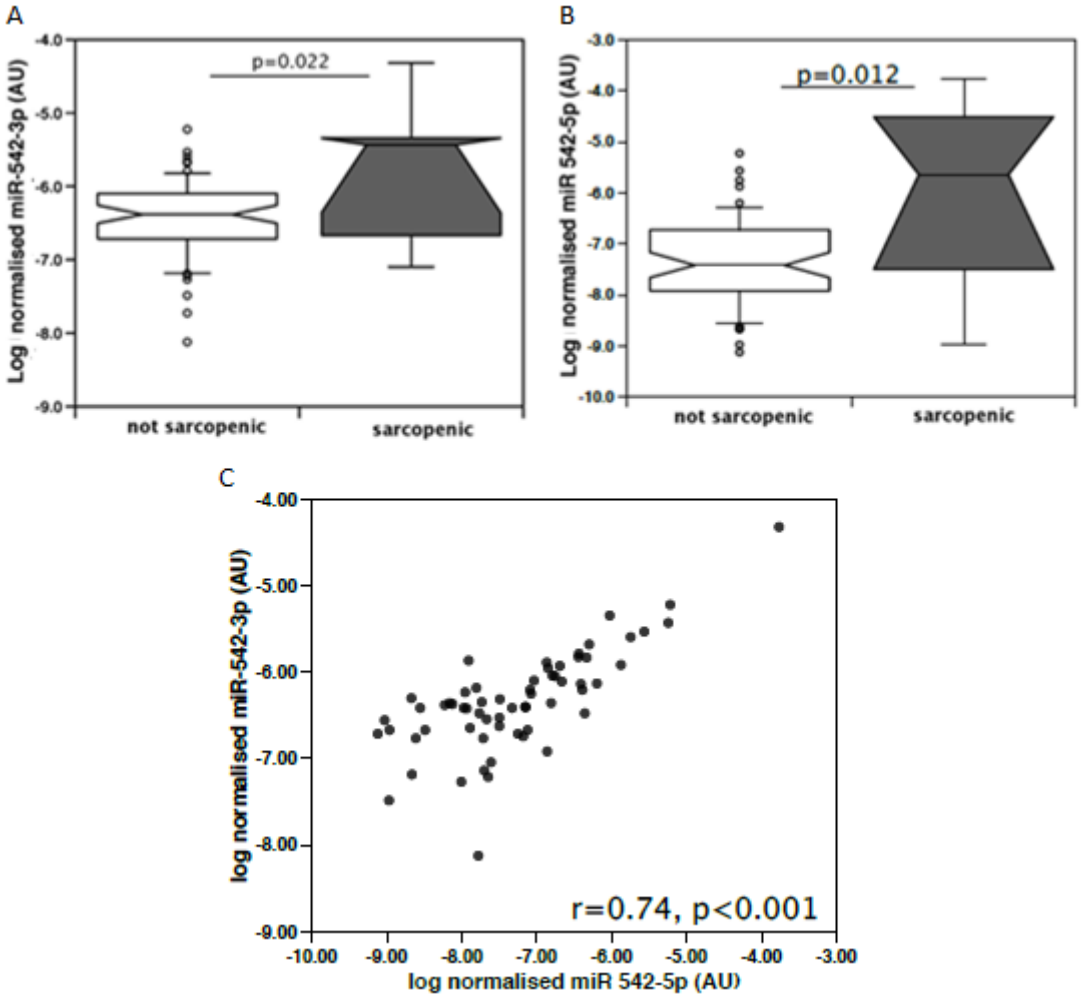


Figure 17- miR-542-3p/5p are elevated in sarcopenia.

miR-542-3p and miR-542-5p were quantified in quadriceps biopsies from male participants in the HSS study. miR-542-3p data were generated by Dr Jen Lee. miR-542-3p/-5p were elevated in patients presenting sarcopenia compared to not sarcopenic [A-B]. There is an association between miR-542-5p expression and miR-542-3p expression in the HSS cohort [C]. Correlations were analysed by Pearson´s test as data had a linear association, showing p and r values. miR-542-3p and miR-542-5p levels were normalised to U6 and RNU48. Box and whiskers plots showing whiskers to 90% with outliers shown.

3.3.4 miR-542-5p levels inversely associated with lung function in a cohort of older people

As miR-542-5p was associated with lung function in COPD patients we compared quadriceps expression of miR-542-5p with available measurements of FEV_1 in the HSS cohort. The lung function measurements were not performed at the same time as the quadriceps biopsies having been taken 3-9 years previously but were the only measurements of lung function available for the HSS cohort.

Comparison of quadriceps expression of miR-542-5p with these historical values of lung function showed an inverse association between the miR levels and FEV_1% (r=-0.39, p=0.002, *Figure 18, B*). miR-542-5p levels were also increased in patients with airflow obstruction compared to normal airflow (p<0.001, *Figure 18, H*), consistent with a role for lung function, hypoxia or oxidative stress in increasing miR-542-5p expression in the quadriceps. Indeed miR-542-5p levels did showed a greater increase in patients with airflow obstruction than miR-542-3p, around 10-fold increase and 1.5-fold increase, respectively. However, unlike miR-542-3p, miR-542-5p was not increased in people with a history of smoking *(Figure 18, D)* nor in individuals with self-reported asthma *(Figure 18, F)*. miR-542-3p data, which was previously obtained in our group, is shown with the only purpose to help comparing miR-542-5p data.

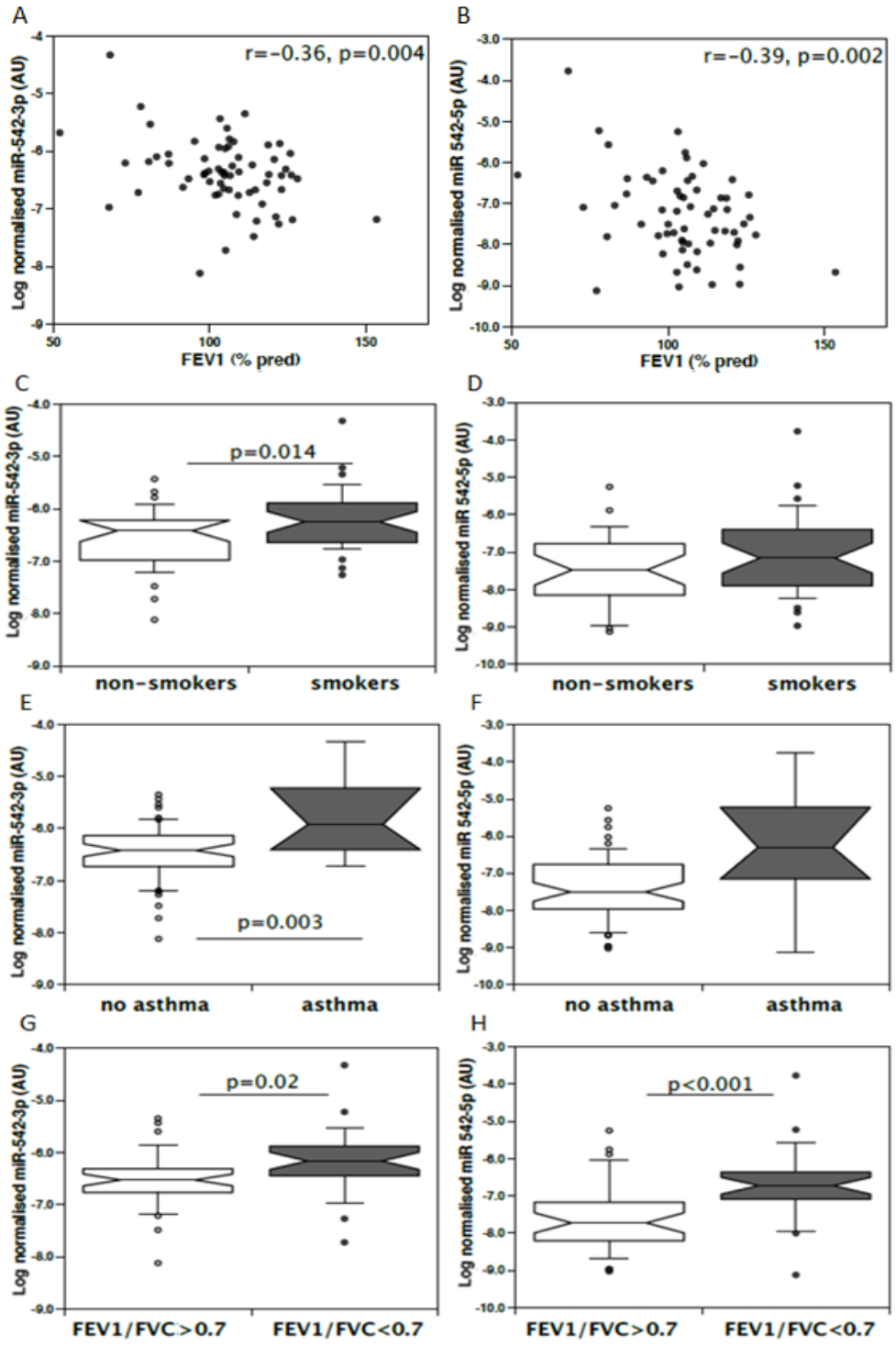


Figure 18- miR-542-3p/5p are associated with lung function in healthy older individuals.

miR-542-3p/-5p were quantified in quadriceps biopsies from male participants in the HS study. miR-542-3p data were generated by Dr Jen Lee. An association between miR-542-3p [A] and miR-542-5p [B] was seen with FEV_1 % predicted. miR-542-3p expression was increased under smoking [C] and asthma conditions [E] compared to non-smokers and non-asthmatic individuals. No difference was seen in miR-542-5p expression under those two conditions [D, F]. Both miR expression was increased in patients with airflow obstruction compared to normal airflow [G-H]. Correlations were analysed by Pearson´s test as data had a linear association, showing p and r values. miR-542-3p and miR-542-5p levels were normalised against U6 and RNU48. Box and whiskers plots showing whiskers to 90% with outliers shown.

3.3.5 miR-542-3p and miR-542-5p levels are increased in patients with ICUAW and associate with days of ICU stay

To determine whether miR-542-3p or -5p were increased in other conditions where muscle dysfunction occurs we determined their expression in quadriceps biopsies from patients with established ICUAW. This disease was chosen as our group had previously seen similar changes in the expression of myomiRs to those we have observed in COPD. In these patients there was a marked elevation of both miR-542-3p and -5p (20 fold, $p<0.001$ and 50 fold, $p<0.001$ respectively, *Figure 19, A-B*) and miR levels directly associated with length of ICU stay (miR-542-3p: $r= 0.58$, $p=0.014$; miR-542-5p: $r=0.57$, $p=0.016$, *Figure 19, C-D*). Together with the data from the COPD patients, these data suggest that miR-542-3p and -5p may be associated with the loss of muscle mass in response to diseases in which oxidative stress and inflammation are thought to be contributory factors. However, data regarding oxidative stress, inflammation, lung function and physical performance were not obtained for this cohort so associations with miR-542 levels could not be examined.

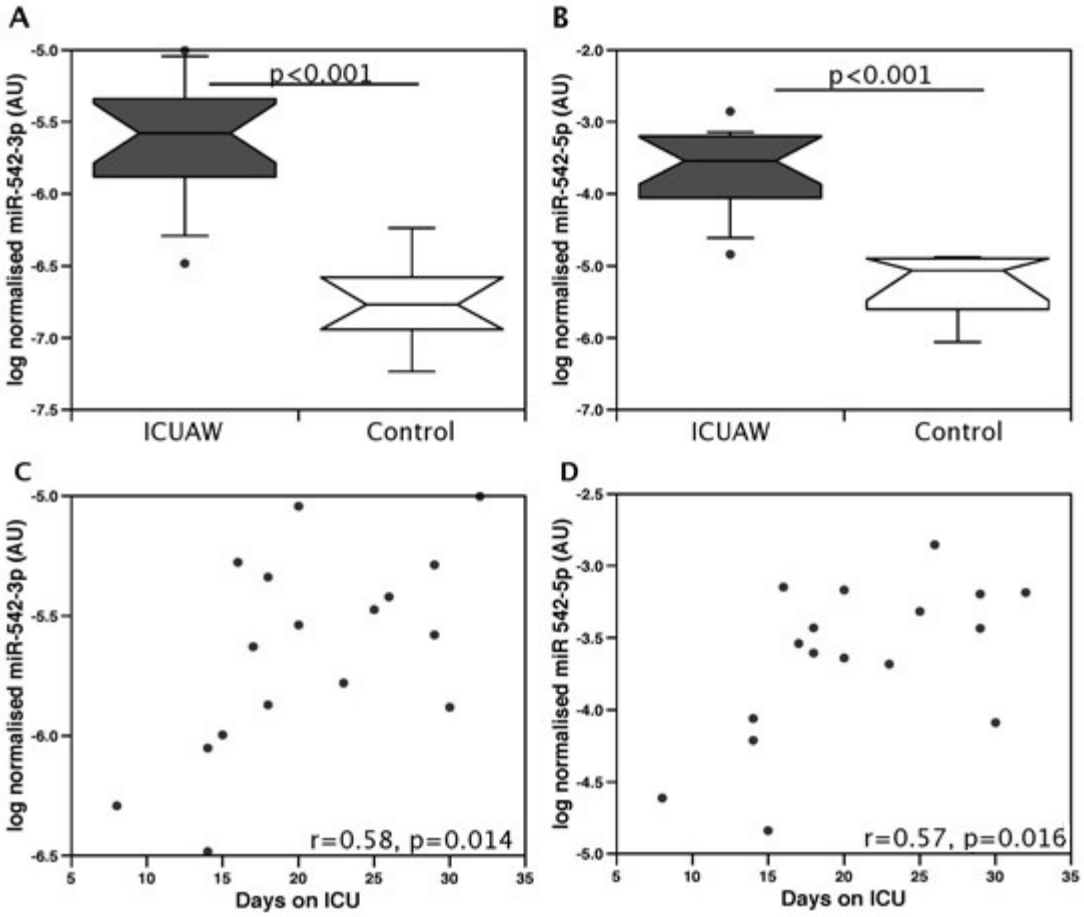


Figure 19- In patients with ICUAW miR-542-3p/5p levels are increased and associate with length on ICU.

miR-542-3p/5p were quantified in quadriceps biopsies from patients (n=17) with established ICUAW and pre-operative controls (n=7). Box and whiskers plots showing that the expression of miR-542-3p (A) and miR-542-5p (B) are increased in patients compared to controls ($p<0.001$ and $p<0.001$ respectively, whiskers to 90% with outliers shown). In patients with ICUAW, miR-542-3p (C) and miR-542-5p (D) expression were positively correlated with length of ICU stay. Correlations were analysed by Pearson´s test as data had a linear association, showing p and r values. miR-542-3p and miR-542-5p levels were normalised against U6.

3.3.6 miR-542-3p expression is increased under hypoxia *in vitro*

The associations between miR-542-3p/-5p and lung function seen in patients with COPD and from the HSS cohort suggest that a driver for expression of these miRs could be hypoxia. To analyse this hypothesis, human myoblasts were cultured under hypoxic (2% O_2) or normoxic conditions for 48, 72 and 96h and miR expression was quantified by TaqMan PCR. An elevation of miR-542-3p expression was seen in hypoxic compared to normoxic myoblasts at 96h (p=0.0303, 1.2-fold increase, *Figure 20, A*). However, miR-542-5p expression was not elevated in response to hypoxia (p=0.4687, *Figure 20, B*).

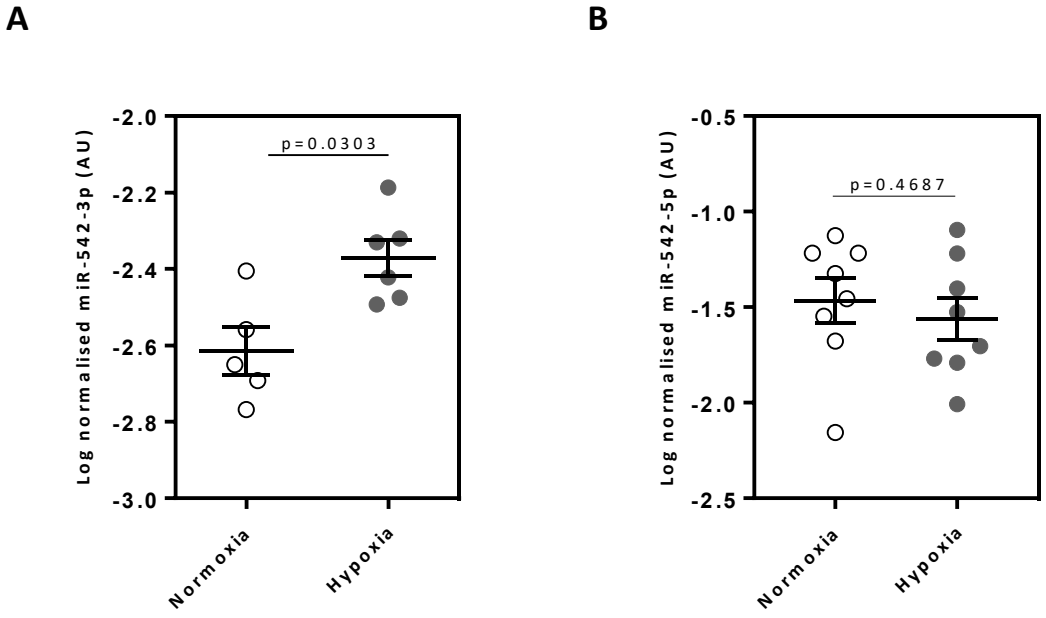


Figure 20- miR-542-3p expression is elevated under hypoxia *in vitro*.

LHCN-M2 myoblasts were cultured and incubated under hypoxia or normoxia for 96h. miRs levels were measured by Taqman PCR and an elevation of miR-542-3p was seen in hypoxic myoblasts compared to normoxia [A]. No difference was seen in miR-542-5p levels [B]. Scatter dot plot shows mean signal± SEM from n=3 independent experiments with 2 [A] and 3 [B] repetitions in each. Statistical analysis was performed using unpaired t-test as samples were normally distributed. miR-542-3p and miR-542-5p levels were normalised against U6.

3.3.7 Bioinformatic analysis predicts important targets for miR-542-3p and miR-542-5p in muscle wasting context

The elevation of miR-542 in conditions associated with muscle wasting and the strong association of miR-542 expression in the patients' quadriceps with physical performance suggest that the elevation of this microRNA may have functional consequences. Previous studies on the role of miR-542-3p showed that it targeted survivin and induced growth arrest (290). Whilst reduced regeneration is a feature of muscle wasting, to inhibit cell proliferation the microRNA would have to be expressed in the satellite cells and myoblasts. Given that miR-542-3p an -5p were readily detectable in the biopsies, it seems likely that the associations between muscle physiology and microRNA expression described above are from the levels of microRNA expressed in differentiated muscle rather than satellite cells suggesting that the microRNA has effects other than on cell proliferation. Therefore, to contribute to the muscle pathophysiology that occurs in the patient groups studied the microRNAs would need to regulate components of the protein synthetic, protein degradation pathways and/or affect energy metabolism. It is likely there is interplay between these systems but the fact that the associations of miR-542-3p/-5p levels are stronger with physical performance than with strength suggests that associations with energy metabolism may be the more important ones in the context of the studies so far. However, the fact that microRNAs have multiple targets and that the pathways may cross-talk makes the study of microRNA effects very complex.

To determine possible targets of miR-542-3p/-5p involved in promoting skeletal muscle atrophy we performed bioinformatic analysis using miRwalk 2.0 (291). miRwalk uses 12 algorithms to detect a pairing between the microRNA seed and the 3'UTR region of a possible mRNA target. To reduce the number of targets and increase specificity, targets had to be predicted by at least 4 algorithms to be considered. The list of targets generated by this method included a striking number of ribosomal proteins from both cytoplasmic and mitochondrial ribosomes. Indeed around 21% and 27% of cytoplasmic and 22% and 32% of mitochondrial ribosomal proteins were predicted to be targeted by miR-542-3p and miR-542-5p respectively *(Table 12, A)*. Moreover, miR-542-3p had previously been shown to promote ribosomal stress in cells

and to activate p53 by targeting the ribosomal proteins (292). By reducing the available ribosomes this approach would suppress maximal protein synthesis a common feature of muscle wasting. A similar effect on mitochondrial ribosomal proteins would not only suppress mitochondrial protein synthesis but reduce energy supply. Given the association of these microRNAs with physical performance measures that have some endurance requirement to a greater extent than those that are more limited to measurements of strength, mitochondrial targets were of great interest.

Secondly, we focused on TGF-β signalling as the bioinformatics analysis predicted a number of possible targets of the miR *(Table 12, B)* in this pathway which is known to contribute to atrophy in studies both by our group and others. For example, GDF-15 was shown to associate with muscle mass in COPD and to promote muscle wasting *in vivo* (197) and also suppresses the expression of microRNAs leading to an increased sensitivity of muscle cells to TGF-β in ICUAW (30). The predicted targets of miR-542 in the TGF-β pathway include a number of inhibitors of the pathway including CTSP proteins, PPM1A and PP2A proteins which de-phosphorylate SMAD proteins as described in the introduction. These are not the only pathways predicted to be targeted by the microRNAS that could contribute to atrophy but there was insufficient time to analyse all the potential pathways.

Table 12- Potential pathways and RNA targets of miR-542-3p/-5p.

miR-542-3p/-5p target important pathways that could contribute to muscle wasting according to miRwalk predictions. Several ribosomal proteins from both the small and the large ribosomal subunit and both from mitochondrial and cytoplasmic origin are potential targets for miR-542-3p/-5p. Targeting is specie specific so differences are seen between mouse and human predicted targets [A]. Molecules from the TGF-β pathway are also predicted targets of those microRNAs including inhibitors of the signalling system [B].

A

MITOCHONDRION				CYTOPLASM			
miR-542-3p		miR-542-5p		miR-542-3p		miR-542-5p	
MOUSE	HUMAN	MOUSE	HUMAN	MOUSE	HUMAN	MOUSE	HUMAN
Large subunit	Large subunit	Large subunit	Large subunit	Large subunit	Large subunit	Large subunit	Large subunit
MRPL1	MRPL10	MRPL3	MRPL11	RLP3L	RPL10	RPL5	RPL10L
MRPL4	MRPL18	MRPL10	MRPL14	RPL7	RPL15	PRL7L1	RPL15
MRPL11	MRPL19	MRPL11	MRPL17	RPL18A	RPL22	RPL15	RPL22
MRPL15	MRPL23	MRPL14	MRPL20	RLP21	RPL22L1	RPL18A	RPL22L1
MRPL16	MRPL30	MRPL15	MRPL27	RPL22	RPL23A	RPL22	RPL24
MRPL17	MRPL35	MRPL16	MRPL28	RPL35A	RPL27A	RPL27A	RPL27A
MRPL19	MRPL49	MRPL17	MRPL32	Small subunit	RPL28	RPL36AL	RPL28
MRPL20	MRPL51	MRPL19	MRPL33	PRS1L3	RPL32	RPL37	RPL32
MRPL35	MRPL52	MRPL21	MRPL33	RPS2	RPL36A	Small subunit	RPL34
MRPL40	Small subunit	MRPL33	MRPL34	RPS13	RPL39	RPS1	RPL35A
MRPL46	MRPS2	MRPL35	MRPL35	RPS15A	Small subunit	RPS9	RPL36A
MRPL50	MRSP10	MRPL36	MRPL40	RPS17	RPS3A	RPS15A	RPL36A-H
MRPL53	MRPS12	MRPL38	MRPL42	RPSA	RPS14	RPS18	RPL37
MRPL55	MRPS18B	MRPL40	MRPL43		RPS20	RPS24	RPL39
Small subunit	MRPS18C	MRPL41	MRPL44		RPS21	RPS25	RPL41
MRPS7	MRPS23	MRPL45	MRPL49		RPS23	RPSA	Small subunit
MRPS9	MRPS25	MRPL49	Small subunit		RPS27L		RPS3
MRPS23	MRPS25	MRPL50	MRPS2		RPS28		RPS15A
MRPS25	MRPS26	MRPL55	MRPS6				RPS21
	MRPS27	Small subunit	MRPS10				RPS24
		MRPS2	MRPS11				RPS27A
		MRPS9	MRPS16				RPS27L
		MRSP10	MRPS18B				RPS29
		MRPS21	MRPS18C				
		MRPS23	MRPS25				
		MRPS24	MRPS27				
		MRPS25	MRPS35				
		MRPS34	MRPS36				

B

TGF-β PATHWAY PREDICTED TARGETS			
miR-542-3p		miR-542-5p	
MOUSE	HUMAN	MOUSE	HUMAN
CTDSP1	CTDSP2	CTDSP1	CTDSP1
CTDSP2	CTDSPL	CTDSPL	CTDSP2
CTDSPL	CTDSPL2	CTDSPL2	CTDSPL
CTDSPL2	PPM1A	PPM1A	CTDSPL2
PPM1A	PPP2CA	PPP2R4	PP2A
PPP2R1A	PPP2R1A	PPP2R5C	PPM1A
PPP2R1B	PPP2R1B	PPP2R5E	PPPR2C
PPP2R3A	PPP2R3A	SMAD2	SMAD2
SMAD2	SMAD2	SMAD3	SMAD3
SMAD3	SMAD3	SMAD7	SMAD7
SMAD4	SMURF1	SMURF1	SMURF1
SMAD7	SMURF2	SMURF2	SMURF2
SMURF1	SNIP1	SNIP1	TGFB2
SMURF2	TGFB2	TGFB	TGFBR3
SNIP1	TGFBR3	TGFBR1	
TGFA		TGFBR2	
TGFB			
TGFBR1			
TGFBR2			
TGFBR3			

3.4 Discussion

3.4.1 Main findings

The data presented in this chapter show that miR-542-5p expression is increased in the quadriceps of COPD patients and associated with physical performance in this disease measured as 6MW distance, MVC or TwQ. Moreover, this microRNA is also associated with physical performance in normal elderly individuals (HSS cohort) similar to previous findings on miR-542-3p, suggesting that miR-542 may promote muscle dysfunction. The data also showed an association between quadriceps miR-542-5p levels and lung function impairment measured as TLco, PaO_2 and FEV_1% in COPD and by FEV_1% in the HSS cohort. Together these data suggest that stress in the lung could increase miR-542 in the muscle and the factors likely to contribute to this increase include inflammation, oxidative stress and hypoxia all of which can occur in response to COPD, smoking and asthma. Furthermore, these same factors are likely to contribute to the increase in miR-542-3p and miR-542-5p seen in patients with ICUAW. Despite the proposed effects of miR-542-3p/5p on muscle atrophy, there was no association of these microRNAs with FFMI. A possible explanation for this lack of association is the regeneration rate of each patient which could mask the effects of miR-542. A previous study showed that FFMI in stable COPD patients is associated with microRNAs that regulate regeneration (271) an observation in line with the findings of *Theriault et al.* who showed reduced regeneration in cachectic COPD patients (123). However, the fact that the associations found between muscle mass and microRNAs were only observed in the COPD disease population and not in the general population suggests that these effects can be due to the imbalance that the stress of the disease confers to these individuals. Moreover, depending on each individual, sensitivity to stresses such as TGF-β signalling and their ability to regenerate which may be determined by genetics and epigenetics, individuals will lose muscle in different rates.

3.4.2 How might miR-542 contribute to muscle dysfunction in disease?

The bioinformatic analyses identified a range of potential pathways by which miR-542 may regulate muscle phenotype. These pathways regulate protein synthesis, protein breakdown and energy metabolism. Of these, energy metabolism may be of particular importance because of the stronger association of miR-542 with physical performance parameters that have an endurance component than purely with strength or with muscle mass. Therefore, we decided to firstly focus on the energetic pathways.

In the literature, there are a number of studies investigating the contribution of mitochondrial number or dysfunction to muscle wasting. Mitochondrial number has been shown to be reduced in the *vastus lateralis* muscle of patients with COPD (293). Moreover, abnormal mitochondrial function such as decreased oxidative capacity and increased ROS production has been described in locomotor and respiratory muscles of COPD patients (75,294). Similarly, an approximate 50% reduction in aerobic ATP synthesis was seen in the skeletal muscle of patients with ICUAW compared to healthy controls in addition to reduced levels of the mitochondrial complexes (295). Mitochondrial dysfunction has also been studied in the context of ageing and decreased mtDNA and several mitochondrial proteins such as NADH dehydrogenase, pyruvate dehydrogenase alpha 1, ubiquitous mitochondrial creatine kinase, citrate synthase and isocitrate dehydrogenase 2 were decreased in older people leading to decreased ATP production (296,297). Although mitochondrial impairment has been described in several situations where muscle wasting also occurs, the mechanism describing how and why this impairment occurs has still not been described. Furthermore, dysfunctional mitochondria are likely to lead to a decrease in ATP in the cell. As energy is essential for protein synthesis this reduction may contribute to muscle loss.

Mitochondrial dysfunction is not the only mechanism leading to reduced protein synthesis nor is it the only mechanism that may be regulated by miR-542. For example, reducing the number of available ribosomes will inhibit maximal protein synthesis as will inhibiting the activity of the IGF-1 pathway. Conversely increasing the sensitivity of the TGF-β pathway would increase myostatin dependent atrophy. All of these

mechanisms have been suggested to contribute to wasting in COPD and/or ICUAW. It is also possible that miR-542 may contribute to the regulation of a number of other mechanisms that lead to muscle loss. Such mechanisms include reduced sensitivity to androgens or increased sensitivity to inflammatory signalling (298,299). However, we did not identify any clear components of these pathways in the bioinformatics analysis.

As mentioned above, it is still unknown what causes the increase in miR-542 expression under the conditions of the studied diseases and ageing. Some of the factors that the three cohorts (COPD, ICUAW and HSS) shared were inflammation and hypoxia. However, despite inflammation being considered a possible cause for the miR increase, no association was seen between miR-542 levels and plasma levels of inflammatory cytokines in the COPD cohort suggesting that systemic inflammatory load at least does not cause the increase in miR-542 (data not shown). Hypoxia has recently been shown to increase the expression of miR-424 another microRNA from miR-542 cluster (300,301) and a study has shown that in human fibroblasts miR-542-5p is increased by oxidative stress causing DNA damage (302). As hypoxia and oxidative stress are known to be associated with both COPD and ICUAW these support a role for hypoxia in the expression of miR-542 in the patients together with my observations of elevated miR-542-3p in response to hypoxia *in vitro*. However, further studies are needed to understand the precise mechanism driving increased miR-542-3p as there was no associated increase in miR-542-5p. Increased ROS in the muscle thereby promoting oxidative damage could also be caused by mitochondrial dysfunction. As mentioned earlier, reduced mitochondrial number and mitochondrial dysfunction have been previously demonstrated in the quadriceps of patients with COPD (303), in ICUAW (295) and in the ageing population (304) and are thought to be important contributors to the loss of physical performance on these patients. These impairments could also lead to a decrease in protein synthesis. Therefore, the role that miR-542-3p/-5p plays in energy production affecting protein synthesis and on the TGF-β pathway are of interest from the point of view of muscle loss and the aim of the following chapters is to elucidate some mechanisms that could help understand the muscle wasting process.

3.5 Conclusions

In conclusion, this chapter identified miR-542-5p to be elevated in several diseases which have muscle wasting as a co-morbidity. In COPD patients and in the elderly population in the Hertfordshire sarcopenia study the expression of microRNA was inversely associated with physical performance and lung function. Both miR-542-3p and miR-542-5p levels were also elevated in the quadriceps of patients with ICUAW compared to age-matched controls. Bioinformatic analysis showed that the microRNA targeted pathways and proteins related to the promotion of muscle dysfunction including mitochondrial and cytoplasmic ribosomal proteins and components of the TGF-β signalling system that will be analysed in the subsequent chapters.

CHAPTER 4: Mechanism of the role of miR-542-3p and miR-542-5p in cytoplasmic and mitochondrial ribosomal stress

4.1 Rationale

Reduced exercise capacity has been identified in patients with COPD and other chronic diseases and is caused by a reduction in both muscle mass and energy supply. These processes are often considered separately with muscle mass regulated by the net result of anabolic and catabolic processes, and energy supply determined by the number and function of mitochondria. However, these processes are connected as muscle protein synthesis requires energy from mitochondria and mitochondrial turnover requires new protein synthesis and mitophagy (305). In addition to the balance of these various processes, fibre proportion also contributes to exercise capacity as described in Chapter 1.

Consistent with such a role for energy production in protein synthesis and the maintenance of muscle mass, mitochondrial myopathies commonly have atrophy as a comorbidity as it is seen in Leigh syndrome (306) and mitochondrial DNA depletion syndrome (307). Furthermore, a loss of mitochondrial function is a common characteristic observed in patients with chronic diseases (135,308) where there is muscle dysfunction. Indeed mitochondrial dysfunction has been proposed as a major cause of muscle wasting both in ICUAW (295,309) and in age related sarcopenia (148,161).

In addition to mitochondrial dysfunction, several studies have shown anabolic resistance in the ageing population (310), which is a reduction in muscle protein synthesis in response to anabolic stimuli. Immobilisation which typically occurs in patients with ICUAW was also reported to promote anabolic resistance (311). Consistent with these observations, in COPD patients an imbalance between catabolic/anabolic factors was also described (312). This anabolic resistance is consistent with mitochondrial function being impaired in these patients reducing the energy supply available for protein synthesis. Moreover, in the ageing population

anabolic stimulators such as insulin or branched chain amino acids had impaired ability to initiate protein translation compared to young individuals (313). Other observations have shown that in older individuals the mTOR signalling pathway seems to be decreased compared to younger individuals, suggesting decreased protein synthesis (314). As mentioned in Chapter 1, other factors inhibiting muscle anabolism have been identified. For example, in ageing population increased levels of NF-κB, TNFα and IL-6 which are known to repress mTOR signalling have been observed (314). Other identified mechanisms are reduced IGF-1 levels and insensitivity to IGF-1, which have been identified in COPD patients (29,315). Moreover, the muscle of ageing individuals requires higher doses of amino acids to activate protein synthesis. Therefore, diet plays an important role in anabolic resistance as the elderly might need to increase protein intake and distribute it throughout the day to promote protein synthesis. Decreased exercise while ageing is another factor that contributes to anabolic resistance as exercise is known to stimulate protein synthesis (316).

Protein synthesis occurs on the ribosomes of either the cytoplasm or the mitochondria and as explained in Chapter 1 both types of ribosomes have different features *(Figure 21)* and translate different proteins. Due to this key role in protein synthesis, ribosomal biogenesis and functionality are likely to be important in the context of atrophy. Given the contribution of microRNAs to the control of cell phenotype, microRNAs are likely to contribute to the regulation of both ribosomal and mitochondrial biogenesis. Consistent with this suggestion, there are a number of studies implicating microRNAs in the control of mitochondrial function and a small number of studies looking at their contribution to ribosomal biogenesis and the control of protein synthesis. The microRNAs involved in mitochondriogenesis include miR-696 which is known to regulate expression of PGC-1α, an important activator of mitochondrial biogenesis (317). Moreover, miR-696 expression is dependent on exercise suggesting a reduction in the expression of this microRNA could occur as a consequence of inactivity in patients with COPD and ICUAW as well as in sarcopenia. However, this microRNA was not identified by the screen of COPD patients described in Chapter 3. miR-210 has been shown to lead to mitochondrial electron transport chain dysfunction by targeting key mitochondrial components, including cytochrome c oxidase assembly protein

(COX10) and iron-sulphur cluster scaffold (ISCU), in hypoxic human placenta (318). However, in the muscle of COPD patients, miR-210 is suppressed suggesting that it does not contribute to mitochondrial dysfunction in this disease (162). In mice, miR-494 impaired mitochondrial biogenesis by targeting mitochondrial transcription factor A (mtTFA) and Forkhead box j3 (Foxj3). The latter protein is a transcriptional activator of the myogenic transcription factor MEF2C which is involved in the regulation of adult muscle fibre type identity and skeletal muscle regeneration (319). Consistent with such a role, the miR-494 levels were suppressed in the muscle of mice following endurance exercise training regime (7x 15-min bouts separated by 5min rest for 7 days) and an increase in mitochondrial content was seen (320). However, again miR-494 was not deregulated in the muscle of COPD patients.

Several microRNAs have been shown to target cytoplasmic ribosomes suggesting a role for these microRNAs in the control of protein synthesis. In C2C12 myotubes, miR-10a was reported to regulate ribosomal synthesis. Interestingly rather than suppressing the expression of its targets this microRNA appears to enhance the expression of the ribosomal proteins RPS6, RPS9, RPS16 by interacting with the 5'UTR of the mRNAs (321). However, analysis of the existing dataset for COPD patients failed to identify any change in miR-10a compared to controls. A role for miR-542-3p in cytoplasmic ribosomal synthesis was described by *Wang, Y. et al* (292). miR-542-3p was shown to suppress the expression of small ribosomal proteins leading to an increase of free RPL11 which acts as a positive regulator of p53 by binding to and inhibiting MDM2, an inhibitor of p53. As part of this ribosomal stress response, they showed that miR-542-3p also reduces 18S ribosomal RNA, which is part of the small ribosomal subunit *(Figure 21).* However, in this study they did not focus directly on studying protein synthesis but it is likely that a mechanism that impairs ribosomal biogenesis could also impair protein synthesis.

Together these data show that microRNAs can contribute to both ribosomal and mitochondrial biogenesis. Of these, the only microRNA identified by the screen as altered appropriately in the muscle of COPD patients was miR-542. Furthermore, we have identified in the previous chapter that this microRNA potentially targets mitochondrial ribosomal proteins as well as cytoplasmic ribosomal proteins. This

observation raises the possibility that this microRNA may promote mitochondrial ribosomal stress and thereby promote mitochondrial dysfunction. Such a role for miR-542 would help to explain the associations of miR-542 with muscle function described in the previous chapter.

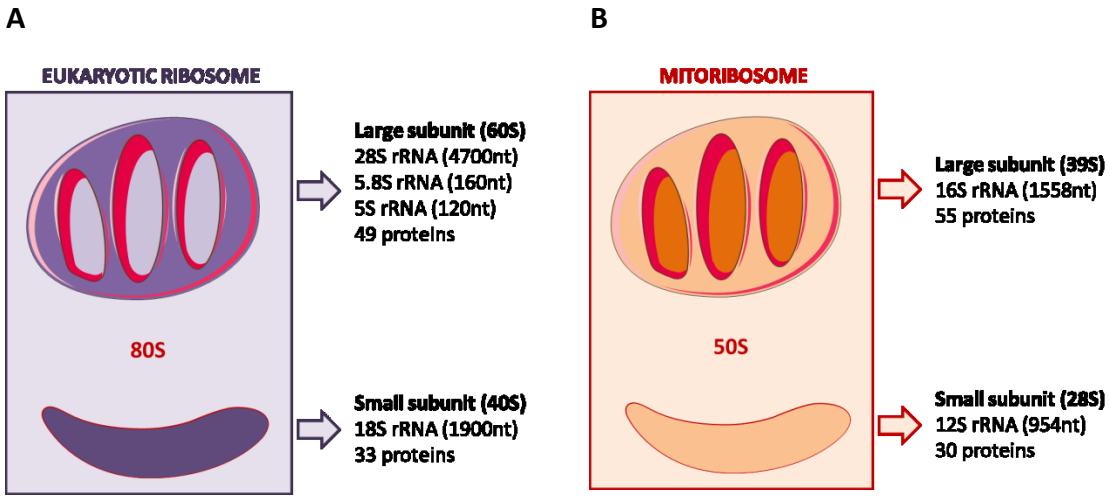


Figure 21- Cytoplasmic and mitochondrial ribosomal subunits.

[A] Cytoplasmic or eukaryotic ribosomes (80S) are made up of 2 subunits, a large subunit (60S) which contains 28S rRNA, 5.8S rRNA, 5S rRNA and 49 proteins, and a small subunit (40S) containing 18S rRNA and 33 proteins. [B] Mitoribosomes or mitochondrial ribosomes (50S) also have 2 subunits, a large subunit (39S) which contains 16S rRNA and 55 proteins, and a small subunit (28S) containing 12S rRNA and 30 proteins.

In this chapter, therefore we aimed to determine whether miR-542-3p/-5p could impair cytoplasmic and mitochondrial ribosomal biogenesis and promote ribosomal stress in muscle cells *in vitro*.

4.2 Hypothesis

The above rationalisation leads to the following hypotheses:

1) miR-542-3p and miR-542-5p would target key mitochondrial ribosomal proteins in skeletal muscle causing a disruption of mitochondrial activity.
2) miR-542-3p and miR-542-5p would target cytoplasmic ribosomal proteins in skeletal muscle inducing ribosomal stress and impairing protein synthesis.

4.3 Results

4.3.1 miR-542-3p targets mitochondrial ribosomal proteins *in vitro*

In the previous chapter, miR-542-3p was predicted to target a significant number of mitochondrial ribosomal proteins *(Table 12)* including MRPS10 (Mitochondrial Ribosomal Protein S10), which forms part of the small 28S subunit of the mitochondrial ribosome. We therefore determined the effect of miR-542-3p on MRPS10 expression by transfection in LHCN-M2 cells. Quantification of Western blots of cell extracts prepared 48h after transfection with the microRNA mimic showed a reduction in MRPS10 in miR-542 transfected cells compared to controls (p=0.0222, 2-fold decrease, *Figure 22*, A-B). The impairment in MRPS10 expression maybe caused by a direct repression of MRPS10 translation or RNA degradation by miR-542-3p.

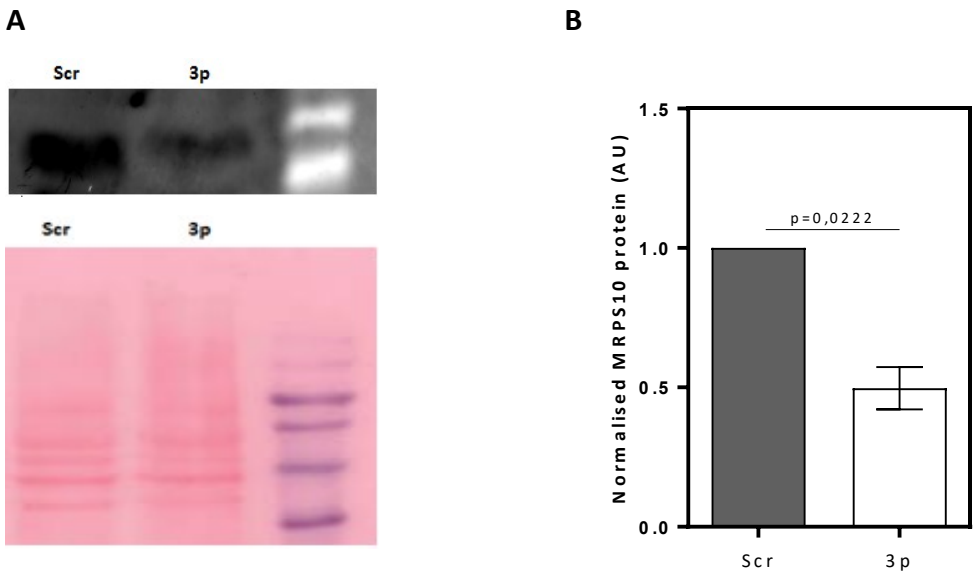


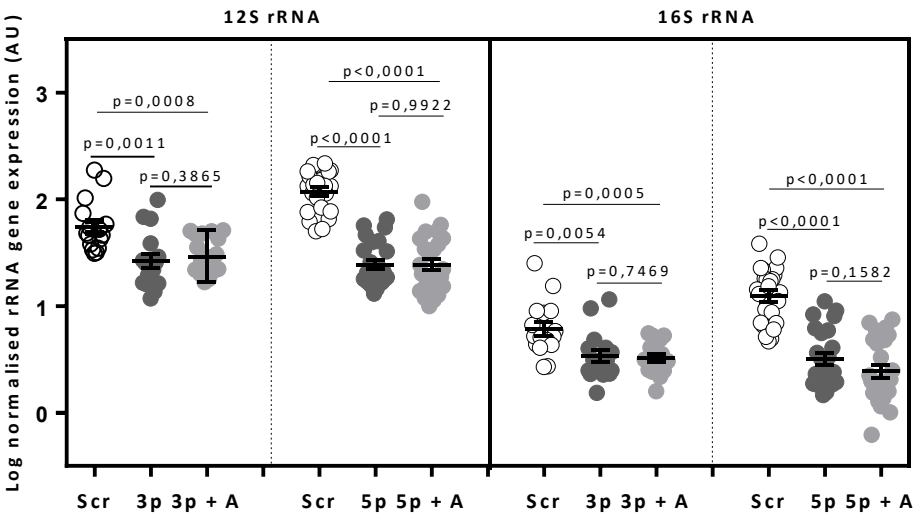
Figure 22- Mitochondrial ribosomal protein is down-regulated by miR-542-3p.

Protein was extracted from LHCN-M2 myoblasts 48h after transfection with scrambled (Scr) or miR-542-3p (3p). As predicted by miRwalk, miR-542-3p decreased MRPS10 levels compared to scrambled treated myoblasts. A decrease of 2-fold by miR-542-3p was seen in MRPS10. Bar chart shows mean signal± SEM from n=3 independent transfections. Statistical analysis was performed using One-sample t-test. Ponceau staining was used as a loading control.

4.3.2 Mitochondrial ribosomal RNA levels are decreased by miR-542-3p and miR-542-5p *in vitro*

The demonstrated decrease in MRPS10 together with the importance of mitochondrial ribosomal proteins for the maturation of rRNAs suggests that the inability to produce ribosomes would lead to ribosomal stress. Therefore, to determine the effect of miR-542 on mitochondrial rRNA levels, the expression of these rRNAs was quantified. 12S rRNA expression was reduced in miR-542-3p transfected LHCN-M2 myoblasts compared to control cells ($p=0.0011$, *Figure 23, A*). 16S rRNA levels were also reduced in the same samples ($p=0.0054$). The effects of miR-542-5p on mitochondrial ribosomal RNA were also determined as this miRNA is also predicted to target mitochondrial ribosomal proteins. Transfection of LHCN-M2 cells with miR-542-5p also decreased mitochondrial rRNAs, 12S ($p<0.0001$, *Figure 23, A*) and 16S rRNA ($p<0.0001$). Moreover, a significant reduction was also seen in the 12S:16S ratio (miR-542-3p: $p=0.0257$; miR-542-5p: $p=0.0108$, *Figure 23, B*) as the reduction in 12S rRNA expression was greater than that of 16S rRNA. Co-transfection with the antagomiR did not rescue the reduction in rRNA caused by miR-542 but did rescue the reduction in the 12S:16S ratio (for further discussion see *Appendix 1*). As the 12S rRNA is stabilised by the formation of the small ribosomal subunit, these data are consistent with mitochondrial ribosomal stress due to impairment in the mitochondrial ribosomal biogenesis.

A



B

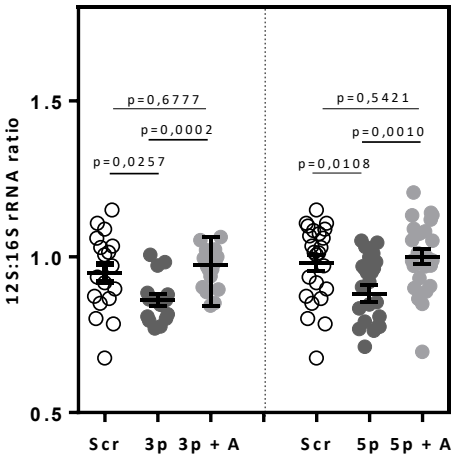


Figure 23- miR-542-3p /-5p decrease levels of 12S and 16S rRNA in LHCN-M2 myoblasts.

LHCN-M2 myoblasts were transfected with scrambled *(Scr)*, miR-542-3p *(3p),* miR-542-5p *(5p),* miR-542-3p together with antagomiR-542-3p *(3p + A)* and miR-542-5p together with antagomiR-542-5p *(5p + A).* 48h later RNA was extracted and rRNA levels were measured by qPCR. [A] miR-542-3p and miR-542-5p transfected myoblasts showed a down-regulation of 12S and 16S rRNA levels compared to control cells. [B] A decrease in 12S:16S [A] ratio was observed in miR-542-3p/-5p transfected cells. Normalisation of the data was performed against hypoxanthine guanine phosphoribosyltransferase (HPRT), and β2-microglobuline (β2M). The results are based on at least n=6 samples repeated in 3 independent experiments. Scatter dot plots show mean signal± SEM and statistical analysis was performed using unpaired t-test as the data were normally distributed.

4.3.3 miR-542-3p decreases CYTB protein levels *in vitro*

To determine whether the mitochondrial ribosomal stress induced by miR-542-3p was sufficient to reduce mitochondrial protein translation we determined the levels of a mitochondrialy encoded protein, cytochrome b (CYTB). CYTB is one of the 10 proteins forming mitochondrial complex III. This complex transfers electrons from ubiquinol to cytochrome C and CYTB plays an essential role as part of the electron transport chain. Transfection of miR-542-3p into LHCN-M2 myoblasts reduced CYTB protein levels compared to transfection with a scrambled oligonucleotide (p=0.0418, 1.3-fold decrease, *Figure 24, A-B*). Decreased levels of CYTB expression may be caused by the direct effect of the miR, repressing CYTB translation or promoting degradation, or by an impairment of mitochondrial ribosomal biogenesis caused by miR-542-3p reducing mitochondrial protein synthesis. However, as there is no evidence for miR-542-3p entering the mitochondria nor for CYTB being targeted by the microRNA the latter explanation seems more reasonable.

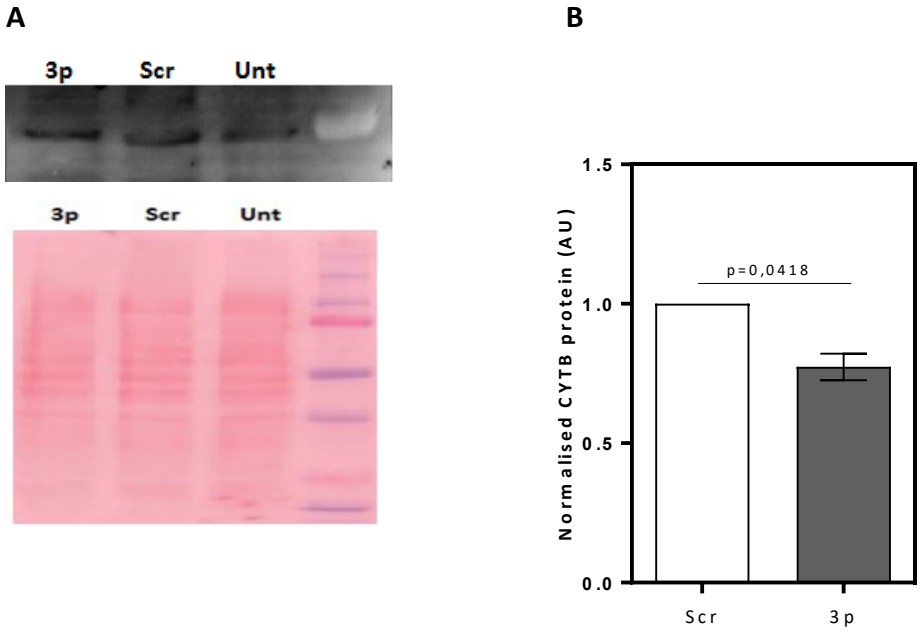


Figure 24- Mitochondrial protein synthesis is down-regulated by miR-542-3p.

Protein was extracted from LHCN-M2 myoblasts 48h after transfection with scrambled (Scr) or miR-542-3p (3p). *(unt)* denotes cells that were not transfected. miR-542-3p decreased the mitochondrially encoded CYTB protein levels in myoblasts compared to scrambled treatment. Bar chart shows mean signal± SEM from n=3 independent transfections. Statistical analysis was performed using One-sample t-test. Ponceau staining was used as a loading control.

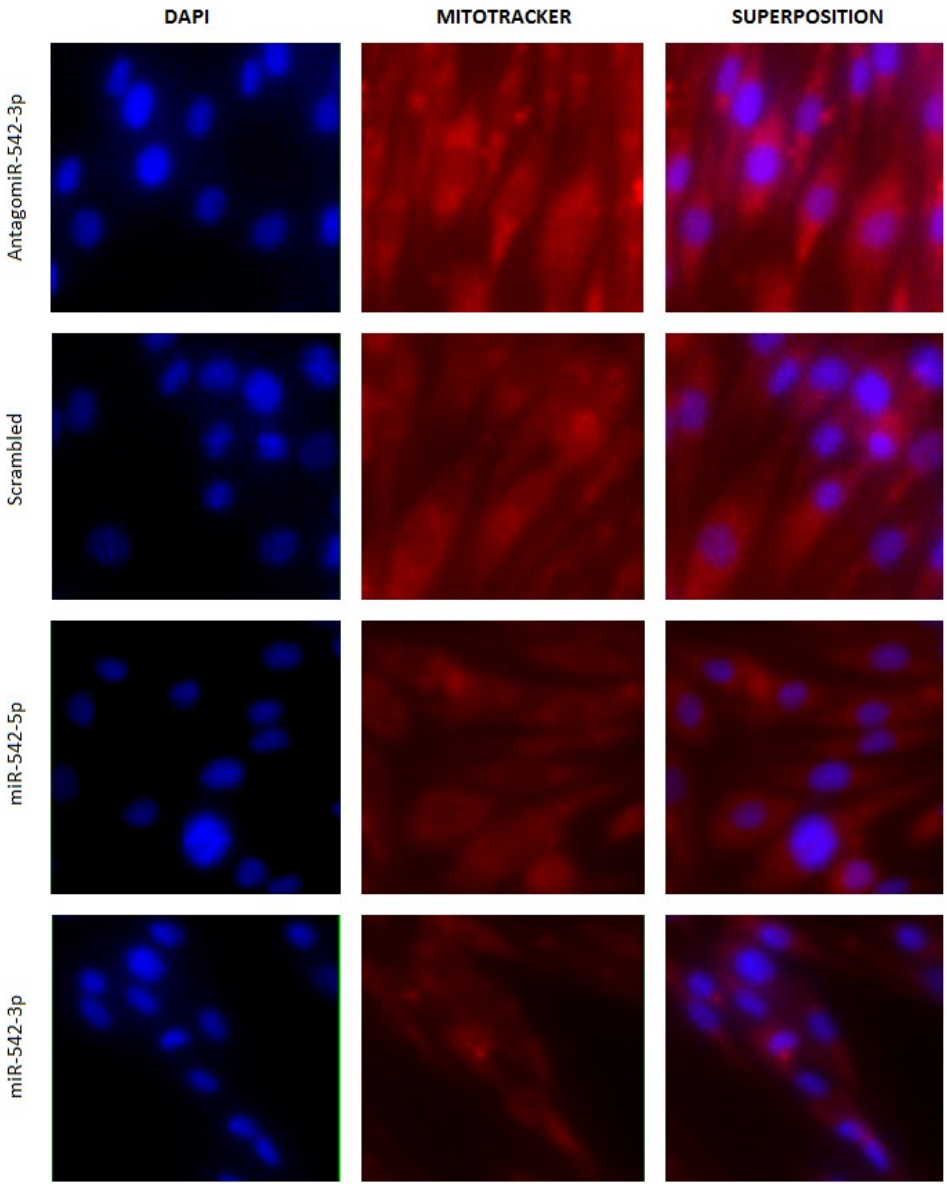
4.3.4 Mitochondrial membrane potential is reduced by miR-542-3p and miR-542-5p *in vitro*

Mitochondrial ribosomal stress is likely to affect the expression of all 13 proteins encoded by the mitochondria that are required for the proper function of complex I, III, IV and V. It seems likely therefore that mitochondrial ribosomal stress would lead to mitochondrial dysfunction, decreasing ATP synthesis. Another effect of such mitochondrial dysfunction might be a reduction in membrane potential. Therefore, the effect of miR-542-3p was determined on membrane potential measured using Mitotracker Red *(Figure 25, A-B)* and JC-1 *(Figure 25, C)* staining. Mitotracker Red staining in LHCN-M2 was reduced 48h after miR-542-3p/-5p transfection compared to scrambled transfection ($p=0.0152$ and $p=0.0411$, respectively). Moreover, fluorescence was restored to control levels by co-transfection with the antagomiR-542-3p/-5p. Uptake of the dye by the myoblasts is dependent on both mitochondrial number and membrane potential. Therefore, to control for the number of mitochondria, 12S DNA was quantified and normalised to 18S DNA. We also measured 16S DNA and we obtained 12S:16S DNA ratio to ensure that there was no deletion of 12S rRNA as both 12S and 16S rRNA are encoded by the mitochondrial chromosome. There was no significant difference between the groups indicating that mitochondrial content was unchanged *(Figure 25, D)* thereby suggesting that the reduction was due to a reduction in membrane potential.

To further confirm the membrane potential was reduced, we measured JC-1 membrane-potential-dependent accumulation in mitochondria. At low concentrations JC-1 is a monomeric dye that emits at ~525nm (green), however after accumulation in the mitochondria in the form of J-aggregates that occurs dependant on membrane potential the dye emission shifts to ~590nm (red). Therefore, mitochondrial membrane potential was extrapolated from the quantification of the red/green fluorescence intensity ratio. This analysis showed a reduction in red/green intensity ratio in LHCN-M2 myoblasts after 48h of miR-542-3p/-5p transfection compared to scrambled transfection ($p<0.0001$ for both). Moreover, the red/green intensity ratio was returned to control levels by antagomiR-542-3p/-5p transfection consistent with a miR-542 dependent reduction in membrane potential. Both analyses showed a bigger

reduction in mitochondrial membrane potential by miR-542-3p compared to miR-542-5p.

A



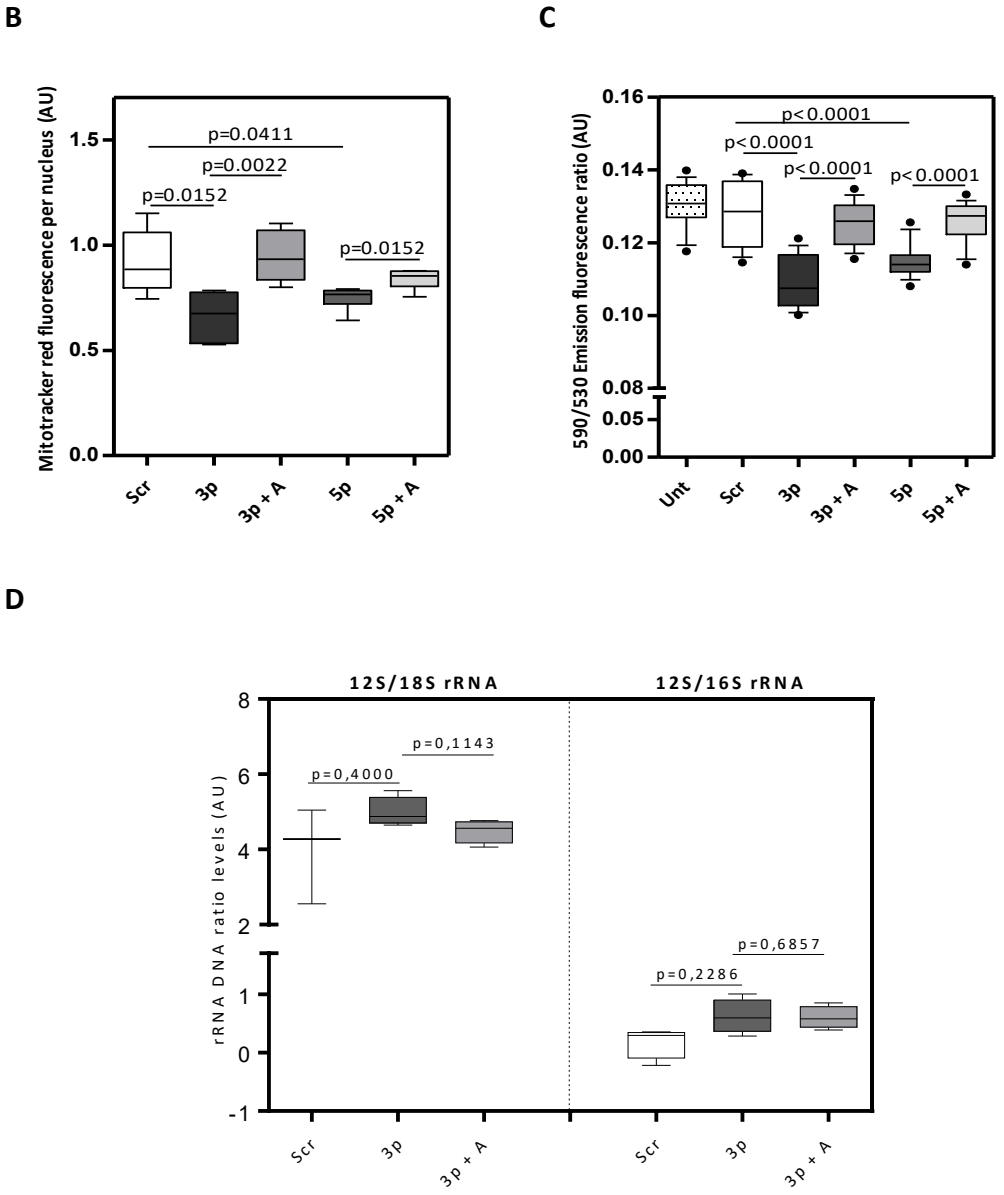


Figure 25- miR-542-3p/-5p inhibit mitochondrial function *in vitro* by decreasing membrane potential.

LHCN-M2 cells were transfected with scrambled mimic (scr), miR-542-3p (3p), miR-542-3p in the presence of its antagomiR (3p + A), miR-542-5p (5p), or miR-542-5p in the presence of its antagomiR (5p + A). Transfected miR-mimic levels were kept constant in all experiments by co-transfection with scr. 48h after transfection, membrane potential measured by Mitotracker Red [A, B] and JC-1 staining [C] showed a reduction by miR542-3p/-5p. Both of these effects were reversed by the antagomiR. The results are based on n=3 independent experiments with 2 samples in each treatment for Mitotracker red and 6 samples in each treatment for JC-1 staining. [C] DNA was extracted from LHCN-M2 myoblasts 48h after miR-542-3p or scrambled transfection. 12S, 16S and 18S rRNA DNA were measured and 12S/18S and 12S/16S ratio were analysed. No significant differences were observed. The results are based on n=4 samples. Box and whiskers plot show 10-90 percentiles and outliers as dots and statistical analysis was performed using Mann Whitney test as samples were not normally distributed.

4.3.5 Mitochondrial ribosomal RNA subunits are down-regulated in patients suffering from muscle wasting (COPD and ICUAW)

To determine whether miR-542-3p dependent mitochondrial ribosomal stress may contribute to muscle wasting, we measured the 12S:16S rRNA ratio in quadriceps samples from the COPD and ICUAW cohorts. RNA was extracted from samples of COPD patients (n=84) and age-matched healthy controls (n=26) and from patients with ICUAW (n=18) and controls (n=7) and 12S and 16S rRNA expression was analysed by qPCR. In both cohorts a reduction of 12S and 16S rRNA was seen in patients compared to controls (COPD: 12S rRNA, $p<0.0001$ and 16S rRNA, $p=0.0005$; ICUAW: 12S rRNA, $p<0.0001$ and 16S rRNA, $p=0.0002$) *(Figure 26, A-B).* These data therefore showed consistency with elevated miR-542-3p/-5p levels measured in patients compared to controls and to *in vitro* data. Moreover, the 12S/16S ratio was also reduced in patients compared to controls in both COPD ($p<0.0001$, *Figure 26, C*) and ICUAW ($p=0.0380$, *Figure 26, D*) cohorts.

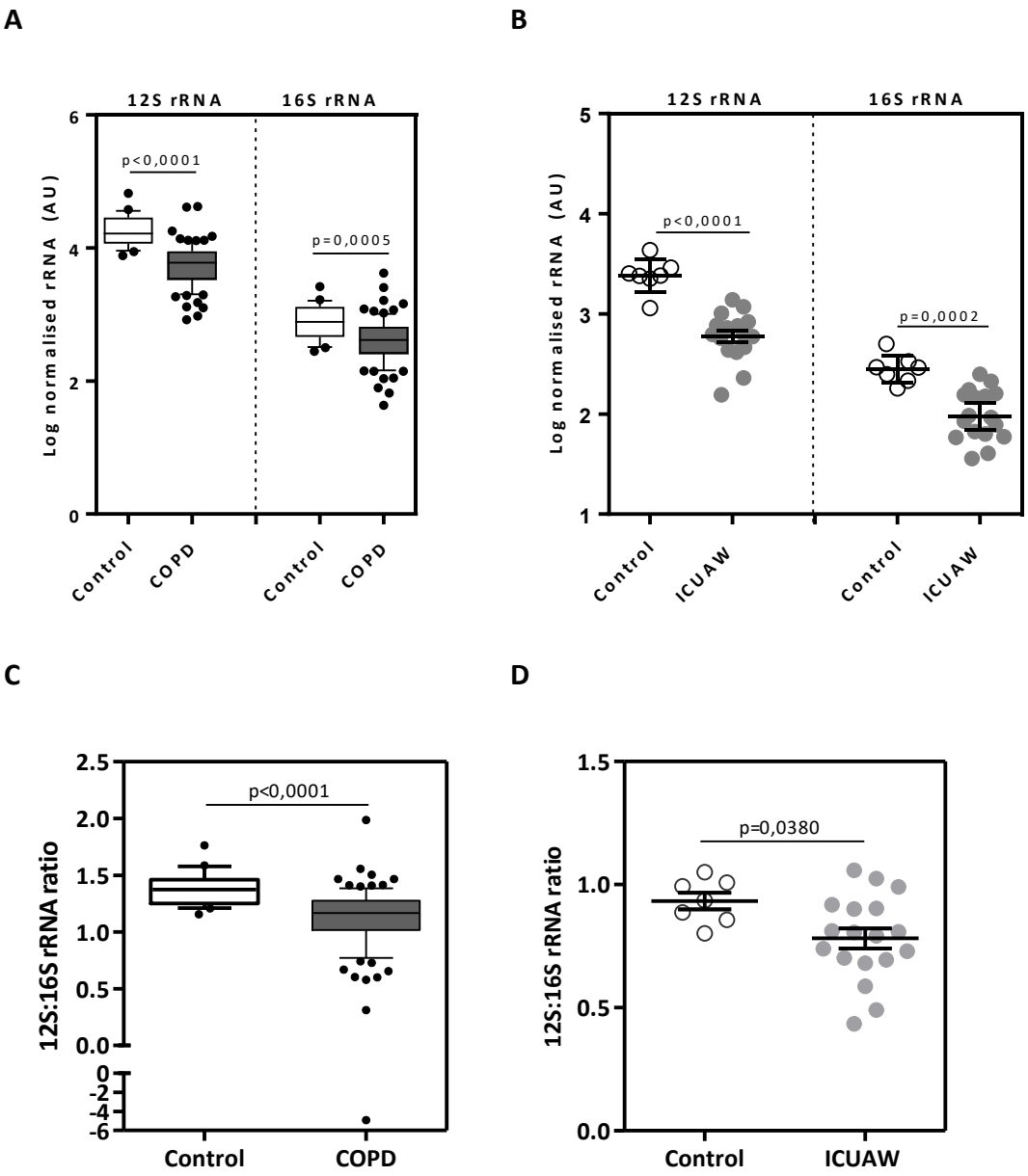


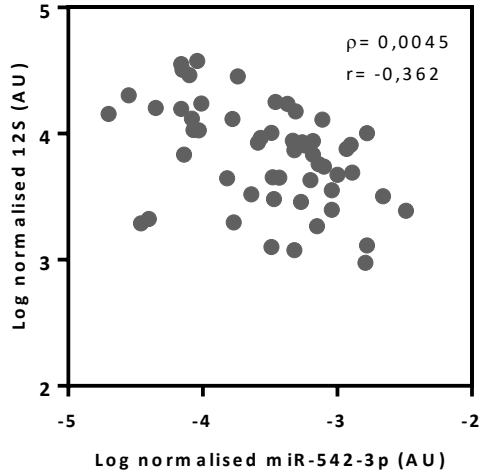
Figure 26- Mitochondrial ribosomal stress in patients with COPD and ICUAW.

12S and 16S rRNA levels were measured in RNA extracted from quadriceps muscle biopsies from 2 different cohorts of patients and showed a decrease in both 12S and 16S levels in COPD and ICUAW patients compared to controls [A,B]. 12S/16S ratio was also decreased in patients of both cohorts compared to controls [C-D]. Box and whiskers plots show 10-90 percentiles and outliers as dots and statistical analysis was performed using Mann Whitney test as the data were not normally distributed. Scatter dot plots show mean signal± SEM and statistical analysis was performed using unpaired t-test as the data were normally distributed. 12S and 16S rRNA levels were normalised against HPRT in COPD cohort and against geomean of HPRT and Beta-2-Microglobulin (B2M) in ICUAW cohort.

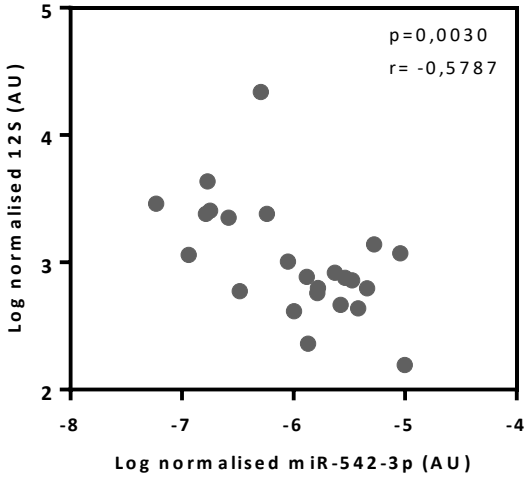
4.3.6 miR-542-3p/-5p levels associate with levels of mitochondrial ribosomal subunits in patients suffering from muscle wasting (COPD and ICUAW)

To study the role of miR-542-3p/-5p in mitochondrial ribosomal stress further, we analysed the associations of 12S and 16S rRNA in patients with COPD and ICUAW. This analysis showed a weak negative correlation between levels of miR-542-3p/-5p and 12S or 16S rRNA in both cohorts. These associations were only seen when both patients and controls were taken into account when performing the analysis in the two cohorts. miR-542-3p expression was associated more strongly with 12S rRNA levels in both cohorts (p=0.0045, r=-0.362 in COPD and p=0.003, r=-0.5787 in ICUAW) *(Figure* 27, *A-B)* than it was with 16S rRNA (p=0.0494, r=-0.2549 in COPD and p=0.0229, r=-0.4623 in ICUAW) *(Figure 27, E-F)*. miR-542-5p also associated with a reduction of 12S rRNA levels in patients in both cohorts (p=0.0034, r=-0.3688 in COPD and p=0.0269, r=-0.4512 in ICUAW) *(Figure* 27*, C-D)* but did not associate with 16S rRNA in COPD patients (p=0.0588, r=-0.2433) *(Figure* 27*, G)* or in patients with ICUAW (p=0.1856, r=-0.2797) *(Figure* 27*, H)* suggesting a stronger effect of the miRs on the small mitochondrial ribosomal subunit than on the large ribosomal rRNA and again consistent with ribosomal stress.

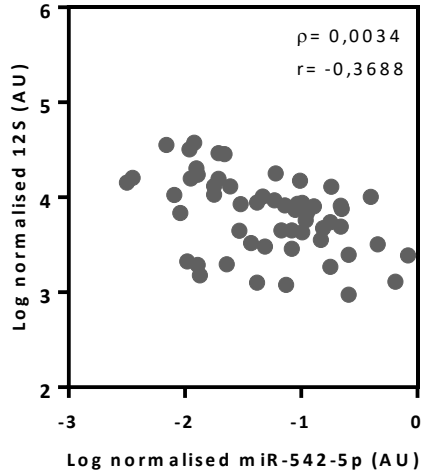
A


ρ= 0,0045
r= -0,362
Log normalised 12S (AU)
Log normalised miR-542-3p (AU)
5
4
3
2
-5
-4
-3
-2

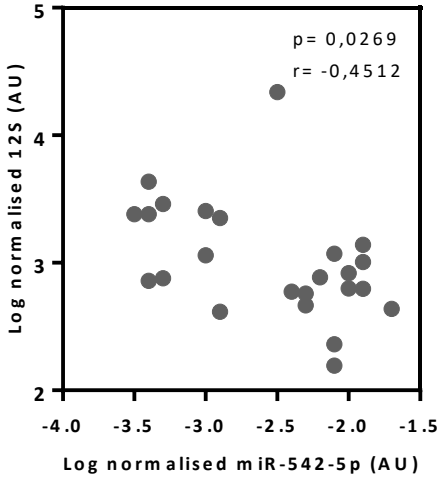
B


p=0,0030
r= -0,5787
Log normalised 12S (AU)
Log normalised miR-542-3p (AU)
5
4
3
2
-8
-7
-6
-5
-4

C


ρ= 0,0034
r= -0,3688
Log normalised 12S (AU)
Log normalised miR-542-5p (AU)
6
5
4
3
2
-3
-2
-1
0

D


p= 0,0269
r= -0,4512
Log normalised 12S (AU)
Log normalised miR-542-5p (AU)
5
4
3
2
-4.0
-3.5
-3.0
-2.5
-2.0
-1.5

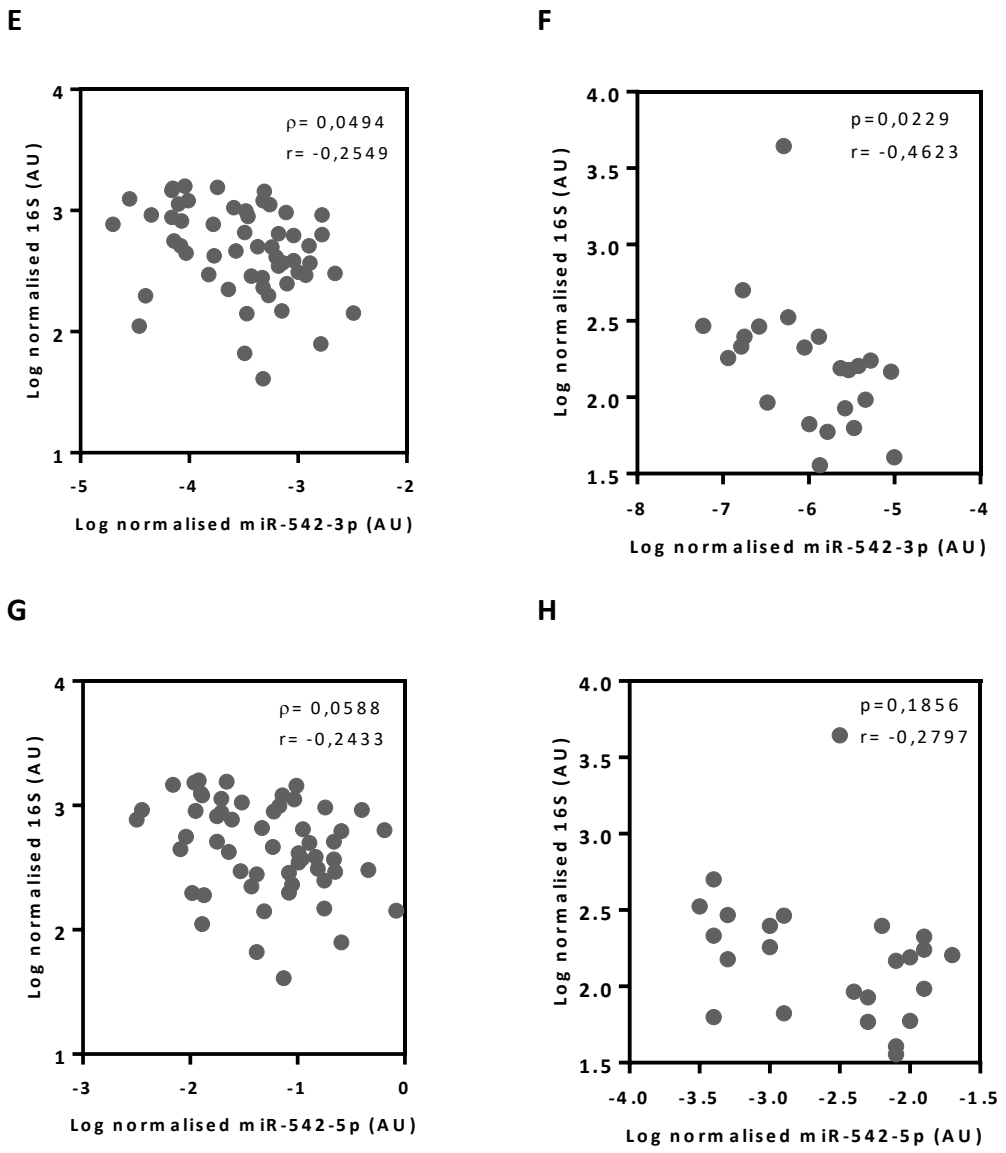


Figure 27- Associations between miR-542-3p/-5p and reduced rRNA in patients with COPD and ICUAW.

12S and 16S rRNA levels in the quadriceps of patients with COPD and ICUAW and the corresponding controls were measured together with miR-542-3p and miR-542-5p levels. Associations were found between miR-542-3p/-5p levels and a decrease of 12S rRNA levels in both cohorts [A-D]. Associations were also seen between miR-542-3p and a reduction in 16S rRNA levels in both cohorts [E-F]. No association was seen between miR-542-5p and a decrease in 16S rRNA in patients with COPD [G] nor with ICUAW [H]. Correlations were analysed by Spearman correlation when data did not have a linear association or by Pearson´s test when data had a linear association showing ρ and r and p and r values, respectively. 12S and 16S rRNA levels were normalised against HPRT in COPD cohort and against geomean of HPRT and Beta-2-Microglobulin (B2M) in ICUAW cohort. miR-542-3p and miR-542-5p levels were normalised against U6.

4.3.7 miR-542-3p targets cytoplasmic ribosomal proteins *in vitro*

miR-542-3p has previously been shown to promote ribosomal stress by inhibiting the expression of a number of cytoplasmic ribosomal proteins (292). To confirm that the same effects could occur in skeletal muscle cells, we examined the role of the microRNA on the expression of RPS23 (Ribosomal Protein S23), a protein forming part of the 40S subunit of cytoplasmic ribosomes together with 18S rRNA. Transfection of LHCN-M2 myoblasts with miR-542-3p caused a reduction in the expression of RPS23 compared to transfection with the scrambled microRNA (p=0.0031, *Figure 28, A-B*).

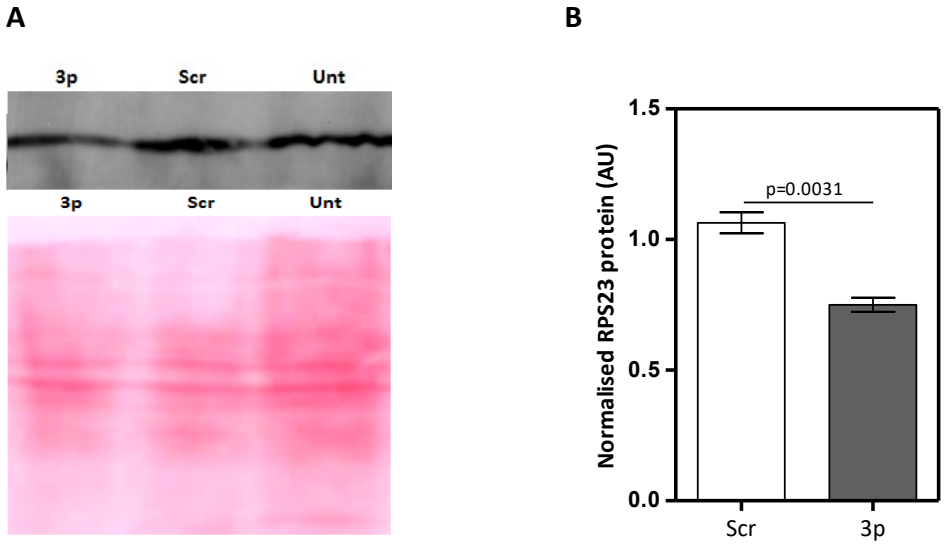


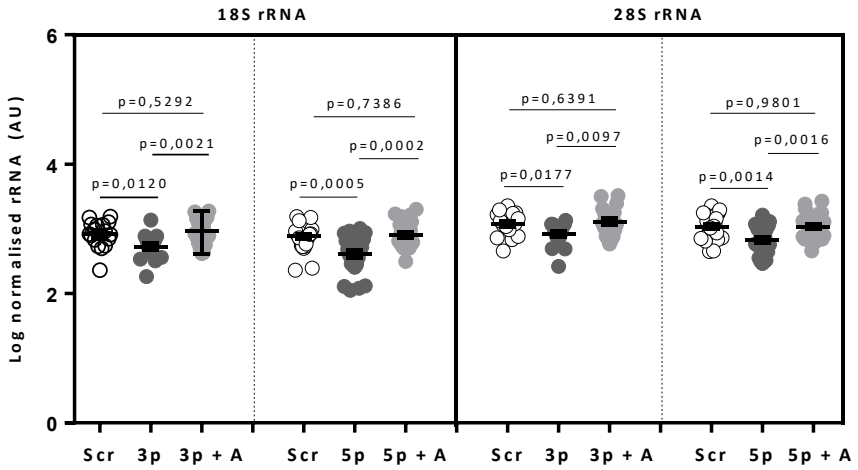
Figure 28- Cytoplasmic ribosomal protein down-regulation by miR-542-3p.

Protein was extracted from LHCN-M2 myoblasts 48h after transfection with scrambled (Scr) or miR-542-3p (3p). *(unt)* denotes cells that were not transfected. As predicted by miRwalk, miR-542-3p decreased RPS23 levels [A] compared to scrambled treated myoblasts and quantification showed 1.33-fold decrease. Bar chart shows mean signal± SEM from n=3 independent transfections. Statistical analysis was performed using unpaired t-test as the data were normally distributed. Ponceau staining was used as a loading control.

4.3.8 Cytoplasmic ribosomal RNA levels were decreased by miR-542-3p and miR-542-5p *in vitro*

To determine whether this reduction in ribosomal protein expression was sufficient to cause cytoplasmic ribosomal stress, the expression of 18S and 28S rRNA was determined under the same conditions as above. In these experiments there was a reduction in 18S rRNA (1.1 fold, p=0.0120, *Figure 29, A*) and a smaller reduction in 28S rRNA levels (1.06 fold, p=0.0177, *Figure 29, A*) in miR-542-3p transfected cells compared to control cells (consistent with the cytoplasmic ribosomal stress shown by *Wang, Y et al.*) *(322).* The effect of the microRNA was greater on the 18S rRNA than on the 28S rRNA leading to a reduction in the 18S:28S ratio *(Figure 29, B)* in miR-542-3p transfected cells compared to control cells (p=0.0249). miR-542-5p also showed similar effects decreasing 18S (p=0.0005) and 28S rRNA (p=0.0014) compared to control myoblasts *(Figure 29, A).* miR-542-5p also decreased the 18S:28S rRNA ratio (p=0.0053). The reduction in 18S and 28S rRNA levels was rescued by co-transfecting the myoblasts with miR-542-3p/-5p antagomiR. The decrease in 18S/28S ratio was rescued by both miR-542-3p/-5p antagomiR, accordingly (further discussion in *Appendix 1*).

A



B

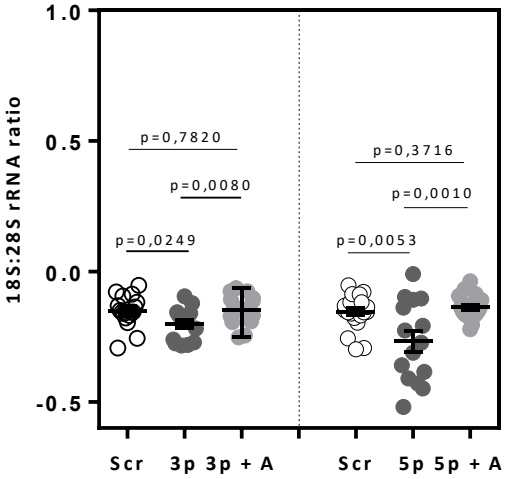


Figure 29- miR-542-3p /-5p decrease 18S and 28S levels of rRNA in LHCN-M2 myoblasts.

LHCN-M2 myoblasts were transfected with scrambled *(Scr)*, miR-542-3p *(3p),* miR-542-5p *(5p),* miR-542-3p together with antagomiR-542-3p *(3p + A)* and miR-542-5p together with antagomiR-542-5p *(5p + A).* 48h later RNA was extracted and rRNA levels were measured by qPCR. [A] miR-542-3p/-5p transfected myoblasts showed a down-regulation of 18S and 28S rRNA. [B] A decrease in 18S:28S ratio was observed in miR-542-3p/-5p transfected cells. The results are based on at least n=6 samples repeated in 3 independent experiments. Scatter dot plots show mean signal± SEM and statistical analysis was performed using unpaired t-test as the data were normally distributed. Normalisation of the data was performed against hypoxanthine guanine phosphoribosyltransferase (HPRT) and β2-microglobuline (β2M).

4.3.9 miR-542-3p and miR-542-5p suppress protein synthesis *in vitro*

Reduced ribosomal content is likely to reduce the maximal protein synthetic capacity of the cells. The effect of the microRNA was therefore determined on protein synthesis using puromycin incorporation. Puromycin is a molecule that resembles the 3'end of the aminoacylated tRNA allowing it to enter the ribosome, to bind and be added to the nascent amino acid chain causing premature translation termination. Puromycin incorporation into nascent proteins can then be determined using an ELISA to measure *de novo* protein synthesis. Myoblasts transfected with either miR-542-3p or miR-542-5p then cultured in the presence of 20% FCS (to promote maximal protein synthesis) had reduced puromycin incorporation into protein ($p<0.0001$, 1.9-fold decrease and $p=0.0016$, 1.4-fold decrease, respectively, *Figure 30*) compared to scrambled treatment suggesting that *de novo* protein synthesis was reduced by the microRNAs.

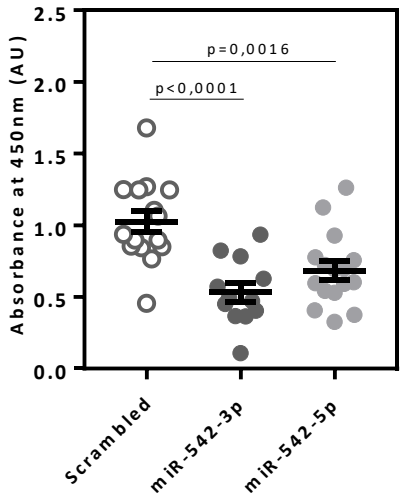


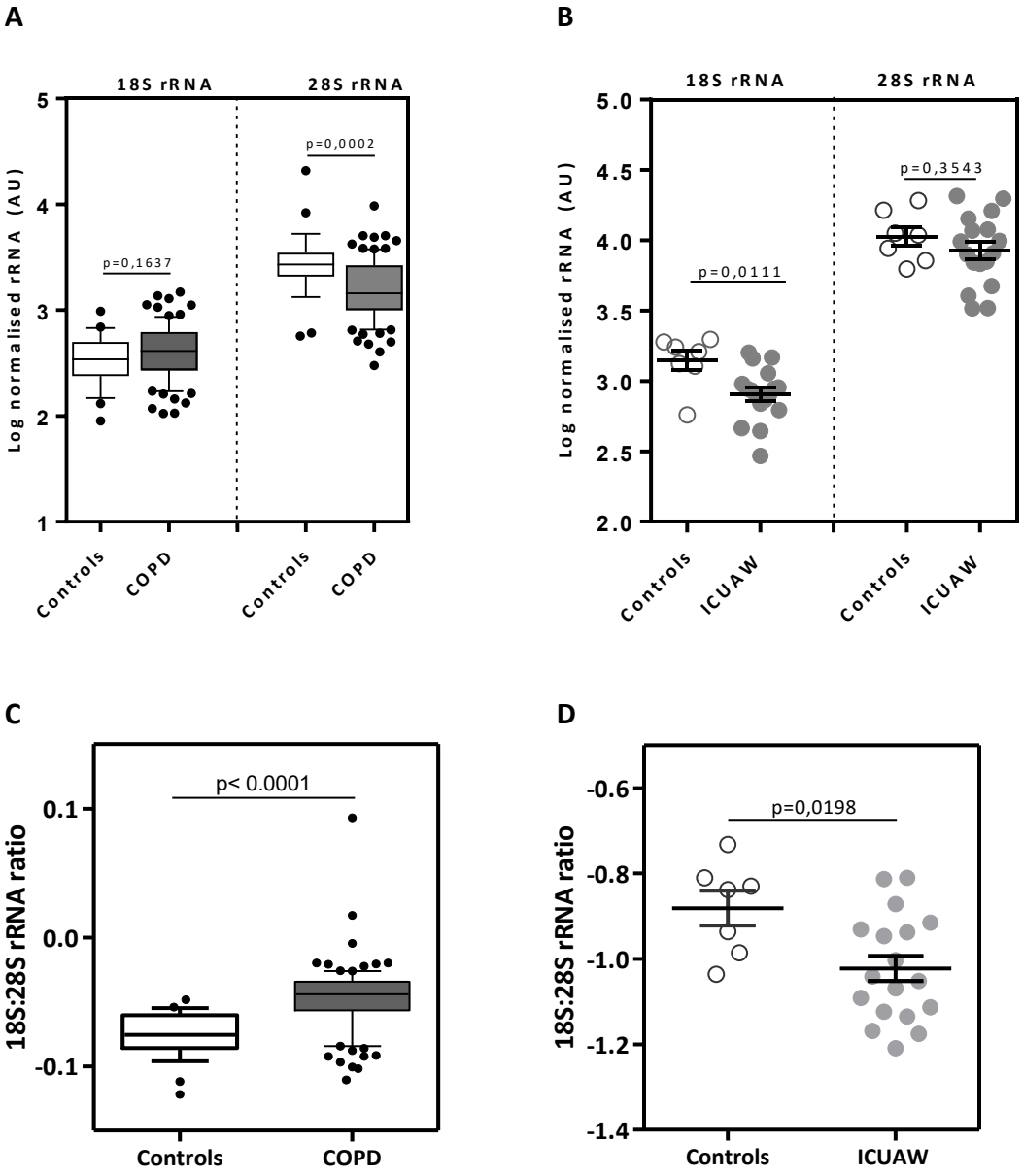
Figure 30- Protein synthesis is decreased by miR-542-3p and miR-542-5p *in vitro*

LHCN-M2 myoblasts were transfected with miR-542-3p/-5p or scrambled and 48h later were incubated with puromycin. The ELISA data showed a decrease of protein synthesis by miR-542-3p/-5p compared to scrambled treatment. Scatter dot plot shows mean signal± SEM from n=3 independent experiments with a minimum of 4 repetitions in each. Statistical analysis was performed using unpaired t-test as the data were normally distributed.

4.3.10 Cytoplasmic ribosomal RNAs are down-regulated in patients suffering from muscle wasting (COPD and ICUAW)

To determine whether miR-542-3p contributes to muscle wasting by causing cytoplasmic ribosomal stress and promoting anabolic resistance we measured 18S and 28S rRNA levels in COPD and ICUAW cohorts. RNA was extracted from samples of the quadriceps of COPD patients (n=84) and age-matched healthy controls (n=26) and from patients with ICUAW (n=18) and controls (n=7) and 18S and 28S rRNA expression was analysed by qPCR. In COPD patients, 18S rRNA levels were constant between patients and controls (p=0.1637) while a reduction in 28S levels was seen in patients (p=0.0002) *(Figure 31, A).* However, in patients with ICUAW a reduction of 18S rRNA (p=0.0111) but no difference in 28S rRNA (p=0.3543) compared to controls was observed. Moreover, there was a reduction in 18S/28S ratio in ICUAW patients compared to controls (p<0.0001, *Figure 31, D*). However, opposite to the *in vitro* data, in COPD patients there was an increase of the 18S/28S ratio in comparison to controls (p=0.0198, *Figure 31, C*).

Other mechanisms might be altering 18S/28S ratio. For example, in mice inoculated with intestinal bacteria it was shown that inflammation positively correlated with a decrease in 28S rRNA and with muscle mass (323). Therefore, the increase in 18S/28S ratio seen in COPD patients could be driven by a reduction in 28S rRNA due to inflammation and consistent with this hypothesis moderate associations between decreased 28S rRNA and circulating interleukins such as IL5 (p=0.0002, r=-0.3236) and IL6 (p=0.0123, r=-0.3042) were observed in the COPD cohort *(Figure 31, E, F)*.


A
18S rRNA
28S rRNA
Log normalised rRNA (AU)
p=0,1637
p=0,0002
Controls
COPD
Controls
COPD
B
18S rRNA
28S rRNA
Log normalised rRNA (AU)
p=0,0111
p=0,3543
Controls
ICUAW
Controls
ICUAW
C
p< 0.0001
18S:28S rRNA ratio
Controls
COPD
D
p=0,0198
18S:28S rRNA ratio
Controls
ICUAW

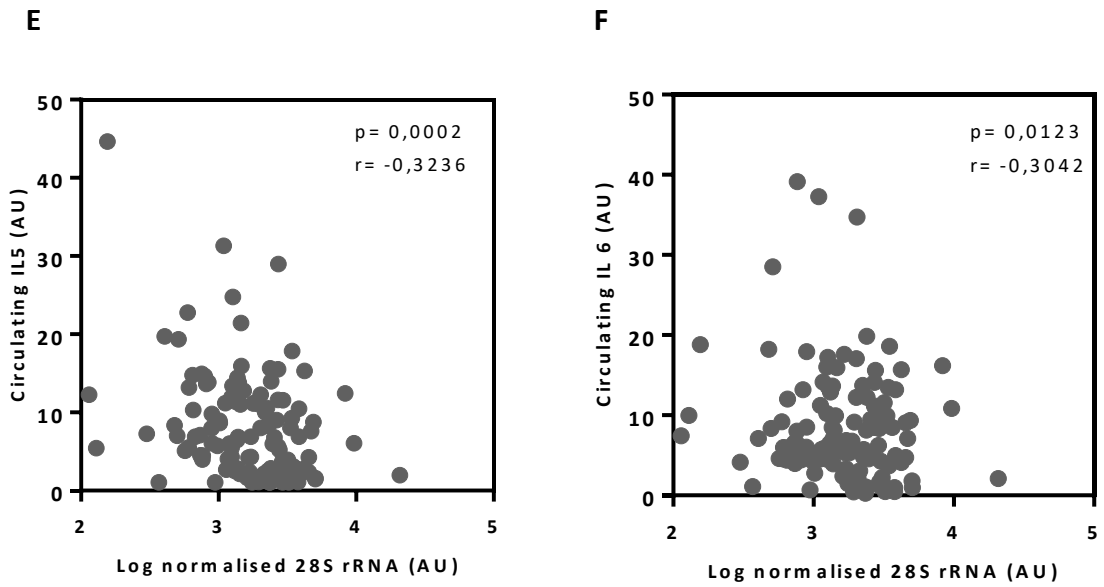


Figure 31- rRNA levels in patients with COPD and ICUAW and associations with interleukins.

18S and 28S rRNA levels were measured in 2 different cohorts. A decrease in 28S rRNAs in COPD patients was seen compared to controls [A] while patients with ICUAW only had decreased levels of 18S rRNA [B]. A decrease in 18S/28S ratio in ICUAW patients [D] but an increase in COPD patients [C] was seen compared to controls. Circulating levels of interleukins in the COPD cohort associated with a decrease of 28S rRNA suggesting inflammation might be driving this effect [E-F]. Box and whiskers plots show 10-90 percentiles and outliers as dots and statistical analysis was performed using Mann Whitney test as samples were not normally distributed. Scatter dot plots show mean signal± SEM and statistical analysis was performed using unpaired t-test as samples were normally distributed. Correlations were analysed by Spearman correlation as data did not have a linear association. 18S and 28S rRNA levels were normalised against HPRT in COPD cohort and against geomean of HPRT and Beta-2-Microglobulin (B2M) in ICUAW cohort.

4.3.11 LHCN-M2 myoblasts under hypoxia decreased the levels of mitochondrial and cytoplasmic ribosomal subunits *in vitro*

In Chapter 3 it was shown that hypoxia increased miR-542-3p expression. If miR-542 promoted both mitochondrial and cytoplasmic ribosomal stress and a reduction in 12S and 18S rRNA levels, it would therefore be expected that hypoxia may also suppress these rRNA levels. Therefore, expression of the mitochondrial and cytoplasmic rRNAs was quantified in LHCN-M2 myoblasts under conditions of normoxia or hypoxia. Consistent with the effects of miR-542-3p, 12S rRNA ($p<0.0001$) was decreased by hypoxia and there was no significant effect on the large rRNA subunit, 16S ($p=0.4907$, *Figure 32, A*). Similarly, 18S rRNA levels were decreased ($p<0.0001$) under hypoxia as well as the large rRNA subunit, 28S ($p=0.0021$, *Figure 32, B*).

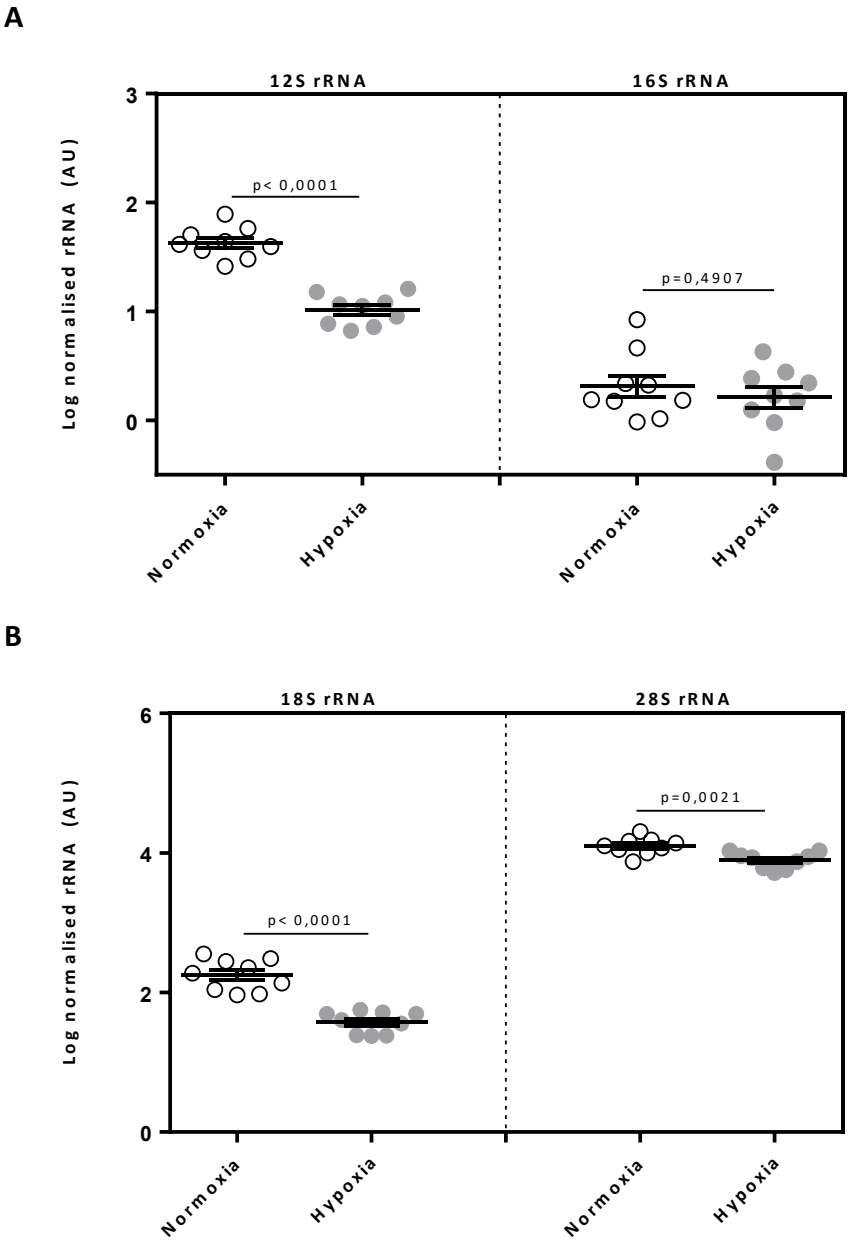


Figure 32- Hypoxia drives down-regulation of 12S and 18S rRNA levels *in vitro.*

RNA from LHCN-M2 myoblasts was extracted after 96h of incubation under normoxia or hypoxia. Decreased levels of [A] 12S and [B] 18S and 28S rRNA were observed in myoblasts incubated under hypoxia. However, hypoxia did not affect 16S rRNA levels in myoblasts. Scatter dot plots show mean signal± SEM from n=3 independent experiments with 3 repetitions in each. Statistical analysis was performed using unpaired t-test as samples were normally distributed. Normalisation of the data was performed against hypoxanthine guanine phosphoribosyltransferase (HPRT) and Glyceraldehyde 3-phosphate dehydrogenase (GAPDH).

4.3.12 miR-542-3p increases GDF-15 expression *in vitro* in a positive feedback manner

Another hallmark of ribosomal stress is an increase in the activity of p53 as described in Chapter 1. A p53 response gene that is important in muscle wasting is GDF-15. We therefore hypothesised that miR-542-3p would increase the expression of GDF-15. Consistent with this hypothesis, transfection of LHCN-M2 with miR-542-3p caused an increase in GDF-15 mRNA expression (p=0.0136, *Figure 33*, *A*) compared to scrambled transfection, suggesting activation of p53. This effect was reversed by transfecting the cells with antagomiR-542-3p (p=0.0017). However, there was no effect due to miR-542-5p transfection (p=0.1927, *Figure 33*, *B*). The reason for the lack of apparent activation of p53 by miR-542-5p even though it causes a reduction in 18S rRNA suggests either that the effect on ribosomes is insufficient or that differences in targets inhibit the activation of GDF-15. One possibility consistent with this suggestion comes from bioinformatics analysis showing that 4 of the 9 databases predict p53 as a target of miR-542-5p, raising the possibility that the microRNA may suppress p53 expression and indirectly suppress GDF-15 levels even in case of ribosomal stress. Conversely only one of the 9 databases predicted that p53 is a target of miR-542-3p making it less likely to be a real target. However, there was insufficient time available to confirm targeting of p53 by miR-542-5p.

We further analysed GDF-15 RNA levels in LHCN-M2 incubated for 96h under hypoxia and normoxia. Hypoxic myoblasts showed increased GDF-15 levels compared to normoxic cells (p<0.0001, *Figure 33, D*), consistent with hypoxia elevating miR-542-3p levels. However, time did not allow us to confirm that this effect was dependent on p53.

To determine whether GDF-15 could increase miR-542-3p in a positive feedback loop, we measured miR-542-3p levels in LHCN-M2 myoblasts 48h after the addition of GDF-15 (50 ng/mL) *(Figure 33, C)*. This treatment caused an increase in miR-542-3p expression in myoblasts compared to treatment with the vehicle (p=0.0360).

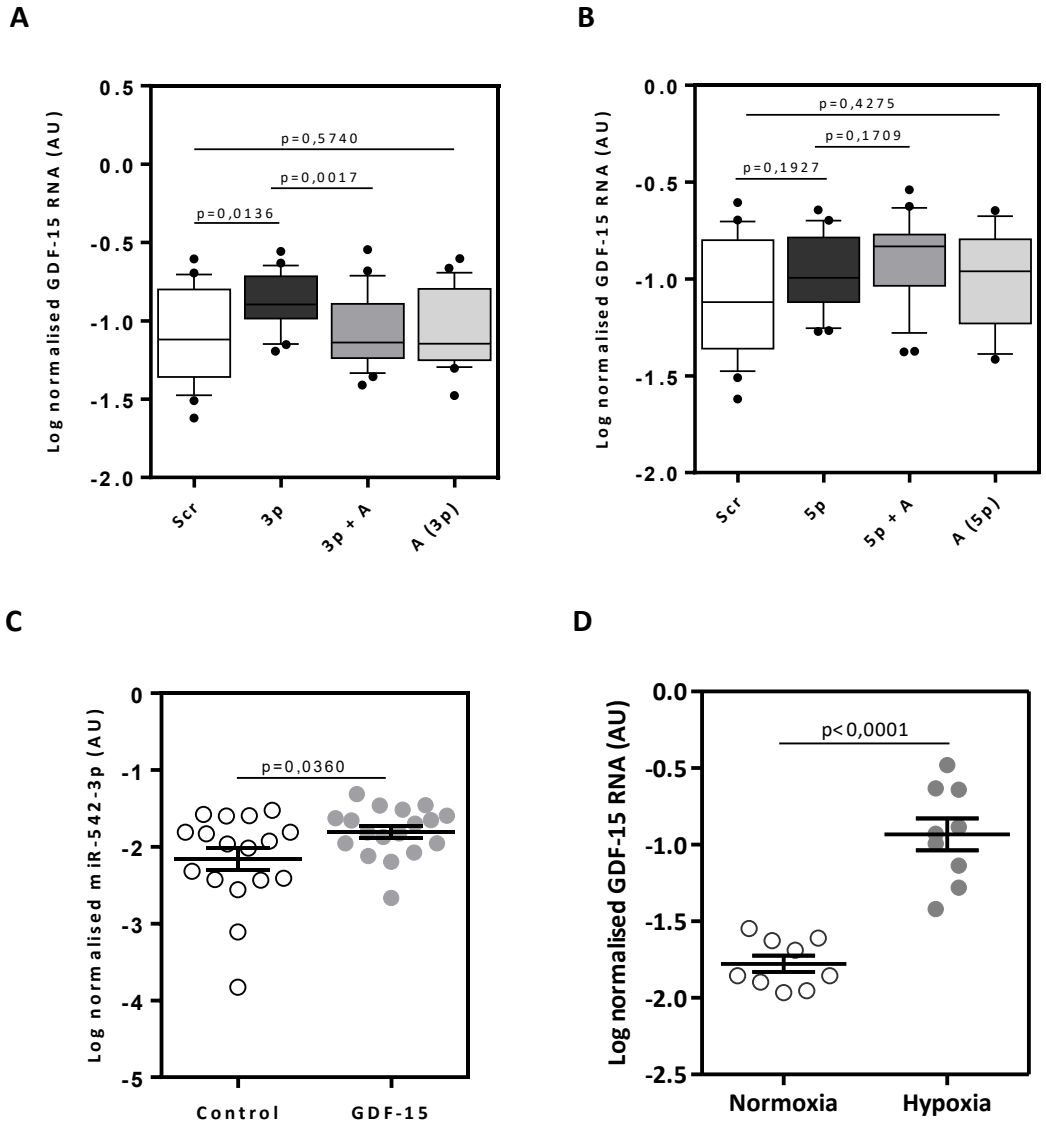


Figure 33- GDF-15 RNA up-regulation by miR-542-3p/-5p *in vitro* and positive feedback.

RNA from LHCN-M2 myoblasts was extracted after 48h of being transfected with scrambled *(Scr)*, miR-542-3p *(3p)*, miR-542-5p, miR-542-3p and antagomiR-542-3p *(3p + A)*, angatomiR-542-3p *(A-3p)*, miR-542-5p *(5p)* and antagomiR-542-5p *(5p + A)*, angatomiR-542-5p *(A-5p)*. An increase in GDF-15 RNA levels was seen in miR-542-3p transfected myoblasts [A] but no effect was shown by miR-542-5p [B]. [C] LHCN-M2 were seeded in 96 well plates and treated 48h with GDF-15 (50 ng/mL). RNA was extracted and miR-542-3p levels were measured and found to be increased by GDF-15 treatment compared to control. [D] RNA from LHCN-M2 myoblasts was extracted after 96h of incubation under normoxia or hypoxia. Increased GDF-15 RNA levels were observed in myoblasts incubated under hypoxia. Transfected miR-mimic levels were kept constant in all experiments by co-transfection with scr. Box and whiskers plots show 10-90 percentiles and outliers as dots from n=3 independent experiments with 6 repetitions in each. Statistical analysis was performed using Mann Whitney test as the data were not normally distributed. Scatter dot plots show mean signal± SEM from n=3 independent experiments with at least 3 repetitions in each. Statistical analysis was performed using unpaired t-test as samples were normally distributed. Normalisation of the data was performed against HPRT, GAPDH and β2M. miR-542-3p was normalised against U6.

4.4 Discussion

4.4.1 Main findings

In this chapter, we have shown that miR-542-3p targets the expression of both mitochondrial and cytoplasmic ribosomal proteins *in vitro* (MRPS10 and RPS23, respectively). As a result of this targeting, the microRNAs induce ribosomal stress in both compartments as shown by a reduction of 12S and 18S rRNA. In the mitochondria, the ribosomal stress leads to mitochondrial dysfunction as the proteins forming part of the electron transport chain and ATP synthase cannot be synthesised as efficiently leading to a reduction in membrane potential. Moreover, decreased ribosomal biogenesis also seems to decrease mitochondrial protein synthesis as shown by reduced CYTB protein levels by miR transfection. In the cytoplasmic compartment, there is a decrease in *de novo* protein synthesis *in vitro* and an increase in GDF-15 levels, a transcriptional target for p53.

Consistent with these data, hypoxia, a condition that increases miR-542-3p, caused similar changes in 12S and 18S rRNA and an increase in GDF-15 RNA levels. Moreover, in patients with COPD and ICUAW there is also evidence of mitochondrial and cytoplasmic ribosomal stress. For example, there was a reduction of 12S/16S rRNA ratio in patients with COPD and ICUAW and associations between 12S and miR-542-3p/-5p were found. The 18S/28S rRNA ratio was also decreased in ICUAW patients compared to controls. These results suggest that miR-542 is a novel contributor to atrophy and muscle dysfunction.

4.4.2 miR-542 promotes mitochondrial ribosomal stress

As described in Chapter 1, mitochondrial dysfunction has been suggested to be an important contributor to muscle wasting in several conditions. The data presented in this chapter identify mitochondrial ribosomal stress in response to elevated miR-542 as a potential key regulator of atrophy. The reduced ability of the muscle to synthesise the proteins encoded by mitochondria would explain the larger reduction in the activity of complexes I, III and IV compared to the activity of complex II that has been

identified in a number of studies. For example, in the skeletal muscle of patients with COPD (308), heart failure (76) and acute disease such as patients with ICUAW (324) a decrease in activity was measured, especially in complex I, III and IV. However, complex II activity was found to be relatively preserved in these patients compared to controls. Furthermore, in the study by *Gifford JR et al*. measurement of complex II activity in the skeletal muscle of COPD patients was not different from controls (325). Similarly, protein extracted from skeletal muscle of patients with ICUAW indicated decreased protein levels in complex III and IV but no change in complex II (295). In ageing, similar patterns have been described with a drop of complexes III, IV and V activity in humans (176,326-329) but no difference in complex II activity. However, some studies fail to observe such complex activity changes (330-332).

Mitochondrial stress measured as a reduction in 12S rRNA has also been reported in other diseases and was attributed to mitochondrial ribosomal protein (MRP) mutations. MRP impairment was shown to decrease mitochondrial activity which is consistent with miR-542-3p targeting MRPs and decreasing mitochondrial complex activities. For example, a mutation in MRPS16 was found in an incidence of agenesis of the *corpus callosum*, a birth defect with incomplete brain development, and was associated with decreased 12S rRNA as well as complex I and IV activity and with increased lactic acid production suggesting that anaerobic glycolysis was used to produce ATP as a result of mitochondrial dysfunction (180). Moreover, some patients with antenatal mitochondrial diseases (skin oedema, hypotonia, cardiomyopathy and tubulopathy) suffer from a mutation in MRPS22 leading to decreased levels of this protein. It has been shown that transfection of MRPS22 cDNA in the cells of those patients restored MRPS22 levels, rescued 12S rRNA levels and restored mitochondrial respiratory chain complexes indicating MRPs play an essential role in mitochondrial function (317).

Whilst our data support a role for miR-542 in hypoxia dependent suppression of mitochondrial function it is possible that other factors also contribute as studies have shown that short term treatment of cells and animals with severe hypoxic stimuli can also modify mitochondrial function and 12S rRNA expression. For example, a hypoxia dependent reduction in 12S rRNA has been shown in rats (comparing coronal sections

of 6h induced-ischemic and control brain) (333) and in chondrocytes in culture under oxidative stress generated by the hypoxanthine-xanthine oxidase system (334). However, a reduction in the 12S:16S ratio has not been described in those cases.

4.4.3 The role of mitochondria in exercise performance

Mitochondrial ribosomal stress leading to mitochondrial function impairment could also lead to reduced exercise capacity since endurance is related to both number and function of mitochondria in skeletal muscle (335). Therefore, the observed mitochondrial ribosomal stress could explain the association between miR-542 expression and 6MW described in the previous chapter. Patients with COPD, ICUAW or older individuals have been reported to have fewer mitochondria in their muscles, therefore are more prone to fatigue. *Killian et al.* firstly reported the limitation in exercise performance in COPD patients. In this study, they reported that 40% of the patients terminated the exercise due to leg fatigue and 30% stated equality between the leg fatigue and the shortness of breath (336). The importance of mitochondria in muscle endurance was also shown in COPD patients where muscle performance correlated with mitochondrial oxidative capacity (337). Moreover, the increase in miR-542 levels observed in those diseases could also cause mitochondrial ribosomal stress leading to decreased ATP production. ATP is essential for muscle plasticity and to allow the muscle to adapt to increasing levels of exercise, situations that trigger an increase in protein synthesis in skeletal muscle. Therefore, the correlation seen between increased miR-542 levels and decreased 6MW distance indicates that patients with higher levels of the miR have a poorer exercise capacity, probably due at least in part to mitochondrial ribosomal stress which causes a decrease in ATP production. Moreover, impairment in ATP synthesis could cause increased production of ROS, leading to increased inflammation thereby contributing to atrophy (135). A decrease in ATP together with an increase in ROS (338) has been reported in sarcopenic patients, consistent with the decline of the maximal rate of oxygen consumption (VO_{2max}) and resting oxygen observed on those patients (339).

4.4.4 miR-542 suppresses protein synthesis

The data presented extend a previous study showing that miR-542-3p can cause cytoplasmic ribosomal stress and we showed that this is accompanied by a reduction in maximal protein synthesis, which could lead to anabolic resistance. *Volpi et al.* firstly demonstrated anabolic resistance in skeletal muscle protein synthesis (MPS) in the elderly by comparing the increased MPS rates of the young controls versus the unchanged rates in the older individuals after consumption of an amino acid and glucose mix (340). Similarly, in older people a lower increase in skeletal MPS was observed compared to young controls after amino acid feeding under insulin clamping conditions (around 40% less) and in response to acute exercise (around 30% less) (341). Anabolic resistance has also been described as a consequence of immobility which leads to a decrease in MPS. One study measured the stimulated protein synthesis in muscles of immobilised legs and compared it to non-immobilised legs after amino acid infusion. A decrease in protein synthesis was reported in the immobilised leg, even when amino acids were infused at higher rates (311). These data suggest that the increase in miR-542-3p levels seen in those patients could contribute to the anabolic resistance by decreasing the number of available ribosomes and thereby maximal protein synthetic rate. As seen in this chapter, hypoxia, which induces miR-542 transcription, also leads to ribosomal stress suggesting it could cause anabolic resistance. Consistent with this hypothesis, a study performed in rats under normoxic or hypoxic conditions for 7 days showed that hypoxia impairs mTOR signalling and enhances muscle loss in the soleus muscle of those animals after injury. These data suggested that protein synthesis could be impaired under those conditions together with satellite cell activity (342).

4.4.5 miR-542-3p elevates GDF-15 expression in muscle

miR-542-3p has been reported to activate p53 by inducing cytoplasmic ribosomal stress (292), suggesting an additional mechanism by which miR-542-3p may regulate muscle mass. GDF-15, which is reported to be a biomarker for acute exacerbations in COPD (343), is a transcriptional target for p53. For example, in COPD patients the

circulating levels of GDF-15 inversely correlated with the *rectus femoris* cross-sectional area and exercise capacity in two separate cohorts (197). Moreover, increased levels of circulating GDF-15 in the plasma and increased levels of mRNA in the muscle were observed in other diseases where muscle wasting is observed, such as in patients with ICUAW (30). Consistent with a role for GDF-15 in atrophy, GDF-15 treatment of mouse myotubes (C2C12) increased the expression of muscle atrophy-related genes such as MuRF-1 and atrogin-1 and down-regulated the expression of some muscle-restricted microRNAs including miR-1, miR-133a and miR-499, which have been shown to repress TGF-β signalling (30). *In vivo*, overexpression of GDF-15 in the *tibialis anterior* muscle of mice caused wasting compared to the control contralateral muscle (197). Therefore, perhaps by activating p53 and thereby increasing GDF-15 levels, miR-542-3p could be inducing another mechanism promoting wasting. Consistent with miR-542 being elevated by hypoxia, previous studies also reported increased levels of GDF-15 expression by hypoxia or oxidative stress in multiple cell types such as cardiomyocytes, hepatocytes and macrophages (344-348).

4.4.6 Critique of the method

The *in vitro* experiments described were performed using C2C12 mouse myoblasts and LHCN-M2 human myoblasts however primary cells or immortalised cell lines from patients could have been used to perform the experiments and might have provided a better insight into the mechanism of the disease. However, there was no guarantee of preserving the epigenetics of the patients and the circulating signalling from the plasma could not have been reproduced so we considered that the approach we have taken is valid to answer our hypothesis.

The clinical data used in this chapter comes from clinical observations from cross-sectional studies therefore we cannot prove a causal link between miR-542-3p/-5p and reduction in ribosomal RNAs and proteins in the patients. However, associations found in two different cohorts (COPD and ICUAW) together with our *in vitro* data suggest a possible mechanism of action that could be confirmed by an animal model and the use of antagomiRs in the model.

4.5 Conclusions

In conclusion, in this chapter we analysed the role of miR-542-3p/-5p in mitochondrial and cytoplasmic ribosomal stress as contributing factors in muscle wasting. We propose that increased miR-542-3p/-5p leads to a reduction in mitochondrial (MRPS10) and cytoplasmic (RPS23) ribosomal proteins resulting in ribosomal stress. In the mitochondria, ribosomal stress causes mitochondrial dysfunction whereas in the cytoplasm, it leads to a reduction in maximal protein synthesis and activation of the expression of GDF-15. Together these activities lead to anabolic resistance and a reduction in energy provision resulting in reduced muscle mass and function *(Figure 34).*

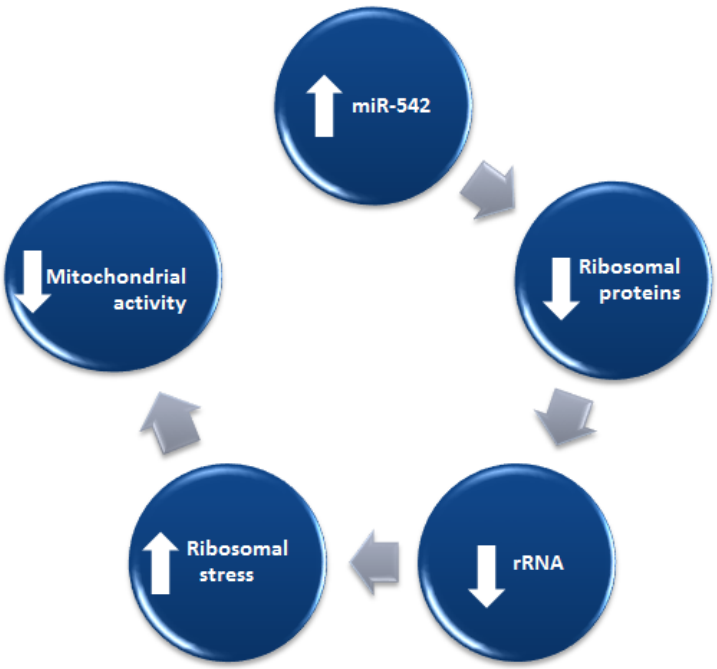


Figure 34- Proposed mechanism of action of miR-542-3p/-5p in cytoplasmic and mitochondrial ribosomal stress

miR-542-3p/-5p target ribosomal proteins which leads to the decrease of ribosomal biogenesis resulting in ribosomal stress, which causes a decrease in mitochondrial activity. Therefore, the total amount of ATP produced is decreased and it is likely to contribute to decreased exercise performance and anabolic resistance seen in patients.

CHAPTER 5: Regulation of SMAD2/3 signalling by miR-542-3p and miR-542-5p

5.1 Rationale

Signalling through the TGF-β pathway has an important role in skeletal muscle by reprograming gene expression, controlling myoblast proliferation and inhibiting myogenic differentiation (349). Indeed, a number of *in vivo* studies have identified the TGF-β family ligands, TGF-β1 and MSTN, as playing a key role in regulating muscle mass and pathogenesis (349). For example, MSTN knockout ($Mstn^{-/-}$) mice have increased muscle mass and strength together with reduced fat compared to wild type mice (350). Moreover, the reduction in MSTN seems to have a beneficial effect in ageing by reducing sarcopenia as shown by a comparison between 24 months $Mstn^{-/-}$ and wild-type mice where $Mstn^{-/-}$ mice lost less muscle mass (351). Similarly, treatment of fibrillin-1 deficient mice with a neutralising TGF-β1 antibody rescued muscle regeneration (352) suggesting that TGF-β1 impaired myoblast proliferation leading to poor regeneration. The relevance of TGF-β signalling to muscle wasting has also been shown in man as several studies have implicated the TGF-β pathway in muscle wasting. In COPD patients, the levels of MSTN in serum were increased compared to controls and inversely associated with muscle mass in male patients (353). Similarly, high serum levels of MSTN were also seen in old individuals with muscle wasting compared to individuals with a normal muscle mass suggesting MSTN contributes to sarcopenia (354).

As described in the introduction, microRNAs are key regulators of cell phenotype and, therefore unsurprisingly, the TGF-β signalling can be regulated by microRNAs targeting key components of the pathway (234,355-357). Some of these microRNAs have been shown to be dysregulated in conditions associated with muscle wasting. Moreover, miR-1 levels were suppressed in the quadriceps of COPD patients compared to controls. miR-1 has been predicted to target HDAC4, which targets follistatin. Follistatin is known to bind and inactivate myostatin suggesting that decreased miR-1 could activate myostatin activity in an indirect manner in those patients.

Other microRNAs that can target a TGF- β ligand are miR-744 (358) and miR-122 (359), which target TGF-β1.

MicroRNAs targeting the receptors of the TGF-β signalling pathway include miR-302, which targets the TGF-β type II receptor leading to down-regulation of TGF-β signalling (360), miR-181b supresses Alk5 and modulated SMAD-dependent and independent TGF-β signalling in A549 cells (adenocarcinomic human alveolar basal epithelial cells) (361) as well as promoting cell proliferation by targeting the cell cycle regulator p27 in hepatocytes (362) which could induce fibrosis. In agreement with this suggestion, elevated levels of this miR were found in the serum of patients suffering from liver fibrosis and cirrhosis (362).

Some microRNAs reduce TGF-β pathway by targeting SMAD protein levels: miR-145 negatively regulates SMAD3 (363) leading to a down regulation of pro-inflammatory cytokines in airway smooth muscle cells in COPD (364). miR-146 targets SMAD4 in hepatic stellate cells and human dermal fibroblasts (365,366) and miR-346 targets both SMAD3 and SMAD4 in mouse kidney cells (367). miR-24 indirectly decreases the expression of total SMAD2, SMAD3, and p-SMAD2 by targeting Tribbles-like protein-3 (Trb3) and also inhibits the TGF-β-induced expression of miR-21 in vascular smooth muscle cells (368). miR-26a decreases levels of SMAD1 and SMAD4 promoting differentiation of myoblasts in mice. Moreover, an inhibition of miR-26a in the *tibialis anterior* muscle delayed regeneration *in vivo* (369).

Other microRNAs target inhibitory components within the pathway and are likely to increase TGF-β signalling and thereby can promote TGF-β signalling so contribute to some pathological processes including fibrosis. miR-21 targets SMAD7 (370) and consistent with a contribution of miR-21 to TGF-β signalling, miR-21 is increased in patients with fibrosis where SMAD7 levels are reduced. Furthermore, both SMAD7 and miR-21 levels return to normal following treatment with bortezomib, an anti-fibrotic drug (370). Similarly, miR-424 targets the 3'UTR of SMAD7, SMURF1 and SMURF2 but only decreases SMURF2 protein levels in HEK293 cells (human embryonic kidney cells) (253). The observation that miR-424 levels are increased in the quadriceps

of COPD patients compared to controls suggests that there may be an increase in TGF-β activity in these patients (371).

The data presented in Chapter 3 showed increased miR-542 levels in COPD patients and in those with established ICUAW as well as a negative association of miR-542 expression with muscle performance. Furthermore, bioinformatic analysis presented in that chapter predicted that this microRNA targeted a number of components of the TGF-β signalling system including inhibitors of the system (SMAD7 and SMURF1), proteins from the PP2A complex (PPP2CA) which dephosphorylate SMAD2/3 after activation, and other phosphatases such as CTDSP1, CTDSP2 and PPM1A. Therefore, the main aim of this study was to determine whether miR-542-3p/-5p could regulate TGF-β signalling. To determine their role in SMAD activation we analysed their effects *in vitro* in both C2C12 (mouse) and LHCN-M2 (human) myoblasts, followed by quantifying the identified targets in quadriceps biopsies from patients with COPD or ICUAW.

5.2 Hypothesis

The above rational prompted the following hypothesis:

1) Increased miR-542-3p and miR-542-5p levels will increase the activity of the TGF-β pathway in skeletal muscle by reducing the expression of a set of inhibitory components of the SMAD signalling system.

5.3 Results

5.3.1 miR-542-3p and miR-542-5p increase SMAD dependent luciferase activity in the absence of added ligand *in vitro*

To determine the effect of miR-542-3p on SMAD reporter luciferase activity and to identify an appropriate concentration of the ligand, C2C12 cells were transfected with the miR-mimic and the reporter components as described in Chapter 2. C2C12 myoblasts were used as they are an extensively studied cell line and results are easily comparable with the literature. Cells were treated with 0, 0.5, 1, 5ng/mL TGF-β1 for 6h and luciferase activity was determined *(Figure 35)*. TGF-β1 increased luciferase activity at all concentrations with the greatest increase at 5ng/mL (approximately 5-fold). In the absence of added TGF-β1, miR-542-3p increased luciferase activity 1.5-fold but in the presence of TGF-β1, miR-542-3p reduced luciferase activity compared to a scrambled control *(Figure 35)*. As the effects of miR-542-3p on TGF-β1 dependent luciferase activity were greatest at 5ng/mL this concentration was chosen for subsequent experiments.

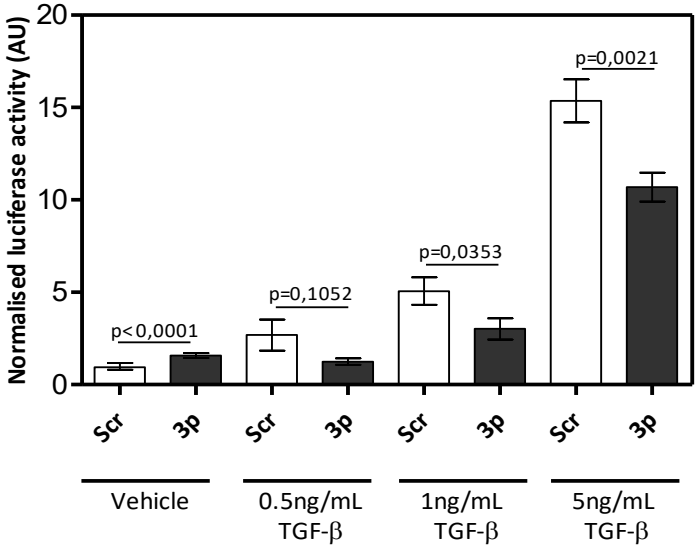


Figure 35- Dose response of TGF-β at 6h activation period in C2C12.

C2C12 cells were transfected with scrambled (Scr) or miR-542-3p (3p) miR-mimics and 24h later were transfected with $CAGA_{12}$ and pRL-TK reporter vectors. Cells were treated for 6h with TGF-β1 at the indicated concentrations to assess which was the minimal concentration of the ligand where a clear activation response was obtained. The results are based on n=6 samples repeated in 3 independent experiments. Firefly luciferase activity was normalised to Renilla luciferase activity. Bar chart shows mean normalised signal± SEM and unpaired t-test was used to perform the statistical analysis as data were normally distributed.

To confirm the effects of miR-542-3p, the experiment was repeated in the presence and absence of an antagomiR using 5ng/mL TGF-β1. These experiments again showed that in the absence of added ligand, miR-542-3p increased luciferase activity by 2-fold (p=0.0018) *(Figure 36)* and that miR-542-3p suppressed luciferase activity in cells stimulated with 5ng/mL TGF-β1, 2-fold (p<0.0001). Both effects of the microRNA were reversed by co-transfecting myoblasts with the antagomiR. On its own, the antagomiR did not affect luciferase activity in the presence or absence of added TGF-β1.

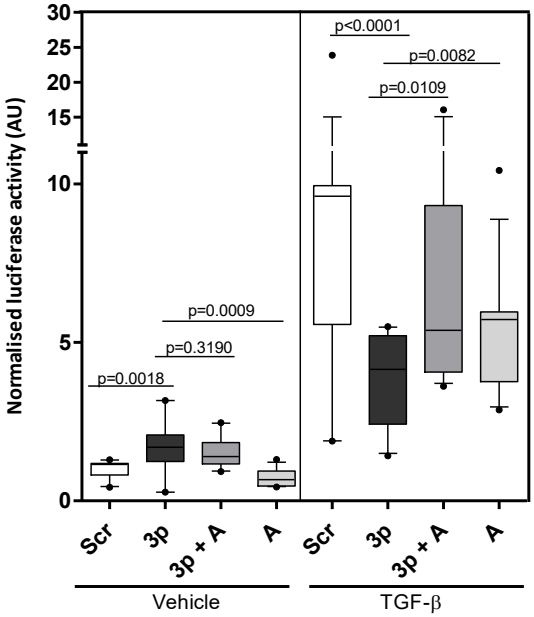


Figure 36- miR-542-3p increases basal level of TGF-β signalling in C2C12.

C2C12 cells were transfected with scrambled (Scr), miR-542-3p (3p), miR-542-3p miR-mimics and antagomiR-542-3p (3p + A) and antagomiR-542-3p (A) and 24h later were transfected with $CAGA_{12}$ and pRL-TK reporter vectors. Cells were treated with BSA (vehicle) or stimulated with 5ng/mL TGF-β1. An increase in the basal levels of TGF-β signalling was observed in unstimulated and miR-542-3p transfected cells. However, a reduction of the signalling was seen in the presence of the miR and TGF-β1 ligand. Transfected miR-mimic levels were kept constant in all experiments by co-transfection with scr. Firefly luciferase activity was normalised to Renilla luciferase activity. Box and whiskers plot shows 10-90 percentiles of normalised luciferase activity signal and outliers as dots. Statistical analysis was performed using Mann Whitney test as the data were not normally distributed.

To determine whether miR-542-3p had a similar effect in human myoblasts the experiment was repeated using LHCN-M2 myoblasts. We also determined the effects of miR-542-5p on TGF-β activity in this cell line. Consistent with the previous experiments, in the absence of added TGF-β1 miR-542-3p and miR-542-5p increased luciferase activity by almost 2-fold (p=0.0003 by miR-542-3p and p=0.0017 by

miR-542-5p) in LHCN-M2 cells *(Figure 37)* and this effect was reversed by addition of the corresponding antagomiR. Furthermore, both miRs suppressed ligand stimulated luciferase activity at 5ng/mL TGF-β1 (p=0.0226 by miR-542-3p and p=0.0002 by miR-542-5p) in an antagomiR reversible manner.

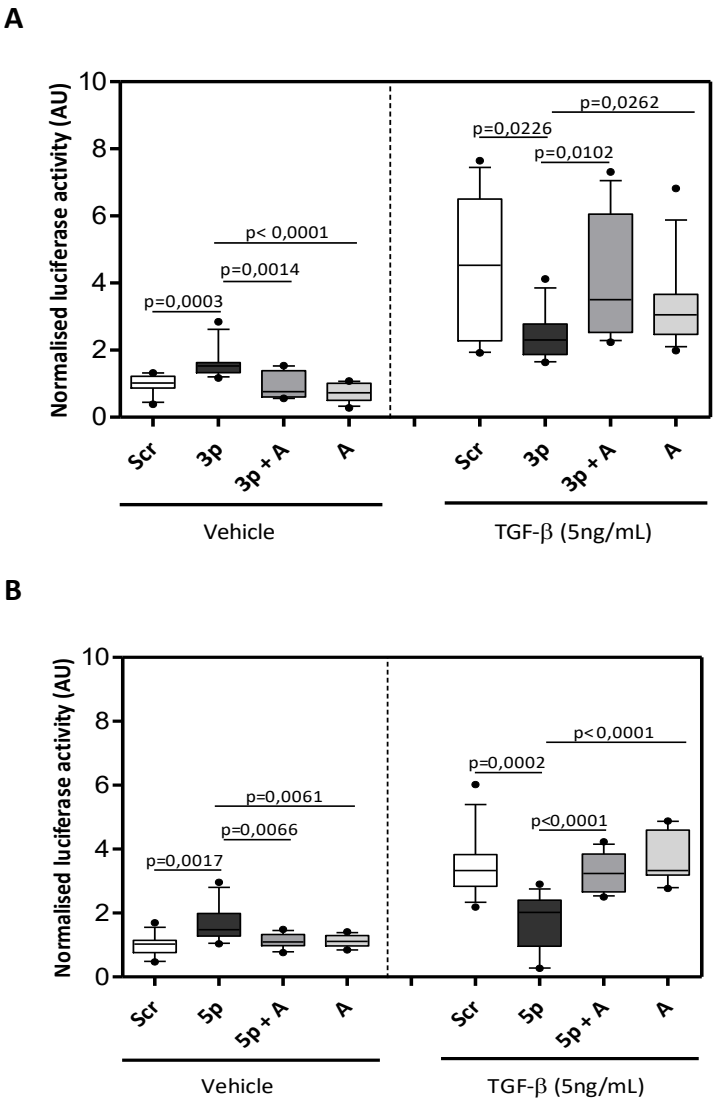


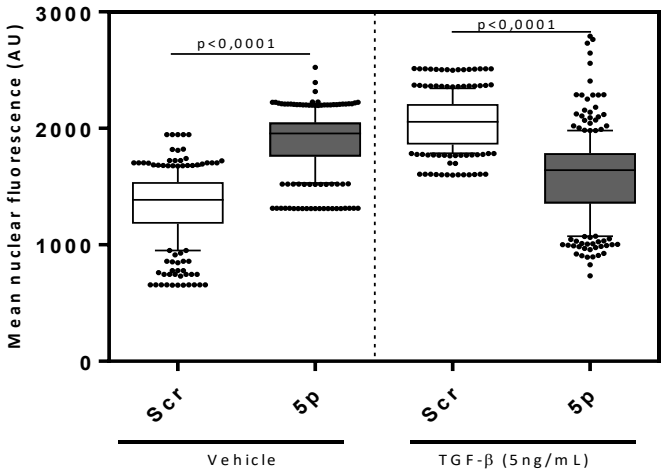
Figure 37- miR-542-3p and miR-542-5p increased basal SMAD2/3 activity in LHCN-M2.

LHCN-M2 myoblasts were transfected with scrambled *(Scr)*, miR mimic miR-542-3p *(3p)* [A]/ miR-542-5p *(5p)* [B], miR-542-3p and antagomiR-542-3p *(3p + A),* miR-542-5p and antagomiR-542-5p *(5p + A)* and antagomiR (A) and 24h later were transfected with $CAGA_{12}$ and pRL-TK reporter vectors. After 24h myoblasts were treated with BSA (vehicle) or with 5ng/mL TGF-β1 for 6h. An increase in the basal levels of TGF-β signalling was observed in non-stimulated cells and in the presence of miR-542-3p/-5p (p=0.0003 and p=0.0017, respectively). However, transfection of the cells with antagomiR-542-3p/-5p (3p+A)/(5p+A) reversed the effect of the miRs. Transfected miR-mimic levels were kept constant in all experiments by co-transfection with *Scr*. The results are based on n=6 samples repeated in 2 independent experiments. Firefly luciferase activity was normalised to Renilla luciferase activity. Box and whiskers plot show 10-90 percentiles of normalised luciferase activity and outliers as dots. Statistical analysis was performed using Mann Whitney test as the data were not normally distributed.

5.3.2 miR-542-5p increase p-SMAD2/3 nuclear localisation independent from TGF-β ligand *in vitro*

The increase in the basal luciferase activity seen in the previous experiment suggested that in the absence of added ligand miR-542-5p could promote the phosphorylation of SMAD2/3 leading to its accumulation in the myoblast nucleus. To determine whether this microRNA increased nuclear p-SMAD2/3, cells were transfected with miR-mimic and the presence of p-SMAD2/3 was assessed by immunofluorescence. To account for any effect of the miR on cell proliferation, average fluorescence of p-SMAD2/3 per nucleus was determined. This assay showed a ligand independent increase in nuclear p-SMAD2/3 in LHCN-M2 cells 48h after transfection with miR-542-5p compared to scrambled oligonucleotide ($p<0.0001$) *(Figure 38, A-B).* Consistent with the luciferase assay data, after 6h of TGF-β1 stimulation miR-542-5p transfected cells showed decreased levels of SMAD activity compared to control cells ($p<0.0001$).

A



B

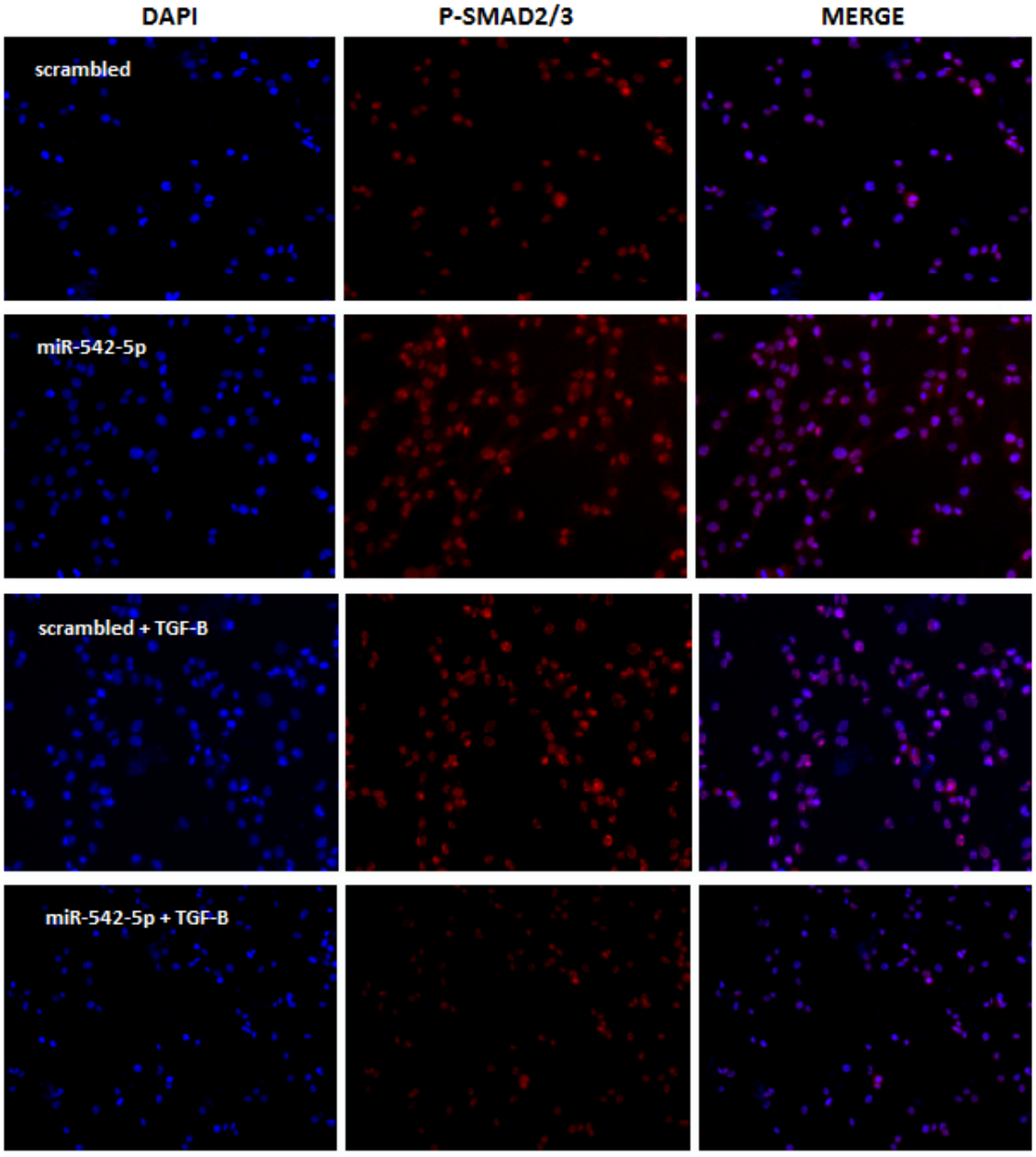


Figure 38- miR-542-5p increases p-SMAD2/3 accumulation in the nuclei.

LHCN-M2 myoblasts were transfected with scrambled *(Scr)* and miR-542-5p *(5p)* miR-mimic and cultured for 48h. Later, myoblasts were treated for 6h with serum free or medium containing 5ng/mL TGF-β1 then fixed and stained for p-SMAD2/3 and DAPI. Firefly luciferase activity was normalised to Renilla luciferase activity. [A] Box and whiskers plots show 10-90 percentiles of mean fluorescence in the nuclei from cells transfected with miR-mimic or scrambled control (3 independent experiments) show an increase in p-SMAD2/3 nuclear localisation in inactivated cells transfected with miR-542-5p in comparison to scrambled transfected cells. Outliers are shown as dots. Statistical analysis was performed using Mann Whitney test as the data were not normally distributed. [B] Images show DAPI staining for nuclei (blue), p-SMAD2/3 staining only (red) and merge of p-SMAD2/3 staining with DAPI.

To determine whether the miR-542 dependent increase in p-SMAD2/3 in the absence of exogenous ligand was due to increased ligand expression, we measured TGF-β1 [A] and MSTN [B] mRNA in LHCN-M2 myoblasts 48h after transfection with miR-542 and scrambled oligonucleotides. This analysis showed a decrease in mRNA levels of both ligands by the microRNA ($p<0.0001$) compared to scrambled control, suggesting that the increase seen in p-SMAD2/3 nuclear localisation is independent of endogenous ligand expression *(Figure 39, A-B).* Transfection with antagomiR showed a partial reversal of the effects of the microRNA.

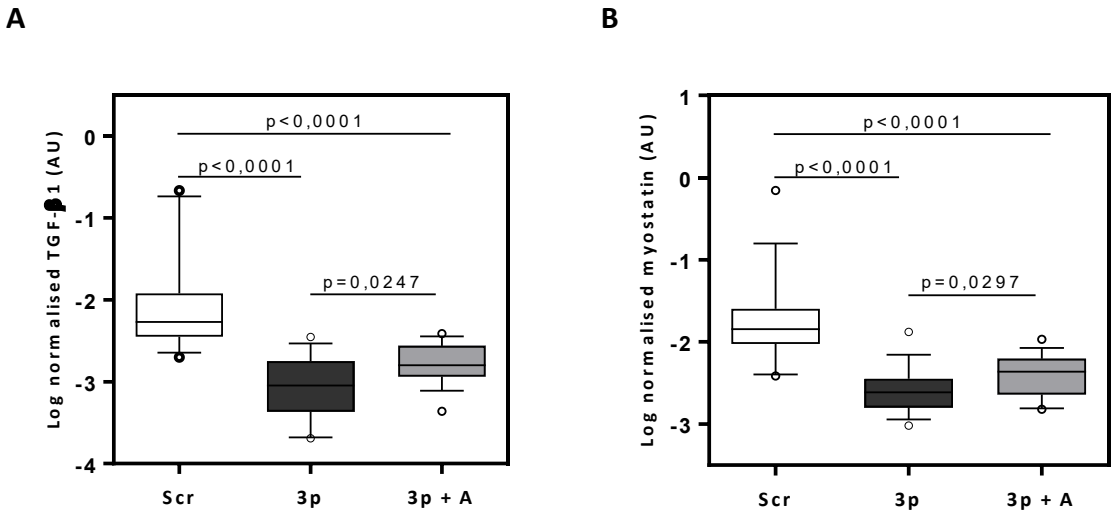


Figure 39- miR-542-3p decreases TGF-β1 and myostatin RNA expression.

RNA was extracted from LHCN-M2 myoblasts 48h after transfection with scrambled *(Scr)*, miR-mimic miR-542-3p *(3p)* and miR-542-3p and antagomiR-542-3p *(3p + A)* and analysed from the expression of TGF-β1 and myostatin. A reduction in TGF-β1 and myostatin RNA levels was seen in miR-542-3p transfected myoblasts ($p<0.0001$). Box and whiskers plots show 10-90 percentiles and outliers as dots from n=3 independent experiments with 6 repetitions in each. Statistical analysis was performed using Mann Whitney test as the data were not normally distributed. Gene normalisation was performed against the geomean of glyceraldehyde-3-phosphate dehydrogenase (GAPDH), Hypoxanthine phosphoribosyltransferase (HPRT) and beta-2-microglobulin (B2M).

Some studies have shown receptor independent mechanisms of SMAD phosphorylation such as via the four and a half LIM domain protein (FHL1) which binds to CK δ and promotes SMAD phosphorylation (266). Therefore, to determine whether the effects of miR-542 were receptor dependent, LHCN-M2 myoblasts were transfected with a dominant inhibitory form of the TGF-β type II receptor (TGFBIIR) and luciferase expression was analysed. Transfection of the inhibitory form of TGFBIIR prevented activation of TGF-β signalling in response to ligand activation compared to transfection with the empty vector (pCDNA.3) indicating a disruption in TGFBIIR functionality *(Figure 40).* miR-542-5p did not elevate basal SMAD activity in the LHCN-M2 myoblasts transfected with a dominant inhibitory TGFBIIR receptor *(p=0.8882)*. However, an increase in TGF-β signalling was seen in the presence of miR-542-5p and pCDNA.3 (p=0.0012) in the absence of the ligand suggesting that the receptor is needed for the miR dependent SMAD activity increase.

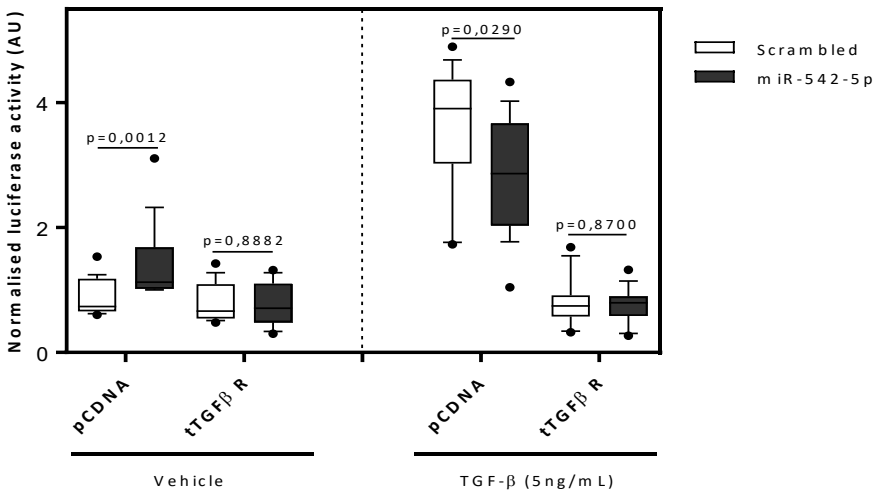


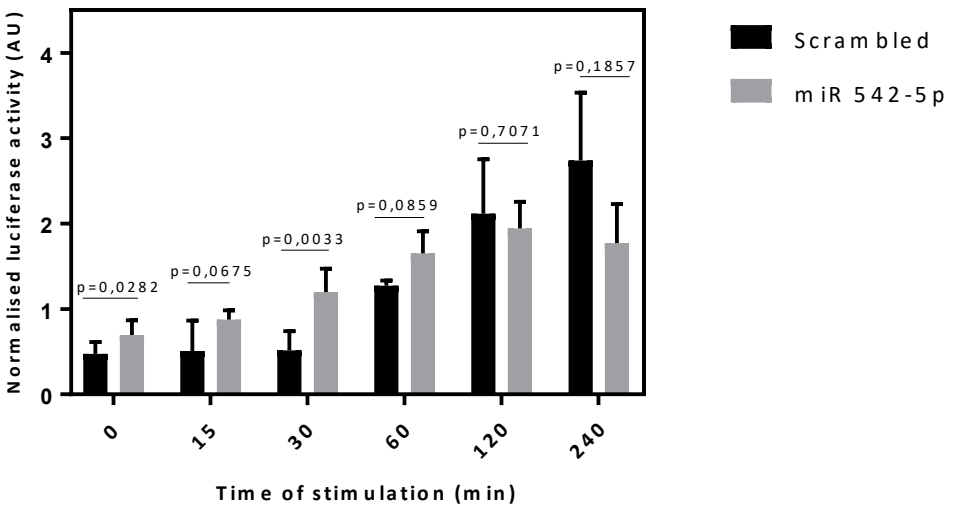
Figure 40- TGF-β receptor complex is required for SMAD phosphorylation in the presence of miR-542-5p.

LHCN-M2 myoblasts were transfected with miR-mimic miR-542-5p or scrambled oligonucleotide followed 24h later by transfection of the luciferase reporter system together with an expression vector for a dominant inhibitory TGFBIIR receptor or an empty control (pCDNA.3). In the presence of the truncated receptor, miR-542-5p did not elevate the basal luciferase activity but did increase basal luciferase activity in cells transfected with pCDNA.3 in comparison to scrambled transfected cells. The results are based on n=2 independent experiments with 6 samples in each. Firefly luciferase activity was normalised to Renilla luciferase activity. Box and whiskers plot shows 10-90 percentiles of normalised luciferase activity and outliers as dots and statistical analysis was performed using Mann Whitney test as data were not normally distributed.

5.3.3 miR-542-3p/-5p effects on TGF-β signalling are time dependent

To further examine the effect of miR-542 in the presence of added ligand we performed a time course of the luciferase response in human myoblasts. In the absence of miR-542, luciferase activity did not increase until 1h after TGF-β1 (5ng/mL) activation and this SMAD dependent increase in activity is still observed at 4h. However, in the presence of miR-542, the luciferase activity increase was significant 30min after activation, but plateaued by 2h. As a result, in the presence of miR-542 at 30min after TGF-β1 addition there is a significantly higher SMAD activity than in the absence of miR-542 (p=0.0033) *(Figure 41, A)*. To confirm the results observed in the standard curve, we measured nuclear p-SMAD2/3 2h after TGF-β1 addition (a time where there is no difference in luciferase activity between scrambled and miR transfection). This assay showed ligand independent increase of nuclear p-SMAD2/3 in LHCN-M2 cells 48h after transfection with miR-542-3p *(Figure 41, B-C)* or miR-542-5p *(Figure 41, D-E)* compared to scrambled (p<0.0001). In the presence of TGF-β1, there is a small difference in SMAD activation between miR-542-3p/-5p or scrambled treated myoblasts. However, it is possible that the statistical difference observed is due to the large amount of data points collected.

A



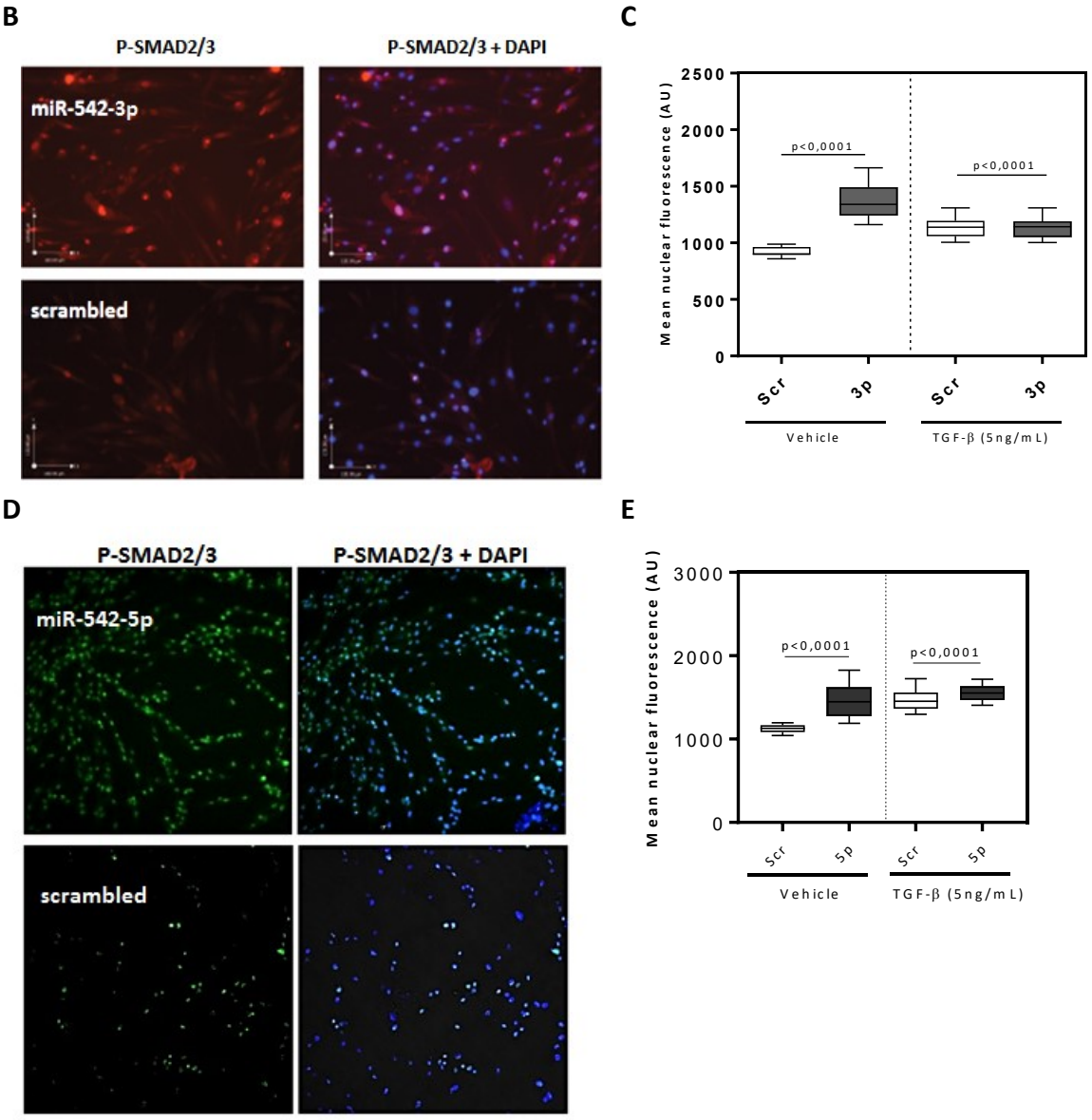


Figure 41- miR-542-3p/-5p effects of TGF-β signalling are time dependent.

LHCN-M2 myoblasts were transfected with scrambled *(Scr)*, miR-mimic miR-542-3p *(3p) [B-C]* and miR-542-5p *(5p) [D-E]* and cultured for 48h. [A] Luciferase assay was performed after 5ng/mL TGF-β1 stimulation for the indicated times, showing an increase of SMAD activity after 30min of activation in the presence of miR-542. [B-E] 48 h after transfection myoblasts were treated during 2h with SF or TGF-β1 and stained for p-SMAD2/3 and DAPI. Images show DAPI staining for nuclei (blue), p-SMAD2/3 staining only (red [C] or green [D]), and merge of p-SMAD2/3 staining with DAPI. Plots of mean fluorescence in the nuclei showed an increase in p-SMAD2/3 nuclear localisation in cells transfected with miR-542-3p/-5p in comparison to scrambled transfected cells in the absence of added ligand. The results are based on n=6 samples repeated in 3 independent experiments. Firefly luciferase activity was normalised to Renilla luciferase activity. Bar chart shows mean normalised signal± SEM and unpaired t-test was used to perform the statistical analysis as data were normally distributed. Box and whiskers plots show 10-90 percentiles. Statistical analysis was performed using Mann Whitney test as data were not normally distributed.

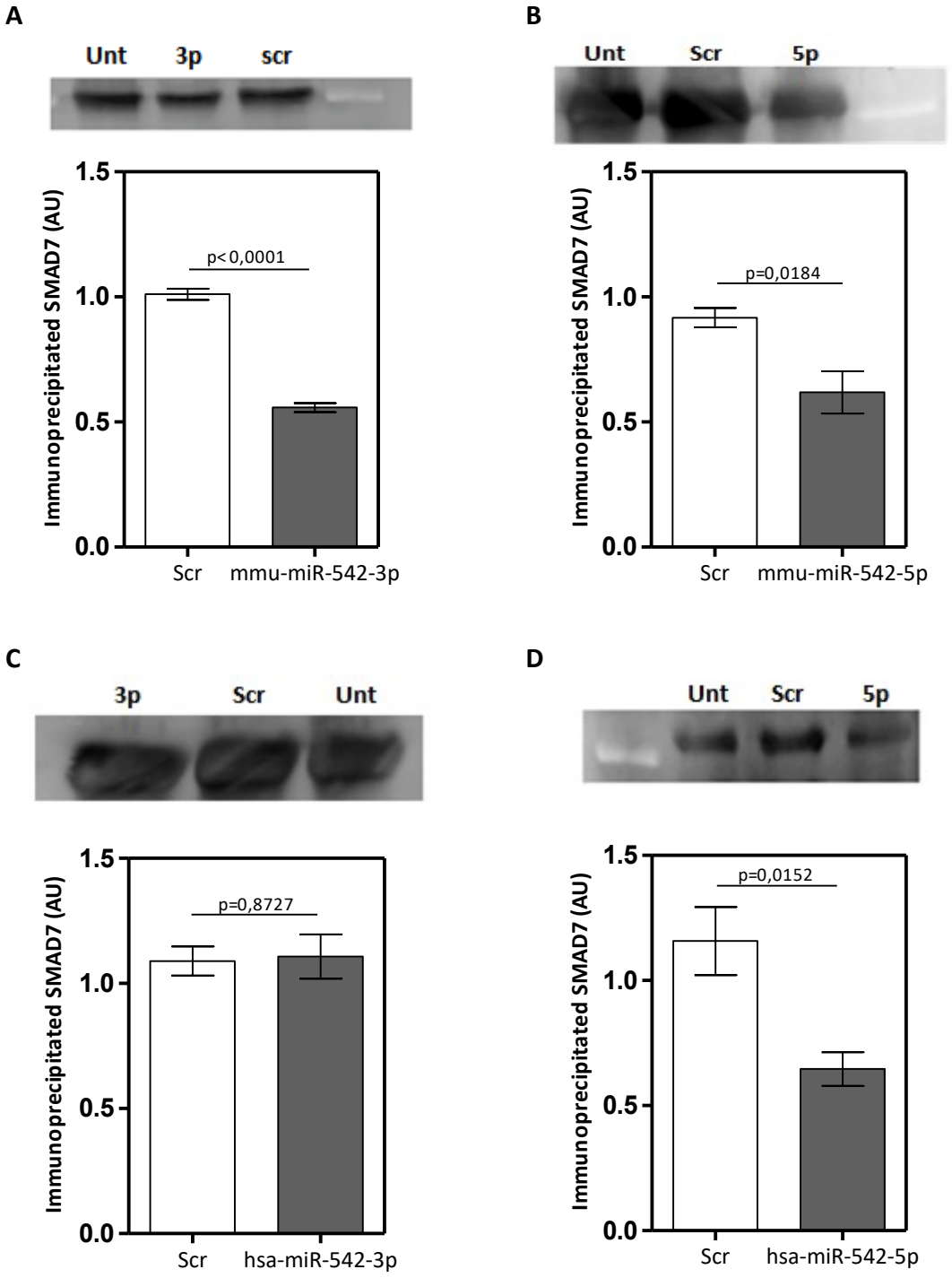
5.3.4 miR-542-3p and miR-542-5p target inhibitors of TGF-β signalling *in vitro*

As described in Chapter 3, bioinformatic analysis predicted that miR-542-3p/-5p would target a number of components of the TGF-β/SMAD signalling pathway that suppress the production of p-SMAD2/3 by inhibiting the receptor complex (SMAD7, SMURF1) or by promoting SMAD2/3 dephosphorylation (components of the Protein phosphatase 2 -PP2A- complex, PPM1A, CTDSP1 and CTDSP2). We chose to analyse first, the effect of miR-542-3p/-5p on SMAD7 (which inhibits TGF-β type I receptor function) and SMURF1 (a ubiquitin ligase which localises SMAD7 to the plasma membrane, making it essential for SMAD7 activity and also promotes TGF-β type I receptor degradation).

5.3.4.1 Effect of miR-542 on SMAD7 and SMURF1

As shown in Chapter 3, *Table 12 [B]* some miR-542-3p and miR-542-5p targets differ between mouse and human as miR-542-3p targets SMURF1 in both species but only targets SMAD7 in the mouse whereas miR-542-5p targets both genes in both species. Transfection of C2C12 myoblasts (mouse) with miR-542-3p and miR-542-5p mimics reduced SMAD7 protein levels by more than 40% ($p<0.0001$ and $p=0.0184$, respectively) *(Figure 42, A-B)* whereas in LHCN-M2 cells (human) only the miR-542-5p mimic reduced the expression of SMAD7 by approximately 50% ($p=0.0152$) *(Figure 42, C-D),* consistent with the proposed specificity. SMURF1 protein levels in LHCN-M2 cells transfected with miR-542-3p appeared to be reduced by 50% ($p=0.0019$) *(Figure 42, E)* in comparison with scrambled oligonucleotide transfected cells. However, the anti-SMURF1 antibody produced a number of bands on Western blots in addition to one at the correct molecular weight suggesting that it was not specific. Consequently, these data are not conclusive of a reduction in SMURF1. Therefore, to further analyse the effect of miR-542 on these TGF-β signalling inhibitors, we measured RNA levels of SMAD7 and SMURF1 in miR-542-3p [F] and miR-542-5p [G] transfected human myoblasts. This analysis showed no difference in SMAD7 RNA levels between miR-542-3p and scrambled transfected LHCN-M2 cells ($p=0.3715$). SMURF1 RNA levels were down regulated by miR-542-3p ($p=0.0377$) suggesting miR-542-3p promotes SMURF1 RNA degradation consistent with the protein analysis. miR-542-5p treated myoblasts had decreased levels of SMAD7 and SMURF1 RNA compared to scrambled treated cells

(p=0.0009 and p=0.0067, respectively). AntagomiR co-transfection only rescued SMAD7 RNA in miR-542-5p transfected myoblasts, for a potential explanation, see *Appendix 1.*



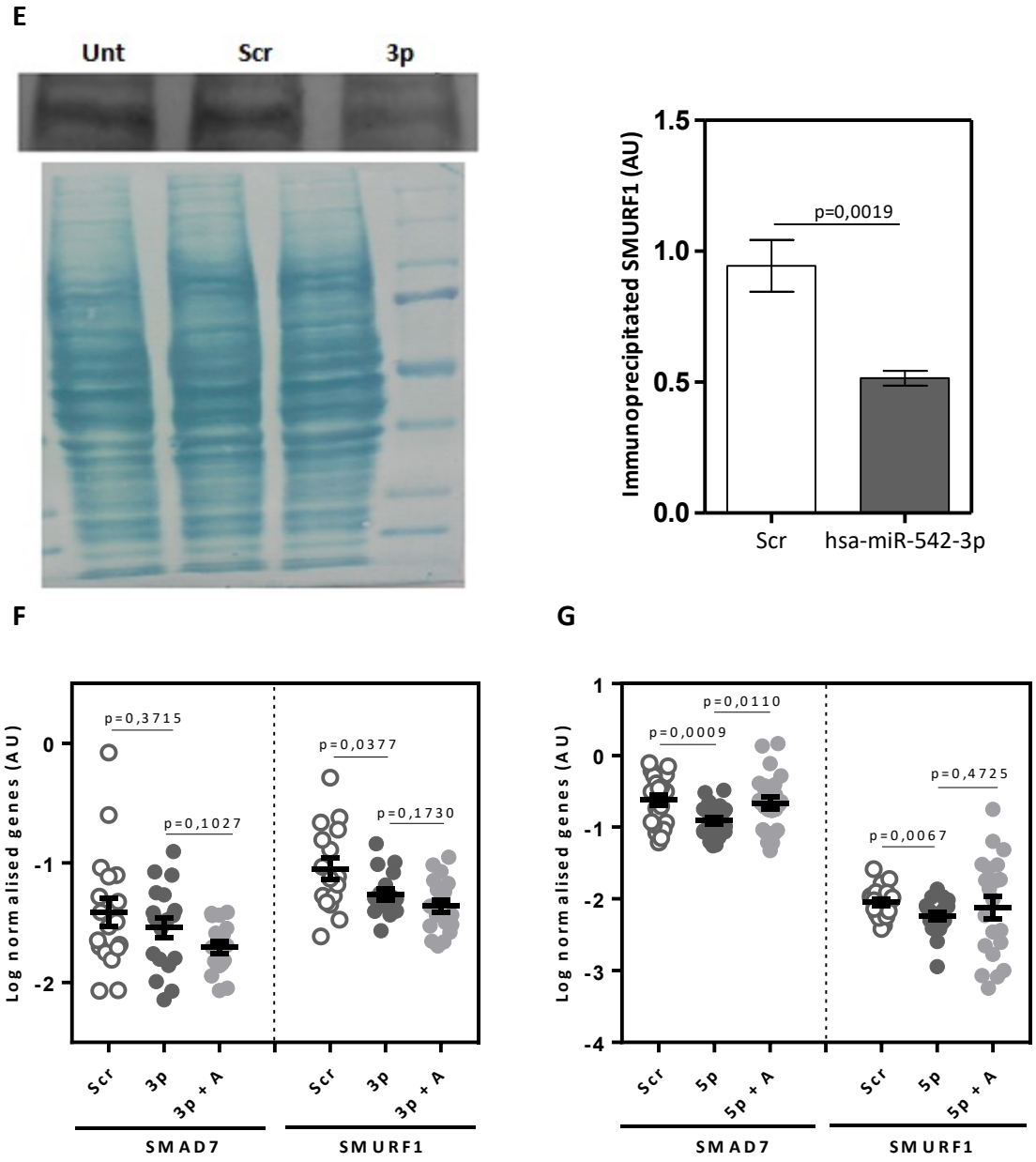


Figure 42- SMAD7 and SMURF1 are targeted by miR-542-3p/-5p.

SMAD7 was immunoprecipitated from C2C12 and LHCN-M2 myoblasts 48h after transfection with scrambled *(Scr)*, miR-mimic miR-542-3p *(3p)* and miR-542-5p *(5p).* Cells cultured for the same length of time but not transfected are denoted *(Unt).* As predicted by miRwalk, in mouse both miR-542-3p and miR-542-5p decreased SMAD7 levels [A-B] but in human only miR-542-5p targets SMAD7 [C-D]. miR-542-3p in human seem to target SMURF1 [E]. SMURF1 RNA levels were down-regulated by miR-542-3p [F] in human myoblasts whereas no effects were seen in SMAD7 RNA levels [F]. miR-542-5p decreased both SMAD7 and SMURF1 RNA levels in human myoblasts [G]. Bar charts and scatter dot plots show mean signal± SEM from n=3 independent transfections. Statistical analysis was performed using unpaired t-test as data were normally distributed. For SMURF1 [E], Amido Black staining was used for controlling for loading. In [F] and [G], each of the 3 independent experiments had 6 repetitions. Gene normalisation was performed against the geomean of GAPDH, HPRT and B2M.

5.3.4.2 Effect of miR-542 on protein phosphatases

After demonstrating that miR-542-3p/-5p could target SMAD7 and SMURF1, we determined whether the PP2A complex was also targeted. miR-542-3p and miR-542-5p were predicted to target several components of the PP2A complex (Chapter 3, *Table 12, B*). Primers were therefore designed for the 5 most highly expressed PP2A components in skeletal muscle according to Gene Atlas *(https://www.ebi.ac.uk)*. The PP2A complex is a trimer made up from a structural, a regulatory and a catalytic subunit. Predicted miR-542-3p/-5p targets were identified in each subunit type: structural (PPP2R1A), regulatory (STRN, PPP2R3A and MOB3B) and catalytic (PPP2CA). MOB3B, PPPR3A and PPP2R1A primers produced multiple bands but there was insufficient time to design new primers and repeat the experiment. However, the primers designed for STRN and the catalytic subunit PPP2CA produced single bands of the correct size and amplified the correct gene as demonstrated by sequencing. To determine whether miR-542-3p/-5p targeted these components we quantified PPP2CA and STRN mRNA in LHCN-M2 myoblasts transfected with either miR-542-3p/miR-542-5p or scrambled mimic.

Transfection of LHCN-M2 cells with miR-542-3p reduced both PPP2CA and STRN mRNA ($p<0.0001$ and $p=0.0084$ respectively) *(Figure 43, A-B)*. The suppression of PPP2CA was partially reversed by co-transfection with the antagomiR ($p=0.0338$) but that of STRN expression was not ($p=0.6938$), see *Appendix 1* for explanation about the antagomiR effect. As hypoxia increases the expression of miR-542-3p, we also analysed PPP2CA and STRN RNA levels in LHCN-M2 incubated for 96h under normoxia or hypoxia. Both PPP2CA and STRN RNAs were reduced in hypoxic compared to normoxic cells ($p<0.0001$) *(Figure 43, C-D).* Similarly, miR-542-5p transfection also reduced both PPP2CA and STRN mRNA ($p=0.0129$ and $p<0.0001$, respectively) *(Figure 43, E-F).* The effect of the microRNA was not inhibited by antagomiR co-transfection ($p=0.9254$ and $p=0.9377$, respectively), see further explanation in *Appendix 1*.

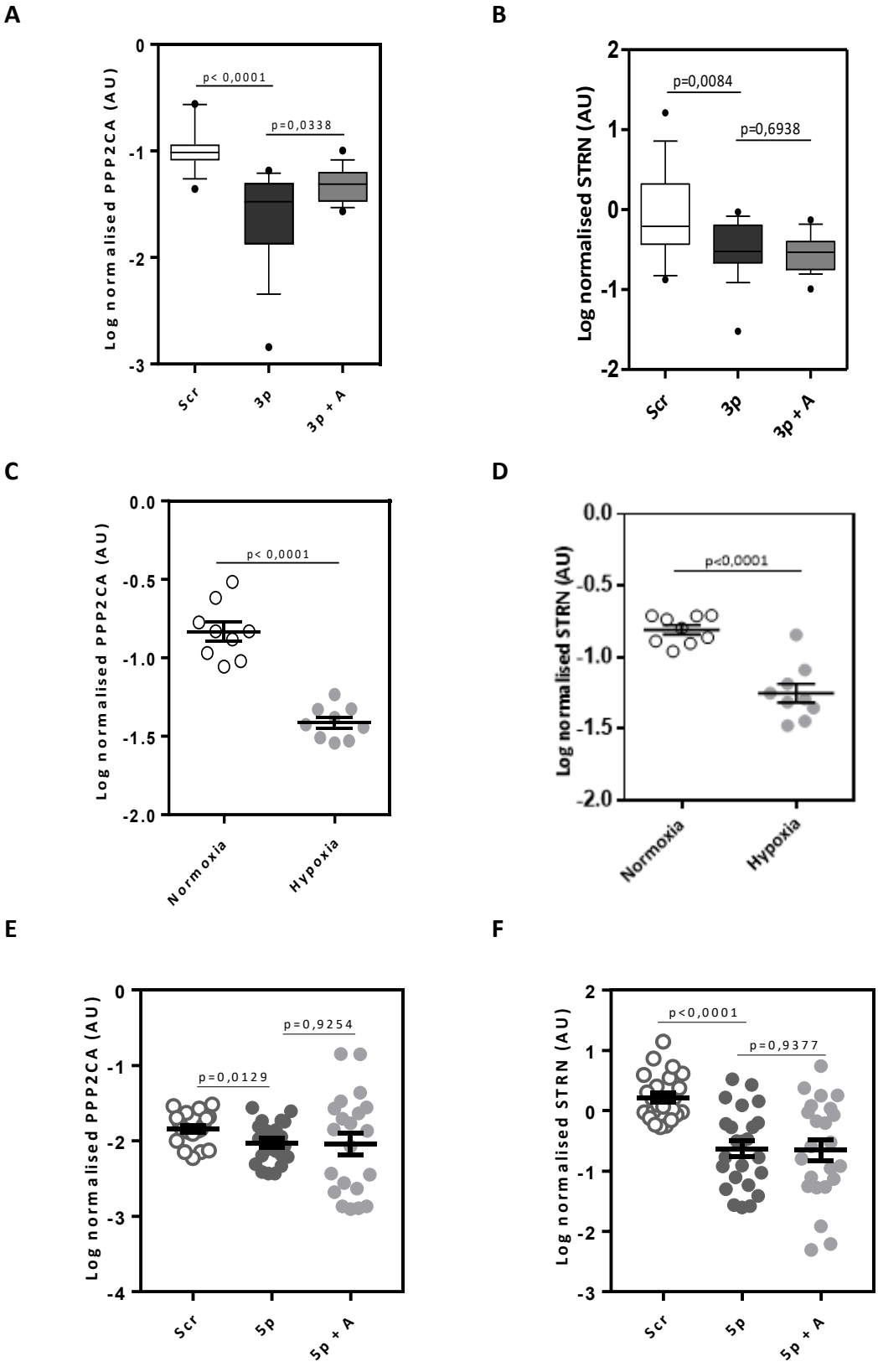


Figure 43- miR-542-3p and miR-542-5p target PPP2CA and STRN *in vitro.*

[A] RNA from LHCN-M2 myoblasts was extracted after 48h of transfection with scrambled *(Scr)*, miR-mimic miR-542-3p *(3p)* or miR-542-5p (*5p)* and miR-542-3p and antagomiR-542-3p *(3p + A)* or miR-542-5p and antagomiR-542-5p *(5p + A).* A reduction in PPP2CA [A] and STRN RNA levels [B] was seen in miR-542-3p transfected myoblasts. Similarly, miR-542-5p also decreased PPP2CA [E] and STRN [F] RNA levels

compared to scrambled transfected myoblasts. RNA from LHCN-M2 myoblasts was extracted after 96h of incubation under normoxia or hypoxia. Decreased levels of PPP2CA [C] and STRN [D] RNA were observed in myoblasts incubated under hypoxia ($p<0.0001$). Transfected miR-mimic levels were kept constant in all experiments by co-transfection with Scr. Box and whiskers plots show 10-90 percentiles and outliers as dots from n=3 independent experiments with 6 repetitions in each. Statistical analysis was performed using Mann Whitney test as the data were not normally distributed. Scatter plots show mean signal± SEM from n=3 independent experiments with 3 [C-D] or 6 [E-F] repetitions in each. Statistical analysis was performed using unpaired t-test as data were normally distributed. Gene normalisation was performed against the geomean of GAPDH, HPRT and B2M.

miR-542-3p/-5p were also predicted to target other SMAD2/3 phosphatases apart from the PP2A complex including PPM1A, CTDSP1 and CTDSP2. To determine whether miR-542-3p/-5p targeted these phosphatases we quantified their RNA levels in miR-542-3p/-5p or scrambled mimic transfected human myoblasts. The three sets of primers were designed and sequencing showed that the amplified product by PPM1A primers was not correct. Therefore, we only measured CTDSP1 and CTDSP2 RNA expression, showing no difference between the treatments (miR-542-3p, $p=0.8868$ [C] and $p=0.8211$ [E], respectively, and miR-542-5p, $p=0.4583$ [D] and $p=0.1391$ [F], respectively) *(*Figure 44*).* The antagomiR effects are further discussed in the *Appendix 1.*

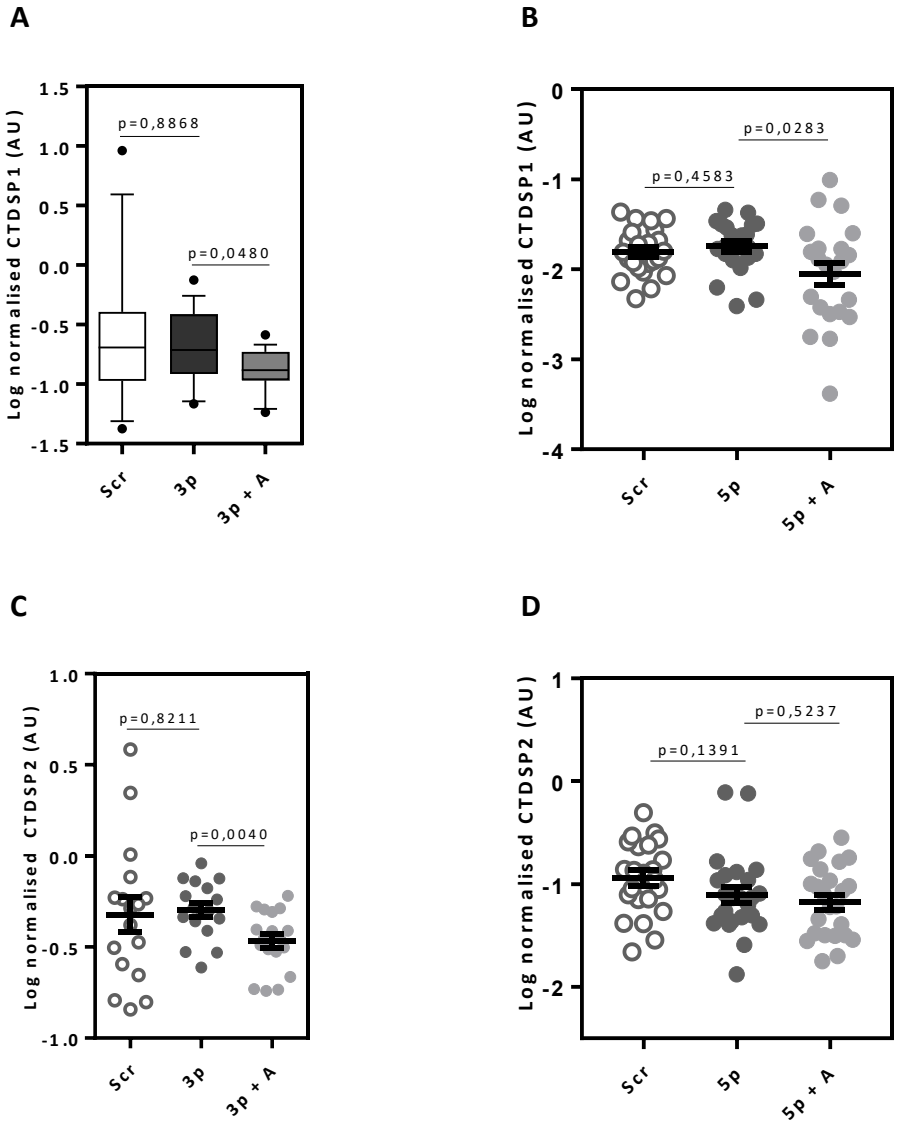


Figure 44- miR-542-3p/-5p do not target CTDSP1 or CTDSP2 *in vitro.*

RNA from LHCN-M2 myoblasts was extracted after 48h of transfection with scrambled (Scr), miR-mimic miR-542-3p (3p) or miR-542-5p (5p) and miR-542-3p and antagomiR-542-3p (3p + A) or miR-542-5p and antagomiR-542-5p (5p + A). No difference was seen in CTDSP1 [A-B] and CTDSP2 [C-D] RNA levels between miR-542-3p/-5p transfected cells compared to control cells. Transfected miR-mimic levels were kept constant in all experiments by co-transfection with Scr. Box and whiskers plot shows 10-90 percentiles and outliers as dots from n=3 independent experiments with 6 repetitions in each. Statistical analysis was performed using Mann Whitney test as data were not normally distributed. Scatter plots show mean signal± SEM from n=3 independent experiments with 3 repetitions in each. Statistical analysis was performed using unpaired t-test as samples were normally distributed. Gene normalisation was performed against the geomean of GAPDH, HPRT and B2M.

5.3.5 miR-542-3p and miR-542-5p did not increase p-SMAD2/3 in the presence of TGF-β ligand *in vitro*

The effects of miR-542 on SMAD7, SMURF1 and SMAD phosphatase expression suggest that the increase in SMAD dependent luciferase activity occurs as a result of a reduced ability to turn off SMAD signalling together with either increased basal SMAD2/3 phosphorylation in the absence of added ligand or a sensitised response to the low levels of ligand present in the culture medium. This observation explains the increased luciferase activity in the absence of exogenous ligand but not the reduction in luciferase activity in the presence of TGF-β1.

A suggestion for this effect is that as p-SMAD2/3 levels in the nucleus were higher in the presence of miR-542, it was not possible to elevate them further, as any such response would be dominated by the effect of TGF-β1 on SMAD degradation. Activation of the TGF-β pathway includes activation of TAK1 promoting phosphorylation of the SMAD2/3 linker region after TGF-β receptor dependent C-terminus phosphorylation. This TAK1-dependent double phosphorylation leads to SMAD2/3 ubiquitination by NEDD4L and degradation. SMAD2/3 degradation can also occur through calpain (proteolytic enzyme) (372).

To determine whether increased/early degradation caused the reduction in luciferase activity 6h after TGF-β1 addition, the effect of the dual specific proteasome/calpain inhibitor MG132 (10μM) was determined in the presence and absence of added TGF-β1. Consistent with previous results, miR-542-5p increased luciferase activity in the absence of added ligand ($p<0.0001$). In the presence of TGF-β1, miR-542-5p decreased luciferase activity compared to scrambled treatment ($p=0.0062$). However, in the presence of MG132 and TGF-β1, there was no difference between miR-542-5p and scrambled treatment ($p=0.0598$) *(Figure 45, A)*. The fold change in luciferase activity in the absence of added ligand between a) miR-542-5p and scrambled transfection and b) miR-542-5p and scrambled transfection in the presence of MG132, was no different. Similarly, in the presence of added ligand, no difference in the luciferase fold change was seen between the same two groups *(Figure 45, B).* Therefore, these data were not conclusive.

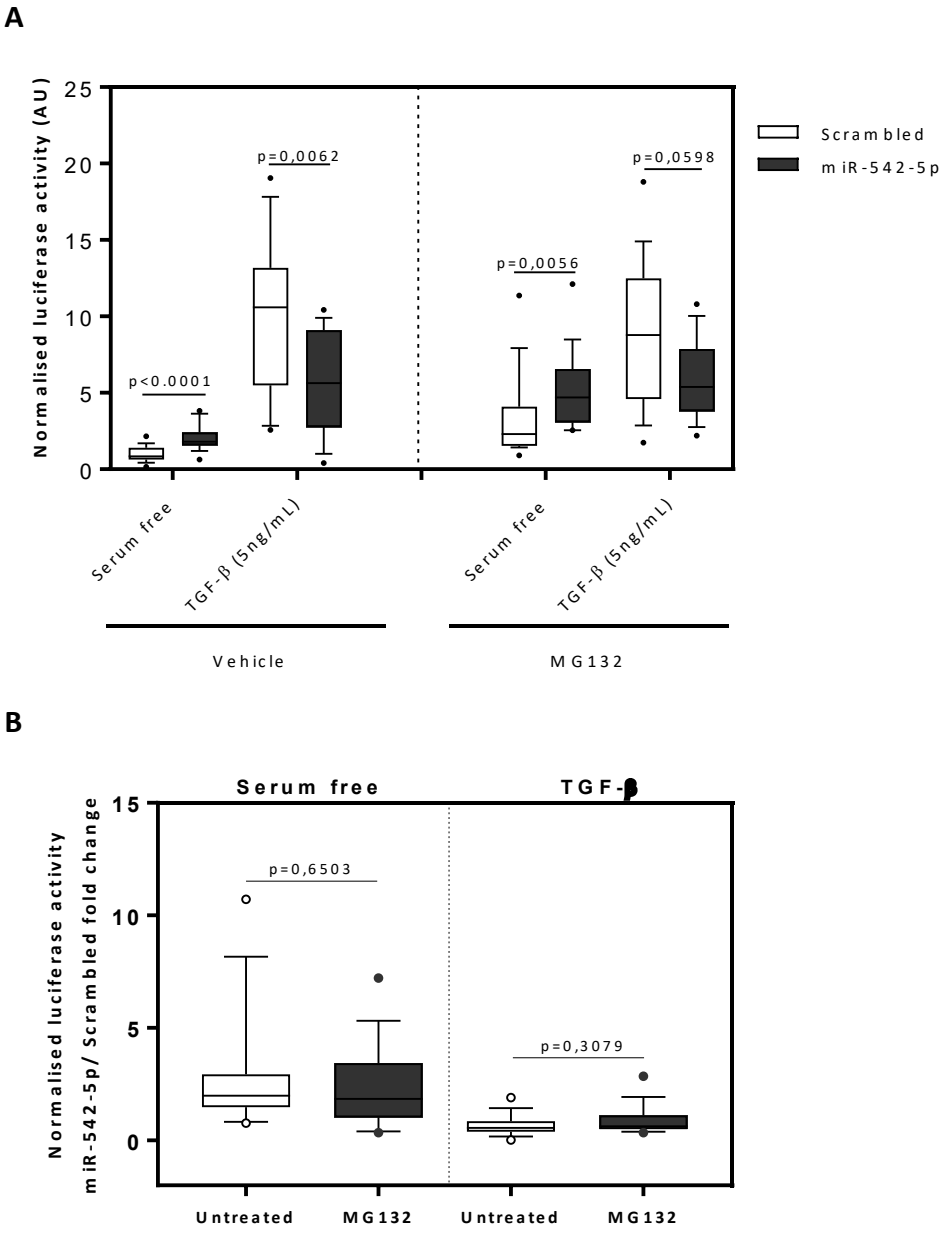


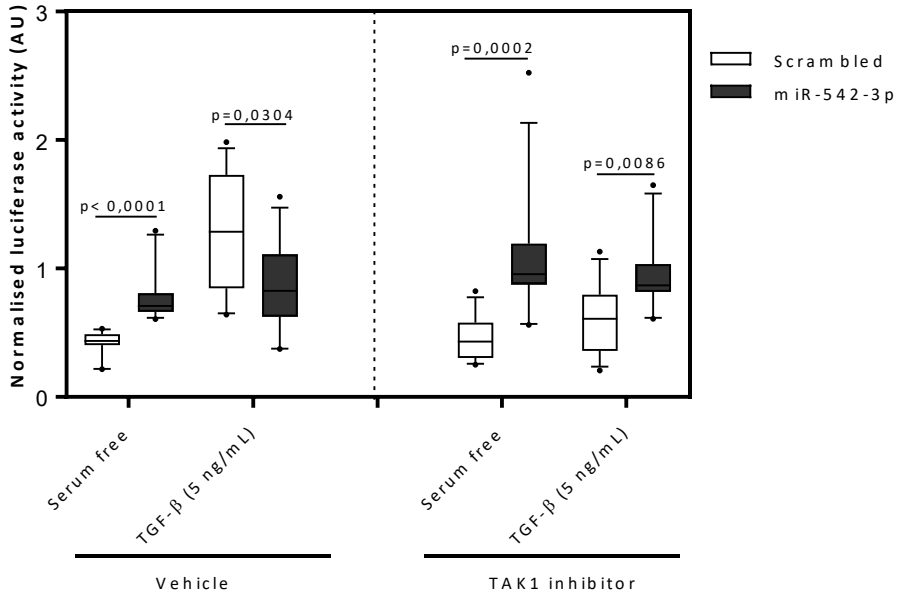
Figure 45- MG132 effects on TGF-β pathway are inconclusive.

LHCN-M2 myoblasts were transfected with miR-mimic miR-542-5p or scrambled oligonucleotide. 24h later, LHCN-M2 were transfected with the luciferase reporter system and next day cells were activated with TGF-β in the presence of MG132 (a proteasome inhibitor). [A] In the presence miR-542-5p, increased SMAD dependent luciferase activity was seen without activation of the system. In the presence of TGF-β1, miR-542-5p decreased SMAD activity. However, in the presence of MG132 and TGF-β1 no difference in luciferase activity was seen between miR-542-5p and scrambled treatment. [B] No effect was seen by MG132 treatment as there was no difference in the luciferase fold change between miR-542-5p and scrambled transfected myoblasts with the presence or absence of MG132. Similarly, no effects by MG132 were seen when the cells were activated. Firefly luciferase activity was normalised to Renilla luciferase activity. The results are based on at least n=6 samples repeated in 2 independent experiments. Box and whiskers plot show 10-90 percentiles of normalised luciferase activity and outliers as dots. Statistical analysis was performed using Mann Whitney test as the data were not normally distributed.

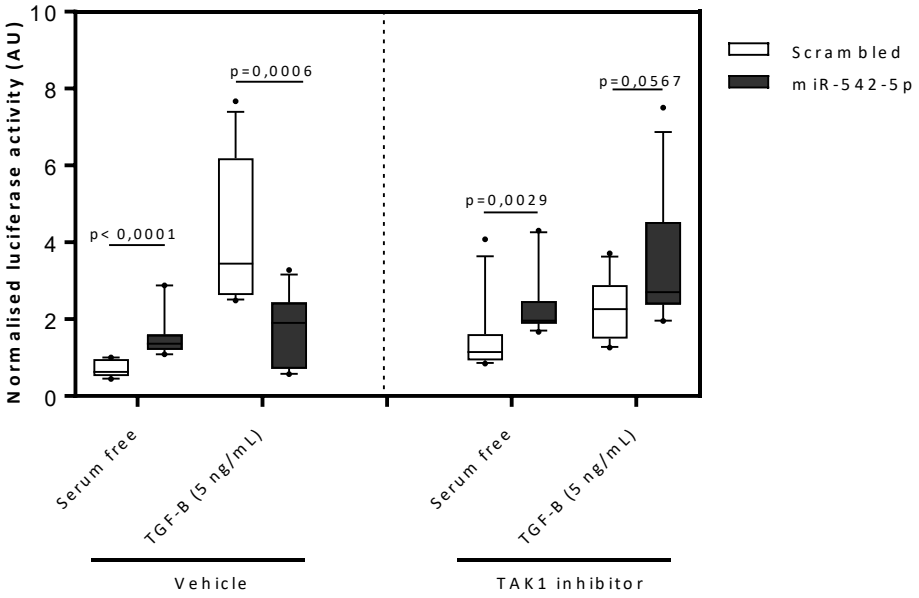
To determine whether inhibition of TAK1 would prevent the reduction in SMAD dependent luciferase in the presence of TGF-β for 6h, the effect of the TAK1 inhibitor ((5Z)-7-Oxozeaenol) (1.5μM) was determined in human myoblasts. (5Z)-7-Oxozeaenol alone had no effect on luciferase activity measured in cells transfected with the scrambled control. In the presence of (5Z)-7-Oxozeaenol and absence of added TGF-β1, miR-542-3p *(Figure 46, A)* increased SMAD activity (2.2 fold, p=0.0002) compared to control cells. Furthermore, in the presence of the TAK1 inhibitor and TGF-β, an increase in SMAD activity was seen by miR-542-3p compared to scrambled. A similar pattern of changes was seen in miR-542-5p transfected cells. However, in the presence of TGF-β and TAK1 inhibitor, a trend towards increased luciferase activity was seen in miR-542-5p transfected cells compared to controls, but it did not reach statistical significance *(Figure 46, B)* (p=0.0567).

In order to analyse the relative effect of the miR in the presence of the TAK1 inhibitor compared to its absence we analysed the luciferase activity fold difference (i.e. comparing [(scr with TAKi)/(scr no TAKi)] with [(miR with TAKi)/(miR no TAKi)]). In the absence of added ligand there was no activity fold change between a) miR-542-3p and scrambled transfection and b) miR-542-3p and scrambled transfection in the presence of TAK1 inhibitor. However, in the presence of added ligand, a difference in the luciferase fold change was seen between the same two groups, showing an increase of TGF-β signalling in the presence of TAK1 (p=0.0002, *Figure 46, C*). Focusing on miR-542-5p, no luciferase activity fold change increase was seen in the absence of added ligand between a) miR-542-5p and scrambled transfection and b) miR-542-5p and scrambled transfection in the presence of TAK1 inhibitor. Similarly, in the presence of added ligand, a difference in the luciferase fold change was seen between the same two groups, showing an increase of TGF-β signalling in the presence of TAK1 (p=0.0022, *Figure 46, D*), suggesting an increased/early breakdown of p-SMAD2/3 causing the reduction in luciferase activity in the absence of TAK1. In both series of experiments, the overall activation of the signalling by TGF-β1 was decreased by TAK1 inhibition, as has previously been reported (373).

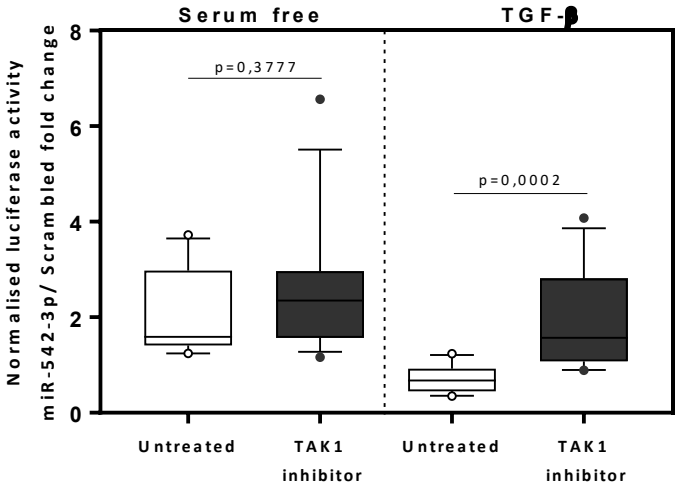
A


Normalised luciferase activity (AU)
0
1
2
3
p< 0,0001
p=0,0304
p=0,0002
p=0,0086
Scrambled
miR-542-3p
Serum free
TGF-β (5 ng/mL)
Serum free
TGF-β (5 ng/mL)
Vehicle
TAK1 inhibitor

B


Normalised luciferase activity (AU)
0
2
4
6
8
10
p< 0,0001
p=0,0006
p=0,0029
p=0,0567
Scrambled
miR-542-5p
Serum free
TGF-B (5 ng/mL)
Serum free
TGF-B (5 ng/mL)
Vehicle
TAK1 inhibitor

C



D

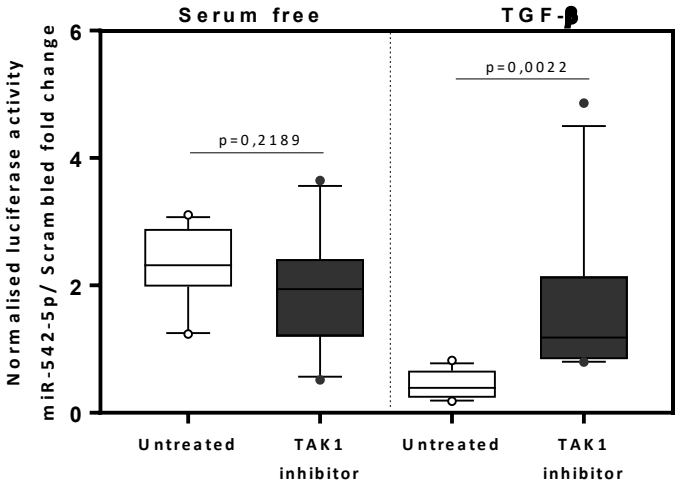


Figure 46- Degradation of p-SMAD2/3 is promoted by TAK1 signalling.

LHCN-M2 myoblasts were transfected with miR-mimic miR-542-3p/miR-542-5p or scrambled oligonucleotide followed 24h later by transfection of the luciferase reporter system. 24h later, cells were activated with TGF-β for 6h in the presence of a TAK1 inhibitor ((5Z)-7-Oxozeaenol). In the presence of TAK inhibitor and under serum free, miR-542-3p [A] and -5p [B] treated cells increased SMAD dependent luciferase activity compared to control treated myoblasts. In the presence of TAK1 inhibitor and TGF-β stimulated cells, miR-542-3p [A] treated cells increased luciferase signal whereas miR-542-5p treated cells showed a similar luciferase activity than the scrambled treated cells. Both, miR-542-3p [C] and miR-542-5p [D] transfected myoblasts under the presence of TAK1 inhibitor showed an increase in SMAD dependent luciferase activity compared to scrambled treated myoblasts. The results are based on at least n=6 samples repeated in 2 independent experiments. Firefly luciferase activity was normalised to Renilla luciferase activity. Box and whiskers plots show 10-90 percentiles of normalised luciferase activity and outliers as dots. Statistical analysis was performed using Mann Whitney test as the data were not normally distributed.

5.3.6 Increased TGF-β signalling in patients suffering from muscle wasting (COPD, ICUAW or older population)

The observation that miR-542-3p/-5p can modulate the TGF-β signalling pathway *in vitro* and are increased in the quadriceps muscle of COPD and ICUAW patients raise the possibility that TGF-β signalling is also increased in these diseases.

TGF-β signalling was indirectly measured by quantifying *CYR61* gene expression as its transcription is known to be induced by the TGF-β pathway (374,375) and has been previously used as a marker of TGF-β activity (30,376). The *CYR61* translational product is an extracellular matrix-associated signalling protein of the CCN family involved in inflammation and tissue repair, playing an important role in chronic inflammatory diseases. Elevation of *CYR61* mRNA levels were previously shown in patients with established ICUAW (30) ($p<0.0001$, *Figure 47, B*). Therefore, we determined whether *CYR61* mRNA was also elevated in COPD patients and in the cohort of older individuals. RNA was extracted from samples of the quadriceps of COPD patients (n=89) and age-matched healthy controls (n=27) and *CYR61* expression was analysed by qPCR. Expression of *CYR61* was higher in COPD patients compared to controls ($p=0.0484$, *Figure 47, A*). However, no correlation was found between *CYR61* and miR-542-3p ($p=0.8521$, $r=0.02893$) or miR-542-5p ($p=0.9711$, $r=0.005562$) in the COPD patients *(results not shown)*. In patients with ICUAW, a strong direct correlation was found between *CYR61* expression and miR-542-3p ($p< 0.0001$, $r=0.8163$*, Figure 47, C*) but no correlation was seen with miR-542-5p ($p= 0.1715$, $r=0.3477$, *Figure 47, D*). In the samples from a cohort of healthy older people from the HSS *CYR61* levels were increased in the sarcopenic individuals (n=5) compared to the non-sarcopenic individuals (n=62) ($p=0.0241$, *Figure 47, E*).

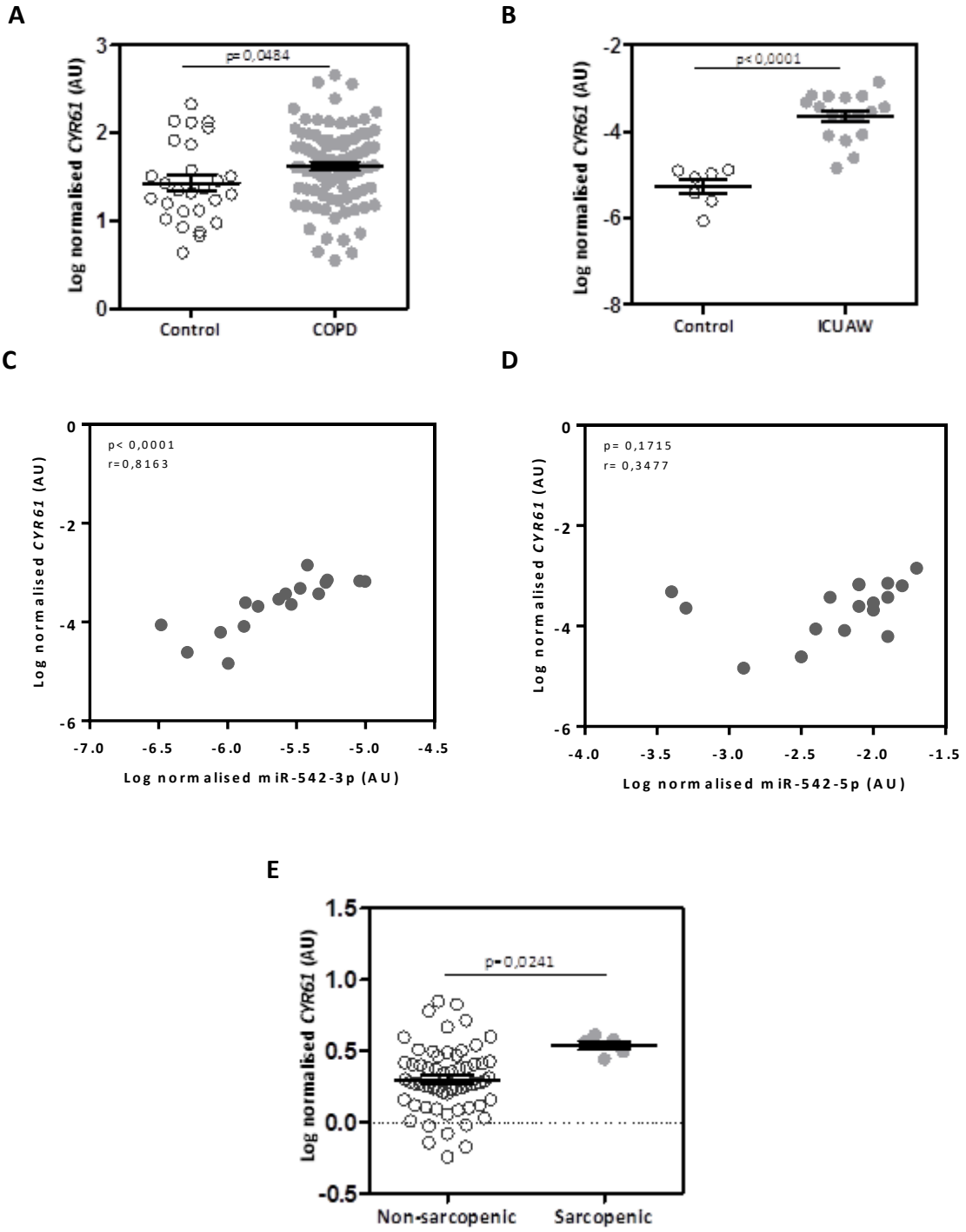


Figure 47- *CYR61* levels in COPD, ICUAW and older people cohort.

CYR61 mRNA levels were measured in quadriceps samples from 3 different cohorts of people. There was an increase of expression in COPD [A] and ICUAW patients [B] as well as in sarcopenic individuals [E]. In ICUAW patients there was a strong direct association between miR-542-3p and *CYR61* mRNA levels [C]. No other associations were seen between miR-542-3p/-5p and *CYR61* RNA levels in the other cohorts. Scatter plots show mean signal± SEM and statistical analysis was performed using unpaired t-test as the data were normally distributed. Correlations were analysed by Pearson´s test as data had a linear association showing r values. Gene normalisation was performed against HPRT the COPD cohort and the geomean of HPRT and B2M in the ICUAW cohort.

5.3.7 Down-regulation of inhibitors of TGF-β system in ICUAW patients

The patients with ICUAW had the largest increase in the expression of miR-542-3p/5p and have previously been shown to have increased nuclear p-SMAD2/3 (363). Therefore, the expression of SMAD7, SMURF1 and PPP2CA was measured in samples from ICUAW patients to determine whether there were consistent changes in the expression of these inhibitors of the TGF-β signalling pathway, with those observed *in vitro*. Quantification of immunoprecipitated SMAD7 *(Figure 48, A)* showed a reduction in protein level in the quadriceps muscle of ICUAW patients (p=0.0017, *Figure 48, B*) compared to controls. Insufficient protein was available for the analysis of other proteins, but the *in vitro* analysis had shown reductions in mRNA for these potential targets so we measured them in those patients. RNA levels of both *SMAD7* and *SMURF1*, were down-regulated in the quadriceps of patients with ICUAW compared to age-matched controls (p=0.0470 and p=0.0334, respectively). Similarly, mRNA levels of PPP2CA were reduced in patients with ICUAW compared to controls (p=0.0340) *(Figure 48, C).*

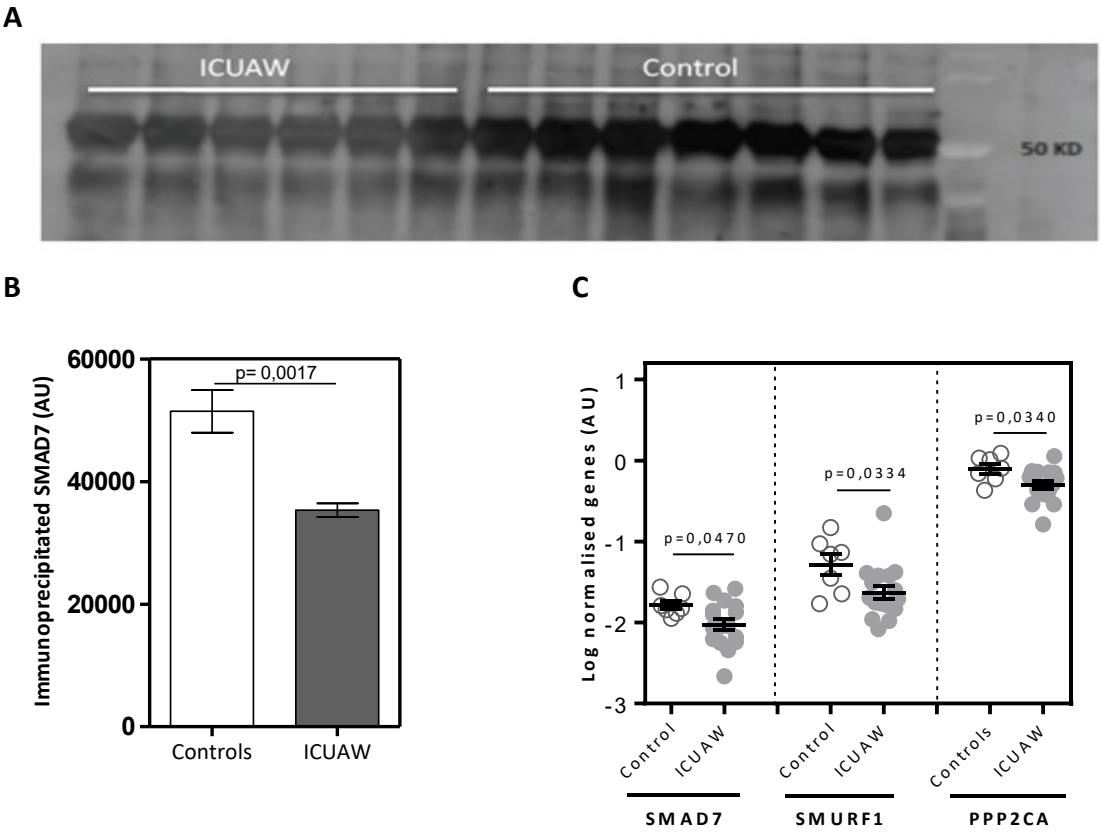


Figure 48- SMAD7 protein expression and *SMAD7*, *SMURF1* and *PPP2CA* RNA levels are decreased in patients with ICUAW.

[A] SMAD7 protein was immunoprecipitated from quadriceps biopsies from patients with established ICUAW or from controls and the intensity of the signals was quantified [B]. There was a significant reduction in SMAD7 protein in the quadriceps of the ICUAW patients [A]. [C] RNA levels of *SMAD7, SMURF1* and *PPP2CA* were measured and found to be decreased in patients with ICUAW in comparison to controls. Bar chart shows mean signal± SEM from n=6 patients with ICUAW and n=7 age matched controls. Scatter dot plots show mean signal± SEM from n=18 patients with ICUAW (except for SMAD7 which has n=17 as a data point was discarded as the SD from two duplicates was too high) and n=7 age matched controls. Statistical analyses were performed using unpaired t-test as the data was normally distributed. Gene normalisation was performed against the geomean of HPRT and B2M.

5.4 Discussion

5.4.1 Main findings

The current study shows that miR-542-3p and miR-542-5p promote the accumulation of p-SMAD2/3 in the nuclei of cells in the absence of added ligand in a receptor dependent manner, as demonstrated by the transfection with the dominant inhibitory TGFBIIR receptor. Analysis of potential targets showed that miR-542-3p/-5p target inhibitors of the SMAD signalling system suggesting that *SMAD7, SMURF1, PPP2CA* and *STRN* down-regulation contribute to the elevation of p-SMAD2/3 activity in the absence of exogenous ligand. Data obtained from skeletal muscle biopsies from patients with ICUAW, COPD and sarcopenia were consistent with the *in vitro* results. An increase in *CYR61* expression was observed in both COPD patients and in individuals with sarcopenia. *CYR61* gene transcription is elevated by TGF-β signalling activation (375) and has already been shown to be up-regulated in patients with ICUAW (30). Moreover, an association was found between *CYR61* gene expression and miR-542-3p in patients with ICUAW suggesting that this microRNA may contribute to the increase in *CYR61* levels. Finally, in the ICUAW cohort where the highest levels of miR-542-3p/-5p were measured, *SMAD7* mRNA and protein levels were down-regulated in patients compared to age-matched controls. Moreover, *SMURF1* and *PPP2CA* RNA levels were also down-regulated in patients with ICUAW. Together these data suggest that increased miR-542 in the muscle of patients with ICUAW, COPD or sarcopenia stimulates the TGF-β/MSTN signalling system either causing the ligand independent activation of SMAD signalling or sensitising the system to low levels of ligand. It therefore seems likely that miR-542 contributes to muscle wasting in these diseases.

5.4.2 Mechanism of SMAD2/3 activation

The most surprising observation presented in this chapter is the activation of SMAD2/3 signalling by miR-542 in the absence of added ligand. As described in Chapter 1, SMAD signalling is controlled by both activators and inhibitors of the phosphorylation of SMAD proteins. The simplest explanation of the presence of p-SMAD2/3 in the nuclei

of miR-542 transfected cells, therefore, is the targeting of proteins that inhibit phosphorylation of SMAD2/3 or promote their dephosphorylation by the microRNAs. However, the data do not really answer the question of why the phosphorylation occurs in the first place. The increased phosphorylation could be attributed either to a low rate of phosphorylation that occurs spontaneously in the absence of the ligand or to the phosphorylation that occurs in response to low levels of ligand in the culture medium following transfection but prior to the assay. Another possibility is that the phosphorylation occurs though a ligand independent route via an alternative mechanism. However, the data show that the receptor is required for SMAD2/3 phosphorylation to occur, therefore, receptor independent mechanisms such as phosphorylation by CKδ or other intracellular kinases seem unlikely. The fact that TGF-β activity was measured 48h following miR transfection may have allowed p-SMAD2/3 accumulation in the nuclei from any or a combination of those mechanisms. Apart from the TGF-β dependent mechanism mentioned above, there are TGF-β independent mechanisms that act via TGF-β receptor such as betaglycan that increases TGF-β signalling via the activation of p38 pathway (377). Betaglycan, also known as TGF-β type III receptor, has been suggested to play a limited role in the direct regulation of TGF-β signal transduction due to its short cytoplasmic tail and the absence of signalling motifs (378). The data presented showed increase p-SMAD2/3 in the nuclei, but phosphorylation of SMAD2/3 does not occur by p38 pathway, which instead modulates SMAD signalling once the activation has occurred so the betaglycan mechanism also seems unlikely in this situation. Therefore, it seems more likely that the mechanism contributing to SMADs phosphorylation is due to TGF-β signalling activation as a consequence of TGF-β1 or MSTN. The endogenous levels of those ligands were measured *in vitro* and their expression decreased due to microRNAs transfection *(Figure 39)*. Therefore, it is likely that the ligands were present in the serum added to the cell media and despite being at low concentrations they could activate the system during the 48h gap from when the cells were transfected until when the analysis was performed. After SMAD phosphorylation, miR-542 targeting of the phosphatases would reduce SMAD dephosphorylation, promoting the accumulation of p-SMAD2/3 in the nuclei. To further validate this hypothesis, the experiments could be repeated in myoblasts cultured in the presence of TGF-β1 and

MSTN neutralising antibodies to block the activity of any protein present in the cell culture media. Considering the function of some of the miR-542 targets, which are the main inhibitors of the TGF-β pathway such as SMAD7, SMURF1 and PP2A complex components (PPP2CA), it seems likely that miR-542 targeting all of them provides a biological mechanism for the increase in p-SMAD2/3 nuclear localisation. However, to confirm this mechanism, and to identify the relative importance of each target, luciferase assays performed in LHCN-M2 myoblasts transfected with a single siRNA, or a combination of siRNAs against the identified targets (siSMAD7, siSMURF1, siPPP2CA and/or siSTRN) would need to be performed.

5.4.3 Time course of SMAD signalling

Under normal conditions in the body, ligand concentration increases progressively allowing time for the cells to adapt. However, under the assay conditions used, a high concentration of ligand was added suddenly. Therefore, the times where we observed a difference on pSMADs levels on the luciferase assay could represent an artificial time, needing more time in a physiological condition to see a similar change. One of the effects of miR-542 described in this chapter is to shorten the apparent time course of the response to TGF-β1, thereby potentially suppressing TGF-β activity. However, it seems likely that this is an artefact of the system being studied as mentioned above. For example, the presence of p-SMAD2/3 in the nuclei of miR-542 transfected cells in the absence of added ligand raises the possibility that the pool of cytoplasmic SMAD2/3 is reduced. As a result, less SMAD2/3 may be available to be phosphorylated in response to the addition of ligand. However, this suggestion is not completely consistent with the observation of the apparent earlier activation of luciferase activity in miR-542 transfected cells seen at 30min after the ligand addition. Alternatively, the fact that some SMAD2/3 is already phosphorylated may indicate it is available for degradation. TGF-β stimulation has been shown to promote SMAD degradation through a number of other pathways including p38 and Jun N-terminal kinase (JNK), mitogen-activated protein kinase (MAPK), Ras-Erk, PI3K-Akt and GTPases (RHOA and CDC42) (379). In this study, we determined the effect of TAK1 inhibition as TAK1 has

been shown to promote degradation of p-SMAD2/3 following TGF-β stimulation by promoting phosphorylation of SMAD2/3 in the linker region (206). Consistent with this proposal, the data suggest that TAK1 signalling promotes the degradation of p-SMAD2/3 in the presence of TGF-β1. However, further experiments need to be performed to elucidate the role of TAK1 signalling in p-SMAD2/3 degradation.

5.4.4 Increased p-SMAD2/3 in the muscle of wasting patients

The observation that miR-542 activates the TGF-β signalling system *in vitro* raises the possibility that it also modulates TGF-β signalling in the muscle of humans. Having showed that both miR-542-3p and miR-542-5p expression are elevated in the muscle of patients with ICUAW, COPD and sarcopenia, it is possible that it promotes muscle wasting in these diseases by activating atrophy through the TGF-β system. The potential for such a role for miR-542 is supported by the following two observations. Firstly, the expression of several targets which are inhibitors of SMAD signalling such as *SMAD7*, *SMURF1* and *PPP2CA* are reduced in patients with ICUAW compared to controls suggesting an effect of the microRNAs on the TGF-β pathway. Secondly, the expression of *CYR61*, a TGF-β induced gene, is increased in all the conditions. Despite the fact that genes normally respond to more than one signalling system, the *CYR61* RNA increased together with a previous demonstration of increased nuclear p-SMAD2/3 in patients with ICUAW (30) suggests that TGF-β activity is elevated in these patients. Consistent with our data, other studies have also reported an increase in *CYR61* RNA levels in COPD patients (380,381) and have shown that ageing elevates *CYR61* expression promoting fibroblast senescence (382). Our data suggest the possibility that the elevation of miR-542 levels seen in patients either sensitises the cells to the increase in MSTN or TGF-β1 or causes a ligand independent increase in p-SMAD2/3 causing an atrophic effect on the muscles. However, this question remains to be determined as our experiments only suggested that the TGF-β receptor was needed for the increase in p-SMAD2/3. To elucidate this question, the luciferase assay should be repeated under the presence of antibodies against MSTN and TGF-β1 in

order to block TGF-β signalling activation by the ligands. In this detailed experiment, an increase in p-SMAD2/3 would suggest that it occurs in a ligand independent manner.

5.4.5 TGF-β signalling and other members of the miR-542 cluster

As described in Chapter 3, 5 out of 6 of the microRNAs elevated in the quadriceps of COPD patients were derived from the genomic region surrounding miR-542 (chromosome Xq26.3). This DNA adjacent to miR-542 contains miR-450a, miR-450b-5 and miR-450b-3p, and within 7KB of these there is the miR-424-503 locus. miR-424 and miR-503 are separated by 383 bases on the genome and are transcribed as part of a single host gene. The expression of these microRNAs is tightly correlated with that of miR-542 in the samples analysed in this thesis (383) raising the possibility that miR-542 is also transcribed as part of the same host gene. However, multiple efforts to identify a single transcript have proven unsuccessful. A study has identified miR-542-3p and miR-542-5p to be induced by miR-424-503 expression but they found that miR-542 levels were much lower (384). Therefore, it remains unclear if there is more than one promoter or two distinct promoters that are similarly regulated. Functionally, there are some similarities in activity as miR-424 and miR-503 have also been shown to regulate TGF-β signalling by supressing SMAD7 expression (253). Furthermore, the expression of miR-424 and miR-503 are promoted by TGF-β pathway raising the possibility of a positive feedback loop (368).

5.4.6 Other roles of miR-542-3p

There are other potential mechanisms by which the increase in miR-542-3p could contribute to muscle wasting. For example, miR-542-3p has been reported to function as a tumour suppressor by targeting survivin and thereby promoting cell cycle arrest. Consistent with such a role, the expression of miR-542-3p is decreased in patients with some cancers (290,385,386). As myoblast proliferation is an important part of muscle regeneration and the maintenance of muscle mass, miR-542-3p may limit myoblast proliferation and suppress regeneration. However, miR-542-5p is not predicted to

target survivin and proliferation assays showed no effect in LHCN-M2 transfected with miR-542-5p compared to scrambled transfected cells *(See Appendix 2)*. The data also do not show whether miR-542 expression was elevated in the satellite cells and myoblasts in patients.

5.4.7 Critique of the method

The clinical data presented in this chapter come from cross-sectional studies. Therefore, even though miR-542-3p/-5p was found to be elevated in 3 different cohorts and associated with muscle wasting, disease severity and skeletal muscle dysfunction this does not prove that miR-542-3p/-5p promotes muscle mass loss in the patients. To be able to demonstrate the effect of miR-542-3p/-5p a generation of an appropriate animal model and the use of antagomiRs in the model would be required. A longitudinal study would also further validate the role of miR-542-3p/-5p in muscle wasting. However, the fact that similar associations are seen in 3 different cohorts suggests that the associations are robust and together with the biological observations seen *in vitro* and in patients, provide evidence of a role of miR-542-3p/-5p in TGF-β signalling. The *in vitro* data have been produced using two different cell lines, C2C12 mouse myoblasts and LHCN-M2 human myoblasts. Other cell lines might have been used and could be considered to be more specific such as primary cell lines from COPD patients. However, the advantages of using immortalised cell lines from patients might be limited as *in vitro* studies are artificial systems used to study biological processes. For example, *in vitro* cell lines are in contact with fetal calf serum which is enriched in growth factors whereas cells in patients are separated from the plasma by a layer of endothelium. Moreover, plasma itself is also distinct from serum being less enriched in growth factors particularly in adults. However, *in vitro* studies were designed to determine whether the microRNAs could regulate the pathways in a muscle cell type. Having demonstrated that the proposed miR effect can occur *in vitro*, the next step is to evaluate whether it could regulate the same pathways in muscle *in vivo (see Chapter 6)*. This approach then implies that regulating these microRNAs may be an appropriate mechanism to controlling muscle mass.

5.5 Conclusions

In conclusion, this chapter evaluated the role of miR-542-3p/-5p in regulating the TGF-β pathway and thereby contributing to muscle wasting. We suggest that the increase in miR-542-3p/-5p leads to suppression of *SMAD7*, *SMURF1* and parts of PPCA complex (*PPP2CA* and *STRN*) decreasing intracellular inhibition of TGF-β signalling and contributing to an increase in SMAD2/3 dependent signalling *(Figure 49)*. Experimentally, we have not been able to prove PPM1A and CTDSP1 as miR-542 targets neither their contribution to alter TGF-β signalling, despite being predicted as miR-542 targets.

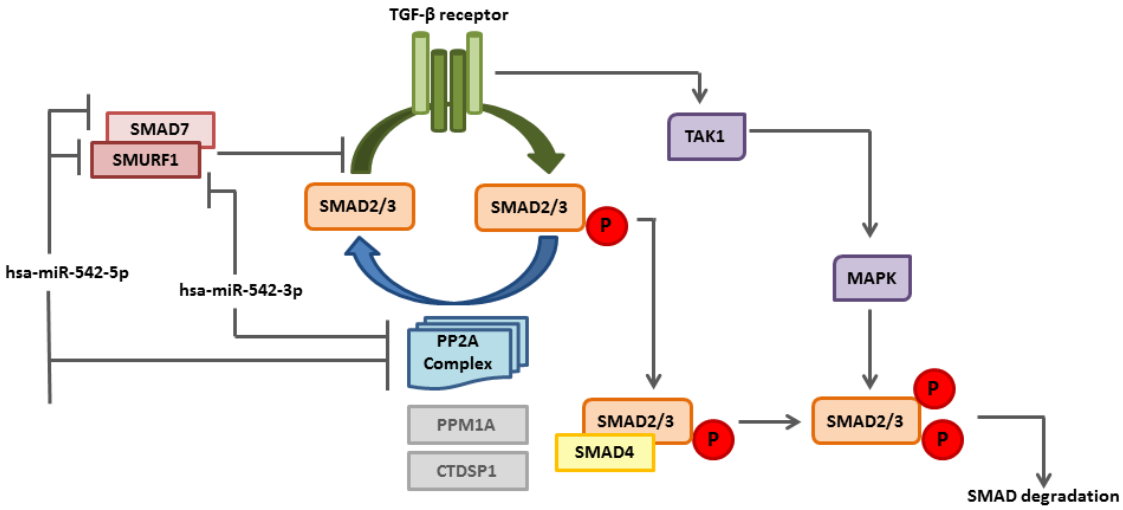


Figure 49- Proposed mechanism of action of miR-542-3p/-5p in the TGF-β pathway.

SMURF1 and PP2A complex are targeted by both miR-542-3p/-5p whereas SMAD7 is only targeted by miR-542-5p in humans. The decrease of the inhibitors of the system could drive the increase in p-SMAD2/3 that binds to SMAD4 and translocates to the nucleus. However, if p-SMAD2/3 is double phosphorylated in a linker region by MAPK it is then degraded by ubiquitylation. Experimentally, we have not been able to proof PPM1A and CTDSP1 as miR-542 targets neither their contribution to alter TGF-β signalling.

CHAPTER 6: Effects of miR-542 *in vivo* via the development of a mouse model

6.1 Rationale

The data presented so far in this thesis has identified miR-542 as a potential key regulator of muscle mass in patients. Furthermore, potential mechanisms by which this microRNA may cause muscle wasting and dysfunction have been described. However, clinical data from human cohorts show correlation but not causation of the microRNA effects and results seen *in vitro* cannot be extrapolated to conclude that similar changes would occur *in vivo* since the whole organism presents more complexity as well as signalling interactions that do not occur *in vitro.* As there is currently no method to modulate miR-542 expression in humans, it is therefore necessary to use an animal model to demonstrate that the microRNA can cause muscle wasting *in vivo*.

There are several approaches to achieve over-expression of the microRNA in muscle. The two main approaches considered were generation or acquisition of an over-expressing miR-542 mouse strain or gene delivery. The generation of transgenic mouse strains has the advantage that there is minimal inter-individual variability so an enhanced reproducibility. However, from a practical point of view it also confers several disadvantages such as cost and overproduction of mice (387) which does not agree with the 3Rs principles of humane experimental techniques. As no transgenic miR-542 mouse strain was available and its generation would have taken too long and been too expensive this option was not possible.

There are a number of potential gene delivery techniques, which use either viral or nonviral methods (388). Viral delivery requires cloning the DNA of interest into a viral vector such as adenovirus, adeno-associated virus, herpes virus, pox virus, human foamy virus, lentivirus or retroviruses which have been modified by deleting regions of their genome to avoid their replication, prevent the production of infectious particles and increase the amount of target DNA that can be inserted (389). Replication and amplification of the viral vector is achieved by the host cellular machinery using a

packaging cell line. The main advantages of this method are high transfection efficiency and stability. However, the use of viruses also has several disadvantages such as high cytotoxicity, immunogenicity which leads to inflammation, insertional mutagenesis, limitation in transgenic capacity size and cost (390). Furthermore, not all viruses target the appropriate tissue restricting the choice of virus for any particular application. In the case of skeletal muscle, the current virus of choice as a gene delivery vector is adeno-associated virus (AAV) such as AAV serotype 8 (AAV-8) and AAV-9 because targeting occurs in dividing and non-dividing cells, transduction is highly efficient and persistent and there is low immunogenicity (391-393).

Nonviral methods of DNA transfer confer several advantages compared to the viral methods as they are less immunogenic, the size of transfected DNA is not limited and they are cost-effective. However, the transfection efficiency of these systems is lower than viral methods (388). Skeletal muscle has the ability to take up and express naked plasmid DNA following intramuscular injection, and expression from the plasmid has been shown to persist at least for 2 months (394,395). However, the main limitation of this technique is the poor transfection efficiency achieved (approximately 1% of fibres become transfected) limiting its use for experimental and therapeutic applications (262). To overcome this limitation several strategies have been developed. For example, transfection efficiency of naked DNA plasmid has been improved 2-fold after 7 days of the injection by using 150 mM sodium phosphate rather than saline as the administration buffer, which helps to reduce plasmid degradation (396). An alternative method of inhibiting DNA degradation is by co-injection of aurintricarboxylic acid (ATA) (a DNAse inhibitor) in the presence of 150 mM sodium phosphate, obtaining 2.5-fold enhanced gene expression compared to injection in the absence of ATA in skeletal muscle (397).

Another methodology used to increase the uptake of naked DNA following injection is electroporation. This method consists of applying a series of controlled electric pulses across the muscle. These pulses induce a voltage across the cell, which facilitates the transport of charged molecules *(Figure* 50*)* (398). Therefore, electroporation increases transgene expression in mouse *tibialis anterior* 5 days after gene transfer by 12-fold (obtaining a transfection efficiency of up to 17%) and reduces inter-individual

variability compared to injection of plasmid alone (262). However, electroporation has a major drawback, particularly in muscle wasting studies, which is tissue damage due to the high voltage (262,399). The need to limit damage and enhance transfection efficiency in skeletal muscle was addressed by several groups and it has been found that pre-treatment of mouse TA muscles with hyaluronidase and electroporation using 50% v/v saline as a vehicle for plasmid DNA increases transgene expression after 5 days of the gene transfer and reduces muscle damage (262,399). Hyaluronidase catalyses the hydrolysis of hyaluronan, which is a component of the extracellular matrix, resulting in decreased hyaluronan viscosity and thereby increasing tissue permeability. Pre-treatment of 0.4U/μL hyaluronidase 2h before electroporation increased transfection efficiency by ~10 fold in mouse TA but in this study lower transfection was achieved by electroporation only in comparison to other studies. Hyaluronidase treatment alone followed by plasmid injection does not improve transfection (262).

Electroporation has become a widely used method for the transient expression of genes in skeletal muscle (a literature search of Pubmed using the terms “electroporation, gene expression and mouse” returns 1566 hits) indicating that it is a widely accepted method of gene transfer. Consequently, considering the advantages and disadvantages of the different techniques, plasmid injection followed by electroporation and pre-treatment with hyaluronidase was chosen as the method for over-expressing miR-542 as it provided a balance between cost and time efficiency, medium transgene expression and low cytotoxicity.

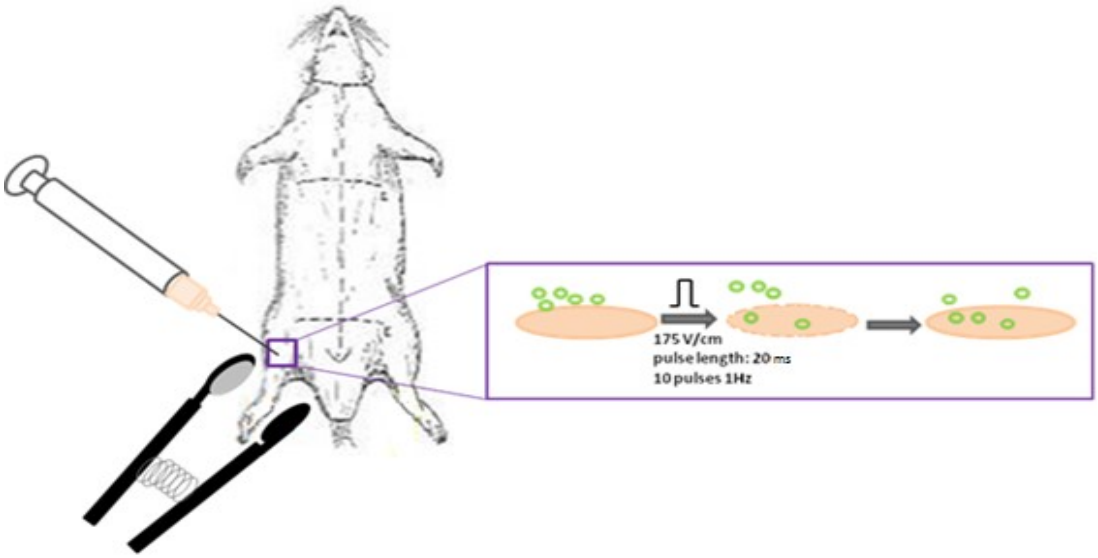


Figure 50- Schematic representation of DNA injection followed by electroporation used in *in vivo* experiments.

Mouse TA is injected with hyaluronidase followed by DNA pCAGGS-EGFP-542 or control plasmid injection and electroporation. Electroporation was performed at 175 V/cm applied in ten 20ms squared wave pulses at 1Hz. The voltage produced across the muscle fibres facilitates the uptake of charged molecule such as DNA.

6.2 Hypothesis

Results presented in Chapters 3, 4 and 5 generated the following hypotheses:

1) Over-expression of miR-542 in muscle would cause muscle wasting *in vivo by:*

   1.1) Causing mitochondrial and cytoplasmic ribosomal impairment by targeting ribosomal proteins.

   1.2) Increasing TGF-β pathway activity by targeting inhibitors of the pathway.

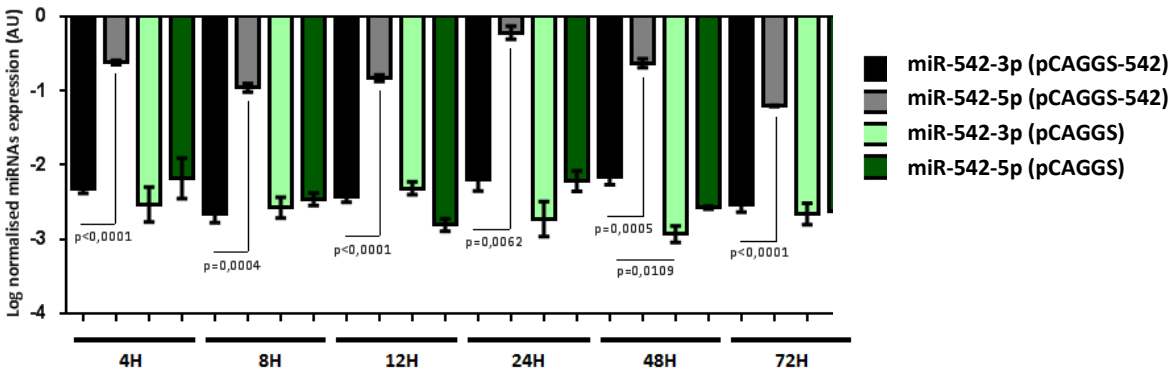
6.3 Results

6.3.1 Predominant miR-542-5p expression from pCAGGS-EGFP-542 vector *in vitro*

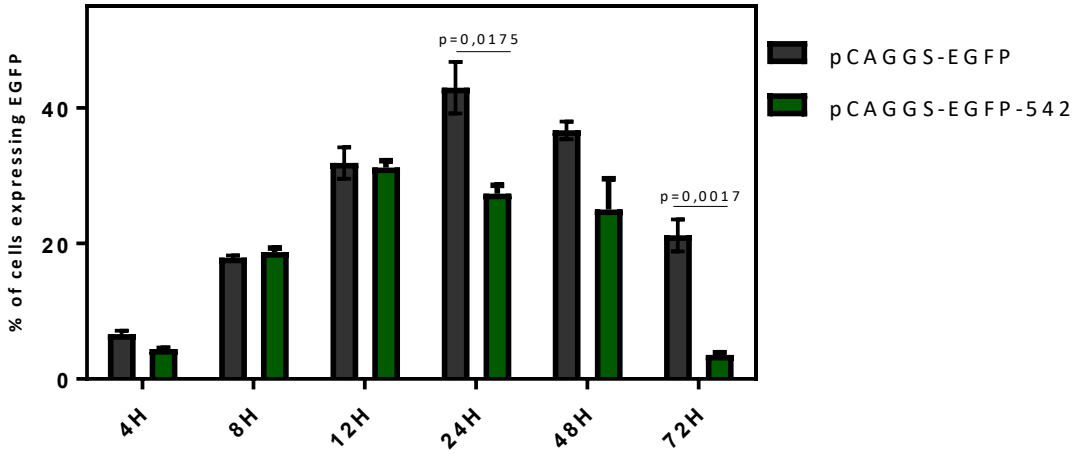
To overexpress miR-542 in mice, we generated a vector (pCAGGS-EGFP-542) containing an EGFP cDNA followed by 500bp of the miR-542 gene including the hairpin region contained within the 3'-UTR of the EGFP under the control of a strong promoter (the CAGS promoter) thereby allowing identification of positive transfected fibres using fluorescence. As a control vector we used pCAGGS containing only the EGFP region (400). To confirm miR-542 expression, C2C12 mouse myoblasts were transfected with the miR-542 or control plasmid and both miR-542-3p and miR542-5p levels were analysed by Taq-PCR and EGFP levels were visualised under a fluorescence microscope at different time points (4h, 8h, 12h, 24h, 48h and 72h). microRNA quantification showed an increase in the expression of miR-542-5p form (*Figure 51, A*) but no marked increase of miR-542-3p compared to control at all the time points (except at 48h, p=0.0109) analysed in the cells transfected with pCAGGS-EGFP-542. The greatest increase (10 fold) in miR-542-5p levels compared to control was observed at 24h after transfection. Elevated expression of miR-542-5p (approx. 2-fold) was still detectable 72h after transfection.

The presence of EGFP allowed identification of transfected cells in the presence and absence of the microRNA (and quantification of these cells, *Figure 51, B*). A different expression profile was seen between myoblasts transfected with the control plasmid (pCAGGS-EGFP) or the miR plasmid (pCAGGS-EGFP-542, *Figure 51, C*). Whereas control plasmid induced an increase in EGFP levels over time, miR-542 plasmid increased EGFP translation in the first 12h but this was followed by a decrease at 24h (p=0.0175) and a progressive decline in EGFP until EGFP expressing cells were almost undetectable at 72h (p=0.0017). This reduction in the proportion of cells expressing detectable EGFP could be due to reduced cell viability or proliferation, a reduction in protein synthesis or a combination of these effects.

A


Log normalised miRNAs expression (AU)
0
-1
-2
-3
-4
p<0,0001
p=0,0004
p<0,0001
p=0,0062
p=0,0005
p=0,0109
p<0,0001
4H
8H
12H
24H
48H
72H
miR-542-3p (pCAGGS-542)
miR-542-5p (pCAGGS-542)
miR-542-3p (pCAGGS)
miR-542-5p (pCAGGS)

B


% of cells expressing EGFP
40
20
0
p=0,0175
p=0,0017
4H
8H
12H
24H
48H
72H
pCAGGS-EGFP
pCAGGS-EGFP-542

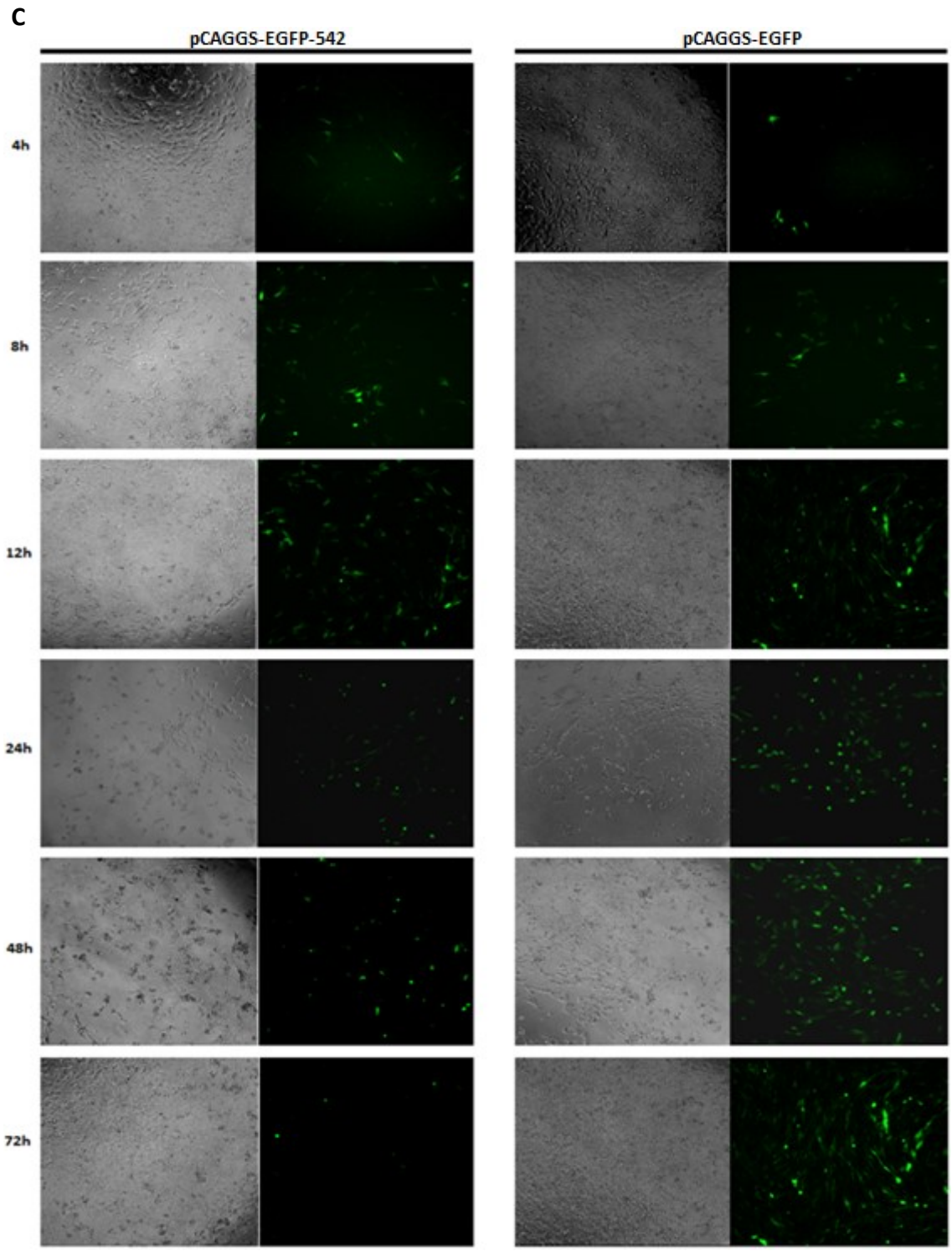


Figure 51- pCAGGS-EGFP-542 vector leads to an increase in miR-542-5p levels *in vitro.*

C2C12 were transfected with pCAGGS-EGFP-542 or pCAGGS-EGFP and miR-542-3p/-5p levels and EGFP protein levels were measured at 4h, 8h, 12h, 24h, 48h and 72h. An increase of the miR-542-5p form was observed over time *in vitro* being the highest increase at 24h after transfection [A]. EGFP protein levels were observed under the fluorescence microscope and showed an increase over time on pCAGGS-EGFP transfected myoblasts but a decrease after 12h of transfection in myoblasts transfected with pCAGGS-EGFP-542. Bar charts show mean signal ± SEM from n=4 independent transfections. Statistical analysis was performed using unpaired t-test as samples were normally distributed. miR-542-3p and miR-542-5p levels were normalised against U6.

6.3.2 miR-542-3p/-5p expression from pCAGGS-EGFP-542 vector *in vivo*

To confirm expression from pCAGGS-EGFP-542 *in vivo*, we measured miR-542-3p/-5p levels at an early time point after electroporation. In the first experiment, the dose of anaesthetic administered was too high as the mouse strain used was more susceptible to the anaesthetic than that used by the group from which we obtained the protocol (262). Therefore, mice did not fully recover and 4h after transfection they were humanely killed and used to determine microRNA expression at this time point. RNA was extracted from the whole TA and showed an increase in miR-542-5p levels in the miR-542-5p expressing TA compared to the control TA (p=0.0173, *Figure 52*). However, no difference in miR-542-3p levels was seen between the two TAs, consistent with the *in vitro* results shown in *Figure 51.*

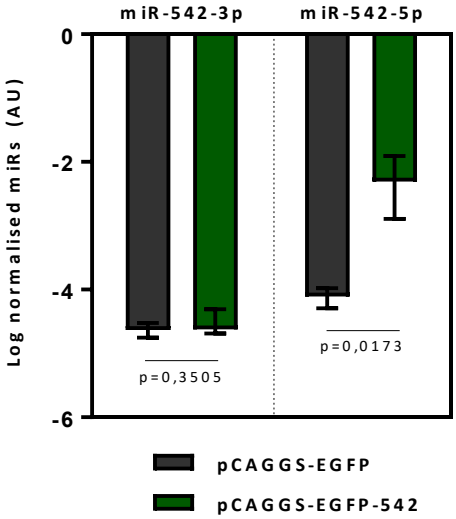


Figure 52- miR-542-3p/-5p expression of pCAGGS-EGFP-542 *in vivo.*

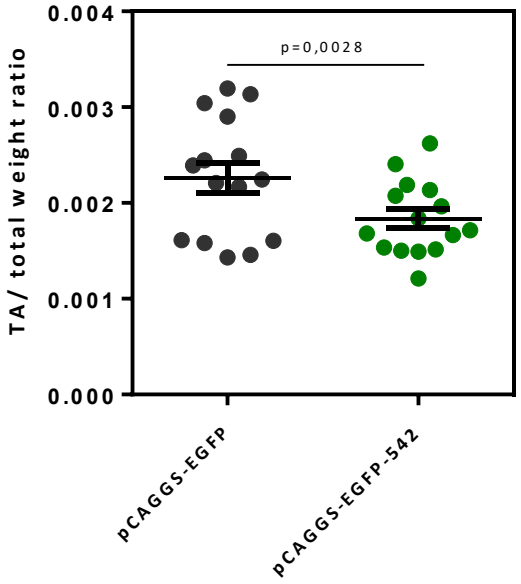
miR-542-3p and miR-542-5p expression from pCAGGS-EGFP-542 were measured at 4h after electroporation. miR-542-5p levels were up-regulated in miR-542 expressing TAs compared to PCAGGS-EGFP control TAs. Bar chart shows mean signal± SEM from n=3 mice. Statistical analysis was performed using unpaired t-test as samples were normally distributed. miR-542-3p and miR-542-5p levels were normalised against U6.

6.3.3 miR-542 induces wasting *in vivo* and electroporation efficiency varies along the TA muscle

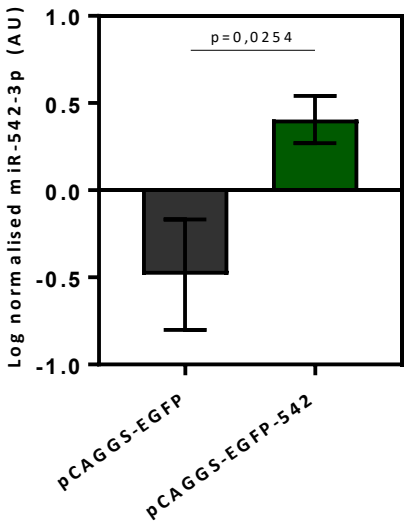
To analyse the effect of miR-542 *in vivo,* we electroporated pCAGGS-EGFP-542 into the right TA and pCAGGS-EGFP on the left TA of the mice. Three days after electroporation the mice were humanely killed and the TAs were dissected out and weighed. Electroporation of the miR-542 plasmid into the TA caused a rapid reduction in muscle weight of about 20% compared to the contralateral muscle expressing EGFP alone (p=0.0028, *Figure 53, A*), suggesting that elevated miR-542 caused muscle wasting. To confirm miR-542 levels were increased after 72h of electroporation, we measured both miR-542-3p and miR-542-5p levels in the TAs. Laser capture microdissection of the samples was performed to restrict the analysis to the positively electroporated fibres. In these samples, miR-542-5p was undetectable by Taq PCR, however, an increase of miR-542-3p was seen in the miR-542 electroporated TA compared to the control leg (p=0.0254, *Figure 53, B*) suggesting a change in the processing of the microRNA over time.

To determine electroporation efficiency after 3 days of the plasmid injection, TAs were sectioned *(as detailed in Chapter 2)* and the percentage of positively electroporated fibres was counted under a fluorescent microscope. To account for differential transfection away from the site of injection along the length of the TA, the muscle was divided into 5 equal regions. This analysis showed that the highest electroporation efficiency (around 40%) was in level 4, close to the site of plasmid injection *(Figure 53, C).* Moreover, electroporation efficiency was more successful in the outside part of the TA than in the centre, possibly due to the fact that higher current reached the outside of the muscle compared to the inner part or due to damage provoked by the needle *(*Figure 53*, D).*

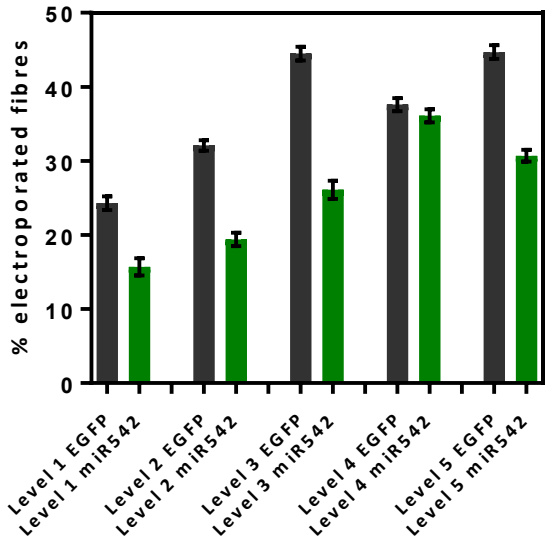
A


p=0,0028
TA/ total weight ratio
0.004
0.003
0.002
0.001
0.000
pCAGGS-EGFP
pCAGGS-EGFP-542

B


p=0,0254
Log normalised miR-542-3p (AU)
1.0
0.5
0.0
-0.5
-1.0
pCAGGS-EGFP
pCAGGS-EGFP-542

C


% electroporated fibres
50
40
30
20
10
0
Level 1 EGFP
Level 1 miR542
Level 2 EGFP
Level 2 miR542
Level 3 EGFP
Level 3 miR542
Level 4 EGFP
Level 4 miR542
Level 5 EGFP
Level 5 miR542

D

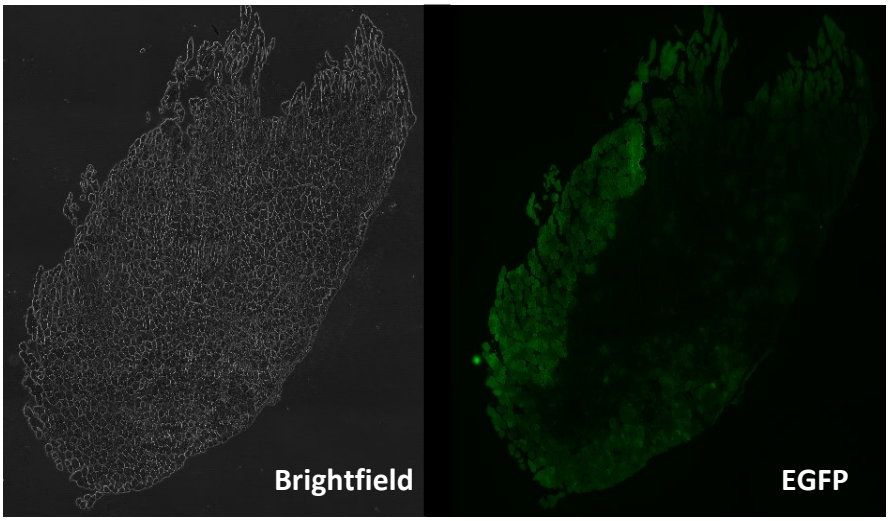


Figure 53- pCAGGS-EGFP-542 electroporation drives muscle wasting *in vivo* and its transfection efficiency varies within the muscle length and depth.

[A] TAs were weighed after dissection and a 20% reduction in mass was seen in TAs electroporated with miR-542 vector compared to the contralateral TAs electroporated only with the EGFP plasmid, (n=15 mice generated in 3 independent experiments of 5 mice per experiment). miR-542-3p and miR-542-5p expression from the pCAGGS-EGFP-542 plasmid was measured at 72h after electroporation and normalised to U6. [B] miR-542-3p levels were increased in the miR-542 expressing TA compared to the control leg (n=4 mice from a single experiment). Electroporation efficiency was proven unequal along the muscle being higher in the middle-down part lengthwise where the vectors injection took place [C] and also higher in the external area of the muscle [D] as current during electroporation might be more intense or the area less damaged due to the plasmid injection (n=10 mice from 2 separate experiments n=5 mice per experiment). Scatter dot plot and bar charts show mean signal ± SEM and statistical analysis was performed using paired t-test as samples were normally distributed.

6.3.4 miR-542 induces fibre diameter and area decrease *in vivo*

To further analyse the effects of miR-542 on muscle *in vivo,* fibre diameter and area of transfected (fluorescent) and non-transfected (non-fluorescent) fibres were measured in both the miR-542 and the EGFP-control electroporated TAs at level 4. There was a 10% decrease in the diameter of the pCAGGS-EGFP-542 transfected fibres compared to both the non-transfected fibres from the same muscle and the pCAGGS-EGFP control fibres from the contralateral TA ($p=0.0015$). There was no significant difference in diameter between the non-transfected fibres of the two TAs ($p=0.2380$) *(Figure 54, A).* As expected, fibre area was also reduced (17%) on the pCAGGS-EGFP-542 transfected fibres compared to both non-transfected fibres from the same muscle and the pCAGGS-EGFP transfected fibres ($p<0.0001$). No significant difference was observed in fibre area between the non-transfected fibres of the two TAs ($p=0.2609$*) (Figure 54, B).*

Binning of the transfected fibres into defined fibre size ranges identified a leftwards shift towards smaller fibres, observed in both fibre diameter *(Figure 54, C)* and area *(Figure 54, D)* of the pCAGGS-EGFP-542 electroporated TA compared to pCAGGS-EGFP expressing TA.

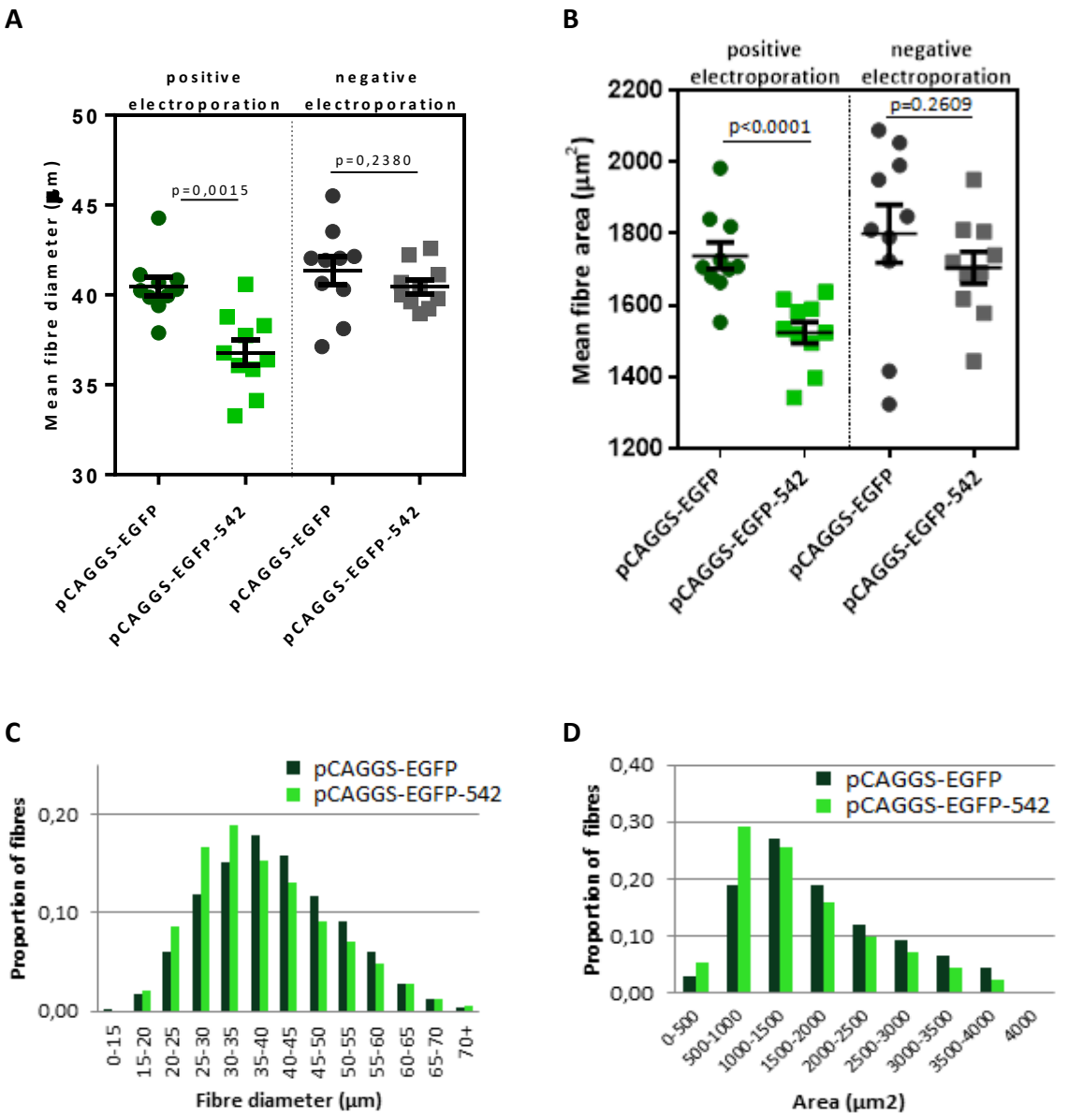


Figure 54- Fibre diameter and area are decreased in miR-542 positively electroporated fibres *in vivo*.

Using fluorescence microscopy, positively electroporated fibres from both TAs of each animal were detected and diameter and area were measured using Image J software. [A] A mean for all the fibre diameters counted per TA was obtained per animal and showed a decrease in the pCAGGS-EGFP-542 electroporated TA compared to the control TA. [B] Similarly, a mean for all the fibre areas counted per TA was obtained per animal and showed a decrease in the pCAGGS-EGFP-542 electroporated TA compared to the control leg. Transfected fibre measurements were split in ranges and proportions were obtained showing an increase in small fibres and a decrease in big fibres in miR-542 expressing TA compared to control TA in both fibre diameter [C] and fibre area [D] graphs. Scatter dot plots and bar charts show mean signal ± SEM and statistical analysis was performed using paired t-test as samples were normally distributed. Results are based on n=2 independent experiments with 5 mice in each repetition.

6.3.5 miR-542 causes mitochondrial impairment *in vivo*

To analyse the effects of miR-542 on mitochondrial function and protein content, mitochondria were prepared from the whole TA *(detailed in Chapter 2),* quantified by Bradford assay and analysed for complex I activity and membrane potential. Quantification of mitochondrial complex I activity (the first component of the electron transport chain) showed a marked reduction in the muscles expressing miR-542 compared to those expressing the control vector (p=0.0286, *Figure 55, A*). Similarly, JC-1 staining of the mitochondria showed a reduction in mitochondrial membrane potential in the muscles expressing miR-542 (p=0.0214, *Figure 55, B*). To determine whether miR-542 caused mitochondrial ribosomal stress we measured *12S* and *16S* rRNAs levels in the samples collected by laser capture microdissection. *12S* rRNA levels were reduced in the pCAGGS-EGFP-542 transfected fibres compared to pCAGGS-EGFP transfected fibres (p=0.0080) but no difference was seen in *16S* rRNA levels (p=0.1051) *(Figure 55, C).* Another measurement of mitochondrial dysfunction was the decrease in *Cytb* RNA (p=0.0414, *Figure 55, D*) in the muscles expressing miR-542 compared to those expressing the control vector, suggesting decreased mitochondria or that the microRNA could also cause cytoplasmic ribosomal stress decreasing the translation of mitochondrial transcription factors. Together these data suggest that over-expression of miR-542 leads to mitochondrial dysfunction and mitochondrial ribosomal stress.

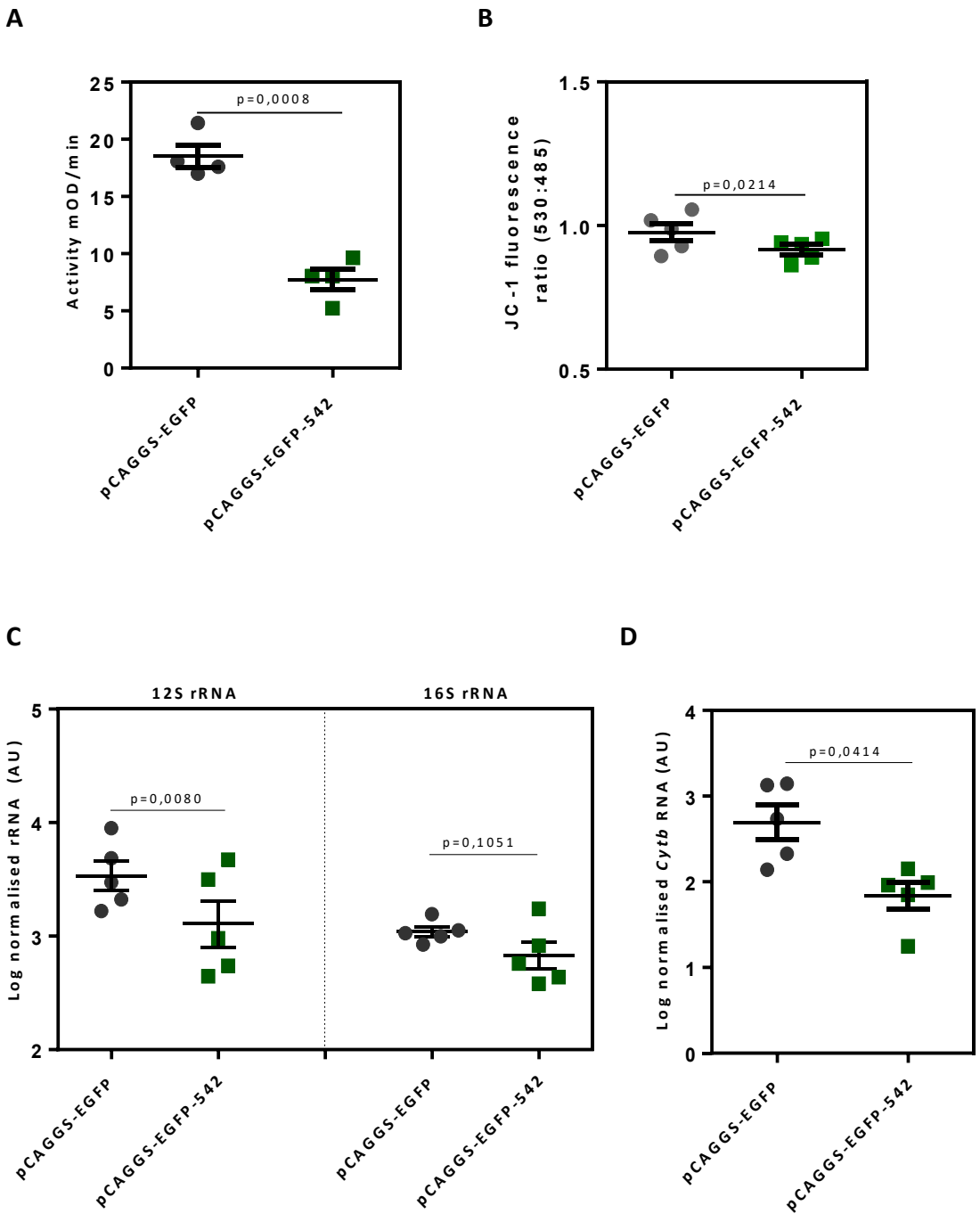


Figure 55- miR-542 causes mitochondrial activity and ribosomal biogenesis impairment *in vivo.*

Mitochondria were isolated from the mice TA and complex I activity [A] and membrane potential (JC-1 assay) [B] were determined. Muscles expressing miR-542 had reduced complex I activity and decreased JC-1 staining suggesting decreased membrane potential. Positively electroporated fibres were selected by laser capture and RNA levels were quantified. Decreased *12S* rRNA levels [C] were seen in TAs expressing miR-542 compared to control TAs but there was no difference in *16S* rRNA levels [C]. *Cytb* RNA [D] was decreased in muscles expressing miR-542 compared to control. Scatter plots show mean signal ± SEM and statistical analysis was performed using paired t-test as samples were normally distributed. Results are based on n=1 independent experiments with 5 mice with the exception of complex I activity measurements for which there was only sufficient protein to perform the assay to four mouse samples. Normalisation of the genes was performed against *Hprt*, *Gapdh* and *B2m*.

6.3.6 miR-542 causes cytoplasmic ribosomal stress *in vivo*

Cytoplasmic ribosomal stress has previously been identified as a response to miR-542 *in vitro* in *Chapter 4.* The effect of miR-542 was therefore determined on *18S* and *28S* rRNA levels in the samples isolated by laser capture microdissection. *18S* rRNA levels were down-regulated in fibres expressing miR-542 compared to those only expressing EGFP (p=0.0213, *Figure 56, A*) whereas there was no significant reduction in *28S* rRNA levels *(p=0.0663, Figure 56, A)* suggesting that over-expression of miR-542 can lead to cytoplasmic ribosomal stress *in vivo*.

To determine whether miR-542 could cause sufficient ribosomal stress to lead to p53 signalling activation, we measured *Gdf-15* RNA levels in the same samples. *Gdf-15* RNA expression was increased in the pCAGGS-EGFP-542 electroporated TA compared to control TA (p=0.0052, *Figure 56, B*), consistent with activation of p53 signalling.

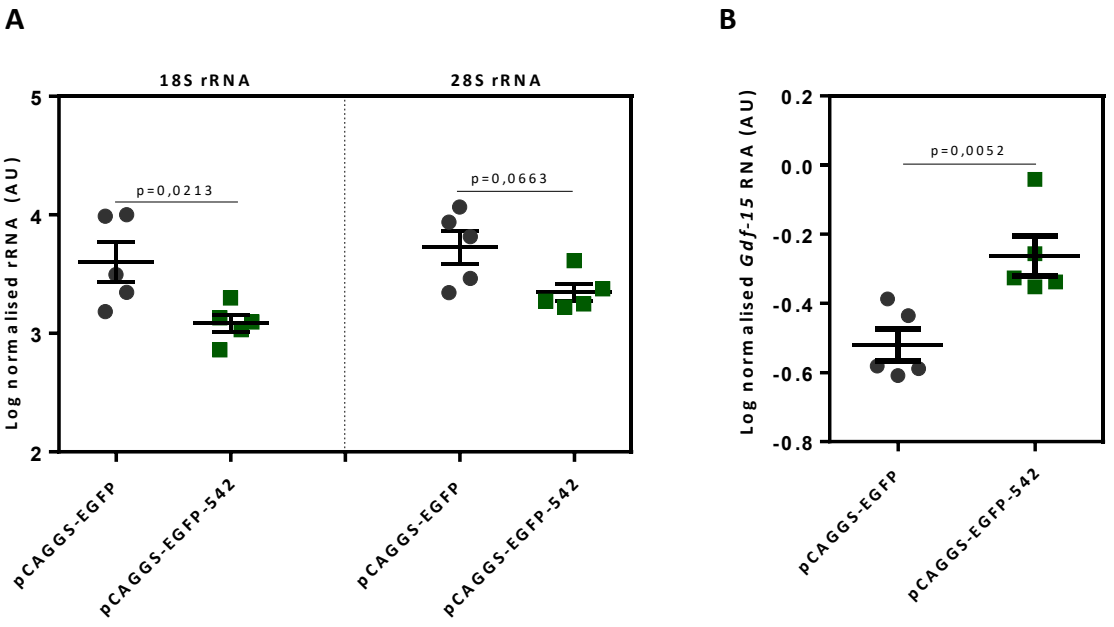


Figure 56- miR-542 causes cytoplasmic ribosomal stress *in vivo.*

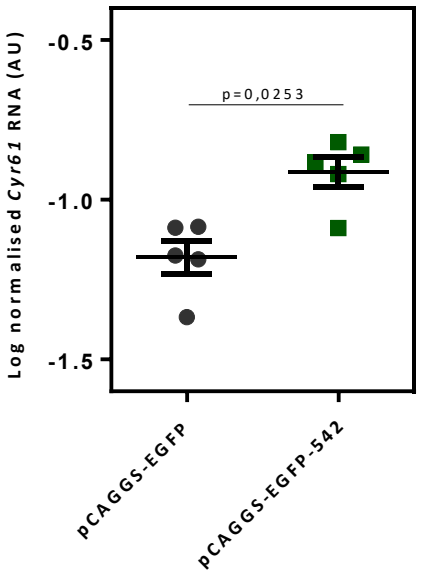
Decrease in *18S* rRNA [A] and increased *Gdf-15* RNA levels [B] in transfected fibres expressing miR-542 were seen compared to EGFP expressing fibres suggesting ribosomal stress. Scatter dot plots show mean signal ± SEM and statistical analysis was performed using paired t-test as samples were normally distributed. Results are based on n=1 independent experiments with 5 mice. Normalisation of the genes was performed against *Hprt*, *Gapdh* and *B2m*.

6.3.7 miR-542 increases TGF-β signalling *in vivo*

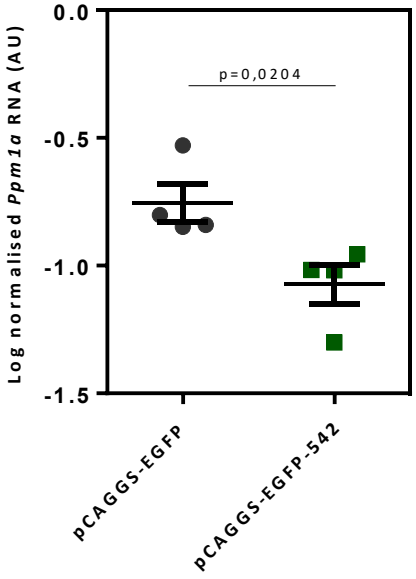
Having demonstrated in the previous chapter that miR-542 can modulate TGF-β signalling *in vitro*, we investigated whether increased miR-542 modulated the same pathway *in vivo*. As previously, TGF-β signalling was indirectly measured by quantifying the expression of *Cyr61* in transfected fibres isolated by laser capture microdissection. Increased *Cyr61* RNA levels were observed in miR-542 transfected fibres compared to EGFP-expressing fibres (p=0.0253, *Figure 57, A*), suggesting increased TGF-β pathway activity.

The effect of miR-542 was determined on the expression of the SMAD pathway inhibitors described previously including components of the *Pp2a* complex (the catalytic subunit *Ppp2ca* and the regulatory subunit *Strn)*, *Ppm1a*, *Smurf1 and Smad7*. This analysis showed a decrease in *Ppm1a* (p=0.0204, *Figure 57, B*) and in *Smurf1* levels in pCAGGS-EGFP-542 transfected fibres compared to pCAGGS-EGFP fibres (p=0.0357, *Figure 57, C*). *Strn* levels were detected in all the fibres expressing EGFP but not in most of the fibres expressing miR-542 suggesting that *Strn* was also reduced. To allow statistical comparison, in samples where *Strn* was below the detectable levels it was assumed that the C_T value was 40 (this would be above the actual C_T so assumes a higher concentration) and they were normalised. This analysis confirmed a decrease in *Strn* levels in fibres expressing miR-542 (p=0.0119, *Figure 57, D*). *Ppp2ca* levels were undetectable by PCR in both TAs and there was no difference in *Smad7* RNA (p=0.2586, *Figure 57, E*) between the TAs. Quantification of SMAD7 protein showed a reduction in protein levels *(Figure 57, F)* in the TA expressing miR-542 compared to the control TA (p=0.0041, *Figure 57, G*).

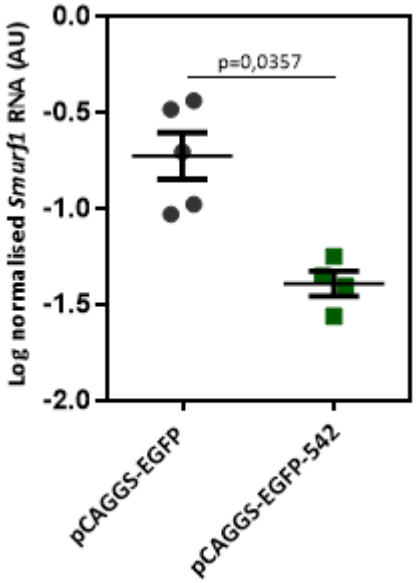
A


Log normalised Cyr61 RNA (AU)
-0.5
-1.0
-1.5
p=0,0253
pCAGGS-EGFP
pCAGGS-EGFP-542

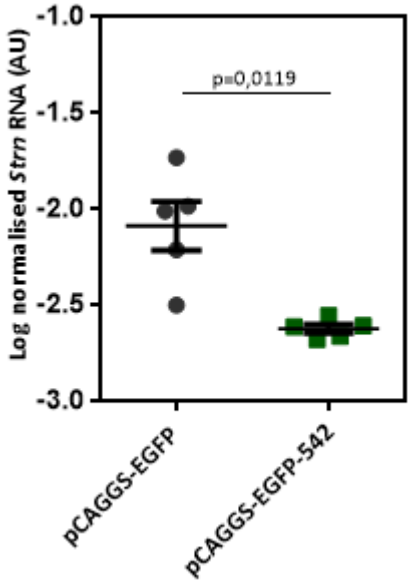
B


Log normalised Ppm1α RNA (AU)
0.0
-0.5
-1.0
-1.5
p=0,0204
pCAGGS-EGFP
pCAGGS-EGFP-542

C


Log normalised Smurf1 RNA (AU)
0.0
-0.5
-1.0
-1.5
-2.0
p=0,0357
pCAGGS-EGFP
pCAGGS-EGFP-542

D


Log normalised Strn RNA (AU)
-1.0
-1.5
-2.0
-2.5
-3.0
p=0,0119
pCAGGS-EGFP
pCAGGS-EGFP-542

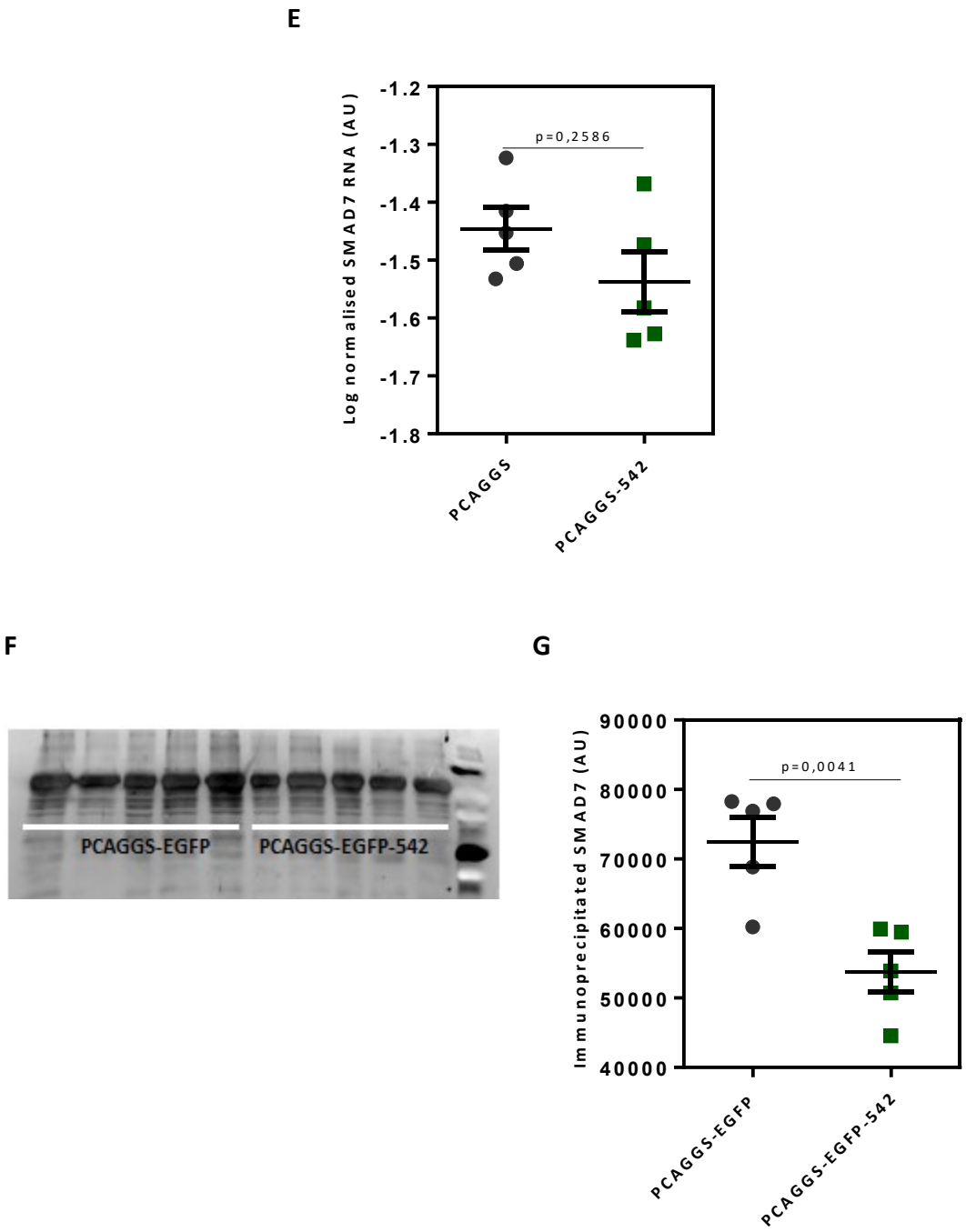


Figure 57- TGF-β signalling was increased by miR-542 *in vivo.*

Increased *Cyr61* RNA was seen in the fibres expressing miR-542 compared to fibres expressing only EGFP suggesting increased TGF-β activity [A]. *Ppm1a* [B], *Smurf1* [C] and *Strn* [D] inhibitors of TGF-β pathway were down-regulated in miR-542 transfected fibres compared to EGFP transfected fibres. Despite no differences in *Smad7* RNA level were seen between legs [E], a decrease in SMAD7 protein level was observed in miR-542 electroporated TAs compared to control TAs [F-G]. Scatter dot plots show mean signal ± SEM and statistical analysis was performed using paired t-test as samples were normally distributed. Results are based on n=1 independent experiments with 5 mice, however for some genes we could only get detectable values in 4 of the mouse samples. Normalisation of the gene expression was performed against *Hprt*, *Gapdh* and *B2m*.

6.4 Discussion

6.4.1 Main findings

This *in vivo* study shows that over-expression of miR-542 in mouse TA induces detectable wasting within 72 hours of electroporation as demonstrated by the 20% reduction in muscle mass of the miR-542 expressing TA compared to the control TA. Consistent with muscle loss, a 10% decrease in fibre diameter and 17% decrease in fibre area were seen in the miR-542 expressing TA compared to control TA. Electroporation efficiency was variable along longitudinal and cross-sectional axes of the TA. Consistent with the results from Chapter 3, mitochondrial functional impairment was observed in the miR-542 expressing TA as demonstrated by a decrease in complex I activity and a decrease in membrane potential. These effects were accompanied by a decrease in *12S* rRNA consistent with mitochondrial ribosomal stress. miR-542 expression also seemed to promote cytoplasmic ribosomal stress causing a down-regulation of *18S* rRNA and an increase of *Gdf-15*. Decreased *Cytb* RNA levels could also suggest a decrease in cytoplasmic protein synthesis, decreasing the translation of mitochondrial transcription factors such as TFAM or simply a reduction in number of mitochondria.

Consistent with results from Chapter 4, miR-542 elevated the expression of *Cyr61* RNA suggesting an increase in TGF-β pathway activity. This interpretation was strengthened by a decrease in the expression of *Ppm1a*, *Strn* and *Smurf1* RNA, together with a decrease in SMAD7 protein levels.

6.4.2 Expression of miR-542-3p/-5p from pCAGGS-EGFP-542 plasmid *in vitro* and *in vivo*

Both *in vitro* and at the early time point (4h) *in vivo* data showed that the major form of miR-542 expressed from pCAGGS-EGFP-542 was miR-542-5p, whereas, at the later time point *in vivo* (72h) the -3p form predominated. Unfortunately, little is known about the control of the microRNA strand selection process. However, microRNA-3p/-5p ratio is known to vary dependent on cell type and developmental stage as well as

changing in response to disease stages suggesting that it is a finely regulated process (401). Therefore, differences in miR-542-3p/-5p expression between the *in vitro* and *in vivo* experiment could be attributed to differences in cell developmental stage since C2C12 are myoblasts whereas *in vivo* the transfected cells are myofibres. Moreover, *in vitro* myoblasts are in contact with serum containing a lot of growth factors whereas *in vivo* muscle fibres are in the presence of plasma, which contains a lower concentration of growth factors which need to diffuse through the endothelium to reach the fibres. However, this argument does not explain the differences in miR-542 strand selection seen between different time points 4h and 72h *in vivo.* It is known that several molecules could play a role in strand selection such as argonaute, DICER, transactivation response RNA-binding protein, protein activator of dsRNA-dependent protein kinase and Xrn-1/2 (401). However, their mechanism of action remains to be elucidated. Several thermodynamic features have also been reported to affect strand selection. For example, the strand with weakest binding at its 5'-end is more likely to become the guide strand (incorporated in DICER complex). The guide strand has also been suggested to have more uracils at the 5'-end and an excess of purines (adenosines and guanines) (401). If we check those features in miR-542, we see that miR-542-5p strand has a single uracil at the 5'-end and the total number of purines is 11 whereas miR-542-3p strand has 2 uracils at the 5'-end and 14 purines in total. Consequently, miR-542-3p might be more likely to become the guide strand agreeing with the higher levels of miR-542-3p seen at 72h *in vivo*. However, the literature does not help to explain changes in strand selection with time. Changes in guide strand selection have been reported in the context of diseases stage (401) suggesting that miR-542 expression could change as atrophy develops in the mouse muscles.

Visualization and measurement of the expression of pCAGGS-EGFP-542 plasmid *in vivo* showed a main drawback of the gene delivery technique. Transfection efficiency varied along both the longitudinal and horizontal axes of the TA. Higher electroporation efficiency levels were seen in level 4 (near the bottom of TA) probably as a result of being closer to the plasmid injection site. Horizontally, the more external fibres of the muscle were transfected. This is likely to be the consequence of the damage caused by the needle during plasmid injection promoting inflammation and protein degradation

on the injured site. Another explanation could be the fact that the current applied by the electrodes was diminished when reaching the muscle fibres in the inner part of the TA.

6.4.3 Muscle wasting is promoted by miR-542 *in vivo*

Transfection of miR-542 plasmid *in vivo* induced a rapid (3 days after electroporation) and marked (20%) reduction in muscle mass and fibre size showing that increased levels of miR-542 can drive muscle atrophy. Compared to other studies analysing molecules pro-muscle wasting, miR-542 effects are more dramatic in terms of provoking muscle mass loss in a short period of time. For example, electroporation of a MSTN plasmid in mouse TA resulted in a 10% decrease of muscle mass 14 days after MSTN plasmid injection and electroporation (266). Similarly, electroporation of a GDF-15 vector in mouse TA resulted in less than a 10% loss of muscle mass after 14 days of the injection (197) suggesting miR-542 plays an important role in muscle wasting. Consequently, these data suggest that an up-regulation of this microRNA could have a similar effect in humans, driving atrophy in the clinical conditions which have elevated miR-542 levels.

Several disease studies have shown that loss in muscle mass for example in sarcopenia involves a decrease in muscle fibre size known as atrophy and in muscle fibre number or hypoplasia (148). In COPD patients, a significant reduction in skeletal muscle mass and cross-sectional areas has also been reported together with fibre atrophy (138) but despite having identified in Chapter 3 higher levels of miR-542 in both of those patient groups (sarcopenia and COPD) compared to controls, miR-542 expression does not associate with muscle mass in COPD patients. However, an association was found in the acute settings of admission to the ICU following surgery (162) between miR-542 and muscle loss suggesting that while miR-542 is a drive to atrophy other factors must be important in determining how muscle responds to wasting. For example, the regeneration rate of muscle, which mainly depends on satellite cells and myogenic progenitors, can have an important role in regulating muscle loss and this process might be independent of the effects of miR-542.

Moreover, other microRNAs can also affect the muscle response to atrophy. For example, in patients with COPD an increase in the maternally imprinted microRNA miR-675 was seen in low FFMI compared to normal FFMI patients, whereas there was reduced expression of the paternally imprinted miR-518e. Moreover, an association was found between low FFMI and an altered methylation of the imprinting control region of miR-675 host gene (H19) in these patients, suggesting that the epigenetic control of this locus may contribute to a susceptibility to a low FFMI (271).

6.4.4 Increased mitochondrial and cytoplasmic ribosomal impairment by miR-542 *in vivo*

miR-542 expression in mouse muscle fibres caused a reduction in mitochondrial function *in vivo* shown by decreased complex I (NADH:ubiquinone oxidoreductase) activity and decreased membrane potential (shown by JC1 staining) compared to control fibres. These data are consistent with *in vitro* results and data obtained from patient biopsies shown in Chapter 3. Consistent with miR-542 causing mitochondrial ribosomal stress, we showed a reduction in *12S* rRNA in miR-542 transfected mouse fibres compared to control contra-lateral leg. Similar results were obtained from *in vitro* and patient data.

Supporting the role for miR-542 promoting ribosomal stress, *18S* rRNA was down-regulated in mouse miR-542 expressing fibres compared to the control fibres indicating an impairment of cytoplasmic ribosomal biogenesis by the miR. These results are consistent with the *in vitro* and the patient data presented in Chapter 4. Finally, *Gdf-15* RNA levels were up-regulated in the pCAGGS-EGFP-542 transfected mouse fibres compared to pCAGGS-EGFP transfected fibres which fits with a p53 activation and a mitochondrial and cytoplasmic ribosomal stress as shown previously by *in vitro* and patient data in Chapter 4.

6.4.5 Increased TGF-β signalling by miR-542 *in vivo*

Data from this chapter suggests that increased expression of miR-542 contributes to muscle wasting by increasing TGF-β signalling in the absence of exogenous ligand measured as increased *Cyr61* RNA. This finding is consistent with both *in vitro* results and data obtained from the ICUAW cohort in Chapter 5.

Some clinical trials have aimed to target TGF-β signalling to reduce muscle wasting, for example by blocking MSTN, as a treatment for patients with ICUAW *(www.clinicaltrials.gov reference NCT01321320)*. However, circulating levels of MSTN did not increase in patients admitted to the ICU following aortic surgery (196). Therefore, the relevance of the results presented in this chapter is that miR-542 can repress TGF-β inhibitors *in vivo* leading to increased TGF-β activity bypassing the need for an increase of the ligands such as MSTN or TGF-β1.

6.4.6 Critique of the method

The experiments performed in this chapter relied on the over-expression of miR-542 in the muscle of mice by electroporation. The analysis of transfection efficiency measured by the proportion of EGFP fluorescent fibres showed that transfection was variable along the TA, being higher in the lower part of the muscle on the longitudinal axis close to the site of plasmid injection. Uniform transfection is obviously an ideal situation and it might be possible to increase uniformity using two injections in the TA to deliver the plasmid rather than a single one which could enhance electroporation efficiency. However, the downsides of multiples injections should also be considered as the penetration of the injection in the muscle causes tissue damage that can lead to increased inflammation masking the effects of the microRNA. Similarly, electroporation efficiency was also higher in the external area of the muscle as current during electroporation might be more intense. Therefore, increasing number of pulses and lowering voltage to prevent damage could be tested to ensure better electroporation efficiency throughout the cross-sectional area of the TA. To overcome the limitations of uneven miR-542 expression throughout the muscle, we selected the

longitudinal level with the highest miR-542 expression (level 4) and we selected single positive electroporated fibres from cross-sectional areas from both TAs (miR-542 expressing and control) using laser capture microdissection. This approach allowed us to analyse gene expression in transfected fibres only and reduced the problem associated with variable transfection as well as allowing us to increase sensitivity and to measure smaller changes in RNA levels due to miR-542 expression. There is, however, one advantage to the fact that not all fibres were transfected and that is we were able to determine the effect of transfection on fibre size within the same muscle. This is important when determining the effect of genes that may alter muscle function, as fibre diameter is highly dependent on activity and could be affected by differential muscle usage with one limb being favoured over the other.

The data also provide evidence for cytoplasmic ribosomal stress but to demonstrate that ribosomal stress impairs *de novo* protein synthesis *in vivo* we would need to measure protein synthesis. Protein synthesis has been widely studied by measuring radioactive isotope (e.g. ^{3}H-phenyalanine or ^{35}S-methionine) or stable isotope (e.g. ^{15}N-lysine, ^{13}C-leucine or [ring-^{13}C6]-phenylalanine) incorporation into proteins. However, radioactive isotopes are difficult to use in animals and are too hazardous for routine human use. Stable isotopes studies require a calculation of fractional protein synthesis that need to be performed in a controlled environment [33]. An alternative tracer is deuterated water ($^{2}H_2O$), which has been successfully used to measure protein synthesis rates in mice, rats, fish and humans. After $^{2}H_2O$ intake, ^{2}H atoms equilibrate within the body H atoms in body water and become incorporated into the C-H bonds of nonessential amino acids. Protein synthesis rates can therefore be measured by protein isolation, degradation and quantification of ^{2}H incorporation into nonessential amino acids, most often alanine, by mass spectrometry (MS). $^{2}H_2O$ can easily be incorporated into the drinking water (402). However, time and the current Home Office licence did not allow the performance of these experiments.

6.5 Conclusions

In conclusion, this chapter evaluated the role of miR-542 *in vivo* identifying miR-542 as a contributing cause for muscle wasting. We suggest that miR-542 promotes a reduction in fibre size leading to a loss of muscle mass. The mechanisms contributing to this wasting *(Figure 58)* are cytoplasmic ribosomal stress (leading to increased *Gdf-15* expression and presumably suppressing protein synthesis), mitochondrial ribosomal stress (leading to mitochondrial dysfunction) and increased TGF-β signalling (leading to activation of the atrophy pathways*).*

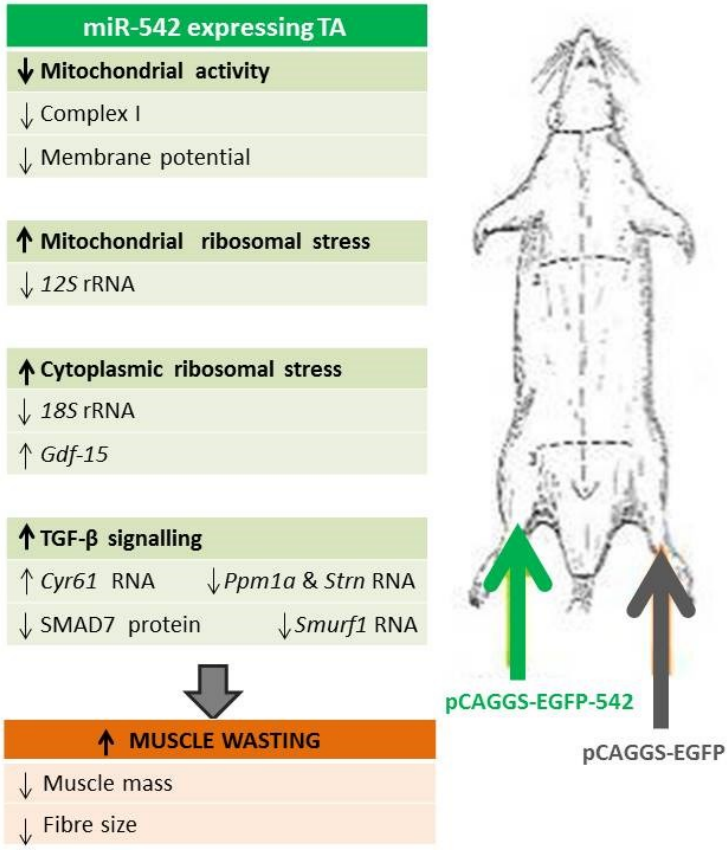


Figure 58- Schematic representation of miR-542 effects *in vivo*.

miR-542 expressing TA had decrease mitochondrial activity shown by complex I activity and JC-1 assay, increased mitochondrial and cytoplasmic ribosomal stress shown by down-regulation of *12S* and *18S* rRNA and up-regulation of *Gdf-15* compared to control TA. miR-542 electroporation causes the down-regulation of inhibitors of the TGF-β pathway (*Ppm1a*, *Strn* and *Smurf1* RNA and SMAD7 protein levels) compared to control TA. All the above mention effects lead to increase muscle wasting shown as a reduction in muscle mass and fibre size in miR-542 expressing leg compared to the counter-leg.

CHAPTER 7: Discussion and further work

7.1 Summary of obtained results

This thesis has examined two main mechanisms, protein synthesis and TGF-β signalling, by which miR-542-3p/-5p contribute to muscle wasting in the context of chronic disease (COPD), acute disease (ICUAW) and normal muscle loss due to ageing. The work in Chapter 3 showed that miR-542-3p/-5p were over expressed in different cohorts of patients suffering from diseases associated with muscle wasting, such as patients with COPD, in ICUAW and older individuals with sarcopenia, compared to age-matched controls and associated with poor exercise performance and poor lung capacity suggesting that these microRNAs could contribute to muscle dysfunction. Results from the bioinformatic analysis suggested several mechanisms by which miR-542 could affect muscle homeostasis. In the fourth chapter, a novel mechanism by which miR-542-3p/-5p could impair protein synthesis was studied. This data showed that these microRNAs decreased mitochondrial ribosomal protein synthesis leading to mitochondrial ribosomal stress and mitochondrial dysfunction *in vitro*. miR-542-3p/-5p also seem to impair cytoplasmic ribosomal biogenesis leading to ribosomal stress seen as decreased rRNA levels. Similar observations were seen *in vivo* shown by decreased mitochondrial complex I activity and membrane potential and in patients as demonstrated by decreased mitochondrial and cytoplasmic ribosomal rRNA (in particular the 12S rRNA). Therefore, there is the possibility that ribosomal stress could be occurring in patients with myopathies contributing to muscle wasting by impairing protein formation needed for muscle growth.

In Chapter 5, a novel role for miR-542-3p/-5p in TGF-β signalling was determined. The TGF-β pathway has previously been reported to be activated in a range of conditions where muscle loss occurs. The *in vitro* studies presented here, showing targeting of these miRs to inhibitors of the TGF-β system, together with the data from the patient samples, showing increased p-SMAD2/3 nuclear localisation and CYR61 mRNA levels and decreased SMAD7 levels in patients compared to controls, suggests that these microRNAs could be contributing to this signalling increase and ultimately contributing

to muscle wasting. Finally, in Chapter 6, the contribution of miR-542-3p/-5p to muscle wasting was analysed *in vivo* by injection of a pCAGGS-EGFP or pCAGGS-EGFP-542 in mouse TA followed by electroporation. Striking results were obtained showing consistency with previous chapters, and showing both mitochondrial ribosomal stress and decreased mRNA levels of TGF-β signalling inhibitors in miR-542 expressing muscles. Moreover, decreased fibre diameter and muscle mass loss 3 days after miR-542-3p/-5p electroporation were seen. Together these results highlight the potential of further study of miR-542-3p/-5p as a possible target to prevent muscle wasting.

7.2 Muscle mass and function regulation: genetics and epigenetics matter

Skeletal muscle is continually turning over with muscle protein being regularly made and removed by the basic muscle growth mechanisms including protein synthesis, mitochondriogenesis and satellite cell recruitment and breakdown mechanisms such as proteolysis, autophagy and apoptosis. There is also a rate of mitochondrial turnover continuously occurring in the muscle. Under normal conditions in healthy adults these processes are in balance but dysregulation of these systems in disease or with increased age can cause muscle wasting.

In patients with diseases such as COPD and ICUAW where muscle wasting occurs several environmental conditions could be contributing to the balance between protein synthesis and degradation such as reduced activity, intermittent hypoxia, oxidative stress or inflammation which have already been shown to provoke a muscle stress response. As we have observed that miR-542-3p/-5p is elevated on these patients compared to appropriate controls and shown that increased miR-542 causes muscle wasting *in vivo,* we compared miR-542 levels to the environmental factors mentioned above to try to identify if any of these conditions was triggering the rise in these miRs levels. However, within the COPD dataset there was no association of miR-542-3p/-5p with plasma levels of inflammatory cytokines suggesting that systemic inflammatory load at least does not cause the increase in miR-542-3p/5p (data not shown). Hypoxia has been shown to increase the expression of miR-424 (403) another

microRNA from this cluster, which is consistent with a role for hypoxia in the expression of miR-542 in the conditions studied here. This suggestion is also supported by the association of miR-542-3p/-5p with pO2 in the COPD patients and a previous study showing that miR-542-3p is elevated by hypoxia (404).

The fact that increased miR-542 expression in mice reduced muscle mass but does not associate with FFMI in the COPD cohort (data not shown) could be seen as a contradiction but there are a number of possible explanation for these observations. Firstly, as the promoter used to drive miR-542 expression in mice is very strong, the increase in miR-542 following electroporation may be much larger than the changes observed in patients. However, the increase measured was not proportionately larger than we observed in patients with ICUAW. Secondly, previous studies have shown that miR-542-3p targets survivin (290), a reduction of which would promote senescence of transfected satellite cells and proliferating myoblasts cells, thereby reducing regeneration and leading to the loss of muscle in response to electroporation. However, if this was the predominant mechanism of muscle loss in the mice the size of the untransfected fibres in the miR-542 expressing leg would be expected to be similar to that of the transfected fibres. The other explanation is that the elevation of miR-542-3p/-5p in COPD patients is a response to chronic stimuli rather than a transient response. There is therefore a significant time for the muscle to adapt, for regeneration to inhibit significant muscle loss and this response may vary between individuals complicating the association of the microRNA with muscle mass. Apart from environmental conditions, genetics and epigenetics factors also contribute to muscle homeostasis. From these factors, one of the most important appears to be the ability to regenerate muscle under stress conditions. As mentioned in Chapter 3, in COPD patients it was found that muscle mass was associated with microRNAs that regulate regeneration (271) suggesting that muscle wasting depends on the regeneration rate of each patient. An alternative confounding factor would be differences in the sensitivity of individuals to the effects of miR-542.

Evidence for such variation in regeneration and the response to signalling come from other studies into the role of microRNAs in muscle wasting performed within the group. For example, the associations of miR-675 expression with FFMI in COPD would

be consistent with a difference in regenerative capacity that contributes to wasting under disease conditions. MiR-675 is known to inhibit cell proliferation and to promote myoblast differentiation (405). Consequently, in patients with intrinsically higher miR-675 expression the balance of satellite cell activation, myoblast proliferation and differentiation may be biased towards a greater commitment to differentiation either reducing any proliferative phase of the regenerative response or reducing the satellite cell pool. Expression of the microRNAs from the C19MC cluster is lower in patients with a low FFMI and these microRNAs seem to be associated with maintenance of the pluripotent phenotype of stem cells (406). This observation is consistent with the idea of differences in the balance of proliferation and differentiation in satellite cells but their role and levels of expression remain unstudied in satellite cells. That neither miR-675 nor miRs from the C19MC are associated with FFMI in normal healthy individuals suggests that there needs to be some stress for their association with FFMI to be important.

Evidence for differential sensitivity to the effects of miR-542 comes from the association of miR-422a with muscle strength in the COPD cohort. This microRNA inhibits the production of SMAD4 as well as of MLH1. The reduction of SMAD4 would lead to reduced activity of SMAD2/3 so reduces the effects of increased miR-542 on TGF-β/MSTN signalling. The reduction in MLH1 would also limit the effects of miR-542 through its effects as a p53 co-activator as the ribosome stress induced by miR-542 promotes p53 activity.

The results described in this thesis have identified that under the studied stress conditions (COPD, ICUAW and sarcopenia) miR-542 levels are elevated and appear to increase the atrophic signalling in muscle. As shown in Chapter 4, miR-542 causes cytoplasmic and mitochondrial ribosomal stress which it is known increases p53 activation. Ribosomal stress could lead to a reduction in muscle mass by impairing protein synthesis which may reduce regeneration rates and could lead to increased protein breakdown to supply needed amino acids to the body or increased autophagy as described by *Artero Castro et al.* (407). As autophagy appears to occur as a result of ribosomal stress, this could drive us to think that maybe also mitophagy occurs. Following this hypothesis, miR-542 could indirectly affect mitochondrial content as a

combined result of protein synthesis impairment and increased mitophagy but further studies are needed to confirm this suggestion. However, miR-542 can also directly affect mitochondria in terms of activity as it targets mitochondrial ribosomal proteins essential for the synthesis of mitochondrial encoded proteins. A lack of translation of those proteins can result in mitochondrial dysfunction and a potential decrease of ATP synthesis in muscle. In turn, decreased ATP production can lead to a reduction of protein synthesis which is a process that requires energy. Therefore, there is a direct effect between reduced protein synthesis and reduced mitochondrial activity and vice versa.

7.3 Ribosomal stress as a contributor to muscle wasting

Reduced mitochondrial number and mitochondrial dysfunction have been previously demonstrated in the quadriceps of patients with COPD (303) and ICUAW (295), and are thought to be important contributors to the muscle dysfunction in these patients. The mitochondrial dysfunction also increases the production of reactive oxygen species in the muscle thereby promoting oxidative damage. Mitochondrial loss and/or dysfunction also occur in skeletal muscle in heart failure (76,408) and in ageing (304) suggesting that maintenance of mitochondrial function is an important part of muscle homeostasis. Indeed, the mitochondrial theory of ageing hypothesises that mitochondrial dysfunction is key to the ageing process (409). In ageing, there is a preferential loss of activity of electron transfer complexes that contain mitochondrially encoded proteins compared to the activity of complex II which is encoded solely by nuclear genes (410). As the synthesis of complexes I, III and IV requires the co-ordinated production of both mitochondrially translated and cytoplasmically translated proteins, mitochondrial ribosomal stress (as demonstrated by the reduction in 12S rRNA and MRPS10) would inhibit normal electron transfer complex formation. Consistent with this suggestion miR-542-3p /-5p reduced mitochondrially encoded CYTB5 protein (a component of Complex III) in cells and Complex I activity in the muscle of mice. miR-542 also reduced mitochondrial membrane potential *in vitro* and *in vivo* suggesting reduced mitochondrial efficiency. It therefore seems likely that the

increase in this microRNA contributes to the mitochondrial dysfunction seen in COPD and in ICUAW patients as well as in ageing. Moreover, in ICUAW patients who had the biggest increase in miR-542-3p/-5p expression, we observed the largest decrease in the 12S:16S ratio even though there was also a decrease observed in samples from COPD patients. Our data therefore indicate that mitochondrial ribosome stress is a contributory factor to muscle dysfunction in these diseases.

The data also show that miR-542-3p/-5p can promote cytoplasmic and mitochondrial ribosome stress and increase the expression of GDF-15 in muscle cells. Cytoplasmic ribosome stress suggests that there is a reduction in the total number of functional ribosomes and therefore a limit on maximal protein synthetic capacity. This observation is consistent with the anabolic resistance seen in sarcopenia. Furthermore, this response may contribute to the marked loss of muscle mass we observed in muscles over-expressing miR-542 *in vivo*.

7.4 TGF-β pathway contributing to atrophy

Changes in the expression of microRNAs that regulate the activity of the TGF-β signalling system is a common theme in the wasting associated with COPD and ICUAW. For example, in both LFFMI COPD patients and ICUAW patients we have found a suppression of miR-1 and miR-499 (30,250). These microRNAs inhibit the production and bioavailability of MSTN (251,411,412) as well as being predicted to inhibit the expression of components of the signalling pathway. Therefore, a suppression of their expression will increase TGF-β activity by removing a level of inhibition. Similarly, the increase in miR-542-3p/-5p described in Chapter 5 will also remove a level of inhibition of the TGF-β signalling pathway. Consistent with our observation that miR-542 reduces the expression of SMAD7, recent data has shown that other microRNAs expressed from the miR-424-503 polycistron also inhibit the production of SMAD7 and promote TGF-β signalling (413). As these microRNAs were also increased in the COPD trial cohort they are likely to contribute to an increase in pSMAD2/3 signalling in these patients. Furthermore, as these microRNAs are also regulated by TGF-β signalling it is possible that they form part of a positive feedback loop (414). Consequently, there is

likely to be a marked sensitization of the muscle of COPD and ICUAW patients to TGF-β signalling. Whether the same changes in sensitivity to TGF-β are seen in normal healthy ageing remains to be established, but the association of miR-542-3p/-5p with physical performance in the HSS cohort provides at least some support for the suggestion.

7.5 General limitations

The study is primarily a cross sectional analysis demonstrating elevation of miR-542-3p/-5p in 3 different conditions associated with muscle wasting (COPD, ICUAW and sarcopenia) and the association of these microRNAs with disease severity and skeletal muscle dysfunction. Therefore, we cannot demonstrate that elevation of the microRNA increases mitochondrial/cytoplasmic ribosomal stress, increases TGF-β signalling or promotes the loss of muscle mass in humans. However, the consistency of the observations across several human diseases suggests that elevation of this microRNA is a common component of muscle dysfunction. Furthermore, the over-expression of this microRNA in cells and in mice caused a reduction in mitochondrial function and muscle mass suggesting that this microRNA can promote wasting at least in animal models. Furthermore, by demonstrating increased SMAD signalling in response to the microRNA and the appropriate effects of these microRNAs on target proteins *in vivo* and *in vitro*, we provide biological plausibility for our observations. Moreover, we demonstrate that there is increased expression of a TGF-β responsive gene (*CYR61*) in ICUAW and COPD patients consistent with an increase in the activity of the signalling pathway as well as showing reduced expression of SMAD7 in ICUAW patients.

7.6 Clinical implications and future work

The results derived from this thesis identify miR-542-3p/-5p as potential therapeutic targets in patients with COPD, ICUAW or ageing healthy people to control muscle wasting. The therapy could consist on a sponge of antagomiRs for miR-542-3p/-5p and maybe also other microRNAs from the same cluster which may target similar pathways or it could be based on suppressing the mechanisms driving the expression of these microRNAs. However, *in vitro* studies should be made transfecting myoblasts with a microRNA sponge which contains the complementary binding sites to microRNA seed region allowing the blockage of the whole family of microRNAs (415) to determine whether they could reverse the effects of miR-542-3p/-5p. Injection of antagomir-542-3p/-5p to a muscle wasting animal model could be used to assess and quantify the ability of these antagomiRs to reverse muscle wasting, measuring fibre diameter and overall muscle weight. rRNA expression and complex I activity could be also measured to assess ribosomal stress and RNA levels and protein expression of inhibitors of TGF-β signalling could be compared between antagomiR treatment, miR treatment and untreated groups. On the other hand, to induce the suppression of microRNA expression, several studies need to be performed to identify the appropriate gene promoter and determine how it gets activated. Moreover, data in the group has shown that the propensity of muscle wasting could be detected by their miR-542 levels. For example, miR-542 levels in patients prior to aortic surgery were higher in patients who lost more than 10% of their *rectus femoris* cross sectional area (RF_{CSA}) in the 7 days following surgery than inthose who lost less than 10% RF_{CSA} (162) suggesting that a therapy could be given to potential wasters prior to major surgery. Moreover, miR-542 levels could be measured in pre-operative individuals and used to stratify patients between high or low risk of muscle atrophy so that high risk patients could receive different diets (high in amino acids) and more intense rehabilitation. The fact that the clinical implications could potentially benefit both acute and chronic wasting is not an isolated case as many pathways such as IGF-1 or GDF-15 have been described to play a role in both (196,197,256). Moreover, in both cases reduced protein synthesis suppression and mitochondrial dysfunction have been reported.

7.7 Conclusions

Expression of miR-542-3p/-5p is increased in patients with COPD and with ICUAW as well as in older individuals who have smoked or suffered from asthma or suffer from sarcopenia. In both COPD patients and in older individuals miR-542-3p/-5p expression is associated with physical performance. We propose that this increase in miR-542-3p/-5p leads to mitochondrial ribosomal stress, which impairs oxidative capacity, and suppresses inhibitors of TGF-β signalling such as SMAD7, SMURF1 and PPP2CA expression leading to increased basal SMAD2/3 dependent signalling. Consequently, miR-542-3p/-5p promotes muscle mass loss and muscle dysfunction in response to the physiological stress of disease.

References

(1) Bentzinger CF, Wang YX, Rudnicki MA. Building muscle: molecular regulation of myogenesis. *Cold Spring Harbor perspectives in biology.* 2012;4(2): 10.1101/cshperspect.a008342.

(2) Bonaldo P, Sandri M. Cellular and molecular mechanisms of muscle atrophy. *Disease models & mechanisms.* 2013;6(1): 25-39.

(3) Katz LD, Glickman MG, Rapoport S, Ferrannini E, DeFronzo RA. Splanchnic and peripheral disposal of oral glucose in man. *Diabetes.* 1983;32(7): 675-679.

(4) Larsen WJ. Human embryology. In: Sherman LS, Potter S Steven. (eds.) *Human embryology.* 3rd ed. New York: Churchill Livingstone; 2001. pp. 86.

(5) Kalcheim C, Cinnamon Y, Kahane N. Myotome formation: a multistage process. *Cell and tissue research.* 1999;296(1): 161-173.

(6) O'Rahilly RR, Müller F. Human Embryology and Teratology. *Human Embryology and Teratology.* 3rd ed. Wiley-Lyss; 2001. pp. 360.

(7) Gilbert SF. Myogenesis: The Development of Muscle. . *Developmental Biology .* 6th ed. Sunderland (MA): Sinauer Associates; 2000.

(8) Konigsberg IR. Clonal analysis of myogenesis. *Science (New York, N.Y.).* 1963;140(3573): 1273-1284.

(9) Freyssenet D. Energy sensing and regulation of gene expression in skeletal muscle. *Journal of applied physiology (Bethesda, Md.: 1985).* 2007;102(2): 529-540.

(10) Hawke TJ, Garry DJ. Myogenic satellite cells: physiology to molecular biology. *Journal of applied physiology (Bethesda, Md.: 1985).* 2001;91(2): 534-551.

(11) Mootoosamy RC, Dietrich S. Distinct regulatory cascades for head and trunk myogenesis. *Development (Cambridge, England).* 2002;129(3): 573-583.

(12) MacIntosh BR, Gardiner PF, McComas AJ. *Skeletal muscle: form and function.* : Human Kinetics; 2006.

(13) Netter FH. Muscles and nerves. *Atlas of human anatomy.* Philadelphia, PA : Saunders/Elsevier; 2011. pp. 168.

(14) Schiaffino S, Reggiani C. Fiber types in mammalian skeletal muscles. *Physiological Reviews.* 2011;91(4): 1447-1531.

(15) Gouspillou G, Sgarioto N, Norris B, Barbat-Artigas S, Aubertin-Leheudre M, Morais JA, et al. The relationship between muscle fiber type-specific PGC-1alpha content and

mitochondrial content varies between rodent models and humans. *PloS one.* 2014;9(8): e103044.

(16) Tirrell T, Cook M, Carr J, Lin E, Ward S, Lieber R. Human skeletal muscle biochemical diversity. *The Journal of Experimental Biology.* 2012(15): 2551.

(17) Soukup T, Zacharova G, Smerdu V. Fibre type composition of soleus and extensor digitorum longus muscles in normal female inbred Lewis rats. *Acta Histochemica.* 2002;104(4): 399-405.

(18) Polla B, D'Antona G, Bottinelli R, Reggiani C. Respiratory muscle fibres: specialisation and plasticity. *Thorax.* 2004;59(9): 808-817.

(19) MacDougall JD, Elder GC, Sale DG, Moroz JR, Sutton JR. Effects of strength training and immobilization on human muscle fibres. *European journal of applied physiology and occupational physiology.* 1980;43(1): 25-34.

(20) Wilson JM, Loenneke JP, Jo E, Wilson GJ, Zourdos MC, Kim JS. The effects of endurance, strength, and power training on muscle fiber type shifting. *Journal of strength and conditioning research.* 2012;26(6): 1724-1729.

(21) Buller AJ, Eccles JC, Eccles RM. Interactions between motoneurones and muscles in respect of the characteristic speeds of their responses. *The Journal of physiology.* 1960;150417-439.

(22) Hargreaves M, Cameron-Smith D. Exercise, diet, and skeletal muscle gene expression. *Medicine and science in sports and exercise.* 2002;34(9): 1505-1508.

(23) Fujita S, Dreyer HC, Drummond MJ, Glynn EL, Cadenas JG, Yoshizawa F, et al. Nutrient signalling in the regulation of human muscle protein synthesis. *The Journal of physiology.* 2007;582(Pt 2): 813-823.

(24) Schiaffino S, Dyar KA, Ciciliot S, Blaauw B, Sandri M. Mechanisms regulating skeletal muscle growth and atrophy. *The FEBS journal.* 2013;280(17): 4294-4314.

(25) Gomes MD, Lecker SH, Jagoe RT, Navon A, Goldberg AL. Atrogin-1, a muscle-specific F-box protein highly expressed during muscle atrophy. *Proceedings of the National Academy of Sciences of the United States of America.* 2001;98(25): 14440-14445.

(26) Eddins MJ, Marblestone JG, Suresh Kumar KG, Leach CA, Sterner DE, Mattern MR, et al. Targeting the ubiquitin E3 ligase MuRF1 to inhibit muscle atrophy. *Cell biochemistry and biophysics.* 2011;60(1-2): 113-118.

(27) Sandri M, Sandri C, Gilbert A, Skurk C, Calabria E, Picard A, et al. Foxo transcription factors induce the atrophy-related ubiquitin ligase atrogin-1 and cause skeletal muscle atrophy. *Cell.* 2004;117(3): 399-412.

(28) Stitt TN, Drujan D, Clarke BA, Panaro F, Timofeyva Y, Kline WO, et al. The IGF-1/PI3K/Akt pathway prevents expression of muscle atrophy-induced ubiquitin ligases by inhibiting FOXO transcription factors. *Molecular cell.* 2004;14(3): 395-403.

(29) Doucet M, Russell AP, Leger B, Debigare R, Joanisse DR, Caron MA, et al. Muscle atrophy and hypertrophy signaling in patients with chronic obstructive pulmonary disease. *American journal of respiratory and critical care medicine.* 2007;176(3): 261-269.

(30) Bloch SA, Lee JY, Syburra T, Rosendahl U, Griffiths MJ, Kemp PR, et al. Increased expression of GDF-15 may mediate ICU-acquired weakness by down-regulating muscle microRNAs. *Thorax.* 2015;70(3): 219-228.

(31) Carvalho RF, Castan EP, Coelho CA, Lopes FS, Almeida FL, Michelin A, et al. Heart failure increases atrogin-1 and MuRF1 gene expression in skeletal muscle with fiber type-specific atrophy. *Journal of molecular histology.* 2010;41(1): 81-87.

(32) Ochala J, Gustafson AM, Diez ML, Renaud G, Li M, Aare S, et al. Preferential skeletal muscle myosin loss in response to mechanical silencing in a novel rat intensive care unit model: underlying mechanisms. *The Journal of physiology.* 2011;589(Pt 8): 2007-2026.

(33) Bloch S, Polkey MI, Griffiths M, Kemp P. Molecular mechanisms of intensive care unit-acquired weakness. *The European respiratory journal.* 2012;39(4): 1000-1011.

(34) Natanek SA, Riddoch-Contreras J, Marsh GS, Hopkinson NS, Moxham J, Man WD, et al. MuRF-1 and atrogin-1 protein expression and quadriceps fiber size and muscle mass in stable patients with COPD. *Copd.* 2013;10(5): 618-624.

(35) Li P, Waters RE, Redfern SI, Zhang M, Mao L, Annex BH, et al. Oxidative phenotype protects myofibers from pathological insults induced by chronic heart failure in mice. *The American journal of pathology.* 2007;170(2): 599-608.

(36) Lecker SH. Ubiquitin-protein ligases in muscle wasting: multiple parallel pathways? *Current opinion in clinical nutrition and metabolic care.* 2003;6(3): 271-275.

(37) Bodine SC, Latres E, Baumhueter S, Lai VK, Nunez L, Clarke BA, et al. Identification of ubiquitin ligases required for skeletal muscle atrophy. *Science (New York, N.Y.).* 2001;294(5547): 1704-1708.

(38) Scheffner M, Nuber U, Huibregtse JM. Protein ubiquitination involving an E1-E2-E3 enzyme ubiquitin thioester cascade. *Nature.* 1995;373(6509): 81-83.

(39) Stewart MD, Ritterhoff T, Klevit RE, Brzovic PS. E2 enzymes: more than just middle men. *Cell research.* 2016;26(4): 423-440.

(40) Fang S, Weissman A,M. Ubiquitin-proteasome system. 2004;61(13): 1546–1561.

(41) Hishiya A, Iemura S, Natsume T, Takayama S, Ikeda K, Watanabe K. A novel ubiquitin-binding protein ZNF216 functioning in muscle atrophy. *The EMBO journal.* 2006;25(3): 554-564.

(42) Reyes-Turcu FE, Ventii KH, Wilkinson KD. Regulation and cellular roles of ubiquitin-specific deubiquitinating enzymes. *Annual Review of Biochemistry.* 2009;78363-397.

(43) Witt SH, Granzier H, Witt CC, Labeit S. MURF-1 and MURF-2 target a specific subset of myofibrillar proteins redundantly: towards understanding MURF-dependent muscle ubiquitination. *Journal of Molecular Biology.* 2005;350(4): 713-722.

(44) Clarke BA, Drujan D, Willis MS, Murphy LO, Corpina RA, Burova E, et al. The E3 Ligase MuRF1 degrades myosin heavy chain protein in dexamethasone-treated skeletal muscle. *Cell metabolism.* 2007;6(5): 376-385.

(45) Lokireddy S, Wijesoma IW, Sze SK, McFarlane C, Kambadur R, Sharma M. Identification of atrogin-1-targeted proteins during the myostatin-induced skeletal muscle wasting. *American journal of physiology.Cell physiology.* 2012;303(5): C512-29.

(46) Lagirand-Cantaloube J, Cornille K, Csibi A, Batonnet-Pichon S, Leibovitch MP, Leibovitch SA. Inhibition of atrogin-1/MAFbx mediated MyoD proteolysis prevents skeletal muscle atrophy in vivo. *PloS one.* 2009;4(3): e4973.

(47) Lassar AB, Buskin JN, Lockshon D, Davis RL, Apone S, Hauschka SD, et al. MyoD is a sequence-specific DNA binding protein requiring a region of myc homology to bind to the muscle creatine kinase enhancer. *Cell.* 1989;58(5): 823-831.

(48) Weintraub H, Davis R, Tapscott S, Thayer M, Krause M, Benezra R, et al. The myoD gene family: nodal point during specification of the muscle cell lineage. *Science (New York, N.Y.).* 1991;251(4995): 761-766.

(49) Sandri M, Sandri C, Gilbert A, Skurk C, Calabria E, Picard A, et al. Foxo transcription factors induce the atrophy-related ubiquitin ligase atrogin-1 and cause skeletal muscle atrophy. *Cell.* 2004;117(3): 399-412.

(50) Cai D, Frantz JD, Tawa Jr NE, Melendez PA, Oh B, Lidov HG, et al. IKKβ/NF-κB activation causes severe muscle wasting in mice. *Cell.* 2004;119(2): 285-298.

(51) Paul PK, Gupta SK, Bhatnagar S, Panguluri SK, Darnay BG, Choi Y, et al. Targeted ablation of TRAF6 inhibits skeletal muscle wasting in mice. *The Journal of cell biology.* 2010;191(7): 1395-1411.

(52) Paul PK, Bhatnagar S, Mishra V, Srivastava S, Darnay BG, Choi Y, et al. The E3 ubiquitin ligase TRAF6 intercedes in starvation-induced skeletal muscle atrophy through multiple mechanisms. *Molecular and cellular biology.* 2012;32(7): 1248-1259.

(53) Kumar A, Bhatnagar S, Paul PK. TWEAK and TRAF6 regulate skeletal muscle atrophy. *Current opinion in clinical nutrition and metabolic care.* 2012;15(3): 233-239.

(54) Attaix D, Ventadour S, Codran A, Béchet D, Taillandier D, Combaret L. The ubiquitin–proteasome system and skeletal muscle wasting. *Essays in biochemistry.* 2005;41173-186.

(55) Bailey JL, Wang X, England BK, Price SR, Ding X, Mitch WE. The acidosis of chronic renal failure activates muscle proteolysis in rats by augmenting transcription of genes encoding proteins of the ATP-dependent ubiquitin-proteasome pathway. *The Journal of clinical investigation.* 1996;97(6): 1447-1453.

(56) Price SR, Bailey JL, Wang X, Jurkovitz C, England BK, Ding X, et al. Muscle wasting in insulinopenic rats results from activation of the ATP-dependent, ubiquitin-proteasome proteolytic pathway by a mechanism including gene transcription. *The Journal of clinical investigation.* 1996;98(8): 1703-1708.

(57) Valimberti I, Tiberti M, Lambrughi M, Sarcevic B, Papaleo E. E2 superfamily of ubiquitin-conjugating enzymes: constitutively active or activated through phosphorylation in the catalytic cleft. *Scientific reports.* 2015;514849.

(58) Jones SW, Hill RJ, Krasney PA, O'Conner B, Peirce N, Greenhaff PL. Disuse atrophy and exercise rehabilitation in humans profoundly affects the expression of genes associated with the regulation of skeletal muscle mass. *FASEB journal : official publication of the Federation of American Societies for Experimental Biology.* 2004;18(9): 1025-1027.

(59) de Boer MD, Selby A, Atherton P, Smith K, Seynnes OR, Maganaris CN, et al. The temporal responses of protein synthesis, gene expression and cell signalling in human quadriceps muscle and patellar tendon to disuse. *The Journal of physiology.* 2007;585(Pt 1): 241-251.

(60) Helliwell TR, Wilkinson A, Griffiths RD, McClelland P, Palmer TE, Bone JM. Muscle fibre atrophy in critically ill patients is associated with the loss of myosin filaments and the presence of lysosomal enzymes and ubiquitin. *Neuropathology and applied neurobiology.* 1998;24(6): 507-517.

(61) Polge C, Attaix D, Taillandier D. Role of E2-Ub-conjugating enzymes during skeletal muscle atrophy. *Frontiers in physiology.* 2015;659.

(62) Mizushima N, Levine B, Cuervo AM, Klionsky DJ. Autophagy fights disease through cellular self-digestion. *Nature.* 2008;451(7182): 1069-1075.

(63) Feng Y, He D, Yao Z, Klionsky DJ. The machinery of macroautophagy. *Cell research.* 2014;24(1): 24-41.

(64) Russell RC, Tian Y, Yuan H, Park HW, Chang YY, Kim J, et al. ULK1 induces autophagy by phosphorylating Beclin-1 and activating VPS34 lipid kinase. *Nature cell biology.* 2013;15(7): 741-750.

(65) Kihara A, Noda T, Ishihara N, Ohsumi Y. Two distinct Vps34 phosphatidylinositol 3-kinase complexes function in autophagy and carboxypeptidase Y sorting in Saccharomyces cerevisiae. *The Journal of cell biology.* 2001;152(3): 519-530.

(66) Itakura E, Kishi C, Inoue K, Mizushima N. Beclin 1 forms two distinct phosphatidylinositol 3-kinase complexes with mammalian Atg14 and UVRAG. *Molecular biology of the cell.* 2008;19(12): 5360-5372.

(67) Heenan EJ, Vanhooke JL, Temple BR, Betts L, Sondek JE, Dohlman HG. Structure and function of Vps15 in the endosomal G protein signaling pathway. *Biochemistry.* 2009;48(27): 6390-6401.

(68) Di Bartolomeo S, Corazzari M, Nazio F, Oliverio S, Lisi G, Antonioli M, et al. The dynamic interaction of AMBRA1 with the dynein motor complex regulates mammalian autophagy. *The Journal of cell biology.* 2010;191(1): 155-168.

(69) Obara K, Sekito T, Ohsumi Y. Assortment of phosphatidylinositol 3-kinase complexes--Atg14p directs association of complex I to the pre-autophagosomal structure in Saccharomyces cerevisiae. *Molecular biology of the cell.* 2006;17(4): 1527-1539.

(70) Narendra DP, Youle RJ. Targeting mitochondrial dysfunction: role for PINK1 and Parkin in mitochondrial quality control. *Antioxidants & redox signaling.* 2011;14(10): 1929-1938.

(71) Youle RJ, Narendra DP. Mechanisms of mitophagy. *Nature reviews Molecular cell biology.* 2010;12(1): 9-14.

(72) Hanna RA, Quinsay MN, Orogo AM, Giang K, Rikka S, Gustafsson AB. Microtubule-associated protein 1 light chain 3 (LC3) interacts with Bnip3 protein to selectively remove endoplasmic reticulum and mitochondria via autophagy. *The Journal of biological chemistry.* 2012;287(23): 19094-19104.

(73) Novak I, Kirkin V, McEwan DG, Zhang J, Wild P, Rozenknop A, et al. Nix is a selective autophagy receptor for mitochondrial clearance. *EMBO reports.* 2010;11(1): 45-51.

(74) Sandri M, Lin J, Handschin C, Yang W, Arany ZP, Lecker SH, et al. PGC-1alpha protects skeletal muscle from atrophy by suppressing FoxO3 action and atrophy-specific gene transcription. *Proceedings of the National Academy of Sciences of the United States of America.* 2006;103(44): 16260-16265.

(75) Puente-Maestu L, Lazaro A, Humanes B. Metabolic derangements in COPD muscle dysfunction. *Journal of applied physiology (Bethesda, Md.: 1985).* 2013;114(9): 1282-1290.

(76) Rosca MG, Hoppel CL. Mitochondrial dysfunction in heart failure. *Heart failure reviews.* 2013;18(5): 607-622.

(77) Peterson CM, Johannsen DL, Ravussin E. Skeletal muscle mitochondria and aging: a review. *Journal of aging research.* 2012;2012194821.

(78) Raben N, Hill V, Shea L, Takikita S, Baum R, Mizushima N, et al. Suppression of autophagy in skeletal muscle uncovers the accumulation of ubiquitinated proteins and their potential role in muscle damage in Pompe disease. *Human molecular genetics.* 2008;17(24): 3897-3908.

(79) Kon M, Cuervo AM. Chaperone-mediated autophagy in health and disease. *FEBS letters.* 2010;584(7): 1399-1404.

(80) Adams V, Jiang H, Yu J, Mobius-Winkler S, Fiehn E, Linke A, et al. Apoptosis in skeletal myocytes of patients with chronic heart failure is associated with exercise intolerance. *Journal of the American College of Cardiology.* 1999;33(4): 959-965.

(81) Borisov AB, Carlson BM. Cell death in denervated skeletal muscle is distinct from classical apoptosis. *The Anatomical Record.* 2000;258(3): 305-318.

(82) Smith HK, Maxwell L, Martyn JA, Bass JJ. Nuclear DNA fragmentation and morphological alterations in adult rabbit skeletal muscle after short-term immobilization. *Cell and tissue research.* 2000;302(2): 235-241.

(83) Primeau AJ, Adhihetty PJ, Hood DA. Apoptosis in heart and skeletal muscle. *Canadian journal of applied physiology = Revue canadienne de physiologie appliquee.* 2002;27(4): 349-395.

(84) Dupont-Versteegden EE. Apoptosis in skeletal muscle and its relevance to atrophy. *World journal of gastroenterology.* 2006;12(46): 7463-7466.

(85) Earnshaw WC, Martins LM, Kaufmann SH. Mammalian caspases: structure, activation, substrates, and functions during apoptosis. *Annual Review of Biochemistry.* 1999;68383-424.

(86) Du J, Wang X, Miereles C, Bailey JL, Debigare R, Zheng B, et al. Activation of caspase-3 is an initial step triggering accelerated muscle proteolysis in catabolic conditions. *The Journal of clinical investigation.* 2004;113(1): 115-123.

(87) Wittmann HG. Structure of Ribosomes. In: Hardesty B, Kramer G. (eds.) *Structure, Function, and Genetics of Ribosomes.* 1st ed. New York: Springer; 1986. pp. 3.

(88) Green R, Noller HF. Ribosomes and translation. *Annual Review of Biochemistry.* 1997;66679-716.

(89) Amunts A, Brown A, Toots J, Scheres SHW, Ramakrishnan V. Ribosome. The structure of the human mitochondrial ribosome. *Science (New York, N.Y.).* 2015;348(6230): 95-98.

(90) Steitz TA. A structural understanding of the dynamic ribosome machine. *Nature reviews.Molecular cell biology.* 2008;9(3): 242-253.

(91) Clemens M,J. Targets and mechanisms for the regulation of translation in malignant transformation. *Oncogene.* 2004;233180.

(92) Taanman JW. The mitochondrial genome: structure, transcription, translation and replication. *Biochimica et biophysica acta.* 1999;1410(2): 103-123.

(93) Hinnebusch AG. Molecular mechanism of scanning and start codon selection in eukaryotes. *Microbiology and molecular biology reviews : MMBR.* 2011;75(3): 434-67, first page of table of contents.

(94) Nakamura Y, Ito K. How protein reads the stop codon and terminates translation. *Genes to cells : devoted to molecular & cellular mechanisms.* 1998;3(5): 265-278.

(95) Temperley R, Richter R, Dennerlein S, Lightowlers RN, Chrzanowska-Lightowlers ZM. Hungry codons promote frameshifting in human mitochondrial ribosomes. *Science (New York, N.Y.).* 2010;327(5963): 301.

(96) Chinnery PF, Hudson G. Mitochondrial genetics. *British medical bulletin.* 2013;106135-159.

(97) Sazanov LA. A giant molecular proton pump: structure and mechanism of respiratory complex I. *Nature reviews.Molecular cell biology.* 2015;16(6): 375-388.

(98) Atherton PJ, Smith K. Muscle protein synthesis in response to nutrition and exercise. *The Journal of physiology.* 2012;590(5): 1049-1057.

(99) Glass DJ. Signalling pathways that mediate skeletal muscle hypertrophy and atrophy. *Nature cell biology.* 2003;5(2): 87-90.

(100) Wu C, Hou S, Orr BA, Youn YH, Roth F, Eberhart CG, et al. mTORC1-mediated inhibition of 4EBP1 is essential for Hedgehog (HH) signaling and can be targeted to suppress HH-driven medulloblastoma. *bioRxiv.* 2017.

(101) Brunet A, Bonni A, Zigmond MJ, Lin MZ, Juo P, Hu LS, et al. Akt promotes cell survival by phosphorylating and inhibiting a Forkhead transcription factor. *Cell.* 1999;96(6): 857-868.

(102) Ramaswamy S, Nakamura N, Sansal I, Bergeron L, Sellers WR. A novel mechanism of gene regulation and tumor suppression by the transcription factor FKHR. *Cancer cell.* 2002;2(1): 81-91.

(103) Rommel C, Bodine SC, Clarke BA, Rossman R, Nunez L, Stitt TN, et al. Mediation of IGF-1-induced skeletal myotube hypertrophy by PI(3)K/Akt/mTOR and PI(3)K/Akt/GSK3 pathways. *Nature cell biology.* 2001;3(11): 1009-1013.

(104) Peng XD, Xu PZ, Chen ML, Hahn-Windgassen A, Skeen J, Jacobs J, et al. Dwarfism, impaired skin development, skeletal muscle atrophy, delayed bone development, and impeded adipogenesis in mice lacking Akt1 and Akt2. *Genes & development.* 2003;17(11): 1352-1365.

(105) Pallafacchina G, Calabria E, Serrano AL, Kalhovde JM, Schiaffino S. A protein kinase B-dependent and rapamycin-sensitive pathway controls skeletal muscle growth but not fiber type specification. *Proceedings of the National Academy of Sciences of the United States of America.* 2002;99(14): 9213-9218.

(106) Musaro A, McCullagh K, Paul A, Houghton L, Dobrowolny G, Molinaro M, et al. Localized Igf-1 transgene expression sustains hypertrophy and regeneration in senescent skeletal muscle. *Nature genetics.* 2001;27(2): 195-200.

(107) Peyssonnaux C, Provot S, Felder-Schmittbuhl MP, Calothy G, Eychene A. Induction of postmitotic neuroretina cell proliferation by distinct Ras downstream signaling pathways. *Molecular and cellular biology.* 2000;20(19): 7068-7079.

(108) McCubrey JA, Steelman LS, Chappell WH, Abrams SL, Wong EW, Chang F, et al. Roles of the Raf/MEK/ERK pathway in cell growth, malignant transformation and drug resistance. *Biochimica et biophysica acta.* 2007;1773(8): 1263-1284.

(109) Pende M, Um SH, Mieulet V, Sticker M, Goss VL, Mestan J, et al. S6K1(-/-)/S6K2(-/-) mice exhibit perinatal lethality and rapamycin-sensitive 5'-terminal oligopyrimidine mRNA translation and reveal a mitogen-activated protein kinase-dependent S6 kinase pathway. *Molecular and cellular biology.* 2004;24(8): 3112-3124.

(110) Cargnello M, Roux PP. Activation and function of the MAPKs and their substrates, the MAPK-activated protein kinases. *Microbiology and molecular biology reviews : MMBR.* 2011;75(1): 50-83.

(111) Silvera D, Formenti SC, Schneider RJ. Translational control in cancer. *Nature Reviews Cancer.* 2010;10254.

(112) Lempiainen H, Shore D. Growth control and ribosome biogenesis. *Current opinion in cell biology.* 2009;21(6): 855-863.

(113) Kressler D, Hurt E, Bassler J. Driving ribosome assembly. *Biochimica et biophysica acta.* 2010;1803(6): 673-683.

(114) Sengupta S, Peterson TR, Sabatini DM. Regulation of the mTOR complex 1 pathway by nutrients, growth factors, and stress. *Molecular cell.* 2010;40(2): 310-322.

(115) Haddad F, Baldwin KM, Tesch PA. Pretranslational markers of contractile protein expression in human skeletal muscle: effect of limb unloading plus resistance exercise. *Journal of applied physiology (Bethesda, Md.: 1985).* 2005;98(1): 46-52.

(116) Glover EI, Oates BR, Tang JE, Moore DR, Tarnopolsky MA, Phillips SM. Resistance exercise decreases eIF2Bepsilon phosphorylation and potentiates the feeding-induced stimulation of p70S6K1 and rpS6 in young men. *American journal of physiology.Regulatory, integrative and comparative physiology.* 2008;295(2): R604-10.

(117) Lecker SH, Jagoe RT, Gilbert A, Gomes M, Baracos V, Bailey J, et al. Multiple types of skeletal muscle atrophy involve a common program of changes in gene expression. *FASEB journal: official publication of the Federation of American Societies for Experimental Biology.* 2004;18(1): 39-51.

(118) Petersson B, Wernerman J, Waller SO, von der Decken A, Vinnars E. Elective abdominal surgery depresses muscle protein synthesis and increases subjective fatigue: effects lasting more than 30 days. *The British journal of surgery.* 1990;77(7): 796-800.

(119) Sundqvist A, Liu G, Mirsaliotis A, Xirodimas DP. Regulation of nucleolar signalling to p53 through NEDDylation of L11. *EMBO reports.* 2009;10(10): 1132-1139.

(120) Fumagalli S, Di Cara A, Neb-Gulati A, Natt F, Schwemberger S, Hall J, et al. Absence of nucleolar disruption after impairment of 40S ribosome biogenesis reveals an rpL11-translation-dependent mechanism of p53 induction. *Nature cell biology.* 2009;11(4): 501-508.

(121) Kirn-Safran CB, Oristian DS, Focht RJ, Parker SG, Vivian JL, Carson DD. Global growth deficiencies in mice lacking the ribosomal protein HIP/RPL29. *Developmental dynamics : an official publication of the American Association of Anatomists.* 2007;236(2): 447-460.

(122) Yablonka-Reuveni Z. The skeletal muscle satellite cell: still young and fascinating at 50. *The journal of histochemistry and cytochemistry : official journal of the Histochemistry Society.* 2011;59(12): 1041-1059.

(123) Theriault ME, Pare ME, Maltais F, Debigare R. Satellite cells senescence in limb muscle of severe patients with COPD. *PloS one.* 2012;7(6): e39124.

(124) Day K, Shefer G, Shearer A, Yablonka-Reuveni Z. The depletion of skeletal muscle satellite cells with age is concomitant with reduced capacity of single progenitors to produce reserve progeny. *Developmental biology.* 2010;340(2): 330-343.

(125) Sacco A, Puri P. *Regulation of Muscle Satellite Cell Function in Tissue Homeostasis and Aging.* 2015.

(126) Murach KA, White SH, Wen Y, Ho A, Dupont-Versteegden E, McCarthy JJ, et al. Differential requirement for satellite cells during overload-induced muscle hypertrophy in growing versus mature mice. *Skeletal Muscle.* 2017;7(1): 14.

(127) Kirby TJ, Patel RM, McClintock TS, Dupont-Versteegden E, Peterson CA, McCarthy JJ. Myonuclear transcription is responsive to mechanical load and DNA content but

uncoupled from cell size during hypertrophy. *Molecular biology of the cell.* 2016;27(5): 788-798.

(128) Man WD, Kemp P, Moxham J, Polkey MI. Skeletal muscle dysfunction in COPD: clinical and laboratory observations. *Clinical science (London, England : 1979).* 2009;117(7): 251-264.

(129) Cooper R, Kuh D, Hardy R, Mortality Review Group, FALCon and HALCyon Study Teams. Objectively measured physical capability levels and mortality: systematic review and meta-analysis. *BMJ (Clinical research ed.).* 2010;341c4467.

(130) Swallow EB, Reyes D, Hopkinson NS, Man WD, Porcher R, Cetti EJ, et al. Quadriceps strength predicts mortality in patients with moderate to severe chronic obstructive pulmonary disease. *Thorax.* 2007;62(2): 115-120.

(131) De Jonghe B, Sharshar T, Lefaucheur JP, Authier FJ, Durand-Zaleski I, Boussarsar M, et al. Paresis acquired in the intensive care unit: a prospective multicenter study. *Jama.* 2002;288(22): 2859-2867.

(132) World Health Organization (. *Chronic obstructive pulmonary disease (COPD) (Fact sheet November).* Available from: http://www.who.int/mediacentre/factsheets/fs315/en/.

(133) Vestbo J, Hurd SS, Agusti AG, Jones PW, Vogelmeier C, Anzueto A, et al. Global strategy for the diagnosis, management, and prevention of chronic obstructive pulmonary disease: GOLD executive summary. *American journal of respiratory and critical care medicine.* 2013;187(4): 347-365.

(134) Global Initiative for Chronic Obstructive Lung Disease, (COLD). *Pocket guide to COPD diagnosis, management and prevention. A guide for health care professionals.* Global Initiative for Chronic Obstructive Lung Disease, Inc. 2017.

(135) Mathur S, Brooks D, Carvalho CR. Structural alterations of skeletal muscle in copd. *Frontiers in physiology.* 2014;5104.

(136) Natanek SA, Gosker HR, Slot IG, Marsh GS, Hopkinson NS, Man WD, et al. Heterogeneity of quadriceps muscle phenotype in chronic obstructive pulmonary disease (Copd); implications for stratified medicine? *Muscle & nerve.* 2013;48(4): 488-497.

(137) Patel MS, Natanek SA, Stratakos G, Pascual S, Martinez-Llorens J, Disano L, et al. Vastus lateralis fiber shift is an independent predictor of mortality in chronic obstructive pulmonary disease. *American journal of respiratory and critical care medicine.* 2014;190(3): 350-352.

(138) Kim HC, Mofarrahi M, Hussain SN. Skeletal muscle dysfunction in patients with chronic obstructive pulmonary disease. *International journal of chronic obstructive pulmonary disease.* 2008;3(4): 637-658.

(139) Hermans G, Van Mechelen H, Clerckx B, Vanhullebusch T, Mesotten D, Wilmer A, et al. Acute outcomes and 1-year mortality of intensive care unit-acquired weakness. A cohort study and propensity-matched analysis. *American journal of respiratory and critical care medicine.* 2014;190(4): 410-420.

(140) Schweickert WD, Hall J. ICU-acquired weakness. *Chest.* 2007;131(5): 1541-1549.

(141) Lacomis D, Zochodne DW, Bird SJ. Critical illness myopathy. *Muscle & nerve.* 2000;23(12): 1785-1788.

(142) Sander HW, Golden M, Danon MJ. Quadriplegic areflexic ICU illness: selective thick filament loss and normal nerve histology. *Muscle & nerve.* 2002;26(4): 499-505.

(143) Friedrich O. Critical illness myopathy: sepsis-mediated failure of the peripheral nervous system. *European journal of anaesthesiology.Supplement.* 2008;4273-82.

(144) Khan J, Harrison TB, Rich MM. Mechanisms of neuromuscular dysfunction in critical illness. *Critical Care Clinics.* 2008;24(1): 165-77, x.

(145) Levine S, Nguyen T, Taylor N, Friscia ME, Budak MT, Rothenberg P, et al. Rapid disuse atrophy of diaphragm fibers in mechanically ventilated humans. *The New England journal of medicine.* 2008;358(13): 1327-1335.

(146) Diaz NL, Finol HJ, Torres SH, Zambrano CI, Adjounian H. Histochemical and ultrastructural study of skeletal muscle in patients with sepsis and multiple organ failure syndrome (MOFS). *Histology and histopathology.* 1998;13(1): 121-128.

(147) Patel HP, Syddall HE, Jameson K, Robinson S, Denison H, Roberts HC, et al. Prevalence of sarcopenia in community-dwelling older people in the UK using the European Working Group on Sarcopenia in Older People (EWGSOP) definition: findings from the Hertfordshire Cohort Study (HCS). *Age and Ageing.* 2013;42(3): 378-384.

(148) Narici MV, Maffulli N. Sarcopenia: characteristics, mechanisms and functional significance. *British medical bulletin.* 2010;95139-159.

(149) Chakravarthy MV, Davis BS, Booth FW. IGF-I restores satellite cell proliferative potential in immobilized old skeletal muscle. *Journal of applied physiology (Bethesda, Md.: 1985).* 2000;89(4): 1365-1379.

(150) Schaap LA, Pluijm SM, Deeg DJ, Visser M. Inflammatory markers and loss of muscle mass (sarcopenia) and strength. *The American Journal of Medicine.* 2006;119(6): 526.e9-526.17.

(151) Visser M, Pahor M, Taaffe DR, Goodpaster BH, Simonsick EM, Newman AB, et al. Relationship of interleukin-6 and tumor necrosis factor-alpha with muscle mass and muscle strength in elderly men and women: the Health ABC Study. *The journals of gerontology.Series A, Biological sciences and medical sciences.* 2002;57(5): M326-32.

(152) Cohen HJ, Pieper CF, Harris T, Rao KM, Currie MS. The association of plasma IL-6 levels with functional disability in community-dwelling elderly. *The journals of gerontology.Series A, Biological sciences and medical sciences.* 1997;52(4): M201-8.

(153) Taaffe DR, Harris TB, Ferrucci L, Rowe J, Seeman TE. Cross-sectional and prospective relationships of interleukin-6 and C-reactive protein with physical performance in elderly persons: MacArthur studies of successful aging. *The journals of gerontology.Series A, Biological sciences and medical sciences.* 2000;55(12): M709-15.

(154) Goodman MN. Tumor necrosis factor induces skeletal muscle protein breakdown in rats. *The American Journal of Physiology.* 1991;260(5 Pt 1): E727-30.

(155) Goodman MN. Interleukin-6 induces skeletal muscle protein breakdown in rats. *Proceedings of the Society for Experimental Biology and Medicine.Society for Experimental Biology and Medicine (New York, N.Y.).* 1994;205(2): 182-185.

(156) Argiles JM, Busquets S, Felipe A, Lopez-Soriano FJ. Molecular mechanisms involved in muscle wasting in cancer and ageing: cachexia versus sarcopenia. *The international journal of biochemistry & cell biology.* 2005;37(5): 1084-1104.

(157) Volpi E, Nazemi R, Fujita S. Muscle tissue changes with aging. *Current opinion in clinical nutrition and metabolic care.* 2004;7(4): 405-410.

(158) Ernster L, Schatz G. Mitochondria: a historical review. *The Journal of cell biology.* 1981;91(3 Pt 2): 227s-255s.

(159) Fernie AR, Carrari F, Sweetlove LJ. Respiratory metabolism: glycolysis, the TCA cycle and mitochondrial electron transport. *Current opinion in plant biology.* 2004;7(3): 254-261.

(160) Ray PD, Huang B, Tsuji Y. Reactive oxygen species (ROS) homeostasis and redox regulation in cellular signaling. *Cellular signalling.* 2012;24(5): 981-990.

(161) Calvani R, Joseph AM, Adhihetty PJ, Miccheli A, Bossola M, Leeuwenburgh C, et al. Mitochondrial pathways in sarcopenia of aging and disuse muscle atrophy. *Biological chemistry.* 2013;394(3): 393-414.

(162) Farre Garros R, Paul R, Connolly M, Lewis A, Garfield BE, Natanek SA, et al. miR-542 Promotes Mitochondrial Dysfunction and SMAD Activity and is Raised in ICU Acquired Weakness. *American journal of respiratory and critical care medicine.* 2017.

(163) Brian Glancy, Hartnell LM, Daniela Malide, Yu ZX, Combs CA, Connelly PS, et al. Mitochondrial reticulum for cellular energy distribution in muscle. *Nature.* 2015;523(7562,): 617-620.

(164) Petersen KF, Befroy D, Dufour S, Dziura J, Ariyan C, Rothman DL, et al. Mitochondrial Dysfunction in the Elderly: Possible Role in Insulin Resistance. *Science.* 2003;300(5622): 1140-1142. . Available from: doi: 10.1126/science.1082889.

(165) Conley KE, Jubrias SA, Esselman PC. Oxidative capacity and ageing in human muscle. *The Journal of physiology.* 2000;526 Pt 1203-210.

(166) Miller BF, Robinson MM, Bruss MD, Hellerstein M, Hamilton KL. A comprehensive assessment of mitochondrial protein synthesis and cellular proliferation with age and caloric restriction. *Aging cell.* 2012;11(1): 150-161.

(167) Poggi P, Marchetti C, Scelsi R. Automatic morphometric analysis of skeletal muscle fibers in the aging man. *The Anatomical Record.* 1987;217(1): 30-34.

(168) Fulle S, Protasi F, Di Tano G, Pietrangelo T, Beltramin A, Boncompagni S, et al. The contribution of reactive oxygen species to sarcopenia and muscle ageing. *Experimental gerontology.* 2004;39(1): 17-24.

(169) Powers SK, Smuder AJ, Criswell DS. Mechanistic links between oxidative stress and disuse muscle atrophy. *Antioxidants & redox signaling.* 2011;15(9): 2519-2528.

(170) Handy DE, Loscalzo J. Redox regulation of mitochondrial function. *Antioxidants & redox signaling.* 2012;16(11): 1323-1367.

(171) Harman D. Aging: a theory based on free radical and radiation chemistry. *Journal of gerontology.* 1956;11(3): 298-300.

(172) Barazzoni R, Short KR, Nair KS. Effects of aging on mitochondrial DNA copy number and cytochrome c oxidase gene expression in rat skeletal muscle, liver, and heart. *The Journal of biological chemistry.* 2000;275(5): 3343-3347.

(173) McKenzie D, Bua E, McKiernan S, Cao Z, Aiken JM, Jonathan Wanagat. Mitochondrial DNA deletion mutations: a causal role in sarcopenia. *European journal of biochemistry.* 2002;269(8): 2010-2015.

(174) Khrapko K, Vijg J. Mitochondrial DNA mutations and aging: devils in the details? *Trends in genetics : TIG.* 2009;25(2): 91-98.

(175) Sylvester JE, Fischel-Ghodsian N, Mougey EB, O'Brien TW. Mitochondrial ribosomal proteins: candidate genes for mitochondrial disease. *Genetics in medicine : official journal of the American College of Medical Genetics.* 2004;6(2): 73-80.

(176) Frontera WR, Hughes VA, Lutz KJ, Evans WJ. A cross-sectional study of muscle strength and mass in 45- to 78-yr-old men and women. *Journal of applied physiology (Bethesda, Md.: 1985).* 1991;71(2): 644-650.

(177) Fattoretti P, Vecchiet J, Felzani G, Gracciotti N, Solazzi M, Caselli U, et al. Succinic dehydrogenase activity in human muscle mitochondria during aging: a quantitative cytochemical investigation. *Mechanisms of ageing and development.* 2001;122(15): 1841-1848.

(178) Crane JD, Devries MC, Safdar A, Hamadeh MJ, Tarnopolsky MA. The effect of aging on human skeletal muscle mitochondrial and intramyocellular lipid ultrastructure. *The journals of gerontology.Series A, Biological sciences and medical sciences.* 2010;65(2): 119-128.

(179) Lanza IR, Short DK, Short KR, Raghavakaimal S, Basu R, Joyner MJ, et al. Endurance exercise as a countermeasure for aging. *Diabetes.* 2008;57(11): 2933-2942.

(180) Miller C, Saada A, Shaul N, Shabtai N, Ben-Shalom E, Shaag A, et al. Defective mitochondrial translation caused by a ribosomal protein (MRPS16) mutation. *Annals of Neurology.* 2004;56(5): 734-738.

(181) Saada A, Shaag A, Arnon S, Dolfin T, Miller C, Fuchs-Telem D, et al. Antenatal mitochondrial disease caused by mitochondrial ribosomal protein (MRPS22) mutation. *Journal of medical genetics.* 2007;44(12): 784-786.

(182) Gordon KJ, Blobe GC. Role of transforming growth factor-beta superfamily signaling pathways in human disease. *Biochimica et biophysica acta.* 2008;1782(4): 197-228.

(183) McCroskery S, Thomas M, Platt L, Hennebry A, Nishimura T, McLeay L, et al. Improved muscle healing through enhanced regeneration and reduced fibrosis in myostatin-null mice. *Journal of cell science.* 2005;118(Pt 15): 3531-3541.

(184) McCroskery S, Thomas M, Maxwell L, Sharma M, Kambadur R. Myostatin negatively regulates satellite cell activation and self-renewal. *The Journal of cell biology.* 2003;162(6): 1135-1147.

(185) Carnac G, Vernus B, Bonnieu A. Myostatin in the pathophysiology of skeletal muscle. *Current Genomics.* 2007;8(7): 415-422.

(186) Zimmers TA, Davies MV, Koniaris LG, Haynes P, Esquela AF, Tomkinson KN, et al. Induction of cachexia in mice by systemically administered myostatin. *Science (New York, N.Y.).* 2002;296(5572): 1486-1488.

(187) Clop A, Marcq F, Takeda H, Pirottin D, Tordoir X, Bibe B, et al. A mutation creating a potential illegitimate microRNA target site in the myostatin gene affects muscularity in sheep. *Nature genetics.* 2006;38(7): 813-818.

(188) McPherron AC, Lee SJ. Double muscling in cattle due to mutations in the myostatin gene. *Proceedings of the National Academy of Sciences of the United States of America.* 1997;94(23): 12457-12461.

(189) Lee SJ, McPherron AC. Regulation of myostatin activity and muscle growth. *Proceedings of the National Academy of Sciences of the United States of America.* 2001;98(16): 9306-9311.

(190) Kambadur R, Sharma M, Smith TP, Bass JJ. Mutations in myostatin (GDF8) in double-muscled Belgian Blue and Piedmontese cattle. *Genome research.* 1997;7(9): 910-916.

(191) Arthur P. Double muscling in cattle: a review. *Crop and Pasture Science.* 1995;46(8): 1493-1515.

(192) McPherron AC, Lawler AM, Lee SJ. Regulation of skeletal muscle mass in mice by a new TGF-beta superfamily member. *Nature.* 1997;387(6628): 83-90.

(193) Schuelke M, Wagner KR, Stolz LE, Hubner C, Riebel T, Komen W, et al. Myostatin mutation associated with gross muscle hypertrophy in a child. *The New England journal of medicine.* 2004;350(26): 2682-2688.

(194) McFarlane C, Plummer E, Thomas M, Hennebry A, Ashby M, Ling N, et al. Myostatin induces cachexia by activating the ubiquitin proteolytic system through an NF-κB-independent, FoxO1-dependent mechanism. *Journal of cellular physiology.* 2006;209(2): 501-514.

(195) Johnen H, Lin S, Kuffner T, Brown DA, Tsai VW, Bauskin AR, et al. Tumor-induced anorexia and weight loss are mediated by the TGF-beta superfamily cytokine MIC-1. *Nature medicine.* 2007;13(11): 1333-1340.

(196) Bloch SA, Lee JY, Wort SJ, Polkey MI, Kemp PR, Griffiths MJ. Sustained elevation of circulating growth and differentiation factor-15 and a dynamic imbalance in mediators of muscle homeostasis are associated with the development of acute muscle wasting following cardiac surgery. *Critical Care Medicine.* 2013;41(4): 982-989.

(197) Patel MS, Lee J, Baz M, Wells CE, Bloch S, Lewis A, et al. Growth differentiation factor-15 is associated with muscle mass in chronic obstructive pulmonary disease and promotes muscle wasting in vivo. *Journal of cachexia, sarcopenia and muscle.* 2016;7(4): 436-448.

(198) McLennan IS. Localisation of transforming growth factor beta 1 in developing muscles: implications for connective tissue and fiber type pattern formation. *Developmental dynamics : an official publication of the American Association of Anatomists.* 1993;197(4): 281-290.

(199) Cusella-De Angelis MG, Molinari S, Le Donne A, Coletta M, Vivarelli E, Bouche M, et al. Differential response of embryonic and fetal myoblasts to TGF beta: a possible regulatory mechanism of skeletal muscle histogenesis. *Development (Cambridge, England).* 1994;120(4): 925-933.

(200) Allen RE, Boxhorn LK. Inhibition of skeletal muscle satellite cell differentiation by transforming growth factor-beta. *Journal of cellular physiology.* 1987;133(3): 567-572.

(201) Burks TN, Cohn RD. Role of TGF-beta signaling in inherited and acquired myopathies. *Skeletal muscle.* 2011;1(1): 19-5040-1-19.

(202) Heydemann A, Ceco E, Lim JE, Hadhazy M, Ryder P, Moran JL, et al. Latent TGF-beta-binding protein 4 modifies muscular dystrophy in mice. *The Journal of clinical investigation.* 2009;119(12): 3703-3712.

(203) Barcellos-Hoff MH. Latency and activation in the control of TGF-beta. *Journal of mammary gland biology and neoplasia.* 1996;1(4): 353-363.

(204) Massague J. TGFbeta signalling in context. *Nature reviews.Molecular cell biology.* 2012;13(10): 616-630.

(205) Shi Y, Massague J. Mechanisms of TGF-beta signaling from cell membrane to the nucleus. *Cell.* 2003;113(6): 685-700.

(206) Bruce DL, Sapkota GP. Phosphatases in SMAD regulation. *FEBS Letters.* 2012;586(14): 1897-1905.

(207) Winbanks CE, Chen JL, Qian H, Liu Y, Bernardo BC, Beyer C, et al. The bone morphogenetic protein axis is a positive regulator of skeletal muscle mass. *The Journal of cell biology.* 2013;203(2): 345-357.

(208) Guo X, Wang X. Signaling cross-talk between TGF-β/BMP and other pathways. *Cell research.* 2008;19(1): 71-88.

(209) Kim RH, Wang D, Tsang M, Martin J, Huff C, de Caestecker MP, et al. A novel smad nuclear interacting protein, SNIP1, suppresses p300-dependent TGF-beta signal transduction. *Genes & development.* 2000;14(13): 1605-1616.

(210) Heikkinen PT, Nummela M, Leivonen SK, Westermarck J, Hill CS, Kahari VM, et al. Hypoxia-activated Smad3-specific dephosphorylation by PP2A. *The Journal of biological chemistry.* 2010;285(6): 3740-3749.

(211) Lin X, Duan X, Liang YY, Su Y, Wrighton KH, Long J, et al. PPM1A Functions as a Smad Phosphatase to Terminate TGFbeta Signaling. *Cell.* 2016;166(6): 1597.

(212) Cohen P. Phosphatase families dephosphorylating serine and threonine residues in proteins. . In: Bradshaw R, Dennis E. (eds.) *Handbook of cell signaling.* 2nd ed. London: Academic Press; 2010. pp. 659-675.

(213) Sapkota G, Knockaert M, Alarcon C, Montalvo E, Brivanlou AH, Massague J. Dephosphorylation of the linker regions of Smad1 and Smad2/3 by small C-terminal domain phosphatases has distinct outcomes for bone morphogenetic protein and transforming growth factor-beta pathways. *The Journal of biological chemistry.* 2006;281(52): 40412-40419.

(214) Ebisawa T, Fukuchi M, Murakami G, Chiba T, Tanaka K, Imamura T, et al. Smurf1 interacts with transforming growth factor-beta type I receptor through Smad7 and induces receptor degradation. *The Journal of biological chemistry.* 2001;276(16): 12477-12480.

(215) Gao S, Alarcon C, Sapkota G, Rahman S, Chen PY, Goerner N, et al. Ubiquitin ligase Nedd4L targets activated Smad2/3 to limit TGF-beta signaling. *Molecular cell.* 2009;36(3): 457-468.

(216) Zhang YE. Non-Smad pathways in TGF-β signaling. *Cell research.* 2008;19(1): 128-139.

(217) Massagué J. Integration of Smad and MAPK pathways: a link and a linker revisited. *Genes & development.* 7th ed. Cold Spring Harbor Laboratory Press; 2003. pp. 2993–2997.

(218) Pessah M, Prunier C, Marais J, Ferrand N, Mazars A, Lallemand F, et al. c-Jun interacts with the corepressor TG-interacting factor (TGIF) to suppress Smad2 transcriptional activity. *Proceedings of the National Academy of Sciences of the United States of America.* 2001;98(11): 6198-6203.

(219) Carnac G, Primig M, Kitzmann M, Chafey P, Tuil D, Lamb N, et al. RhoA GTPase and serum response factor control selectively the expression of MyoD without affecting Myf5 in mouse myoblasts. *Molecular biology of the cell.* 1998;9(7): 1891-1902.

(220) Meriane M, Charrasse S, Comunale F, Gauthier-Rouviere C. Transforming growth factor beta activates Rac1 and Cdc42Hs GTPases and the JNK pathway in skeletal muscle cells. *Biology of the cell.* 2002;94(7-8): 535-543.

(221) Chen S, Crawford M, Day RM, Briones VR, Leader JE, Jose PA, et al. RhoA modulates Smad signaling during transforming growth factor-beta-induced smooth muscle differentiation. *The Journal of biological chemistry.* 2006;281(3): 1765-1770.

(222) Lim LP, Lau NC, Garrett-Engele P, Grimson A, Schelter JM, Castle J, et al. Microarray analysis shows that some microRNAs downregulate large numbers of target mRNAs. *Nature.* 2005;433(7027): 769-773.

(223) Lee RC, Feinbaum RL, Ambros V. The C. elegans heterochronic gene lin-4 encodes small RNAs with antisense complementarity to lin-14. *Cell.* 1993;75(5): 843-854.

(224) Griffiths-Jones S, Saini HK, van Dongen S, Enright AJ. miRBase: tools for microRNA genomics. *Nucleic acids research.* 2008;36(Database issue): D154-8.

(225) Bartel DP. MicroRNAs: genomics, biogenesis, mechanism, and function. *Cell.* 2004;116(2): 281-297.

(226) Lee Y, Ahn C, Han J, Choi H, Kim J, Yim J, et al. The nuclear RNase III Drosha initiates microRNA processing. *Nature.* 2003;425(6956): 415-419.

(227) Lund E, Guttinger S, Calado A, Dahlberg JE, Kutay U. Nuclear export of microRNA precursors. *Science (New York, N.Y.).* 2004;303(5654): 95-98.

(228) Krol J, Loedige I, Filipowicz W. The widespread regulation of microRNA biogenesis, function and decay. *Nature reviews.Genetics.* 2010;11(9): 597-610.

(229) Carthew RW, Sontheimer EJ. Origins and Mechanisms of miRNAs and siRNAs. *Cell.* 2009;136(4): 642-655.

(230) Friedman RC, Farh KK, Burge CB, Bartel DP. Most mammalian mRNAs are conserved targets of microRNAs. *Genome research.* 2009;19(1): 92-105.

(231) Rhoades MW, Reinhart BJ, Lim LP, Burge CB, Bartel B, Bartel DP. Prediction of plant microRNA targets. *Cell.* 2002;110(4): 513-520.

(232) Brodersen P, Voinnet O. Revisiting the principles of microRNA target recognition and mode of action. *Nature reviews.Molecular cell biology.* 2009;10(2): 141-148.

(233) Winter J, Jung S, Keller S, Gregory RI, Diederichs S. Many roads to maturity: microRNA biogenesis pathways and their regulation. *Nature cell biology.* 2009;11(3): 228-234.

(234) Chen JF, Callis TE, Wang DZ. microRNAs and muscle disorders. *Journal of cell science.* 2009;122(Pt 1): 13-20.

(235) Ono K, Kuwabara Y, Han J. MicroRNAs and cardiovascular diseases. *The FEBS journal.* 2011;278(10): 1619-1633.

(236) Sokol NS, Ambros V. Mesodermally expressed Drosophila microRNA-1 is regulated by Twist and is required in muscles during larval growth. *Genes & development.* 2005;19(19): 2343-2354.

(237) Williams AH, Valdez G, Moresi V, Qi X, McAnally J, Elliott JL, et al. MicroRNA-206 delays ALS progression and promotes regeneration of neuromuscular synapses in mice. *Science (New York, N.Y.).* 2009;326(5959): 1549-1554.

(238) van Rooij E, Quiat D, Johnson BA, Sutherland LB, Qi X, Richardson JA, et al. A family of microRNAs encoded by myosin genes governs myosin expression and muscle performance. *Developmental cell.* 2009;17(5): 662-673.

(239) Safdar A, Abadi A, Akhtar M, Hettinga BP, Tarnopolsky MA. miRNA in the regulation of skeletal muscle adaptation to acute endurance exercise in C57Bl/6J male mice. *PloS one.* 2009;4(5): e5610.

(240) Nielsen S, Scheele C, Yfanti C, Akerstrom T, Nielsen AR, Pedersen BK, et al. Muscle specific microRNAs are regulated by endurance exercise in human skeletal muscle. *The Journal of physiology.* 2010;588(Pt 20): 4029-4037.

(241) Eisenberg I, Eran A, Nishino I, Moggio M, Lamperti C, Amato AA, et al. Distinctive patterns of microRNA expression in primary muscular disorders. *Proceedings of the*

National Academy of Sciences of the United States of America. 2007;104(43): 17016-17021.

(242) Russell AP, Wada S, Vergani L, Hock MB, Lamon S, Leger B, et al. Disruption of skeletal muscle mitochondrial network genes and miRNAs in amyotrophic lateral sclerosis. *Neurobiology of disease.* 2013;49107-117.

(243) Sylvius N, Bonne G, Straatman K, Reddy T, Gant TW, Shackleton S. MicroRNA expression profiling in patients with lamin A/C-associated muscular dystrophy. *FASEB journal : official publication of the Federation of American Societies for Experimental Biology.* 2011;25(11): 3966-3978.

(244) McCarthy JJ, Esser KA, Andrade FH. MicroRNA-206 is overexpressed in the diaphragm but not the hindlimb muscle of mdx mouse. *American journal of physiology.Cell physiology.* 2007;293(1): C451-7.

(245) Gregory RI, Yan KP, Amuthan G, Chendrimada T, Doratotaj B, Cooch N, et al. The Microprocessor complex mediates the genesis of microRNAs. *Nature.* 2004;432(7014): 235-240.

(246) Cacchiarelli D, Incitti T, Martone J, Cesana M, Cazzella V, Santini T, et al. miR-31 modulates dystrophin expression: new implications for Duchenne muscular dystrophy therapy. *EMBO reports.* 2011;12(2): 136-141.

(247) Perbellini R, Greco S, Sarra-Ferraris G, Cardani R, Capogrossi MC, Meola G, et al. Dysregulation and cellular mislocalization of specific miRNAs in myotonic dystrophy type 1. *Neuromuscular disorders : NMD.* 2011;21(2): 81-88.

(248) Gambardella S, Rinaldi F, Lepore SM, Viola A, Loro E, Angelini C, et al. Overexpression of microRNA-206 in the skeletal muscle from myotonic dystrophy type 1 patients. *Journal of translational medicine.* 2010;848-5876-8-48.

(249) Fernandez-Costa JM, Garcia-Lopez A, Zuniga S, Fernandez-Pedrosa V, Felipo-Benavent A, Mata M, et al. Expanded CTG repeats trigger miRNA alterations in Drosophila that are conserved in myotonic dystrophy type 1 patients. *Human molecular genetics.* 2013;22(4): 704-716.

(250) Lewis A, Riddoch-Contreras J, Natanek SA, Donaldson A, Man WD, Moxham J, et al. Downregulation of the serum response factor/miR-1 axis in the quadriceps of patients with COPD. *Thorax.* 2012;67(1): 26-34.

(251) Sun Y, Ge Y, Drnevich J, Zhao Y, Band M, Chen J. Mammalian target of rapamycin regulates miRNA-1 and follistatin in skeletal myogenesis. *The Journal of cell biology.* 2010;189(7): 1157-1169.

(252) McCarthy JJ, Esser KA, Peterson CA, Dupont-Versteegden EE. Evidence of MyomiR network regulation of beta-myosin heavy chain gene expression during skeletal muscle atrophy. *Physiological genomics.* 2009;39(3): 219-226.

(253) Xiao X, Huang C, Zhao C, Gou X, Senavirathna LK, Hinsdale M, et al. Regulation of myofibroblast differentiation by miR-424 during epithelial-to-mesenchymal transition. *Archives of Biochemistry and Biophysics.* 2015;56649-57.

(254) Donaldson A, Natanek SA, Lewis A, Man WD, Hopkinson NS, Polkey MI, et al. Increased skeletal muscle-specific microRNA in the blood of patients with COPD. *Thorax.* 2013;68(12): 1140-1149.

(255) Puig-Vilanova E, Ausin P, Martinez-Llorens J, Gea J, Barreiro E. Do epigenetic events take place in the vastus lateralis of patients with mild chronic obstructive pulmonary disease? *PloS one.* 2014;9(7): e102296.

(256) Puig-Vilanova E, Martinez-Llorens J, Ausin P, Roca J, Gea J, Barreiro E. Quadriceps muscle weakness and atrophy are associated with a differential epigenetic profile in advanced COPD. *Clinical science (London, England : 1979).* 2015;128(12): 905-921.

(257) Martin KM, Cooper WN, Metcalfe JC, Kemp PR. Mouse BTEB3, a new member of the basic transcription element binding protein (BTEB) family, activates expression from GC-rich minimal promoter regions. *The Biochemical journal.* 2000;345 Pt 3529-533.

(258) Zhu CH, Mouly V, Cooper RN, Mamchaoui K, Bigot A, Shay JW, et al. Cellular senescence in human myoblasts is overcome by human telomerase reverse transcriptase and cyclin-dependent kinase 4: consequences in aging muscle and therapeutic strategies for muscular dystrophies. *Aging cell.* 2007;6(4): 515-523.

(259) Ellis PD, Smith CW, Kemp P. Regulated tissue-specific alternative splicing of enhanced green fluorescent protein transgenes conferred by alpha-tropomyosin regulatory elements in transgenic mice. *The Journal of biological chemistry.* 2004;279(35): 36660-36669.

(260) Livak KJ, Schmittgen TD. Analysis of relative gene expression data using real-time quantitative PCR and the 2(-Delta Delta C(T)) Method. *Methods (San Diego, Calif.).* 2001;25(4): 402-408.

(261) Cronan JE,Jr, Narasimhan ML, Rawlings M. Insertional restoration of beta-galactosidase alpha-complementation (white-to-blue colony screening) facilitates assembly of synthetic genes. *Gene.* 1988;70(1): 161-170.

(262) McMahon JM, Signori E, Wells KE, Fazio VM, Wells DJ. Optimisation of electrotransfer of plasmid into skeletal muscle by pretreatment with hyaluronidase -- increased expression with reduced muscle damage. *Gene therapy.* 2001;8(16): 1264-1270.

(263) Gollins H, McMahon J, Wells KE, Wells DJ. High-efficiency plasmid gene transfer into dystrophic muscle. *Gene therapy.* 2003;10(6): 504-512.

(264) Shepherd AJ, Mohapatra DP. Tissue preparation and immunostaining of mouse sensory nerve fibers innervating skin and limb bones. *Journal of visualized experiments : JoVE.* 2012;(59):e3485. doi(59): e3485.

(265) Mohan D, Lewis A, Patel MS, Curtis KJ, Lee JY, Hopkinson NS, et al. Using laser capture microdissection to study fiber specific signaling in locomotor muscle in COPD: A pilot study. *Muscle & nerve.* 2017;55(6): 902-912.

(266) Lee JY, Lori D, Wells DJ, Kemp PR. FHL1 activates myostatin signalling in skeletal muscle and promotes atrophy. *FEBS open bio.* 2015;5753-762.

(267) Russell AP, Lamon S, Boon H, Wada S, Guller I, Brown EL, et al. Regulation of miRNAs in human skeletal muscle following acute endurance exercise and short-term endurance training. *The Journal of physiology.* 2013;591(18): 4637-4653.

(268) Davidsen PK, Gallagher IJ, Hartman JW, Tarnopolsky MA, Dela F, Helge JW, et al. High responders to resistance exercise training demonstrate differential regulation of skeletal muscle microRNA expression. *Journal of applied physiology (Bethesda, Md.: 1985).* 2011;110(2): 309-317.

(269) Mueller M, Breil FA, Lurman G, Klossner S, Fluck M, Billeter R, et al. Different molecular and structural adaptations with eccentric and conventional strength training in elderly men and women. *Gerontology.* 2011;57(6): 528-538.

(270) McGregor RA, Poppitt SD, Cameron-Smith D. Role of microRNAs in the age-related changes in skeletal muscle and diet or exercise interventions to promote healthy aging in humans. *Ageing research reviews.* 2014;1725-33.

(271) Lewis A, Lee JY, Donaldson AV, Natanek SA, Vaidyanathan S, Man WD, et al. Increased expression of H19/miR-675 is associated with a low fat-free mass index in patients with COPD. *Journal of cachexia, sarcopenia and muscle.* 2016;7(3): 330-344.

(272) Rabe KF, Hurd S, Anzueto A, Barnes PJ, Buist SA, Calverley P, et al. Global strategy for the diagnosis, management, and prevention of chronic obstructive pulmonary disease: GOLD executive summary. *American journal of respiratory and critical care medicine.* 2007;176(6): 532-555.

(273) Owens GR, Rogers RM, Pennock BE, Levin D. The diffusing capacity as a predictor of arterial oxygen desaturation during exercise in patients with chronic obstructive pulmonary disease. *The New England journal of medicine.* 1984;310(19): 1218-1221.

(274) Wijkstra PJ, TenVergert EM, van der Mark TW, Postma DS, Van Altena R, Kraan J, et al. Relation of lung function, maximal inspiratory pressure, dyspnoea, and quality of life with exercise capacity in patients with chronic obstructive pulmonary disease. *Thorax.* 1994;49(5): 468-472.

(275) Cukic V. The changes of arterial blood gases in COPD during four-year period. *Medical archives (Sarajevo, Bosnia and Herzegovina).* 2014;68(1): 14-18.

(276) Vestbo J, Edwards LD, Scanlon PD, Yates JC, Agusti A, Bakke P, et al. Changes in forced expiratory volume in 1 second over time in COPD. *The New England journal of medicine.* 2011;365(13): 1184-1192.

(277) Young RP, Hopkins R, Eaton TE. Forced expiratory volume in one second: not just a lung function test but a marker of premature death from all causes. *The European respiratory journal.* 2007;30(4): 616-622.

(278) Swanney MP, Ruppel G, Enright PL, Pedersen OF, Crapo RO, Miller MR, et al. Using the lower limit of normal for the FEV1/FVC ratio reduces the misclassification of airway obstruction. *Thorax.* 2008;63(12): 1046-1051.

(279) Sahebjami H, Gartside PS. Pulmonary function in obese subjects with a normal FEV1/FVC ratio. *Chest.* 1996;110(6): 1425-1429.

(280) Mohamed Hoesein FA, Zanen P, Lammers JW. Lower limit of normal or FEV1/FVC < 0.70 in diagnosing COPD: an evidence-based review. *Respiratory medicine.* 2011;105(6): 907-915.

(281) Redelmeier DA, Bayoumi AM, Goldstein RS, Guyatt GH. Interpreting small differences in functional status: the Six Minute Walk test in chronic lung disease patients. *American journal of respiratory and critical care medicine.* 1997;155(4): 1278-1282.

(282) Cahalin LP, Mathier MA, Semigran MJ, Dec GW, DiSalvo TG. The six-minute walk test predicts peak oxygen uptake and survival in patients with advanced heart failure. *Chest.* 1996;110(2): 325-332.

(283) Jay SJ. Reference equations for the six-minute walk in healthy adults. *American journal of respiratory and critical care medicine.* 2000;161(4 Pt 1): 1396.

(284) Troosters T, Gosselink R, Decramer M. Six minute walking distance in healthy elderly subjects. *The European respiratory journal.* 1999;14(2): 270-274.

(285) Podsiadlo D, Richardson S. The timed "Up & Go": a test of basic functional mobility for frail elderly persons. *Journal of the American Geriatrics Society.* 1991;39(2): 142-148.

(286) Luo Y, Zhou L, Li Y, Guo S, Li X, Zheng J, et al. Fat-Free Mass Index for Evaluating the Nutritional Status and Disease Severity in COPD. *Respiratory care.* 2016;61(5): 680-688.

(287) Ju CR, Chen RC. Quadriceps strength assessed by magnetic stimulation of femoral nerve in patients with chronic obstructive pulmonary disease. *Chinese medical journal.* 2011;124(15): 2309-2315.

(288) Sayer AA, Dennison EM, Syddall HE, Jameson K, Martin HJ, Cooper C. The developmental origins of sarcopenia: using peripheral quantitative computed

tomography to assess muscle size in older people. *The journals of gerontology.Series A, Biological sciences and medical sciences.* 2008;63(8): 835-840.

(289) Sayer AA, Syddall HE, Gilbody HJ, Dennison EM, Cooper C. Does sarcopenia originate in early life? Findings from the Hertfordshire cohort study. *The journals of gerontology.Series A, Biological sciences and medical sciences.* 2004;59(9): M930-4.

(290) Yoon S, Choi YC, Lee S, Jeong Y, Yoon J, Baek K. Induction of growth arrest by miR-542-3p that targets survivin. *FEBS letters.* 2010;584(18): 4048-4052.

(291) Dweep H, Sticht C, Pandey P, Gretz N. miRWalk--database: prediction of possible miRNA binding sites by "walking" the genes of three genomes. *Journal of Biomedical Informatics.* 2011;44(5): 839-847.

(292) Wang Y, Huang JW, Castella M, Huntsman DG, Taniguchi T. p53 is positively regulated by miR-542-3p. *Cancer research.* 2014;74(12): 3218-3227.

(293) Gosker HR, Hesselink MK, Duimel H, Ward KA, Schols AM. Reduced mitochondrial density in the vastus lateralis muscle of patients with COPD. *The European respiratory journal.* 2007;30(1): 73-79.

(294) Puente-Maestu L, Perez-Parra J, Godoy R, Moreno N, Tejedor A, Gonzalez-Aragoneses F, et al. Abnormal mitochondrial function in locomotor and respiratory muscles of COPD patients. *The European respiratory journal.* 2009;33(5): 1045-1052.

(295) Jiroutkova K, Krajcova A, Ziak J, Fric M, Waldauf P, Dzupa V, et al. Mitochondrial function in skeletal muscle of patients with protracted critical illness and ICU-acquired weakness. *Critical Care (London, England).* 2015;19448-015-1160-x.

(296) Short KR, Bigelow ML, Kahl J, Singh R, Coenen-Schimke J, Raghavakaimal S, et al. Decline in skeletal muscle mitochondrial function with aging in humans. *Proceedings of the National Academy of Sciences of the United States of America.* 2005;102(15): 5618-5623.

(297) Trounce I, Byrne E, Marzuki S. Decline in skeletal muscle mitochondrial respiratory chain function: possible factor in ageing. *Lancet (London, England).* 1989;1(8639): 637-639.

(298) Van Vliet M, Spruit MA, Verleden G, Kasran A, Van Herck E, Pitta F, et al. Hypogonadism, quadriceps weakness, and exercise intolerance in chronic obstructive pulmonary disease. *American journal of respiratory and critical care medicine.* 2005;172(9): 1105-1111.

(299) Gan WQ, Man SF, Senthilselvan A, Sin DD. Association between chronic obstructive pulmonary disease and systemic inflammation: a systematic review and a meta-analysis. *Thorax.* 2004;59(7): 574-580.

(300) Zhang D, Shi Z, Li M, Mi J. Hypoxia-induced miR-424 decreases tumor sensitivity to chemotherapy by inhibiting apoptosis. *Cell death & disease.* 2014;5e1301.

(301) Ghosh G, Subramanian IV, Adhikari N, Zhang X, Joshi HP, Basi D, et al. Hypoxia-induced microRNA-424 expression in human endothelial cells regulates HIF-alpha isoforms and promotes angiogenesis. *The Journal of clinical investigation.* 2010;120(11): 4141-4154.

(302) Faraonio R, Salerno P, Passaro F, Sedia C, Iaccio A, Bellelli R, et al. A set of miRNAs participates in the cellular senescence program in human diploid fibroblasts. *Cell death and differentiation.* 2012;19(4): 713-721.

(303) Taivassalo T, Hussain SN. Contribution of the Mitochondria to Locomotor Muscle Dysfunction in Patients With COPD. *Chest.* 2016;149(5): 1302-1312.

(304) Barazzoni R. Skeletal muscle mitochondrial protein metabolism and function in ageing and type 2 diabetes. *Current opinion in clinical nutrition and metabolic care.* 2004;7(1): 97-102.

(305) Maltais F, LeBlanc P, Whittom F, Simard C, Marquis K, Belanger M, et al. Oxidative enzyme activities of the vastus lateralis muscle and the functional status in patients with COPD. *Thorax.* 2000;55(10): 848-853.

(306) Trounce I, Neill S, Wallace DC. Cytoplasmic transfer of the mtDNA nt 8993 T-->G (ATP6) point mutation associated with Leigh syndrome into mtDNA-less cells demonstrates cosegregation with a decrease in state III respiration and ADP/O ratio. *Proceedings of the National Academy of Sciences of the United States of America.* 1994;91(18): 8334-8338.

(307) Spinazzola A, Invernizzi F, Carrara F, Lamantea E, Donati A, Dirocco M, et al. Clinical and molecular features of mitochondrial DNA depletion syndromes. *Journal of inherited metabolic disease.* 2009;32(2): 143-158.

(308) Sureshbabu A, Bhandari V. Targeting mitochondrial dysfunction in lung diseases: emphasis on mitophagy. *Frontiers in physiology.* 2013;4384.

(309) Schefold JC, Bierbrauer J, Weber-Carstens S. Intensive care unit-acquired weakness (ICUAW) and muscle wasting in critically ill patients with severe sepsis and septic shock. *Journal of cachexia, sarcopenia and muscle.* 2010;1(2): 147-157.

(310) Burd NA, Gorissen SH, van Loon LJ. Anabolic resistance of muscle protein synthesis with aging. *Exercise and sport sciences reviews.* 2013;41(3): 169-173.

(311) Rennie MJ. Anabolic resistance in critically ill patients. *Critical Care Medicine.* 2009;37(10 Suppl): S398-9.

(312) Debigare R, Marquis K, Cote CH, Tremblay RR, Michaud A, LeBlanc P, et al. Catabolic/anabolic balance and muscle wasting in patients with COPD. *Chest.* 2003;124(1): 83-89.

(313) Guillet C, Prod'homme M, Balage M, Gachon P, Giraudet C, Morin L, et al. Impaired anabolic response of muscle protein synthesis is associated with S6K1 dysregulation in elderly humans. *FASEB journal : official publication of the Federation of American Societies for Experimental Biology.* 2004;18(13): 1586-1587.

(314) Cuthbertson D, Smith K, Babraj J, Leese G, Waddell T, Atherton P, et al. Anabolic signaling deficits underlie amino acid resistance of wasting, aging muscle. *FASEB journal : official publication of the Federation of American Societies for Experimental Biology.* 2005;19(3): 422-424.

(315) Sanders KJ, Kneppers AE, van de Bool C, Langen RC, Schols AM. Cachexia in chronic obstructive pulmonary disease: new insights and therapeutic perspective. *Journal of cachexia, sarcopenia and muscle.* 2016;7(1): 5-22.

(316) Breen L, Phillips SM. Skeletal muscle protein metabolism in the elderly: Interventions to counteract the 'anabolic resistance' of ageing. *Nutrition & metabolism.* 2011;868-7075-8-68.

(317) Aoi W, Naito Y, Mizushima K, Takanami Y, Kawai Y, Ichikawa H, et al. The microRNA miR-696 regulates PGC-1{alpha} in mouse skeletal muscle in response to physical activity. *American journal of physiology.Endocrinology and metabolism.* 2010;298(4): E799-806.

(318) Colleoni F, Padmanabhan N, Yung HW, Watson ED, Cetin I, Tissot van Patot MC, et al. Suppression of mitochondrial electron transport chain function in the hypoxic human placenta: a role for miRNA-210 and protein synthesis inhibition. *PloS one.* 2013;8(1): e55194.

(319) Alexander MS, Shi X, Voelker KA, Grange RW, Garcia JA, Hammer RE, et al. Foxj3 transcriptionally activates Mef2c and regulates adult skeletal muscle fiber type identity. *Developmental biology.* 2010;337(2): 396-404.

(320) Yamamoto H, Morino K, Nishio Y, Ugi S, Yoshizaki T, Kashiwagi A, et al. MicroRNA-494 regulates mitochondrial biogenesis in skeletal muscle through mitochondrial transcription factor A and Forkhead box j3. *American journal of physiology.Endocrinology and metabolism.* 2012;303(12): E1419-27.

(321) Orom UA, Nielsen FC, Lund AH. MicroRNA-10a binds the 5'UTR of ribosomal protein mRNAs and enhances their translation. *Molecular cell.* 2008;30(4): 460-471.

(322) Gianni P, Jan KJ, Douglas MJ, Stuart PM, Tarnopolsky MA. Oxidative stress and the mitochondrial theory of aging in human skeletal muscle. *Experimental gerontology.* 2004;39(9): 1391-1400.

(323) Figueiredo VC, Markworth JF, Durainayagam BR, Pileggi CA, Roy NC, Barnett MP, et al. Impaired Ribosome Biogenesis and Skeletal Muscle Growth in a Murine Model of Inflammatory Bowel Disease. *Inflammatory bowel diseases.* 2016;22(2): 268-278.

(324) Brealey D, Singer M. Mitochondrial Dysfunction in Sepsis. *Current infectious disease reports.* 2003;5(5): 365-371.

(325) Gifford JR, Trinity JD, Layec G, Garten RS, Park SY, Rossman MJ, et al. Quadriceps exercise intolerance in patients with chronic obstructive pulmonary disease: the potential role of altered skeletal muscle mitochondrial respiration. *Journal of applied physiology (Bethesda, Md.: 1985).* 2015;119(8): 882-888.

(326) Lopez MF, Kristal BS, Chernokalskaya E, Lazarev A, Shestopalov AI, Bogdanova A, et al. High-throughput profiling of the mitochondrial proteome using affinity fractionation and automation. *Electrophoresis.* 2000;21(16): 3427-3440.

(327) Chabi B, Mousson de Camaret B, Chevrollier A, Boisgard S, Stepien G. Random mtDNA deletions and functional consequence in aged human skeletal muscle. *Biochemical and biophysical research communications.* 2005;332(2): 542-549.

(328) Capel F, Rimbert V, Lioger D, Diot A, Rousset P, Mirand PP, et al. Due to reverse electron transfer, mitochondrial H2O2 release increases with age in human vastus lateralis muscle although oxidative capacity is preserved. *Mechanisms of ageing and development.* 2005;126(4): 505-511.

(329) Pastoris O, Boschi F, Verri M, Baiardi P, Felzani G, Vecchiet J, et al. The effects of aging on enzyme activities and metabolite concentrations in skeletal muscle from sedentary male and female subjects. *Experimental gerontology.* 2000;35(1): 95-104.

(330) Safdar A, Hamadeh MJ, Kaczor JJ, Raha S, Debeer J, Tarnopolsky MA. Aberrant mitochondrial homeostasis in the skeletal muscle of sedentary older adults. *PloS one.* 2010;5(5): e10778.

(331) Boffoli D, Scacco SC, Vergari R, Solarino G, Santacroce G, Papa S. Decline with age of the respiratory chain activity in human skeletal muscle. *Biochimica et biophysica acta.* 1994;1226(1): 73-82.

(332) O'Connell K, Ohlendieck K. Proteomic DIGE analysis of the mitochondria-enriched fraction from aged rat skeletal muscle. *Proteomics.* 2009;9(24): 5509-5524.

(333) Gillardon F, Lenz C, Waschke KF, Krajewski S, Reed JC, Zimmermann M, et al. Altered expression of Bcl-2, Bcl-X, Bax, and c-Fos colocalizes with DNA fragmentation and ischemic cell damage following middle cerebral artery occlusion in rats. *Brain research.Molecular brain research.* 1996;40(2): 254-260.

(334) Vincent F, Corral-Debrinski M, Adolphe M. Transient mitochondrial transcript level decay in oxidative stressed chondrocytes. *Journal of cellular physiology.* 1994;158(1): 128-132.

(335) Zoll J, Sanchez H, N'Guessan B, Ribera F, Lampert E, Bigard X, et al. Physical activity changes the regulation of mitochondrial respiration in human skeletal muscle. *The Journal of physiology.* 2002;543(Pt 1): 191-200.

(336) Killian KJ, Leblanc P, Martin DH, Summers E, Jones NL, Campbell EJ. Exercise capacity and ventilatory, circulatory, and symptom limitation in patients with chronic airflow limitation. *The American Review of Respiratory Disease.* 1992;146(4): 935-940.

(337) Rabinovich RA, Bastos R, Ardite E, Llinas L, Orozco-Levi M, Gea J, et al. Mitochondrial dysfunction in COPD patients with low body mass index. *The European respiratory journal.* 2007;29(4): 643-650.

(338) Hiona A, Leeuwenburgh C. The role of mitochondrial DNA mutations in aging and sarcopenia: implications for the mitochondrial vicious cycle theory of aging. *Experimental gerontology.* 2008;43(1): 24-33.

(339) Johnson ML, Robinson MM, Nair KS. Skeletal muscle aging and the mitochondrion. *Trends in endocrinology and metabolism: TEM.* 2013;24(5): 247-256.

(340) Volpi E, Mittendorfer B, Rasmussen BB, Wolfe RR. The response of muscle protein anabolism to combined hyperaminoacidemia and glucose-induced hyperinsulinemia is impaired in the elderly. *The Journal of clinical endocrinology and metabolism.* 2000;85(12): 4481-4490.

(341) Cuthbertson DJ, Babraj J, Smith K, Wilkes E, Fedele MJ, Esser K, et al. Anabolic signaling and protein synthesis in human skeletal muscle after dynamic shortening or lengthening exercise. *American journal of physiology.Endocrinology and metabolism.* 2006;290(4): E731-8.

(342) Etheridge T, Atherton PJ, Wilkinson D, Selby A, Rankin D, Webborn N, et al. Effects of hypoxia on muscle protein synthesis and anabolic signaling at rest and in response to acute resistance exercise. *American journal of physiology.Endocrinology and metabolism.* 2011;301(4): E697-702.

(343) Mutlu LC, Altintas N, Aydin M, Tulubas F, Oran M, Kucukyalin V, et al. Growth Differentiation Factor-15 Is a Novel Biomarker Predicting Acute Exacerbation of Chronic Obstructive Pulmonary Disease. *Inflammation.* 2015;38(5): 1805-1813.

(344) Schlittenhardt D, Schober A, Strelau J, Bonaterra GA, Schmiedt W, Unsicker K, et al. Involvement of growth differentiation factor-15/macrophage inhibitory cytokine-1 (GDF-15/MIC-1) in oxLDL-induced apoptosis of human macrophages in vitro and in arteriosclerotic lesions. *Cell and tissue research.* 2004;318(2): 325-333.

(345) Kempf T, Eden M, Strelau J, Naguib M, Willenbockel C, Tongers J, et al. The transforming growth factor-beta superfamily member growth-differentiation factor-15 protects the heart from ischemia/reperfusion injury. *Circulation research.* 2006;98(3): 351-360.

(346) Hsiao EC, Koniaris LG, Zimmers-Koniaris T, Sebald SM, Huynh TV, Lee SJ. Characterization of growth-differentiation factor 15, a transforming growth factor beta superfamily member induced following liver injury. *Molecular and cellular biology.* 2000;20(10): 3742-3751.

(347) Zimmers TA, Jin X, Hsiao EC, McGrath SA, Esquela AF, Koniaris LG. Growth differentiation factor-15/macrophage inhibitory cytokine-1 induction after kidney and lung injury. *Shock (Augusta, Ga.).* 2005;23(6): 543-548.

(348) Zimmers TA, Jin X, Hsiao EC, Perez EA, Pierce RH, Chavin KD, et al. Growth differentiation factor-15: induction in liver injury through p53 and tumor necrosis factor-independent mechanisms. *The Journal of surgical research.* 2006;130(1): 45-51.

(349) Kollias HD, McDermott JC. Transforming growth factor-beta and myostatin signaling in skeletal muscle. *Journal of applied physiology (Bethesda, Md.: 1985).* 2008;104(3): 579-587.

(350) Mendias CL, Marcin JE, Calerdon DR, Faulkner JA. Contractile properties of EDL and soleus muscles of myostatin-deficient mice. *Journal of applied physiology (Bethesda, Md.: 1985).* 2006;101(3): 898-905.

(351) Siriett V, Platt L, Salerno MS, Ling N, Kambadur R, Sharma M. Prolonged absence of myostatin reduces sarcopenia. *Journal of cellular physiology.* 2006;209(3): 866-873.

(352) Cohn RD, van Erp C, Habashi JP, Soleimani AA, Klein EC, Lisi MT, et al. Angiotensin II type 1 receptor blockade attenuates TGF-beta-induced failure of muscle regeneration in multiple myopathic states. *Nature medicine.* 2007;13(2): 204-210.

(353) Ju CR, Chen RC. Serum myostatin levels and skeletal muscle wasting in chronic obstructive pulmonary disease. *Respiratory medicine.* 2012;106(1): 102-108.

(354) Yarasheski KE, Bhasin S, Sinha-Hikim I, Pak-Loduca J, Gonzalez-Cadavid NF. Serum myostatin-immunoreactive protein is increased in 60-92 year old women and men with muscle wasting. *The journal of nutrition, health & aging.* 2002;6(5): 343-348.

(355) Williams AH, Liu N, van Rooij E, Olson EN. MicroRNA control of muscle development and disease. *Current opinion in cell biology.* 2009;21(3): 461-469.

(356) Ge Y, Chen J. MicroRNAs in skeletal myogenesis. *Cell cycle (Georgetown, Tex.).* 2011;10(3): 441-448.

(357) Gagan J, Dey BK, Dutta A. MicroRNAs regulate and provide robustness to the myogenic transcriptional network. *Current opinion in pharmacology.* 2012;12(3): 383-388.

(358) Martin J, Jenkins RH, Bennagi R, Krupa A, Phillips AO, Bowen T, et al. Post-transcriptional regulation of Transforming Growth Factor Beta-1 by microRNA-744. *PloS one.* 2011;6(10): e25044.

(359) Beaumont J, Lopez B, Hermida N, Schroen B, San Jose G, Heymans S, et al. microRNA-122 down-regulation may play a role in severe myocardial fibrosis in human aortic stenosis through TGF-beta1 up-regulation. *Clinical science (London, England : 1979).* 2014;126(7): 497-506.

(360) Faherty N, Curran SP, O'Donovan H, Martin F, Godson C, Brazil DP, et al. CCN2/CTGF increases expression of miR-302 microRNAs, which target the TGFbeta type II receptor with implications for nephropathic cell phenotypes. *Journal of cell science.* 2012;125(Pt 23): 5621-5629.

(361) Wang X, Chen X, Meng Q, Jing H, Lu H, Yang Y, et al. MiR-181b regulates cisplatin chemosensitivity and metastasis by targeting TGFbetaR1/Smad signaling pathway in NSCLC. *Scientific reports.* 2015;517618.

(362) Wang B, Li W, Guo K, Xiao Y, Wang Y, Fan J. miR-181b promotes hepatic stellate cells proliferation by targeting p27 and is elevated in the serum of cirrhosis patients. *Biochemical and biophysical research communications.* 2012;421(1): 4-8.

(363) Megiorni F, Cialfi S, Cimino G, De Biase RV, Dominici C, Quattrucci S, et al. Elevated levels of miR-145 correlate with SMAD3 down-regulation in cystic fibrosis patients. *Journal of cystic fibrosis : official journal of the European Cystic Fibrosis Society.* 2013;12(6): 797-802.

(364) O'Leary L, Sevinc K, Papazoglou IM, Tildy B, Detillieux K, Halayko AJ, et al. Airway smooth muscle inflammation is regulated by microRNA-145 in COPD. *FEBS letters.* 2016;590(9): 1324-1334.

(365) He Y, Huang C, Sun X, Long XR, Lv XW, Li J. MicroRNA-146a modulates TGF-beta1-induced hepatic stellate cell proliferation by targeting SMAD4. *Cellular signalling.* 2012;24(10): 1923-1930.

(366) Liu Z, Lu CL, Cui LP, Hu YL, Yu Q, Jiang Y, et al. MicroRNA-146a modulates TGF-beta1-induced phenotypic differentiation in human dermal fibroblasts by targeting SMAD4. *Archives of Dermatological Research.* 2012;304(3): 195-202.

(367) Zhang Y, Xiao HQ, Wang Y, Yang ZS, Dai LJ, Xu YC. Differential expression and therapeutic efficacy of microRNA-346 in diabetic nephropathy mice. *Experimental and therapeutic medicine.* 2015;10(1): 106-112.

(368) Chan MC, Hilyard AC, Wu C, Davis BN, Hill NS, Lal A, et al. Molecular basis for antagonism between PDGF and the TGFbeta family of signalling pathways by control of miR-24 expression. *The EMBO journal.* 2010;29(3): 559-573.

(369) Dey BK, Gagan J, Yan Z, Dutta A. miR-26a is required for skeletal muscle differentiation and regeneration in mice. *Genes & development.* 2012;26(19): 2180-2191.

(370) Zhu H, Luo H, Li Y, Zhou Y, Jiang Y, Chai J, et al. MicroRNA-21 in scleroderma fibrosis and its function in TGF-beta-regulated fibrosis-related genes expression. *Journal of clinical immunology.* 2013;33(6): 1100-1109.

(371) Ezzie ME, Crawford M, Cho JH, Orellana R, Zhang S, Gelinas R, et al. Gene expression networks in COPD: microRNA and mRNA regulation. *Thorax.* 2012;67(2): 122-131.

(372) Cui W, Zhou J, Dehne N, Brune B. Hypoxia induces calpain activity and degrades SMAD2 to attenuate TGFbeta signaling in macrophages. *Cell & bioscience.* 2015;536-015-0026-x. eCollection 2015.

(373) Freudlsperger C, Bian Y, Contag Wise S, Burnett J, Coupar J, Yang X, et al. TGF-beta and NF-kappaB signal pathway cross-talk is mediated through TAK1 and SMAD7 in a subset of head and neck cancers. *Oncogene.* 2013;32(12): 1549-1559.

(374) Hesler RA, Huang JJ, Starr MD, Treboschi VM, Bernanke AG, Nixon AB, et al. TGF-beta-induced stromal CYR61 promotes resistance to gemcitabine in pancreatic ductal adenocarcinoma through downregulation of the nucleoside transporters hENT1 and hCNT3. *Carcinogenesis.* 2016;37(11): 1041-1051.

(375) Bartholin L, Wessner LL, Chirgwin JM, Guise TA. The human Cyr61 gene is a transcriptional target of transforming growth factor beta in cancer cells. *Cancer letters.* 2007;246(1-2): 230-236.

(376) Parisi MS, Gazzerro E, Rydziel S, Canalis E. Expression and regulation of CCN genes in murine osteoblasts. *Bone.* 2006;38(5): 671-677.

(377) Santander C, Brandan E. Betaglycan induces TGF-beta signaling in a ligand-independent manner, through activation of the p38 pathway. *Cellular signalling.* 2006;18(9): 1482-1491.

(378) Garamszegi N, Dore JJ,Jr, Penheiter SG, Edens M, Yao D, Leof EB. Transforming growth factor beta receptor signaling and endocytosis are linked through a COOH terminal activation motif in the type I receptor. *Molecular biology of the cell.* 2001;12(9): 2881-2893.

(379) Mu Y, Gudey SK, Landstrom M. Non-Smad signaling pathways. *Cell and tissue research.* 2012;347(1): 11-20.

(380) Jin Y, An CH, Liang X, Ifedigbo E, Choi AMK. Cyr61 Is A Novel Regulator In The Pathogenesis Of Cigarette Smoking Induced Emphysema. *Sticky situation: multi-fate of cell and matrix interactions.* American Thoracic Society; 2012. pp. A5550-A5550.

(381) Zhang M, Mo L, Chen Z, Ifedigbo E, Choi AMK, Jin Y. Cigarette Smoking Induces Cyr61 Expression And Secretion In Pulmonary Epithelial Cells Via Egr-1 Mediated Pathways. *Regulating cell growth and survival: apoptosis, survival and senescence.* American Thoracic Society; 2010. pp. A4931-A4931.

(382) Du J, Klein JD, Hassounah F, Zhang J, Zhang C, Wang XH. Aging increases CCN1 expression leading to muscle senescence. *American journal of physiology.Cell physiology.* 2014;306(1): C28-36.

(383) Kemp PaC, Paul R, Farre GR, Natanek, Bloch, Lee J, et al. miR-424-5p reduces rRNA and protein synthesis in muscle wasting. *Journal of Cachexia, Sarcopenia and Muscle.*

(384) Forrest AR, Kanamori-Katayama M, Tomaru Y, Lassmann T, Ninomiya N, Takahashi Y, et al. Induction of microRNAs, mir-155, mir-222, mir-424 and mir-503, promotes monocytic differentiation through combinatorial regulation. *Leukemia.* 2010;24(2): 460-466.

(385) Butz H, Liko I, Czirjak S, Igaz P, Korbonits M, Racz K, et al. MicroRNA profile indicates downregulation of the TGFbeta pathway in sporadic non-functioning pituitary adenomas. *Pituitary.* 2011;14(2): 112-124.

(386) Oneyama C, Morii E, Okuzaki D, Takahashi Y, Ikeda J, Wakabayashi N, et al. MicroRNA-mediated upregulation of integrin-linked kinase promotes Src-induced tumor progression. *Oncogene.* 2012;31(13): 1623-1635.

(387) Casellas J. Inbred mouse strains and genetic stability: a review. *Animal : an international journal of animal bioscience.* 2011;5(1): 1-7.

(388) Nayerossadat N, Maedeh T, Ali PA. Viral and nonviral delivery systems for gene delivery. *Advanced biomedical research.* 2012;127-9175.98152. Epub 2012 Jul 6.

(389) Huang Y, Liu X, Dong L, Liu Z, He X, Liu W. Development of viral vectors for gene therapy for chronic pain. *Pain research and treatment.* 2011;2011968218.

(390) Gardlik R, Palffy R, Hodosy J, Lukacs J, Turna J, Celec P. Vectors and delivery systems in gene therapy. *Medical science monitor : international medical journal of experimental and clinical research.* 2005;11(4): RA110-21.

(391) Louboutin JP, Wang L, Wilson JM. Gene transfer into skeletal muscle using novel AAV serotypes. *The journal of gene medicine.* 2005;7(4): 442-451.

(392) Yue Y, Ghosh A, Long C, Bostick B, Smith BF, Kornegay JN, et al. A single intravenous injection of adeno-associated virus serotype-9 leads to whole body skeletal muscle transduction in dogs. *Molecular therapy: the journal of the American Society of Gene Therapy.* 2008;16(12): 1944-1952.

(393) Lu QL, Bou-Gharios G, Partridge TA. Non-viral gene delivery in skeletal muscle: a protein factory. *Gene therapy.* 2003;10(2): 131-142.

(394) Wolff JA, Malone RW, Williams P, Chong W, Acsadi G, Jani A, et al. Direct gene transfer into mouse muscle in vivo. *Science (New York, N.Y.).* 1990;247(4949 Pt 1): 1465-1468.

(395) Wolff JA, Ludtke JJ, Acsadi G, Williams P, Jani A. Long-term persistence of plasmid DNA and foreign gene expression in mouse muscle. *Human molecular genetics.* 1992;1(6): 363-369.

(396) Hartikka J, Bozoukova V, Jones D, Mahajan R, Wloch MK, Sawdey M, et al. Sodium phosphate enhances plasmid DNA expression in vivo. *Gene therapy.* 2000;7(14): 1171-1182.

(397) Blomberg P, Eskandarpour M, Xia S, Sylven C, Islam KB. Electroporation in combination with a plasmid vector containing SV40 enhancer elements results in increased and persistent gene expression in mouse muscle. *Biochemical and biophysical research communications.* 2002;298(4): 505-510.

(398) Golzio M, Mora MP, Raynaud C, Delteil C, Teissie J, Rols MP. Control by osmotic pressure of voltage-induced permeabilization and gene transfer in mammalian cells. *Biophysical journal.* 1998;74(6): 3015-3022.

(399) Schertzer JD, Plant DR, Lynch GS. Optimizing plasmid-based gene transfer for investigating skeletal muscle structure and function. *Molecular therapy: the journal of the American Society of Gene Therapy.* 2006;13(4): 795-803.

(400) Niwa H, Yamamura K, Miyazaki J. Efficient selection for high-expression transfectants with a novel eukaryotic vector. *Gene.* 1991;108(2): 193-199.

(401) Meijer HA, Smith EM, Bushell M. Regulation of miRNA strand selection: follow the leader? *Biochemical Society transactions.* 2014;42(4): 1135-1140.

(402) Gasier HG, Fluckey JD, Previs SF. The application of 2H2O to measure skeletal muscle protein synthesis. *Nutrition & metabolism.* 2010;731-7075-7-31.

(403) Seymour JM, Ward K, Sidhu PS, Puthucheary Z, Steier J, Jolley CJ, et al. Ultrasound measurement of rectus femoris cross-sectional area and the relationship with quadriceps strength in COPD. *Thorax.* 2009;64(5): 418-423.

(404) Agrawal R, Pandey P, Jha P, Dwivedi V, Sarkar C, Kulshreshtha R. Hypoxic signature of microRNAs in glioblastoma: insights from small RNA deep sequencing. *BMC genomics.* 2014;15686-2164-15-686.

(405) Keniry A, Oxley D, Monnier P, Kyba M, Dandolo L, Smits G, et al. The H19 lincRNA is a developmental reservoir of miR-675 that suppresses growth and Igf1r. *Nature cell biology.* 2012;14(7): 659-665.

(406) Ruiz S, Panopoulos AD, Montserrat N, Multon MC, Daury A, Rocher C, et al. Generation of a drug-inducible reporter system to study cell reprogramming in human cells. *The Journal of biological chemistry.* 2012;287(48): 40767-40778.

(407) Artero-Castro A, Perez-Alea M, Feliciano A, Leal JA, Genestar M, Castellvi J, et al. Disruption of the ribosomal P complex leads to stress-induced autophagy. *Autophagy.* 2015;11(9): 1499-1519.

(408) Wust RC, Myers DS, Stones R, Benoist D, Robinson PA, Boyle JP, et al. Regional skeletal muscle remodeling and mitochondrial dysfunction in right ventricular heart failure. *American journal of physiology. Heart and circulatory physiology.* 2012;302(2): H402-11.

(409) Bratic A, Larsson NG. The role of mitochondria in aging. *The Journal of clinical investigation.* 2013;123(3): 951-957.

(410) Kwong LK, Sohal RS. Age-related changes in activities of mitochondrial electron transport complexes in various tissues of the mouse. *Archives of Biochemistry and Biophysics.* 2000;373(1): 16-22.

(411) Drummond MJ, Glynn EL, Fry CS, Dhanani S, Volpi E, Rasmussen BB. Essential amino acids increase microRNA-499, -208b, and -23a and downregulate myostatin and myocyte enhancer factor 2C mRNA expression in human skeletal muscle. *The Journal of nutrition.* 2009;139(12): 2279-2284.

(412) Rosenberg MI, Georges SA, Asawachaicharn A, Analau E, Tapscott SJ. MyoD inhibits Fstl1 and Utrn expression by inducing transcription of miR-206. *The Journal of cell biology.* 2006;175(1): 77-85.

(413) Li Y, Li W, Ying Z, Tian H, Zhu X, Li J, et al. Metastatic heterogeneity of breast cancer cells is associated with expression of a heterogeneous TGFbeta-activating miR424-503 gene cluster. *Cancer research.* 2014;74(21): 6107-6118.

(414) Llobet-Navas D, Rodriguez-Barrueco R, Castro V, Ugalde AP, Sumazin P, Jacob-Sendler D, et al. The miR-424(322)/503 cluster orchestrates remodeling of the epithelium in the involuting mammary gland. *Genes & development.* 2014;28(7): 765-782.

(415) Ebert MS, Sharp PA. MicroRNA sponges: progress and possibilities. *RNA (New York, N.Y.).* 2010;16(11): 2043-2050.

Appendix 1

AntagomiR addition to some of the *in vitro* experiments seems not to have fully reversed the effect of the microRNA. The reason why that occurs is not entirely clear but some potential explanations are given below.

The efficiency with which the antagomiR recognises the microRNA can vary between the -3p and the -5p strand which could explain why in some cases the antagomiR-542-3p has reversed the effect of the miR-542-3p but the antagomiR-542-5p could not do so such as PPP2CA *(Figure 43)* and CTDSP1 *(Figure 44)* RNA.

In other cases, none of the antagomiRs has been able to reverse the action of the microRNA such as 12S, 16S *(Figure 23)* rRNA as well as SMURF1 *(Figure 42)* and STRN *(Figure 43)* RNA. Depending on how much microRNA is needed freely to trigger those responses, it is possible that the small amount of free microRNA is enough to provoke a decrease in the target. Moreover, the spread in the samples of some experiments could also be one of the causes for not having identified a potential reverse action by antagomiR. This reason could explain why when we ratio 12S/16S and 18S/28S rRNA values we see how the antagomiR reverses the effect of the microRNA which did not happened with 12S and 16S *(Figure 23)* rRNA.

Appendix 2

miR-542-3p is known to target surviving and to affect cell growth (290). miR-542-5p was not predicted to target surviving, but to determine that it was not affecting cell growth we performed a proliferation assay. No changes in proliferation were seen in LHCN-M2 transfected with miR-542-5p compared to scrambled transfected cells.

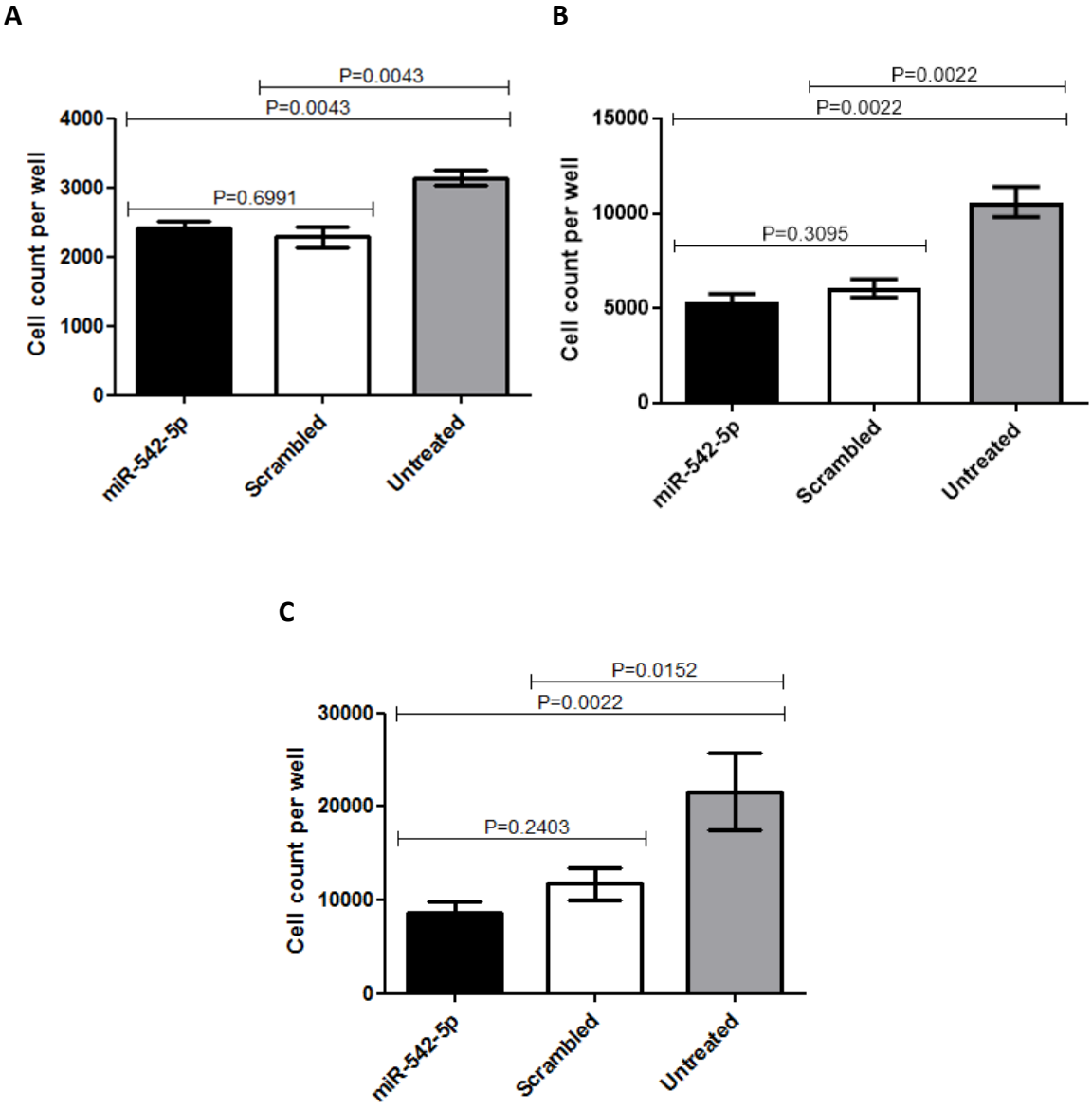


Figure 59- miR-542-5p does not affect proliferation *in vitro*.

LHCN-M2 myoblasts were transfected with miR-542-5p or scrambled as control and cell number was counted at different time points: [A] 24, [B] 48 and [C] 72h. Untreated myoblasts were used as a control of the effect of transfection in proliferation. No effect on proliferation at any of the time points was seen due to miR-542-5p transfection compared to scrambled transfection *in vitro*. However, the transfection technique seems to decrease cell proliferation compared to untreated cells in all the time points.